



ANDREW

SIDELOBE REDUCTION TECHNIQUES
FOR EARTH STATION ANTENNAS

Queen
P
91
C655
L55
1982

SIDELobe REDUCTION TECHNIQUES
FOR EARTH STATION ANTENNAS



Government
of Canada

Gouvernement
du Canada

Department of Communications

DOC CONTRACTOR REPORT

DOC-CR-SP -82-031

DEPARTMENT OF COMMUNICATIONS - OTTAWA - CANADA

SPACE PROGRAM

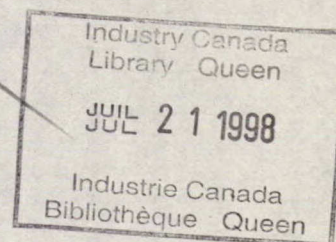
TITLE: ⁽²⁾ Sidelobe Reduction Techniques for
Earth Station Antennas

AUTHOR(S): ⁽¹⁾ S.H. Lim/
R. Boyko
R. Yang



ISSUED BY CONTRACTOR AS REPORT NO:

PREPARED BY: Andrew Antenna Co. Ltd
606 Beech Street
Whitby, Ontario
L1N 5S2



DEPARTMENT OF SUPPLY AND SERVICES CONTRACT NO: 06ST-36001-1-182

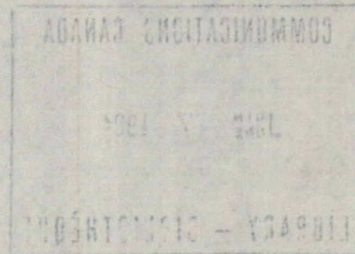
DOC SCIENTIFIC AUTHORITY: Dr. Marcel Bouchard

CLASSIFICATION: Unclassified

This report presents the views of the author(s). Publication of this report does not constitute DOC approval of the reports findings or conclusions. This report is available outside the department by special arrangement.

DATE: 31 May 1982

040



P
91
C655
L55
1982

DD 4504103
DL 4504122

Abstract

A study of sidelobe reduction techniques for earth station antennas (ESA) required to produce radiation pattern envelopes (RPE) 3 to 6dB below the current FCC curve requirement ($32-25\log\theta$) was performed. Included was a comparative study of the procedure for generating RPE by the CCIR, FCC and Intelsat rules with a discussion on possible new methods of improving the procedure. Detail data on antenna performance include the RPE of three different antenna plotted using different rules. The major factors causing co-polar and cross-polar antenna sidelobes were considered together with the techniques for their reduction. Details of studies on reflector coma, astigmatism and temperature distortion are included. The application of sidelobe reduction techniques to upgrade existing antennas was described. Six antenna designs which use the techniques studied were described. These include two new proposed configurations. The first is a large (8-12m) near-field cassegrain antenna with a hollow foam-cone supported subreflector. The second is a dual-polarized axially supported feed for small antennas ($<4.5\text{M}$). Comparative cost of the new antennas and also upgraded antennas were included.

Identifiers

Parabolic Antennas, antenna radiation patterns, sidelobe reduction, horn reflector antennas, offset reflector antenna, near-field Cassegrain, dielectric feed, axially supported feed, antenna feeds, corrugated feed, antenna configurations.

INDEX

| SECTION | DESCRIPTION | PAGE NO. |
|---------|--|----------|
| 1.0 | Introduction | 1 |
| 2.0 | Antenna Radiation Pattern Envelope | 2 |
| 2.1 | Antenna Pattern Measurements | 5 |
| 2.1.1 | Linear Polarized Antenna | 7 |
| 2.1.2 | Circular Polarized Antenna | 8 |
| 2.2 | Methods of Generating RPE's | 10 |
| 2.2.1 | Peak Pattern Envelope | 10 |
| 2.2.2 | CCIR Envelope | 11 |
| 2.2.3 | Intelsat Envelope | 12 |
| 2.2.4 | FCC Envelope | 13 |
| 2.3 | RPE's for Selected Antennas | 13 |
| 2.3.1 | CCIR Envelopes for the Selected Antennas | 14 |
| 2.3.2 | FCC Envelopes for the Selected Antennas | 21 |
| 2.4 | Discussion and comments on RPE Generation | 22 |
| 2.4.1 | The CCIR Method | 22 |
| 2.4.1.1 | Patterns used in Data Base | 23 |
| 2.4.1.2 | Window Intervals | 24 |
| 2.4.1.3 | Distribution of Sidelobe Peaks | 25 |
| 2.4.1.4 | Judgement of Curve Compliance by CCIR Method | 27 |
| 2.4.1.5 | The Relative Level Method | 28 |
| 2.4.2 | Definition of a sidelobe peak | 29 |
| 3.0 | Antenna Sidelobe Performance | 31 |
| 3.1 | Control of Aperture Distribution | 32 |
| 3.1.1 | Antenna Configurations | 32 |
| 3.1.2 | Shaping Techniques | 35 |
| 3.2 | Effect of Aperture Distribution on Sidelobes | 37 |
| 3.3 | Cross-polarization Fields | 40 |
| 3.4 | Antenna Aperture Blockage | 42 |
| 3.4.1 | Support Configurations and Blockage | 42 |
| 3.4.1.1 | Conventional Supports for Feeds and Subreflectors. | 42 |

| SECTION | DESCRIPTION | PAGE NO. |
|---------|-------------------------------------|----------|
| 3.4.1.2 | Conical Tube Support | 45 |
| 3.4.1.3 | Foam Support for Subreflectors | 45 |
| 3.4.1.4 | Axially-supported Feeds | 46 |
| 3.4.2 | Central Aperture Blockage | 47 |
| 3.4.2.1 | Feed and Subreflector Blockage | 47 |
| 3.4.2.2 | Blockage Reduction and Compensation | 49 |
| 3.5 | Diffraction and Scattering | 51 |
| 3.5.1 | Diffraction Fields of | 51 |
| 3.5.2 | Scattering from Supports | 53 |
| 3.5.3 | Scattering from Feeds | 55 |
| 3.6 | Reflector Errors | 57 |
| 3.6.1 | Axial Defocus Error | 57 |
| 3.6.2 | Astigmatism | 58 |
| 3.6.3 | Coma Distortion | 66 |
| 3.6.4 | Spherical Aberration | 69 |
| 3.6.5 | Surface Errors | 70 |
| 3.7 | Antenna Feeds | 73 |
| 3.7.1 | Feeds for Dual-Reflector Systems | 73 |
| 3.7.2 | Prime Focus Feeds | 77 |
| 3.8 | Environmental Effects | 79 |
| 3.8.1 | Temperature Effects | 79 |
| 3.8.2 | Gravitational Sag | 82 |
| 4 | Upgrading Of Existing Antennas | 84 |
| 4.1 | Large ESA's | 84 |
| 4.1.1 | Upgrade methods for 8m, 10m and 12m | 84 |
| 4.1.2 | 10m & 12m Antenna at 4/6 GHz | 84 |
| 4.1.3 | 8m at 4/6 and 12/14 GHz | 85 |
| 4.2 | Small ESA's | 86 |
| 4.2.1 | Upgrade Methods | 86 |
| 4.2.2 | J Hook Feed Antennas | 86 |
| 4.2.3 | Cassegrainian Antennas at 4/6 GHz | 87 |
| 4.2.4 | Cassegrainian Antennas at 12/14 GHz | 87 |
| 4.3 | Summary of Upgrade Costs | 87 |

| SECTION | DESCRIPTION | PAGE NO |
|------------|---|---------|
| 5 | New Antenna Designs | 88 |
| 5.1 | Large ESA Designs | 88 |
| 5.1.1 | New 8-12m Antennas | 88 |
| 5.1.2 | Offset Antennas | 95 |
| 5.1.3 | Horn Reflector Antenna | 95 |
| 5.2 | Small ESA Designs | 96 |
| 5.2.1 | Antenna with axially supported feed | 98 |
| 5.2.2 | Dielguide Antenna | 100 |
| 5.2.3 | Fiberglass Tube Support Antenna | 103 |
| 6.0 | Conclusion and Comments. | 105 |
| Appendix A | A Method of Producing any Aperture Distribution | 108 |
| Appendix B | Circular Polarization Power Transfer | 112 |
| Appendix C | Scattered Field From a Reflector | 116 |
| Appendix D | Temperature Effects of 8m Antenna | 121 |
| Appendix E | Dielguide Paraboloid System | 123 |
| | Reference | 124 |
| | Figures | 133 |

1.0 Introduction

The recent FCC proposal to decrease the orbital spacing of geostationary satellites to 2° means that a new generation of earth station antennas (ESA) would be required. This requirement has become important because the useable satellite positions in the synchronous satellite orbit are relatively limited for any one nation.

This study was initiated to explore the antenna problems associated with the introduction of a more restrictive radiation pattern envelope (RPE) requirements. It studies the feasibility and cost of introducing new antenna designs. In addition methods of upgrading existing antennas and the associated cost are also considered.

To be able to compare antenna sidelobe of different antennas data must be presented in the same format using a common set of rules. The ideal situation would be one set of rules that is universally applied. Unfortunately many different sets of rules exist. Section 2 gives a general survey of antenna pattern measurement and discuss the four main methods used to present antenna RPE for earth station antennas. A discussion of the rules with suggestions on methods to overcome possible problems is also included. Section 3 presents the results of a study into the causes of sidelobe degradation and discuss

the sidelobe reduction techniques available. Section 4 applies the results of the sidelobe reduction study to the possible upgrading for existing ESA designs. Current Andrew designs are used as an example. It showed that while patterns can be improved the existing antenna cannot meet the proposed envelopes (see below). Section 5 presents six possible antenna configurations that deserve further investigation because they have a potential of giving very good sidelobe performance. In most cases details of existing designs are given to illustrate the improvement possible. Two of the proposed configurations are new designs. A conceptual study of a 8m to 12m near-field cassegrain is presented. This system uses a horn-reflector as a feed and use a hollow foam subreflector support to eliminate strut blockage. A dual polarized axially supported feed system for small antennas is also proposed.

The four antenna pattern envelopes listed below are the proposed design goals for this study. They would be referred to within this report as proposed envelopes (1) to (4).

- | | | | |
|-----|-------------------------------|----|--------------------------------------|
| (1) | $G = 29 - 25 \log \theta$ | dB | for $\theta < 36.3^\circ$ |
| | $G = -10$ | dB | $\theta \geq 36.3^\circ$ |
| (2) | $G = 26.25 \log \theta$ | dB | $\theta < 27.5^\circ$ |
| | $G = -10$ | dB | $\theta \geq 27.5^\circ$ |
| (3) | $G = 29 - 25 \log \theta$ | dB | $\theta < 10^\circ$ |
| | $G = 24.6 - 20.6 \log \theta$ | dB | $10^\circ \leq \theta \leq 48^\circ$ |
| | $G = -10$ | dB | $\theta > 48^\circ$ |
| (4) | $G = 26 - 25 \log \theta$ | dB | $\theta < 10^\circ$ |
| | $G = 17.2 - 16.2 \log \theta$ | dB | $10^\circ \leq \theta \leq 48^\circ$ |
| | $G = -10$ | dB | $\theta > 48^\circ$ |

where G is the gain of any peak sidelobe

Figure 1.1 illustrates the relationship of these envelopes to the current FCC requirement ($32 - 25 \log \theta$). Proposed envelopes (1) and (3) are the FCC envelopes reduced by 3dB and 6dB respectively. Proposed envelopes (2) and (4) are more relaxed versions of proposed envelopes (1) and (3). In each case the region from 10° to 48° tends toward the current FCC envelope. This relaxation from the more stringent envelopes should be useful for Cassegrainian antenna system where the feed spillover is within this region.

Antennas of different physical sizes are generally manufactured using different methods. They generally fall into four broad categories and are usually referred to as such in the report. Antennas below about 18' (5m) are small enough

so that they can be easily made using a spinning process. These antennas are called small antennas. Antennas below about 5' (1.5m) has become so small that the support structure and mounting arrangement can be different from say a 15' (4.5m) antenna. These are referred to as very small antennas. Antenna from 5m to 12m in diameter are too large to be manufactured by the spinning process. They are usually assembled from a few identical panels on a back-structure. These are known as large antennas in this report. Antennas more than 25m in diameter (e.g. Intelsat type A antennas) are referred to as very large antennas. Back structure design and assembly for such very large antennas are quite different from those of large antennas.

These categories are chosen because in most cases it is the physical size of the antenna that determines the antenna configuration and support details rather than the size in wavelengths. An example is the Andrew 8m and 10m antenna operating at 12/14 and 4/6 respectively. Although electrically the 8m is almost the equivalent a very large antenna at 4/6 the design details and mechanical problems are not the same as an Intelsat type A antenna. Instead the design problems are very similar to that of the 10m antenna. Naturally the size in wavelength is often important so that reference is also made to antennas in terms of wavelengths where this is more useful. In such cases the usual dividing line is 100 wavelengths.

2.0 Antenna Radiation Pattern Envelope

Antenna sidelobe characteristics are usually studied by use of the radiation patterns. However radiation patterns differ from each other at each frequency. It is therefore necessary to generate a means of representing the sidelobe characteristics of an antenna throughout its specific frequency band. The Radiation Pattern Envelope (RPE) is widely used to provide a very convenient and efficient way of representing the radiation performance of an antenna.

This section of the report describes the different regulations and rules used by different administrations in North America and compares them by using antennas with diameter greater and less than 100 wavelengths at 12/14 GHz and 4/6 GHz band.

2.1 Antenna Pattern Measurements

Before going into the description of the different rules and regulations for RPE generation, it may be useful to briefly describe how the radiation patterns are typically measured and define some of the terms used.

The antenna under test is usually measured as a receive antenna. A standard transmit antenna is placed so that it is in the far field for the receive antenna. For each frequency band, measurements are generally taken at three different frequencies; the two band edges and the mid band frequency.

The receive antenna is placed on a rotating table which allows, the antenna to be rotated horizontally from -180° to 180° with 0° when the boresights of the two antennas are aligned.

In order to obtain better resolution of the radiation pattern near boresight, recording charts having three different angular scales (typically -5° to 5° , -30° to 30° and -180° to 180°) are used (Figure 2.1(a), 2.1(c)).

After checking the alignment of the transmit and receive antennas, the gain of the receiver is adjusted so that the reading is 0dB at the pattern peak. The range of the recorder and the rotator are set to be 5° . The receive antenna is then rotated from -5° to 5° . Quite often some sidelobe levels would drop by more than the recording chart would allow. If this happens, measurements in this region would be done in two stages. Only the main beam and its adjacent sidelobes that are within the chart's range are recorded first. The receiver sensitivity is then boosted so that the maximum of rest of the sidelobe peaks (in the $\pm 5^\circ$ region) are within 10dB of the top of the chart. These are recorded on the same chart.

Advancing to a new chart, the sensitivity of the receiver is increased to bring the maximum peak in the 5° to 30° region within 10dB of the top of the recording chart.

Generally a 20 to 30dB boost is required. The range of the recorder and the rotor are set to be 30° . The antenna is then rotated from -30° to 30° . After recording, the chart paper is advanced. The sensitivity of the receiver is boosted as required (generally by another 10dB) and the range of the recorder and the rotor are set to be 180° . The antenna is then rotated from -180° to 180° .

Depending on whether the receiving antenna is linear polarized or circular polarized, different orientations of the receive and transmit antenna are used while measurements are being taken.

2.1.1 Linear Polarized Antenna

If the antenna under test is linear polarized, four sets of patterns are measured at each frequency; E plane, H plane, E cross and H cross.

The E plane patterns are taken with the E fields of both the receive and transmit antennas in horizontal positions.

The H plane patterns are taken with the E fields of both the receive and transmit antennas in vertical positions.

The E cross patterns are taken with the E field of the transmit antenna in vertical position while the E field of the receive antenna is in horizontal position.

The H cross patterns are taken with the E field of the transmit antenna in horizontal position while the E field of the receive antenna is in vertical position. The cross patterns are taken by first aligning the receive antenna with the transmit antenna. The signal level is recorded. The transmit antenna is then rotated by 90° so that the electric fields are crossed. Final alignment is made by adjusting the transmit antenna until the signal level is a minimum.

2.1.2 Circular Polarized Antenna

For a circular polarized antenna, a simplified procedure can usually be used during the development of an antenna. A linearly polarized transmit antenna with very good beam symmetry is used since most test ranges are already equipped with such antennas. Usually two sets of patterns are taken at each frequency. The two antennas are first aligned. Without turning the receive antenna, the recorder pen is dropped while the E field of the transmit antenna is rotated by 360° . This records, at boresight, the axial ratio of the receive antenna.

The E field of the transmit antenna is rotated again until maximum signal is received. The orientations of the transmit and receive antenna including the feeds are recorded. The receiver sensitivity is adjusted so that the signal level is 0dB at boresight. One set of patterns is taken. After returning the receive antenna to 0° , the E field of the transmit antenna is rotated until minimum signal is received.

The orientations of the antennas and their feeds are again recorded. Without readjusting the receiver sensitivity, a second set of patterns is taken by superimposing on the first set. If it is required, more patterns will be taken by superimposing them on the same charts. In this case, the orientations of the receive and/or the transmit antenna are varied. The former provides the radiation pattern of the receive antenna along cuts on other axes. Rotation of the transmit antenna about different planes provide further information about the received antenna axial ratio. As long as enough transmit antenna orientations are used the complete axial ratio performance of the antenna is obtained.

In the above method when only two patterns are used complete axial ratio information is not provided at angles other than $\theta=0^\circ$ (boresight). A second method called the rotating dipole method will indicate both the axial ratios and sidelobe levels on one set of patterns for all angles. The two antennas are first aligned and the maximum signal level is adjusted to be 0dB at boresight as before. This time patterns are taken while the transmit antenna is being rotated rapidly. Different cuts of the received antenna taken with this method can be used to plot the circularly polarized RPE.

If a circularly polarized source of good circularity is available the patterns can be taken using such a source. This simplifies the measurement procedure. Radiation patterns for cross polar field can be obtained if the transmit antenna is also circular polarized but with opposite sense to that of the receive antenna. Radiation patterns close to the theoretical ones can be measured if the polarization of the transmit antenna is perfectly circular. Practical antennas will usually lead to some error.

2.2 Methods of Generating RPE's

There are many different methods used by various antenna manufacturing industries and other administrations. Given below are four types of methods which are more commonly used.

2.2.1 Peak Pattern Envelope

This is a curve that encloses all sidelobe peaks in the $-180^\circ < \theta$ and $\theta > 180^\circ$ region. By using the peak of the antenna as a reference (0dB), all radiation patterns are aligned and superimposed on top of each other. A curve is drawn so that it encloses all the sidelobe peaks in the $-180^\circ < \theta < 0^\circ$ region. Another curve is drawn so that it encloses all the sidelobe peaks in the $0^\circ < \theta < 180^\circ$ region. When drawing these curves, straight-line approximation method is to be used as much as possible. These two curves are then folded along the centre ($\theta = 0^\circ$). A third curve (the pattern envelope) is drawn so that it encloses the two folded curves. This third curve is then plotted on the pattern envelope chart using the Y-axis as the antenna directivity and the X-axis as the azimuth degrees from main beam. This method is commonly used by antenna industry for microwave antennas used in point-to-point communications.

2.2.2 CCIR Envelopes

Complete details of these rules and regulations are described in the CCIR "Report 391-3" (2) and "Recommendations 465-1" (1). Only a brief description of the rules is given in this section.

The CCIR rules are based on the assumption that it is appropriate to use a radiation pattern based on the level exceeded by a small percentage of the sidelobe peaks for the determination of co-ordination distance and for the assessment of interference between earth and terrestrial stations.

The peak sidelobes levels for all the patterns of the same frequency band are first converted to isotropic level and then recorded together with the associated angles. The data on the negative side ($\theta < 0^\circ$) is combined with data on the positive side ($\theta > 0^\circ$).

The azimuth angular range is divided into several sections (called windows) of various width (Figure 2.2). Within each window, the isotropic level exceeded by 10% of the sidelobe peaks is calculated. This level is then plotted at the middle of each window on the RPE chart. The performance of the antenna is considered to be acceptable if its RPE is below the reference radiation pattern defined by:

$$G = 32 - 25 \log \theta \quad \text{dBi} \quad 1^\circ < \theta \leq 48^\circ$$

$$G = -10 \text{ dBi} \quad \theta > 48^\circ$$

where θ = angle between axis of main beam and direction in question (degrees). G is the gain relative to isotropic antenna.

2.2.3 Intelsat Envelope

There are essentially three different types of standards used by Intelsat to generate RPE. Basically all three standards follow the CCIR rules and regulations. As an example, under the rules and regulations of "Standard C", the RPE is to be generated exactly in the same manner as the CCIR rules with the exception that there is only one window which covers $1^\circ < |\theta| < 180^\circ$. Details of these rules and regulations can be found under the INTELSAT "Performance characteristics of earth stations in the Intelsat V system" (3).

In practice measurements are made on site using an operating antenna. Measurements are only made within $\pm 3^\circ$ of the geostationary arc using the satellite as a source. All the peaks and nulls across the arc are recorded (measurement discontinued when the system noise became significant). A computer program is then used to calculate the number of peaks above reference radiation envelope as defined by

$$G = 32 - 25 \log \theta \quad \text{dBi} \quad 1^\circ < \theta \leq 48^\circ$$

$$G = -10 \text{ dBi} \quad \theta > 48^\circ$$

where G and θ are defined the same way as in 2.2.2.

The performance of the antenna is considered acceptable if no more than 10% of the total peaks exceeds the reference radiation envelope.

2.2.4 FCC Envelope

The FCC rules and regulations for generating RPE resemble the CCIR rules for pattern envelope generation with the exception that averaging is allowed where the peaks exceed the reference radiation envelope. The peak gain of an individual sidelobe may be reduced by averaging its peak level with the peaks of the nearest sidelobes on either side, or with the peaks of two nearest sidelobes on either side, provided that the level of no individual sidelobe exceeds the reference radiation envelope defined in 2.2.2 by more than 6dB.

Details of the rules and regulations can be found in the FCC "Rules and regulations" section 25.209 (4).

2.3 RPE's for Selected Antennas

RPE's of three antennas, two with diameter to wavelength ratio (D/λ) greater than 100 and one with diameter to wavelength ratio less than 100, were analysed in order to study the difference between the CCIR and FCC rules and regulations for RPE generation.

The first antenna is the Andrew original 10 meter ESA. The antenna is designed to operate in the 4/6GHz band and uses a Gregorian Subreflector. D/λ ratio is 132 at 3.95 GHz.

This original 10m antenna was not designed to meet the FCC specification. The gain was optimized without a serious attempt to control the feed spillover. Feed spillover effects are clearly visible in the RPE included. This design has since been superceded by the current 10m antenna which uses an improved feed and subreflector as described in Section 4. The RPE's are included since the effects of sidelobe improvement techniques used in the current 10m design is well illustrated by comparing the RPE for the original design with the RPE for the current design given in Section 4.

The second antenna is a 8 metre Gregorian type ESA. This antenna is designed to operate in the 12/14 GHz band. D/λ ratio is 319 at 11.95 GHz. It is an example of a state-of-the-art high performance ESA design. It is referred to as the Andrew 8M antenna throughout the text of this report.

The third antenna is a 15 feet ESA. It is designed to operate as a TVRO antenna in the 4/6 GHz band. D/λ ratio is 60 at 3.95 GHz.

2.3.1 CCIR Envelopes for the selected Antennas

A computer program was developed to calculate the 10% level within each window. The program essentially follows the CCIR rules and regulations as indicated in their "Report 391-3" (1). A brief description of the algorithm used in the program is given in the following paragraphs.

Input to the computer.

The major input to the computer is a file (stored on disk) containing pairs of data which were generated by a digitizer. Each pair of data consists of the angle and the amplitude corresponding to each peak in the radiation pattern.

Program Logic

When the pairs of data are read, the corresponding antenna gains are added to bring all levels to isotropic.

The angle range (-180° to 180°) is divided symmetrically (with respect to 0°) into sections of various width (windows). A histogram consists of 33 classes is constructed for each window. The class frequency is the total number of input data (with angles belong to that particular window) that has amplitude value between the class limit. For each histogram, the 1st decile, median and 9th decile (10% level) are computed by computing the points which divide the area under the histogram into ratios of 1:9, 1:1 and 9:1 respectively. The maximum amplitude, minimum amplitude, average amplitude and average power are also computed.

Output of the program

The program will process one set of data (one pattern) at a time. The program will store the histogram if it is the first set of data. It will accumulate the previously stored histogram data to the newly generated data and uses this accumulated data to compute the statistical results. The program will also generate a printout of all the window boundaries and the corresponding statistical results.

The program can also superimpose the class frequencies on the negative side ($-180^{\circ} < \theta < 0^{\circ}$) of the radiation pattern on the positive side ($0^{\circ} < \theta < 180^{\circ}$). Computation will then be done by using this combined histogram. In other words, the radiation pattern is folded at the centre ($\theta = 0^{\circ}$) and computation is done on this folded pattern.

The program also provides the option of using the value $32-25\log|\theta|$ (θ is the angle of each input data pair) as an amplitude reference level.

Radiation Pattern Envelope (CCIR)

The radiation patterns of the three selected antennas were analysed by the computer. Results were plotted (Figure 2.3 to 2.18). The following symbols are used in plotting the results.

- maximum
 - ▲ 9th decile (10% level)
 - median
 - ▼ 1st decile
 - minimum
- X,Y X = total number of data within the window.
 Y = total number of data exceeds the value $32-25\log\theta$

Two types of window boundaries and widths are used:

θ , angle between axis of
main beam and direction
in question (degrees)

Type A

Type B

| | |
|-------|-------|
| 0 | 0 |
| .2 | .2 |
| .4 | .4 |
| .7 | .6 |
| | .8 |
| 1.0 | 1.0 |
| 2.0 | 2.0 |
| 4.0 | 4.0 |
| 7.0 | 6.0 |
| | 8.0 |
| 10.0 | 10.0 |
| | 12.0 |
| | 14.0 |
| | 16.0 |
| | 18.0 |
| 20.0 | 20.0 |
| | 30.0 |
| 40.0 | 40.0 |
| | 50.0 |
| | 60.0 |
| 70.0 | 70.0 |
| | 80.0 |
| | 90.0 |
| 100.0 | 100.0 |
| | 120.0 |
| | 140.0 |
| | 160.0 |
| 180.0 | 180.0 |

Except for figure 2.3, all computations were done by using the
combined (folded) histogram data.

| Figure | Antenna Type | Pattern Type | | Window Type |
|--------|--------------|----------------|--------------|-------------|
| | | Frequency | Polarization | |
| | | (GHz) | | |
| 2.3 | Original 10m | 3.7,3.9,4.2 | E & H | A |
| 2.4 | Original 10m | 3.7,3.9,4.2 | E & H | A |
| 2.5 | Original 10m | 3.7,3.9,4.2 | E & H | A** |
| 2.6 | Original 10m | 3.7,3.9,4.2 | E & H | B |
| 2.7 | 8m | 11.7,11.9,12.2 | E & H | A |
| | | 14.0,14.2,14.5 | | |
| 2.8 | 8m | 11.7,11.9,12.2 | E & H | B |
| | | 14.0,14.2,14.5 | | |
| 2.9 | 8m | 11.7,12.2 | E & H | A |
| 2.10 | 8m | 11.7,12.2 | E & H | B |
| 2.11 | 8m | 14.0,14.5 | E & H | A |
| 2.12 | 8m | 14.0,14.5 | E & H | B |
| 2.13 | 8m | 11.7,11.9,12.2 | E & H | A |
| 2.14 | 8m | 11.7,11.9,12.2 | E & H | B |
| 2.15 | 8m | 14.0,14.2,14.5 | E & H | A |
| 2.16 | 8m | 14.0,14.2,14.5 | E & H | B |
| 2.17 | 15 | 3.7,3.9,4.2 | E & H | A |
| 2.18 | 15 | 3.7,3.9,4.2 | E & H | B |

** $32-25\log\theta$ (θ = corresponding angle to each peak) is subtracted from the input data. The level $32-25\log\theta$ is used as the reference level.

TABLE 2.1 Summary of the types of antenna, frequencies, polarization and window boundary types.

Table 2.1 gives a summary of the types of antenna, frequencies, polarizations and window boundary types for each figure. All statistical results were plotted at the mid point of each window. Also plotted in the figures are the curve $32-25\log\theta$ (solid line) and the curve $29-25\log\theta$ (dotted line).

A relative level method using the value $32-25\log\theta$ as the reference level was also developed. The value $32-25\log\theta$ was subtracted from all amplitude values before they were statistically analysed by the program. Results of the program's output were plotted in Figure 2.5. Section 2.4.1.5 discuss the method in more detail.

The effects of reducing window sizes were also studied. Different window sizes do have a different weighting on the statistical results. Using a smaller window size (Type B) will track the radiation pattern more precisely. However, the window size of type A is found to be adequate.

Using the 9th decile (10% level) points as a guide, it is quite obvious that the equation $32-25\log\theta$ ($\theta < 48^\circ$) fits those points better than the equation $29-25\log\theta$ for the 10th antenna. The opposite is true for the 8M antenna. It is understandable that the recently developed 8M antenna (1979) has a better performance than the 10M antenna which was developed in 1975.

For the 15' antenna, the equation $32-25\log\theta$ fits the 9th decile points better than the equation for $0 < 1.5^\circ$. For $0 > 1.5^\circ$ the latter equation is a better one.

A study on the difference in levels between the cross and parallel polarized radiation patterns shows that at boresight the two levels differ by 33 to 47dB. This difference in levels gradually decreases as the azimuth angle becomes larger. At around 180° the difference are about 3-10dB. The following table shows the difference in level of the three antennas being studied.

Difference in levels (dB)

| Antenna Type | Original | | | |
|-----------------|-----------|---------|---------|---------|
| | 8M | 10M | 15' | |
| Freq.Range(GHz) | 11.7-12.2 | 14-14.5 | 3.7-4.2 | 3.7-4.2 |
| Azimuth Angle | | | | |
| 0 | 45 | 47 | 42 | 33 |
| .5 | 35 | 27 | 28 | 34 |
| 1 | 18 | 23 | 29 | 27 |
| 3 | 20 | 22 | 21 | 18 |
| 5 | 18 | 6 | 18 | 18 |
| 6.12 | 14 | 13 | 13 | 12 |
| 12-18 | 10 | 8 | 13 | 11 |
| 18-24 | 8 | 8 | 8 | 7 |
| 24-72 | 8 | 8 | 8 | 7 |
| 72-180 | 8 | 8 | 4 | 7 |

The cross polarized radiation pattern envelope can be generated by lowering the parallel polarized radiation pattern envelop the corresponding amount as shown in the above table. In analysing the cross polarized patterns, the level $4-15\log\theta$ dBi ($.2^\circ < \theta < 18.48^\circ$) -15 dBi ($\theta > 18.48^\circ$) seems to represent a reasonable envelope for the 8m ESA and 15' ESA. The cross polarized envelope of the original 10m ESA is found to be best represented by:

$$G = 8-10\log\theta \text{ dBi } (.2^\circ < \theta < 15.8^\circ)$$

$$G = 20-20\log\theta \text{ dBi } (15.8^\circ < \theta < 56.2^\circ)$$

$$G = -15 \text{ dBi } (\theta = 56.2^\circ)$$

2.3.2 FCC Envelopes for the Selected Antennas

The FCC envelopes of the three antennas are shown in Figure 2.19-2.21. It can be seen from Figure 2.19 that the FCC envelope for the original 10m ESA is below the reference RPE except for $30^{\circ} < \theta < 60^{\circ}$. As for the 8m ESA, the FCC envelopes are below the reference RPE at both frequency bands. The FCC rules and regulations also reveal the fact that the more recently developed 8m ESA has a better performance than the original 10m ESA. The RPE for the 15' ESA is below the reference RPE except in the $80^{\circ} < \theta < 115^{\circ}$ region.

2.4 Discussion and Comments on RPE Generation Methods

The Sub-Sections above have described the methods of pattern measurement and RPE generation and also have provided some RPE data to serve as the basis for this review on the subject. Most of the discussion would be confined to the CCIR method.

2.4.1 The CCIR Method

There are many references to antenna patterns within the text of the various current CCIR documents. However the reference pattern envelope for earth station antennas is determined only by Recommendation 465-1 (1). This recommendation defines the provisional $32-25\log\theta$ envelope (See Figure 1.1). and states that it will be applied only beyond 1° to antennas larger than $100 D/\lambda$. It is important to recognize that the purpose of Recommendation 465-1 was to define a general typical antenna pattern to be used for co-ordination purposes, only when the real pattern of the specific antenna was not known. For this purpose the data came from calculated patterns averaged for several antenna types, none of which fell wholly below the $32-25\log\theta$ curve. Recommendation 465-1 refers to CCIR Study Group 4 Report 391-3 (2) from which the envelope is derived, and the material in Report 391-3 must be taken as the accepted CCIR method of presentation of pattern data.

The concept behind the method is good since it enables much essential data to be presented in a form that is visually easy to interpret. At the same time it is also simple to add the results presented to a data-base for further computer analysis.

However the method can be improved. There are many ambiguities and defects which should be clarified and corrected. Report 391-3 does not recommend or describe any particular method of data presentation. Instead it gives examples of sidelobe data and the presentation in these examples is generally taken as the current CCIR preferred method of presentation.

Some of the details that Report 391-3 is ambiguous about are:-

- a) Number and type of patterns to be used to obtain the samples.
- b) Window sizes to be used.
- c) How the worst 10%, median and best 10% values are derived. And also how to treat small samples.
- d) Judgement of pattern compliance

2.4.1.1 Patterns used in Data Base

The entire CCIR method of presentation depends on the analysis of samples within specified window areas. This means the number of samples used and how they are derived are important. Results with too few samples may present a misleading picture of the antenna. However Report 391-3 does not specify the number of patterns or the kind of patterns that must or can be used. Generally an antenna is specified by patterns at the band edges and mid-band frequency band for both E and H plane. (0° and 90° for circular polarization). This gives a minimum of 12 sets of data (the left and right side each contribute one set) from which the sample can be taken.

For antennas close to $100 D/\lambda$ this may not represent sufficient sample points for the intervals from 1° - 10° . In that case other patterns for the antenna might be considered. For many ESA applications patterns are taken at each assigned channel frequency instead of the usual three frequencies referred to above. These patterns can be used to increase the number of samples available.

In view of different pattern that can be used some consideration should be given to a standard method for selecting patterns to be used. It would be useful to require that each RPE should also note the number of patterns used. Any patterns that do not conform to conventional practice (such as measurement of the pattern out to 20° only) should also be indicated.

2.4.1.2 Window Intervals

Window interval type A of this report follows the CCIR example while window type B divides the pattern further to test the effect of window sizes. Type A window size seem to be adequate. However for larger antenna and where many samples are available a finer window interval such as type B may give a better picture. It should be noted that the data used to obtain the $32-25\log\theta$ curve itself is plotted using 1° windows. Window sizes become less important if the relative level method (See Section 2.4.1.4) of data presentation is used.

2.4.1.3 Distribution of Sidelobe Peaks

The derivation of the distribution of peaks will affect the specification compliance of a particular antenna which is being judged against a specification permitting averaging. The CCIR-based curve $32-25 \log \theta$ is frequently used in this way. Recommendation 465 is based on permitting "a small percentage of excess peaks", as indicated in Considerings (b). This applies to the main body of the antenna pattern beyond the first few sidelobes. Near the main lobe, Considerings (c) suggests only the peak envelope. The statistical approach to the main body of the pattern is justified because this is the region which affects interference with terrestrial stations. That type of interference is normally scattered over many stations, has a cumulative effect in the noise performance of the terrestrial system and is usually subject to some type of statistical propagation factor. On the other hand, interference with other space stations is more predictable and has no statistical base. For this reason, peak envelope has some validity immediately adjacent to the main lobe.

Report 391-3 is the definitive document for the curve $32-25 \log \theta$. It defines 10% as the "small percentage of excess peaks" permitted in Recommendation 465-1. It also calls for measured data on actual antennas to be presented as shown in Figure 6 of that Report. This calls for a plot in the center of each window of the worst 10% of peaks, together with maximum, median, best 10% and minimum values.

Section 2.3.1 describe the approach used in this report to obtain the data presented in Figures 2.3 to 2.18. The medium, worst 10% and best 10% values are defined to be essentially the same as that normally used for class distribution analysis. An alternative method would be to find the number of peaks that represent 10% (or just less than 10%) of the peaks. The value of the peak just outside this 10% range is then designated as the worst 10% case value.

Both approaches give approximately the same results when the sample size is large. However a significant difference between them can exist when the sample sizes are small. Section 2.1 of Report 391-3 notes the problem caused by the small sample population below 1°.

Another example of the treatment of small samples is that of Intelsat in their submission to Draft Report 391-3 (MOD1) (5). It stated that all data with less than 10 peaks are treated as a case where the 10% value is equal to the maximum. This in effect means no averaging is allowed if the data contains less than 10 peaks. Since a stray peak may be 3 to 10dB above the next highest peak a considerable difference in RPE can exist for the same antenna when the sample size is 9 and when the sample size is 10. There is of course nothing at present to stop anyone faced with the above situation from adding another pattern to the data base to bring the sample size above 10. The use of the class frequency method would tend to smooth out such abrupt transitions*. The CCIR method of presentation makes it axiomatic that the sample size must be appreciably greater than 10 in order to utilize the statistics upon which their report is based. The problem of small sample size is one that needs further consideration.

*Abrupt transitions can also occur in certain cases with the class frequency method.

2.4.1.4 Judgement of Curve Compliance by CCIR Method

The CCIR method of plotting pattern data against the curve gives a distorted picture of the merit of an antenna with regard to the 10% rule. The CCIR practice is to plot, in the middle of the window, the actual dBi values of the maximum, worst 10% etc. Figure 2.22 (a) shows the theoretical case of an antenna that has nearly all peaks touching the CCIR curve. Since many antennas do have peak envelopes that closely follow the slope of the CCIR curve, this is not an unusual case. Note that the median lies on the CCIR curve while the maximum and worst 10% values lie well above the curve. Although this antenna pattern meets the CCIR perfectly for all the peaks yet the CCIR plot shows the false result that even the worst 10% value fails the standard by 3dB. On the other hand Figure 2.22(b) shows an antenna pattern which actually fails to meet the standard by a big margin but which appears to be acceptable when plotted by the CCIR method. This is the case for an antenna where all the sidelobes are approximately the same for the window considered. Curves of this kind can occur when spillover energy is superimposed on the intrinsic antenna pattern. It is not possible to deduce from the distribution that a full 50% of the peaks exceed the CCIR curve.

The situation described above has come about because the windows chosen cover a significant portion of a pattern. The CCIR curve was originally obtained using data calculated from a 1° window. For such a narrow window the amplitude change of the CCIR curve is very small. However, such a small window was only possible because data was sampled from many different antennas. For assessing a single antenna, much wider windows are necessary. CCIR Report 393 shows sampling windows where the difference between the start and end of the window can be as much as 7.5 dB. This is why peaks below the curve at the start of the window can show up as a maximum that is apparently well above the curve.

This situation shows up for almost all the RPE's given in Section 2.2. An example is Figure 2.9, for the 0.2° to 4° region the distribution shows that both the peak and worst 10% value is above the CCIR curve. The distribution data given shows that there were 12 samples none of which was above the CCIR curve. The distributions given by Intelesat in their submission (5) also illustrates the point. The distribution for the B standard antennas (Figure 4 in their report) shows that all maximum and 10% points are either above or on the CCIR curve. Yet according to their compliance data (Figure 5 of their report) only 4 out of 64 antenna fail to comply with the CCIR curve.

2.4.1.5 The Relative Level Method

Although the problem is too wide a window size, the solution does not lie in reducing the window size. The window must always be large enough to give a reasonable number of sample points. If size is reduced there will no longer be enough samples to give a meanful results for antennas close to 100 D_h. The best solution is to use the level relative to the CCIR curve instead of the dBi value for each sample point (See Section 2.3.1) This means that the distribution data obtained is that relative to the CCIR curve. Using this method would mean that if a peak or worst 10% point is plotted above the curve it shows non-compliance with either the peak or 10% rule.*

*After the completion of this report the author's attention have been drawn to CCIR DOC 4/269-E where a similar method was proposed.

Judgement of compliance now becomes very simple and unambiguous. Figure 2.22(c) and 2.22(d) shows the distribution of Figure 2.22(a) and 2.22(b) replotted for this method. This shows the difference between the dBi method and the relative level method. Figure 2.23 is a RPE plotted using the relative level method. It can be compared directly with Figure 2.4 which is plotted from the same data using the dBi level method. It can be seen that the distribution spread is generally less for the relative level method. Also the distribution for the 2° to 4° window shows the peak level below CCIR curve while that for Figure 2.4 shows it more than 2dB above the curve.

2.4.2 Definition of a Pattern Peak

No problem exist where a pattern have pronounced peaks and nulls. However in many regions of the pattern the nulls and peaks may be replaced by ripples or shoulders. Such regions usually occur where there is feed or subreflector spillover or where blockage effects are strong. Since the existance of a peak is important in all method of averaging, a means must be devised to treat such cases. One generally acceptable method is to define a null (and hence peaks) by specifying that the amplitude must drop by at least a certain amount (usually 1dB).

Even this method can sometimes lead to the acceptance of "broad" peaks which contain much more energy than that of a equivalent normal size peak. Since both the FCC and CCIR method of averaging assumes that peaks are of the same relative width, "broad" peaks can lead to errors. One way to avoid this is to assume the peaks are present even if they are not. As an example if there is a "broad" peak that extend over a 10° region where normally peaks extend over 1° then the

"broad" peak is divided into 10 regions and each region is treated as a peak. This will ensure that all peaks used in data calculation have the same relative weight. This method may however be difficult to implement for actual patterns since the "normal" peak spacing is sometimes a matter of subjective judgement.

3.0 Antenna Sidelobe Performance

Introduction

Factors effecting antenna sidelobes

With the notable exception of the torus antenna most of the earth station antennas currently in use have a circular radiating aperture. The discussions that follow would therefore be limited to such antennas. Any radiating aperture has an intrinsic sidelobe pattern which depends solely on the amplitude distribution across the aperture. This is why the aperture distribution control is perhaps the single most important part of any modern antenna design. Section 3.1 sets out briefly the control techniques available while Section 3.2 shows how antenna performance is affected by different aperture distributions. Throughout this section cross-polarization performance of an antenna is considered where appropriate. However the general problems specifically associated with cross-polarization fields are briefly described in Section 3.3.

The actual measured antenna pattern is never identical to the intrinsic pattern. Departures of an antenna sidelobe pattern from the ideal are caused by many factors. One major effect is that of aperture blockage by support struts and subreflectors. Section 3.4 discusses this effect.

Diffraction and Scattering effects are discussed in Section 3.5. The contribution of the five major causes of reflector aberrations to sidelobe degradation is considered in Section 3.6. Feed design and the effects of main and subreflector spillover on sidelobe performance are detailed in Section 3.7. Finally environmental effects such as temperature, and gravitational distortion are treated in Section 3.8.

3.1 Control of Aperture Distribution

For an ideal antenna the radiation pattern envelope depends solely on the amplitude and phase distribution at the aperture. In practice this ideal or intrinsic pattern is modified by factors such as blockage, struts, feed and subreflector spillover, reflector errors and environmental effects which are all considered in many of the sections that follow. Since these factors generally serve only to degrade the pattern it is important to start with an intrinsic pattern that is better than the radiation envelope required. To achieve this it becomes necessary to understand the factors affecting aperture distribution and the control techniques available. Section 3.1.1 gives a brief review of main antenna configurations used in ESA designs together with factors affecting aperture distribution for each. Methods of reflector shaping which is the most important aperture control technique available in modern antenna design is described in Section 3.1.2.

3.1.1 Antenna Configurations

Figures 3.1.1 (a) to (f) show the six main antenna configurations that have been used in ESA designs. Figure 3.1.1(a) shows the prime-focus paraboloid which is the most simple reflector antenna configurations available. The feed is placed at the paraboloid focus so that a uniform phase

distribution appears at the aperture. This is true as long as the feed has a distinct phase centre so that it radiates a spherical wave. Aperture distribution corresponds directly to the feed distribution with the addition of a parabolic space attenuation term.

Figure 3.1.2 (a) and (b) give a curve of the parabolic space attenuation and illustrates how it can be used to calculate the aperture amplitude distribution. The F/D ratio given represent that of dish with the corresponding maximum angle. Thus in the example for the aperture point which subtends a half angle of 72° at the focus the feed pattern shows a taper of -10dB. The additional space attenuation is given by the curve as -3.6dB. This means that the aperture distribution is -13.6dB down from the axial point. Energy from the feed going past the paraboloid becomes spillover energy and appears as such in the antenna far field patterns. Prime focus systems can therefore be controlled only by varying either the reflector F/D or by changing the feed pattern.

Figure 3.1.1 (b) shows a dual-reflector system which is at present the most popular system for ESA designs. This system uses a paraboloid and a subreflector which can be convex (Cassegrainian system) or concave (Gregorian system).

The dual-reflector system generally used is a shaped system. Shaping is usually used to increase the efficiency of the system (>70% with up to 95% claimed for some Intelsat type A designs). The aperture distribution is generally shaped to be nearly uniform with a sharp edge taper. The near uniform illumination produces high gain while the edge taper serves to reduce spillover of the feed past the main reflector. Such a distribution can meet the FCC specification provided care is taken to keep the spillover past the main and subreflector low. Subreflector spillover (from 15° to 40° typical) can affect the near-in sidelobes. In addition, blockage by the struts (Section 3.4.1.1) and subreflector contribute to degradation of the near-in sidelobe.

To produce patterns that can meet the proposed envelopes, aperture distribution would have to be shaped to produce low sidelobe. This shaping may mean a reduction in efficiency so that they become comparable to those for the prime focus system. Gaussian type distributions, with -20dB edge tapers, can produce sidelobe levels below -38dB for the first and second sidelobes. However for the small antennas ($<4.5\text{m}$) the aperture blockage tends to negate most of the sidelobe improvement.

Figure 3.1.1 (c) shows one method of implementing a near field Cassegrainian system. This configuration is used in the proposed new 8 to 12m antenna and is described fully in Section 5.1.1. Aperture control is the same as that for the dual-reflector system described above. Subreflector spillover of the type described for the dual-reflector system is absent since any spillover is almost along the reflector boresight axis. Because of their circular symmetry, the reflectors for all three paraboloid systems reviewed here contribute very little cross-polarization energy ($<-45\text{ dB}$). Most of the cross-polarization energy present in the systems are from the feed.

Figures 3.1.1(d) to (e) show offset systems where the feed is no longer on the reflector axis. These systems are described in Section 5.1.2 and 5.1.3. The Horn Reflector (Figure 3.1.1 (e) and the single reflector offset antenna (Figure 3.1.1 (d) are equivalent to the prime-focus paraboloid in that no subreflector shaping is possible. For the horn reflector scattering from the reflector edges can be a serious problem. Control techniques used include absorber linings and special edge-geometry blinders.

The single reflector offset antenna is an attractive system for very small antennas ($<2\text{m}$ in diameter) where they can be made out of a single or two-piece stamping. The main problem for such antennas is the relatively high cross-polarization levels encountered.

The recent interest in offset parabolic reflectors centers on the use of shaping techniques, to improve the illumination and cross-polarization discrimination. A typical shaped offset parabolic reflector can now achieve a cross-polarization discrimination of better than -30 dB compared with $>-25\text{ dB}$ for an offset reflector fed with a horn. Sidelobes can be below -25 to -30 dB with an aperture efficiency of about 70%.

The main advantage of the offset designs is the improvement in sidelobes that comes from a clean and unblocked aperture. The offset configuration also removes some of the limitations on feed and subreflector sizes inherent in small dual-reflector paraboloid. The problem of high feeder spillovers still remains. The spillover is however no longer symmetrical about the boresight axis. Much of that spillover may not be on the principal planes and so sometimes becomes "hidden". It should also be noted that offset reflectors have much greater manufacturing cost.

3.1.2 Shaping Techniques

Nearly all the large dual-reflector antennas are now designed using a reflector shaping technique. The concept of controlling aperture phase and amplitude distribution by shaping the reflector profiles has become a major tool in antenna design.

Antenna reflector shaping was first proposed by Green (6) and Galindo (7) in 1963. Since the manuscripts were submitted within a month of each other (February and March respectively) they should probably receive joint credit, for the concept. However Dunbars work on doubly curved radar antennas (8) in 1949 is perhaps the first recorded instance of reflector shaping in microwave antennas. Williams (9), whose paper in 1965 is perhaps the most widely cited, was the first to present experimental results of a shaped reflector.

The technique provides control of the aperture amplitude and phase distribution by shaping the profiles of the main and subreflector of an antenna. Many of the published work on shaping concentrate on shaping to produce a uniform illumination for large antennas. However to produce the low sidelobes required by proposed envelopes (1) to (4) it is necessary to taper the illumination. Appendix A presents a generalized treatment of shaping which can be used to obtain any specified aperture distribution. It should also be noted that small shaped systems cannot simply be scaled down versions of larger shaped antennas. Thus the design considerations for a small shaped Cassegrains (<5m in diameter) differs in many respects from that for a large shaped antenna such as the Andrew 8m antenna.

An improvement on ray-optics shaping is the shaping techniques based on physical optics or spherical modes. Such techniques have been described by Wood (10), Rusch (11) as well as Elliot and Poulton (12). They allow the designer to optimize a system based on physical optics and can be used to optimize additional antenna parameters such as VSWR and feed spillover.

The importance of these shaping techniques lies in the fact that they give an antenna designer control over the aperture distributions. It becomes possible, by studying how different aperture distributions affect the sidelobe levels and gain, to choose an optimum distribution for a particular application.

3.2 Effect of Aperture Distribution on Sidelobes

To design antennas for low sidelobe performance requires a study of the intrinsic behaviour of a circular radiating aperture. Far field behaviour of a radiating aperture can generally be predicted from theory. A Kirchhoff-Huygens integration of the aperture field can be used to predict the far field. Alternatively physical optics (or diffraction theory) can also be used. This has the advantage that it allows feed or subreflector spillover fields to be taken into account.

Many authors (13) (14) (15) (16) have studied the way aperture distributions can be used to produce low sidelobes with a minimum loss of gain. The ideal antenna pattern is one with a main beam and no sidelobes. This can be obtained by the use of a Gaussian distribution with a zero power edge taper in an infinite aperture. Unfortunately the aperture efficiency also approaches zero. This sums up one of the main problems with Gaussian distributions. While they have desirable pattern behaviour they are also highly inefficient.

The Taylor distribution is one type of distribution that can achieve low sidelobes with reasonable gain loss. The distribution for circular aperture was introduced by Taylor (17) in 1960. It approaches the ideal space factor. Figure 3.2.1 shows typical Taylor aperture distributions used to produce sidelobes below 25 to 35 dB. A shaped subreflector can be used to produce these distribution at the main reflector. However some factors should be also considered in the practical application of such distributions.

First diffraction effects would produce a ripple across the aperture which would degrade sidelobes to some extent. Secondly it is impossible to produce a sharp cut-off at the edge. Finally subreflector (and struts if present) blockage would raise the sidelobes above those predicted for a zero blockage aperture. In many cases the final pattern envelope is almost strictly limited by subreflector blockage. Figure 3.2.2 shows the subreflector pattern required to produce the -30dB Taylor distribution for a main reflector with an F/D of 0.2. This distribution is one of those that was used for a proposed 10m antenna design (see Section 5.1.1).

The most commonly used distribution is one which provides zero-power in the blocked central region and a taper towards the edge to improve sidelobe level and reduce backlobes. Sidelobe levels and beamwidth are affected by the size of the zero-power region (generally the size of the blocked area), and the position of the start and the type of edge taper. A study of the way these factors affect the far field has been conducted for circularly symmetric apertures.

It is assumed that the total power from the feed is radiated from the aperture. This assumption is valid only if shaping can be used to ensure that, in practice, very little power in fact appears in the region. It is not true for a conventional Cassegrain where power does appear in this region. In this case power is then blocked by the subreflector so that in addition to a gain loss due to the 'hole' appearing in the aperture pattern there is also a gain loss due to the power that is blocked and not radiated. The effect is generally small.

Most of the studies for such distributions assume that the aperture taper must start from the boresight position. In actual shaped systems this is seldom the case. The most popular distribution is one that is uniform for most of the aperture. Near the outside of the aperture the field then drops as quickly as possible to provide a low edge taper at the rim of the main reflector. It is thus also important to study cases where the taper starts at points away from the boresight axis. The curves shown in Figure 3.2.3 to 3.2.10 show how the gain and 1st sidelobe levels of a radiating aperture is related to the degree of edge taper and the position at which the taper starts. Both linear and square law tapers are considered. The effect of central aperture blockage is also illustrated by cases of 0,1,3 and 5% blockage (of the area). It can be seen that for low blockages, it is possible to decrease sidelobe levels considerably while for higher blockages, this become progressively more difficult and the total reduction in sidelobe levels become smaller. By using these design curves it would be possible to estimate the gain and 1st sidelobe for a given aperture distribution. It becomes possible to find the distribution that would give minimum loss of gain for a given reduction in sidelobe level. It can be seen that the central region blockage (by a feed or subreflector) greatly affects the sidelobe performance.

3.3 Cross Polarization

Cross polarization effects are considered in many parts of this study together with the co-polar field. However a brief description of cross-polarization effects in general would be presented here.

The studies have been published on cross-polarization effects contain the details required to analyse any antenna system. No attempt would be made to describe the studies or reproduce the results reported here. Instead a few basic references to studies of interest would be cited in this report.

For linear polarization the most appropriate method of measuring cross-polarization is the definition 3 as given by Ludwig (18), who consider the problem of defining cross-polarization. The intrinsic contribution of a paraboloid reflector to the true antenna secondary field is generally low enough to be ignored when practical feeds are used. Safak and Delogue (19), Wood (20), Thomas (21) and Watson and Ghobrial (22) have all published studies on antenna cross-polarization. Most of the disagreement between the authors are on definition of the feed used as a source.

Cross polarization effects for circular polarization has also been studied recently . For offset reflectors Chu and Turrin (23) showed that the reflector gives rise to cross-polarized fields in the plane of asymmetry. They also show why there is a squint of the main beam due to cross-polarization effects for circular polarization. Dijk et al (24) show how the offset configuration tend to compare unfavourably with circularly symmetrical reflectors using Huygen source feeds.

The presence of cross-polarization (or more properly contra-polarization) energy in a circularly polarized source shows up as an increase in axial ratio of the field (see Section 2.1:2).

Thus measurement of the axial ratio of a source is also a measurement of the cross-polarization field. Figure 3.3.1 show how the axial ratio is related to the cross-polarization of the field. As shown in figure 3.3.1 the amount of cross-polarized energy transferred depends on the orientation of the polarization ellipse of the transmitter and source. This illustrates the fact that one antenna (either the source or the transmitter) must be perfectly circular for the power transfer between them to be truly independent of orientation angle.

Figure 3.3.1 gives curves for minimum and maximum power transfer. Appendix B gives a table of power transfers for antennas with the same sense of polarization as well as antenna of opposite sense of polarization. The design practice is to take the worst case results for both co-polar and cross-polar power transfer in system calculations. Because neither the source nor the receive antenna are perfectly circular for actual antennas there will always be an orientation for minimum and maximum power transfer. The fact that circularly polarized antenna can often be rotated to provide additional discrimination against a strong interference source may be a useful design tool. Thus if provision to rotate the feed can be provided for little additional cost it can become a useful design feature.

3.4 Antenna Aperture Blockage

The feed system arrangement for reflector antennas generally requires supports which can contribute significantly to the sidelobe levels. The supports as well as the subreflector(s) if used can cause aperture blockage as well as scattering. This section gives the effects of blockage while section 3.5 describes the effects of scattering and diffraction. Section 3.4.1 describes the various feed system support methods and their blockage effects. Sections 3.1.1 and 5.1.2 to 5.1.3 describes the effects of central aperture blockage caused by feeds and subreflectors. Obviously the best way to eliminate support blockage is to remove it entirely. Section 5.1.2-5.1.3 describes antennas such as the Horn reflector and offset reflector which have no aperture blockage at all.

3.4.1 Support Configuration and Blockage

The support struts for a feed or subreflector can contribute significantly to sidelobe degradation of an antenna. The Sub-Sections below consider the blockage effects of conventional support struts as well as describe other support methods that can be used to eliminate or minimize such blockage effects.

3.4.1.1 Conventional Supports for feeds and Subreflector

Figures 3.4.1 (a)-(f) show typical feed and subreflector support configurations and the blockage shadows produced by the support. These shadow areas are usually calculated using ray-optics. The effective shadow areas are generally larger in practice. Aperture gain is reduced in proportion to the blockage area. In addition the blockage also increases sidelobe levels.

Figures 3.4.1 (a)-(d) show the ways a feed for a prime-focus paraboloid can be supported. Figure 3.4.1 (a) shows the centrally-mounted J-hook feed which is widely used. This feed is popular because polarization adjustment can easily be obtained by rotating the mounting hub. Feeder line connection is also very simple. Unfortunately the optical shadow on the aperture is the largest for this type of feed. The side-mounted J-hook feed (Figure 3.4.1 (b)) has less blockage but cannot be adjusted for polarization. This means the entire antenna has to be rotated to obtain polarization adjustment. However it can be used in cases where polarization adjustment is unnecessary (such as circularly polarized antennas) because of the smaller blockage produced. By mounting the support at the rim of the reflector (Figure 3.4.1 (c)) spherical wave blockage is eliminated. This reduces blockage to a minimum for such struts. This arrangement results in long and inconvenient feeder lines.

In applications such as TVRO (Television Receive-Only) where the receive electronics package can be placed behind the feed it is possible to use the strut supported feed arrangement shown in Figure 3.4.1 (d). Here the weight of the feed and electronics-package can be supported by very thin struts to reduce the blockage. The feeder is a small diameter co-axial cable which is supported behind the struts. Polarization adjustment, if required, can either be mechanical (rotating the feed or a polarizer vane) or electrical (ferrite rotator).

Figures 3.4.1 (e) and (f) show two methods by which subreflectors are supported. Both the tripod and quadripod configurations can either be from the reflector edge or within the reflector surface. If the base is from the reflector edge spherical wave blockage is eliminated so that the ray optics shadow is the same size as the cross-section of the struts themselves. Studies have shown that in general quadripods have a smaller effect on the fields in the principal planes of the antenna. The size of the struts is determined by mechanical considerations. One method of reducing the optical shadow is to use two or more members in place of one large member for the support struts.

Figures 3.4.2 (a)-(b) show the use of two struts of circular cross-section in place of a single strut. In both cases the ray optics shadow is the same since the second strut lies in the shadow on the first. However a thin-wire induced current analysis of these two cases by Rusch (25) shows that the actual effective shadow is larger. Figures 3.4.3 (a) and (b) present E and H polarization results obtained by Rusch for the two cases.

The results are for the effective percentage blockage of the second strut. It can be seen that in both cases the blockage for H polarization is much higher than that for the E polarization. The results for square cross-section struts are similar to that for circular cross-section. The use of multiple member struts is generally advantageous for very large (>30m) antennas where the subreflector system is heavy enough to require a strut of high structural strength. In such cases a large single member can be replaced by a multiple member strut with a reduction in both effective aperture blockage and material cost. However this solution is not useful for smaller antennas.

Sections 3.4.1.2 and 3.4.1.3. below show how strut blockage can also be reduced by the use of dielectric supports. However there is little advantage in replacing the conventional metal struts with dielectric struts of about the same dimensions since a material with a high dielectric constant such as fibreglass has to be used. Such struts do not decrease the blockage shadow.

3.4.1.2 Conical Tube Support

One method of supporting a subreflector without any additional blockage is to use the conical tube support shown in Figure 3.4.4. Here a thin sheet of dielectric material is formed into a conical tube which is used to support the subreflector. For this method to be successful the material used must be thin enough to be almost transparent at the operating frequency. The system thus works best at the lower frequencies for smaller antennas. It can be used successfully in the 4/6 GHz bands for antennas up to 4.5m. Details of an actual antenna and the application of this technique for new antennas are given in Section 5.2.3.

3.4.1.3 Foam Support for Subreflectors

One method of eliminating subreflector supports is to use the dielguide shown in Figure 3.4.5.(a). Here a specially shaped subreflector is supported by a solid dielectric foam cone. This system means that blockage is reduced solely to that for the subreflector. It allows the use of a smaller feed and subreflector than is possible with a conventional feed/subreflector system. In addition it provides higher efficiencies than a conventional paraboloid/hyperboloid antenna system. Because of this factor it can be considered for small ($<50\lambda$) antennas where feed and subreflector blockage becomes very significant. Details of an actual antenna design and the application of this configuration to new small earth station antennas are given in Section 5.2.2.

The dielguide feed described above can be used successfully for antennas up to about 5 m. in diameter. Its electrical advantage disappears for larger antennas. However support blockage is still a serious problem for antennas of 8 to 12 m diameter. Figure 3.4.5 (b) shows a proposed foam support for such antennas when used in near-field cassegrain configuration (see Section 3.7.1). Here a foam core is used merely as a shadow-free support for the subreflector. Details of the proposed use of such a support are given in Section 5.1.1.

3.4.1.4 Axially Supported Feeds

Figures 3.4.6 (a) and (b) show axially supported feeds which can be used to reduce support blockage. These are single-polarized feeds (a proposed dual polarized version is described in Section 5.2.1). The feed is supported by a transmission line mounted on the axis of the reflector. Since the support is in the blockage shadow of the feed itself it does not contribute any additional ray-optics shadow. Figure 3.4.6 (a) shows an axially supported feed using a co-axial line which can be used when the frequency is below about 3 GHz. This concept is used by Andrew for their standard microwave antennas in the 1.7 to 2.7 Ghz range. For such antennas the feed is a co-axial cavity excited by short dipole probes.

At higher frequencies a waveguide transmission line has to be used to support the feed. (See Figure 3.4.6 (b)). This type of feed arrangement can be used in antennas with very good sidelobe performance. The support configuration is similar to that of the well known culter feed which however has a different cavity arrangement. Because the culter feed is generally associated with poor VSWR and pattern performance, the generic name "axially supported feed" is used in reference to the high performancec feed systems described in Sections 5.2.1.

Because feed blockage is always much smaller than subreflector blockage this configuration can be used in very small antennas (e.g. DBS antennas) where subreflector blockage becomes excessive. Details of such antennas are given in Section 5.2.1.

3.4.2 Central Aperture Blockage

The previous Sections (3.4.1.2 to 4) have shown that the effects of conventional strut supports can be eliminated by the use of the special support configurations described. It is therefore meaningful to consider the effects of the central aperture blockage caused by feeds and subreflectors alone. Section 3.4.2.1 discusses the effects of such blockage while Section 3.4.2.2 show ways reducing and eliminating the effects.

3.4.2.1 Feed and Subreflector Blockage

For the case of a subreflector or a prime focus feed the effect is a ray optics circular shadow on the aperture of the same size as the subreflector or feed. (See Figure 3.4.1). This is because the blockage is a plane wave blockage. For a feed/subreflector system the feed blockage is a spherical wave blockage so that the shadow is magnified. To avoid this additional feed shadow it is a good design practice to place the feed so that it is in the shadow region of the subreflector (See Figure 3.4.7).

The circular blockage shadow has two main effects. Energy from the feed within the shadow region is blocked and scattered. This power loss reduces the gain. However the effect is not serious for most antennas. As an example a 2% blockage reduces the gain by 0.09dB while a 5% blockage causes a gain loss of 0.72dB. The second more serious effect of the shadow is to cause an increase in sidelobe levels. Figure 3.4.7 shows the simple physical model of the antenna which can

be used to analyse the effect. The blocked aperture with a "hole-in-the-centre" distribution is equivalent to the two unblocked aperture shown. The first is equivalent to the unblocked antenna aperture and has a pattern equivalent to the intrinsic pattern for that particular aperture distribution.

The second aperture is equal in diameter to the blockage shadow and radiates a pattern that is 180 degrees out of phase to the first aperture. The radiation pattern is that from a aperture with uniform distribution. Figure 3.4.9 (a) illustrates how these two patterns can be used to produce the actual radiation pattern. The main beam and the even order sidelobes are reduced in amplitude while the first and other odd order sidelobes are increased.

The effect on pattern and gain of such blockage effects for different distributions have already been given in Section 3.2. Figure 3.4.8 illustrates the relative effects of subreflector and feed blockage calculated for a 15' (4.5m) antenna at 11.95 GHz. A blockage diameter of 5 wavelengths is selected for the feed blockage since most high preformance antennas use either wide angle scalar feeds or waveguide radiators with efficiency plates. The subreflector blockage of 21 wavelengths is chosen as the upper limit of such subreflectors. While smaller subreflectors can be used subreflector of 15-21 wavelengths in diameter offer many advantages (See Sections 3.5.2 and 3.7.2). It represents a blockage of only 1.4% of the area. It can be seen that the lower primary feed blocked aperture has sidelobes that are about 2 to 3 dB lower than that for the subreflector-blocked aperture. Both configurations have envelopes below the $32-25\log\theta$ and $29-25\log\theta$ curves. However the subreflector blocked antenna cannot meet the $26-25\log\theta$ curve. Also see Section 5.1.1 for a similar comparison for a 10m antenna.

3.4.2.2 Blockage Reduction and compensation

Blockage can be reduced by using feeds and subreflectors of smaller sizes. However there are practical limits to the size of both for efficient operation. (See Sections 3.5.2 and 3.7). Where blockage is serious, it may be possible to compensate for this electrically. The basic compensating method is to use a radiator to cancel out the field produced by the blocked region.

Figure 3.4.9 illustrates the way blockage compensation is achieved. Figure 3.4.9 (a) shows how the far-field pattern of the aperture is obtained from the summation of the no blockage field and the field of the blocked region. The compensating radiator can be designed to produce a field which substantially cancels the blockage field as shown in Figure 3.4.9(b). The result approximates that of the unblocked aperture alone. It is also possible to overcompensate as shown in Figure 3.4.9 (c). This results in an improved first sidelobe and a much more gradual drop in sidelobe levels for the near-in sidelobes. Slight over-compensation can be used to advantage where an exceptionally low first sidelobe is required. The first sidelobe occurs at about 2 degrees for a 15' (4.5m) antenna at 4 GHz or a 5' (1.5m) antenna at 12 GHz.

Figure 3.4.10 shows possible methods of blockage compensation. Figure 3.4.10 (a) shows how compensation can be achieved for feeds in general. Figure 3.4.10 (b) shows how it can actually be implemented for an axially supported feed (see Sections 3.4.14 and 5.2.1). Figure 3.4.10 (c) shows how it can be used for a subreflector.

Figure 3.4.11 shows the use of absorbers to provide selective compensation of antenna sidelobes. This is a technique that is normally used as a "last-resort" method of reducing interference in an existing antenna installation. In practice

two pieces of absorbers are positioned experimentally until they cancel or reduce an unwanted interference that is experienced on site. This method increases the overall sidelobe levels as well as the noise temperature. The sidelobe reduction is selective in frequency and direction (ie it is not axially symmetric). It is normally not used as a design feature in new antennas. Janky et al (36) give some measured and predicted results for this method which show that the first and second sidelobes can be reduced.

3.5 Diffraction and Scattering

Scattering from various sources has a very significant effect on the radiation pattern of all earth station antennas. Because most of the antenna sidelobe behaviour can be predicted fairly accurately by diffraction theory it is used extensively to model antenna designs. Section 3.5.1 shows how diffraction theory is used to predict overall antenna performance from the calculation of subreflector and main reflector patterns. Section 3.5.2 describes how scattering from struts affect the radiation pattern envelopes of antennas. Section 3.5.3 discusses the effect of scattering from feeds.

3.5.1 Diffraction Fields of Reflectors

With the use of high speed computers it becomes possible to apply diffraction theory to the prediction of the pattern behaviour of antennas. Appendix C gives a general description of the induced current method calculating the diffraction fields of reflectors. It gives, in a format suitable for computer analysis, the equations that can be used to calculate the scatter field of any symmetrical reflector of arbitrary cross-section.

For front feed systems the feed pattern is used with the main reflector to obtain a complete diffraction pattern of the reflector. Example of such far field patterns showing the effects of the blockage of the feed is given by Figures 4.1.17 and 4.1.19. For a dual-reflector system the subreflector/feed pattern must first be calculated.

This pattern would be one varying in amplitude as well as phase. For shaped reflector the phase variation is usually quite large (over 90°). This composite pattern is then used to illuminate the main reflector to obtain the final diffraction pattern. Thus the final pattern include all diffractions effects of the subreflector (as well as any feed spillover) in addition to the main reflector contribution. Figure 3.5.1 shows the diffraction pattern for a 69 wavelength subreflector for shaped dual-reflector system. Here the shaping is to produce an approximately uniform subreflector pattern (note:- not a uniform main reflector distribution).

This is an example of a very large subreflector in terms of wavelengths. Note how well the ray optics pattern is followed and how sharp the roll-off is. The spillover of the subreflector energy pass the main reflector, is only 3.2%. Figures 3.5.2 is a plot of the far field of a 529 wavelength antenna that is illuminated by the subreflector pattern of Figure 3.5.1. The gain gives an efficiency of 81%. Further examples of subreflector and main reflector diffraction field can be found in Figures 5.1.2 and 5.1.3. The discussion of these Figures in Section 5.1.1 also brings out many characteristics of such diffraction patterns which would not be repeated here.

3.5.2 Scattering From Supports

Scattering from supports can affect the antenna patterns starting from the near-in sidelobes (4th or 5th sidelobes) up to the back-lobe region (100° - 120°). The level of the scatter fields is dependent on factors such as size, orientation and surface of the supports as well as the level of the aperture fields. Interactions between nearby objects (multiple reflections) can also increase the effect beyond that predicted from theory.

Figures 3.5.3 (a) and (b) illustrate very well the effect of scattering (as opposed to blockage considered in Section 3.4.1.1) from a J-hook support. An examination of the left side of Figure 3.5.3 (a) which shows a 12' J-hook antenna at 11.7 GHz may lead one to believe that sidelobes from the 5th onwards ($>5^{\circ}$) may be mainly due to blockage of the intrinsic antenna pattern. However a comparison with Figure 3.5.3 (b) would immediately dispel this impression. Figure 3.5.3 (b) is the same antenna with the addition of absorber to the J-hook support. There is about a 3dB effect even at 5th sidelobe while the effect is 5 to 12dB further out. This dramatic improvement in pattern shows one reason why feed or subreflector supports are so undesirable in antennas which must have very good sidelobe performance.

The J-hook scattering described represents one common type of support scatter. It is relatively large and intercept a very significant amount of energy. It has surfaces oriented at different angles to the axis connected by bends (where the radius of curvature changes rapidly). In general it has a continuous effect over a significant region of the pattern.

In contrast, the long support struts of either tripod or quadrapod has in theory a much sharper effect over a more limited region. Figure 3.5.4 shows how the support strut of a reflector scatters energy. The scattering has a peak along a conical region about the strut as shown. Thus if a pattern is taken along the plane of the strut two peaks would be encountered. One in along the boresight axis while the other at an angle of 2α where α is the angle that the strut makes with the reflector axis. Energy associated with the first peak serves to reduce the gain and affects the sidelobe levels. Energy from the second peak can sometimes show up as very distinct scatter source. As an example an analysis is carried out for the struts of the Andrew 10m antenna. This has an angle (α) of 50.5° and at 3.95 GHz is 80 wavelengths long. The analysis employs a thin wire approximation of the strut. Figures 3.5.5. shows the envelope of the peaks of the patterns of the strut plotted in relation to an actual pattern. No attempt is made here to relate the actual level of the envelope to the level of the measured pattern. Calculation of an absolute gain involves many uncertainties. Figures 3.5.5 serves mainly to illustrate the width of such a peak in relation to the intrinsic pattern peaks. It can be seen that the peak produced by a strut is only about twice the width of an intrinsic peak. Figures 3.5.6. uses measured patterns to illustrate the same point. Figures 3.5.6 (a) shows a pattern for a 12' antenna at 14.4 GHz with a very pronounced peak due to scattering from a strut. Figure 3.5.6(b) shows the same antenna with absorber placed on the struts. Note the complete absence of the peak and also how little the rest of the pattern is affected by the absorber.

3.5.3 Scattering From Feeds

Some energy is always back scattered by a reflector into the feed. Some of this energy appears at the feed input as reflected power which can contribute substantially to the system VSWR. The rest appears as a spurious scatter field coming from the feed.

Poulton et al (28) have described the method that can be used to predict such effects. It can be shown that feed scattering is relatively small for front-fed paraboloids. The effect is however much larger for dual reflector systems. This is because the feed is much nearer the reflecting surface for such systems. To keep this feed scatter energy to a minimum it is generally desirable to design a subreflector that gives a zero energy region which corresponds to the subreflector blockage. Figure 3.4.7 illustrates the use of a 'tip' at the subreflector vertex to produce a low-energy region. This reduces both the feed reflected power and the spurious scatter field. To further reduce the scatter field it is generally necessary to push the feed further back so that it is well within the 'shadow' region (see Fig. 3.4.7). Similar considerations apply in the case of the Gregorian subreflector system. Because the subreflector is concave (as opposed to convex) the feed to vertex distance is longer than that for an equivalent Cassegrainian system. This is one of the advantages of a Gregorian system since it leads to lower feed backscatter. Instead of a vertex 'tip' a dielectric vertex plate can also be used to produce the zero energy region.

A major source of possible sidelobe degradation is that caused by reflector aberrations due either to misalignment or reflector surface errors.

Errors of this type cause a variation in aperture phase which can be represented by a power series of the form:-

$$\text{Phase} = 1 + B_1 x + B_2 x^2 + B_3 x^3 + B_4 x^4 \dots$$

The first x term represents a linear phase which merely shifts the beam direction without affecting the sidelobes or gain. The second x term represents the focus and astigmatic error which occurs when the feed phase centre moved axially away from the focus. This leads to gain loss and higher first sidelobe levels. However it is a second order term so that the sidelobes are still symmetrical. The third x term is the coma distortion of a reflecting system. This is due to a lateral displacement of the feed from the reflector focus. The fourth x term is caused by spherical aberration.

All these factors are discussed in the Sub-Sections that follow.

3.6.1 Axial Defocus Error

One of the most common forms of reflector errors encountered in practice is the axial displacement of the feed system phase centre from the reflector focus. This kind of error usually arises because of uncertainty in the location of the effective phase centre of the feed system. For small-aperture circular waveguide feeds the phase centre can be modified by currents flowing outside the waveguide. These currents are usually changed by the use of choke rings or efficiency plates. Generally, however, the feed phase centre is fairly close to the feed aperture. This is not true for larger diameter (>1 wavelength) feed horns. For such horns the phase centre is typically from 1 to 5 wavelengths behind the aperture.

Initial design information for horn phase centres can generally be obtained using the method of Hu (29) or that of Ohtera and Hiroshi (30) for scalar horns. However the effective phase centre should also be measured where possible. The final design phase centre should be determined by actual axial movement of the feed system in the reflector. The position of the feed system which gives maximum antenna gain is regarded as one where the feed system effective phase centre coincides with the reflector phase centre. Reference to the feed system above can be taken to apply equally to a primary feed as well as a feed horn/subreflector combination. Such a combination can be regarded as a feed system with its own effective phase centre. For shaped systems the feed/subreflector combination will not have a true phase centre. It is still possible however to eliminate or minimize the axial defocus error by moving the feed system. In this case the optimum position occurs when the phase error of the feed/subreflector field is corrected by the main reflector shaping.

The effect of defocus error has been treated by several authors (31) (32) (33). It is mainly a quadratic error which does not affect antenna pointing. The sidelobes are affected equally on both sides. Generally the 1st sidelobe tends to increase and the null becomes smaller. As the defocus error increases the nulls disappear and the 1st sidelobe blends into the mainbeam. The amount of focus error (P_f in degrees) is given by

$$P_f = \frac{45dF}{(F/D)^2}$$

where dF = axial feed displacement (in wavelength)
 F/D = Focal length to Reflector diameter Ratio

Figure 3.6.1 shows the effect of axial movement on aperture phase for F/D of 0.2 to 0.5. It can be seen that this effect is particularly serious for "deep" dishes.

Generally a small (in terms of wavelength) movement of the feed system can lead to gain and sidelobe changes. The example below for a very deep reflector (effective $F/D = 0.2$) brings out this point very clearly. Figure 3.6.2 (a) shows the effect of defocus error on a 84 wavelength diameter shaped Cassegrain. It can be seen that even a 0.1 wavelength movement of the feed has a noticeable effect on the gain and 1st sidelobe level. Figure 3.6.2 (b) shows the calculated defocus error this time for a very shallow dish ($F/D=0.44$). As would be expected from Figure 3.6.1 the shallow dish is much less sensitive to axial movements. The gain and sidelobe level shown in Figures 3.6.2 (a) and (b) are obtained using a diffraction analysis of the feed system and main reflector. The effect on the main beam and sidelobes is similar to that for reflector astigmatism which is treated in Section 3.6.2 below.

3.6.2 Astigmatism

If a reflector is perfectly circularly symmetric and the feed has the E and H plane phase centres at the same point then it would be possible to eliminate all second order aberrations. This can be achieved by the elimination of all the defocus errors as described in Section 3.6.1. Astigmatism is another second order aberration which can be caused either by a difference in E and H plane feed phase centres or by the shape of the reflector. Astigmatic phase error has been investigated by authors such as Cogdell and Davis (34) and Hoerner and Wong (35). The former described how such errors can be detected and suggested ways of correcting them in large antennas. Feeds used in most earth station antennas are generally designed to have the E and H plane phase centres very close together. Thus the main source of astigmatic phase error is generally in the reflector and subreflector. Astigmatism is present when an "out-of-round" condition exists in either the main reflector or subreflector. The reflector aperture is an ellipse instead of a circle.

Physically the reflector can be regarded as one with two different foci. The section of the reflector cutting the minor diameter of the elliptical aperture has a deeper parabolic curve than that through the major diameter. Instead of a point focus the reflector now has a line focus. This leads to a broadening of the main beam and a loss in gain as well as sidelobe degradation.

This effect can be serious for the 12/14/17 GHz frequency bands. It is the reason why reflectors for the higher frequency bands must be very carefully designed. The back-structure and reflector supports must be designed to ensure that gravitational sag (and other factors such as wind loads) does not cause significant astigmatism.

It is useful to have a method of estimating the degree of reflector astigmatism when the antenna is mounted in its operating position. If the rim is well defined it would be possible to measure aperture diameters and estimate the maximum difference in diameter. However for many dishes the rim is not well defined. During the spinning process the reflector edge is turned back to form a flat or round flange at the aperture. This aperture flange adds significantly to the rigidity of the reflector. However it means that there is no sharp transition from the edge of the parabolic surface to the flange. In such cases an alternative measurement method can be used. Because of the turning process the flange should lie quite accurately on a plane. Any distortion such as gravitational sag would produce high and low points on the aperture flange which would no longer lie on a plane. Once the high and low points are located it becomes possible to measure the difference in depth between these points. One simple method which can be used in the field is to stretch two strings across the points. The distance between the skew lines represented by the strings (Δa) gives a measure of aperture distortion.

The effect of such aperture distortion is dependent on the reflector F/D and operating frequency. Aperture distortion is defined and its effects are presented in Figures 3.6.3. and 3.6.4. Figure 3.6.3 gives a plot of the estimated gain loss verses aperture distortion (Δa) for typical paraboloid reflectors with F/D ratio from 0.3 to 0.38 at 13.2 GHz. The gain loss due to random errors (RMS error = 0.014 inches) is also included in the calculation. Figure 3.6.3 shows the importance of keeping aperture distortion low at the 12/14 GHz band. As the aperture distorts, the focus is no longer a point but becomes a line. Figure 3.6.4 shows the spread of the focal line as a function of aperture distortion. This spread of the focal region is the main cause of the gain loss. Figure 3.6.4 also shows the relationship between aperture distortion and the change in the aperture diameter. It shows that the average change in aperture diameter (Δd) is almost equal to the aperture distortion.

Figures 3.6.5 to 3.6.12 show the results of a study into how reflector astigmatism affects gain and sidelobe performance. A 10 foot (3m) antenna (Andrew P10-122D) was first measured to obtain reference patterns for an undistorted reflector. Astigmatism was then artificially introduced by applying forward forces to the reflector edges as shown in Figure 3.6.5. This produced the high and low points, hence aperture distortion, that was described above. Antenna patterns and gains were obtained for diameter distortion (Δd) of 0.25 inches and 0.5 inches. This corresponds approximately to Δa of 0.25 inches and 0.5 inches.

Using Figures 3.6.1 and 2.6.4(b) it can be seen that this represents a maximum aperture phase change of about 250. Figures 3.6.6 to 3.6.8 gives a comparison of the normal E plane pattern and the distorted pattern (for $\Delta d = 0.5$ inches). Figure 3.6.6(a) shows the undistorted pattern to $+5^\circ$ while the corresponding distorted pattern Figure 3.6.6(b) shows the severe effect of the astigmatic error on the main beam and near-in sidelobes. The 3dB beamwidth has broadened from 0.55° to 1.38° . The broadening effect is such that both the first and second sidelobes have merged with the main beam. The third sidelobe is increased from an average of -30.7dB to -23dB . The average boresight gain was 6.6 dB below that for the undistorted reflector. The sidelobe behaviour from 5° to 30° is compared in Figures 3.6.7(a) and 3.6.7(b). Considering the large aperture phase change involved the sidelobe structure has remained relatively unchanged. If the gain loss of the distorted pattern is taken into account it can be seen that the overall isotropic levels of the sidelobes have remained relatively constant. This would indicate that the predominant radiation in this region is independent of the drastic aperture phase change.

It is therefore also interesting to note that the predominant side-lobe structure in this region is one with peaks at about every 4° . A calculation shows that the pattern structure is produced by a source with an effective separation of about 9 inches. The surface of the J-hook support extends about 10 inches from the reflector axis. The relatively unchanged sidelobe radiation in this region is therefore probably due to the fact that the J-hook support effect predominates in this region. Figures 3.6.8(a) and (b) can be used to study the difference between the normal and distorted side-lobe pattern for the 30° to 180° region. In the 30° to 70° region some large differences occur between the patterns, although the overall level remains about the same. The region from 70° to 110° is mainly due to the feed spill over and run illumination of the reflector by the feed. Here again the pattern structure and dBi levels have remained relatively unchanged because the predominant radiation source is not affected by aperture distortion.

Figures 3.6.9 to 3.6.11 give a comparison of the undistorted H plane pattern for the same diameter distortion ($d = 0.5$ inches). A study of these figures confirm that the sidelobe behaviour in the various regions of the pattern is very similar to that for the E plane described above. One notable fact is the asymmetry between the left and right side of the pattern in the 6° and 30° region. This is typical of J-hook supports. For the H plane measurement the J-hook is along the measurement plane and now provides asymmetrical blockage and scattering. The fact that the distorted patterns have the same structure and isotropic level as the undistorted pattern is further proof that the J-hook support is the dominant radiation source in this region.

Figures 3.6.12(a) and (b) illustrate the effect of a smaller amount of astigmatic error. Here the aperture distortion is half of that shown in Figures 3.6.6.-3.6.11. It can be seen that the beam broadening is less. Sidelobe performance for wider angle sidelobes is closer to the undistorted patterns. They are not included since they are similar to those described above. Table 3.6.1 summarizes the main characteristics of the normal and distorted patterns.

The calculated gain loss given in the table is that obtained using Figures 3.6.3 and 3.6.4. It can be seen that there is fairly good agreement between the measured results and those estimated using Figures 3.6.3 and 3.6.4.

TABLE 3.6.1. EFFECT OF ASTIGMATIC ERROR ON 10' ANTENNA

| Antenna Parameter | No Distortion | | Dia. Distortion $\Delta d = 1/4"$ | | Dia. Disortion $\Delta d = 1/2"$ | |
|---------------------------------|---------------|---------|--------------------------------------|---------|-------------------------------------|---------|
| | E-plane | H-plane | E-plane | H-plane | E-plane | H-plane |
| (1) 3dB beamwidth | .55° | .55° | 1.11 | 0.98 | 1.38° | 1.2° |
| (2) 10dB beamwidth | .97° | 1.0° | 1.88 | 1.61 | 2.67° | 2.2° |
| (3) 1st sidelobe level (dB) | -27 | -30.2 | - | - | - | - |
| (4) 2nd sidelobe level (dB) | -26 | -32.45 | 27.95 | -32.5 | - | -28.4 |
| (5) 3rd sidelobe level (dB) | -30.75 | -42.05 | -26.2 | -35.4 | -23.1 | 29.85 |
| (6) Measured Gain (dBi) | 49.5 | | 46.9 | | 42.9 | |
| (7) Measured Gain loss(dB) | - | | 2.6 | | 6.6 | |
| (8) Calculated Gain loss(dB) | - | | 2.3 | | 8.3 | |

Astigmatic error is best avoided in the smaller dish sizes (< 5m) by a proper design of the reflector and the reflector supports. As shown in Section 3.8.1 some degree of astigmatic error due to gravitational sag is always present for larger reflectors. Fortunately for earth station antennas operating with geostationary satellites the elevation angles remain relatively constant. In such cases astigmatism due to gravitation sag is best corrected by the alignment of the reflector panels in the operating position. Where this method cannot be applied it may be necessary to design reflector structure so that gravitation sag deforms the reflector from one paraboloid to another. The feed system can then be moved so that it follows the position of the focus. Another method of reducing astigmatism is to use a deformable subreflector that can be squashed to compensate for main reflector astigmatism.

3.6.3 Coma Distortion

The effect of coma distortion on antenna side-lobes is illustrated in Figure 3.6.13 for the three major antenna configurations. Figure 3.6.13 (a) for a front-fed system shows the basic effect of lateral feed displacement. It can be seen that the ^{high}sidelobe levels are measured on the same side as the lateral feed displacement. In addition the sidelobe levels on the opposite side is decreased relative to the normal levels. This unbalance in near-in sidelobe is characteristic of coma distortion. Figures 3.6.13(b) and (c) show the way the subreflector tilt can create coma lobes in Cassegrain and Gregorian antenna systems.

The effect of lateral feed displacement on antenna performance has been the subject of many studies. Earlier studies include that of Jones (36) as well as that of Kelleher and Colman (37) who presented results for four different focal lengths and 2 different aperture illuminations. They showed that displacement in either the E or H plane is essentially the same. Some of the later studies on the subject included mathematical models of the displacement effect as well as results of computer analysis and measurements. Figures 3.6.14(a) and (b) are computer outputs of the Andrew program "Defocus" which is based mainly on the analysis given by Imbriale et. al. (38). The problem was also analysed by Ruze (39) who is perhaps best known for his work on reflector surface error. In addition to other cases he presented the case of a reflector with uniform illumination which corresponds most closely to the actual illumination of most high efficiency shaped antenna systems. All the studies indicate that gain loss is small for the feed displacements typical of misalignment. Gain loss only becomes significant when coma lobes become very severe. Figure 3.6.15 shows the relationship between coma lobes expected of the Andrew 8m antenna and the gain loss. It is based on the assumption that aperture illumination is uniform and the unperturbed 1st. sidelobe level is -15 dB. It can be seen that the gain loss is very small for coma lobes as high as 12.5 dB (this usually represents a 1st. sidelobe unbalance of up to 5 dB for the antenna).

The effect of coma is maximum at the 1st sidelobe and decreases with increasing angle. Figures 3.6.16 (a) and (b) are actual patterns taken on the Andrew 8m antenna which show the effect of coma on the sidelobe and cross-polarization. Figure 3.6.16 (a) shows the antenna with a 1st sidelobe difference of 1.6dB. Figure 3.6.16 (c) shows the antenna pattern after the subreflector has been adjusted to remove the coma distortion. It only recorded the first 4 sidelobes and the cross-polarization since the effect on the further outside lobes are generally small. A comparison of the difference in sidelobe levels (left side) of Figures 3.6.16 (a) and (c) gives:-

| | Difference |
|--------------|------------|
| 1st sidelobe | 0.8 dB |
| 2nd sidelobe | 0.4 dB |
| 3th sidelobe | 0.3 dB |
| 4th sidelobe | 0.4 dB |

This shows that the effect is maximum at the first sidelobe. Safak and Delogne have recently published a fairly comprehensive treatment of reflector antenna cross-polarization. One of the cases they considered was that of a general feed misalignment that excluded roll (rotation about the boresight axis) using a Huygens source as a feed. The analysis showed that the antenna does not suffer depolarization due to that type of misalignment. The experimental results of Kelleher and Coleman tend to confirm this for actual antennas since they found that cross-polarization levels remain fairly constant for the lateral feed displacements they introduced.

Measured results obtained on the Andrew 8m antenna are also in agreement with this. The Andrew 8m antenna does not have an ideal Huygens source. However the large diameter aperture corrugated feed used is an approximation of such a source. Figure 3.6.16 (b) shows the cross-polarization pattern of the antenna when the 1st sidelobe unbalanced is 1.6 dB. The boresight cross-polarization is -48 dB. Figure 3.6.16 (c) is the pattern after first sidelobes are balanced. The boresight cross-polarization level has become 44.4 dB. The boresight cross-polarization has actually improved when coma was present! However in this case a fairer and more realistic way of comparing the two cases would be to use peak cross-polarization levels. In practice when antennas have cross-polarization levels as low as that considered here the cross-polarization pattern structure is seldom the classical twin-lobe with null on boresight pattern shown in text-books. The actual pattern measured often has a single peak close to the boresight axis. The worst-case cross-polarization occurs when the cross-polarization peak is exactly on boresight. This is in fact the case for Figure 3.6.16 (b) where the peak cross-polarization is also the boresight cross-polarization. For Figure 3.6.16 (c) the peak cross-polarization (-43.9 dB) occurs away from the boresight axis so that the boresight cross-polarization is only -48dB. Therefore a comparison on the peak cross-polarization levels would give:-

| | |
|---|------------|
| Cross-polarization for pattern with no coma | = -44.4 dB |
| Cross-polarization for pattern with coma | = -43.9 dB |

It would be useful to briefly summarize the main effects of coma distortion on earth station antennas. The greatest effect of coma is on the near-in sidelobe. Figures 3.6.16 (a)-(c) showing the cause of coma can be used as a guide in the field for correcting coma.

3.6.4 Spherical Aberration

Spherical aberration is represented by the fourth power x term in the equation representing antenna aperture phase (Seidel) aberrations (See section 3.6). Unlike all the other terms it is independent of the position of the object in the field of view. This means that it affects the off-axis as well as the axial image.

The effects of spherical aberration are similar to those of defocussing (see Section 3.6.1) and in practice can be regarded as a second order focus error. Spherical aberration should be considered in the analysis of spherical reflecting systems such as the multiple feed torus antenna. In paraboloid systems the effect is small.

3.6.5 Surface Errors

All the antennas aberrations discussed in the subsections above are "systematic" errors caused by system misalignment or distortion. In contrast, surface errors are usually random errors which are the result of the manufacturing process. These errors are dependent on the manufacturing method as well as the size of the reflectors. As an example reflectors manufactured by the use of a spinning technique would generally have approximately the same RMS tolerance. This is because the main source of errors is the random departure of the reflector surface from the spinning chuck. Typically such dishes can be manufactured to an average RMS error of 0.006-0.015 inches for reflectors up to 12' in diameter.

Profile errors on the reflector and subreflector appear mainly as phase errors in the aperture distributions of a reflector. The effect of antenna tolerance on gain and sidelobes has been considered by Ruze (40) who gives the gain G as

$$G = \eta \left(\frac{\pi D^2}{\lambda} \right) \exp \left(- \frac{4\pi \epsilon}{\lambda} \right)^2$$

Where η = aperture efficiency

D = reflector diameter

λ = wavelength,

ϵ = surface RMS error

The effect on the sidelobes can be considered by separating the radiation field into a no-error pattern and a scatter pattern. The gain loss due to r.m.s. errors can be calculated using the above formula. The power represented by this gain loss appears as the scatter pattern. The distorted antenna pattern is given by:-

$$G(\theta) = G_0(\theta) e^{-\bar{\delta}^2} + \left(\frac{2\pi c}{\lambda}\right)^2 e^{-\bar{\delta}^2} \sum_{n=1}^{\infty} \frac{\bar{\delta}^{2n}}{n \cdot n!} e^{-(\pi c u / \lambda)^2 / n}$$

Where

$G(\theta)$ = the distorted antenna pattern,

$G_0(\theta)$ = the no-error antenna pattern,

c = the radius of the correlation region,

u = $\sin\theta$,

$\bar{\delta}^2 = \left(\frac{4\pi e}{\lambda}\right)^2$

Figures 3.6.17 can be used to estimate the gain loss due to r.m.s. errors for earth station antennas operating in both the 4/6 and 12/14/17 GHz bands. Most small earth station antennas have r.m.s. tolerances chosen to give low gain loss (0.1-0.2dB). This normally means that contribution to sidelobes due to reflector errors is small. For large and very large ESA the method of construction may determine the tolerance possible. In some cases the gain loss are higher than 0.2dB.

The worst-case effect of random errors occurs when the correlation intervals for the errors are all approximately the same. This is when the errors would have a large effect at a particular antenna angle. Figure 3.6.18 is a plot of the envelope for the worst-case surface error contribution to an antenna pattern. Curve A is the case when the antenna gain loss due to surface error is 0.1dB. Marked on the curve are regions where a given correlation interval is expected to predominate. As an example Curve A indicates that at 10° off boresight the worst-case surface error contribution would be -7.5dBi where the predominant correlation interval would be two wavelengths. Curve B gives the same data as curve A for a gain loss of 0.4dB. Gain loss due to surface errors is estimated from the equations given above or from Figure 3.6.17. Curve C is

the current CClR curve. It can be seen from Figure 3.6.18 that surface error must be considered if the acceptance envelope becomes 3 to 6dB lower. Figure 3.6.19 shows the typical error contour for one surface panel of a large earth station antenna (>5m). Such antennas are assembled from several individual panels.

The surface error can be separated into two components. The first component is the random error due to each panel which is a function of fixtures and manufacturing method used.

As an example of the tolerance achievable the Andrew 8m antenna has panels with an RMS error of 0.010" to 0.015". The second error component is that due to relative misalignment of the reflector panels. This error can generally be kept small by the use of an optical alignment method. As an example the theodolite method used by Andrew to align such antennas gives an estimated alignment accuracy of 0.005"

Feeds are the first link in the radiation chain that finally produces an antenna far-field pattern. As such their contribution to good sidelobe performance should never be underrated. This section reviews some of the critical design feed parameters required as well as briefly describes the more important feed configurations used. Circularly polarized feeds are not treated separately since they generally require the same characteristics as a high performance linearly polarized feed. For most ESA designs circular polarization is achieved by adding a polarizer to a linearly polarized feed. For a circularly symmetric feed with good input VSWR the feed axial ratio is dependent mainly on the polarizer design. Feed requirements of dual-reflector systems are very similar to those for prime-focus systems. However, they do have some significant differences. Desirable characteristics common to both systems are described first in Section 3.7.1 for dual-reflector systems while Section 3.7.2 for prime focus systems brings out some of the differences.

3.7.1 Feeds For Dual-Reflector Systems

A high performance feed for dual reflector system should ideally have the following characteristics:-

- (a) Circularly symmetric pattern with equal E and H plane fields.
- (b) Low cross-polarization.
- (c) A smooth pattern with a very sharp amplitude roll-off where it illuminates the subreflector edge.
- (d) A distinct phase centre which is at the same point for both the E and H planes. The phase distribution should be constant out to the start of the sharp amplitude taper (variations $< 30^\circ$).
- (e) Low VSWR (< 1.1) and loss ($< 0.1\text{dB}$)
- (f) Broad band behaviour of (a) to (e) over a 50-60% frequency band.

These factors contribute to high performance and low sidelobes in various ways. Thus circular symmetry is required for efficient shaping. If the feed pattern is unequal, spillover cannot be kept low over the entire reflector edge. Low feed cross-polarization is needed because for a well designed reflector the main contribution to the cross-polarization within the main beam comes from the feed. A smooth pattern is necessary since ripples cannot be corrected and will lead to a very significant increase in sidelobe levels. A steep roll-off is necessary to produce a low edge taper. A low edge taper is necessary to produce low feed spillover as well as to minimize rim diffraction effects. This is one of the most important feed characteristic for good sidelobe performance. Generally the larger the feed aperture size the steeper the roll-off can be designed to be. The introduction of higher order modes can also serve to enhance the roll-off. A separation of the H and E plane phase centres can lead to astigmatic errors (see Section 3.6.2). A flat feed phase characteristic which is associated with a distinct phase centre makes the production of a smooth uniform aperture phase much easier. It should be noted that if shaping is used on the subreflector it can also be used to correct for any deficiencies in the feed phase pattern. This is true as long as the feed phase change is fairly smooth and does not vary significantly with frequency. Broad band behaviour is necessary for feed phase distribution. It is also essential for amplitude distribution as well as such factors as feed VSWR.

The requirements for a high performance feed enumerated above means that the designer has very little real choice of feeds. The two most popular choices are the corrugated horn and the multimode horn. A diagonal horn can also be used. Another possibility for future high-volume low-cost applications is a dielectric guide used either as a subreflector support or solely as a pure radiator (see Section 5.2.2).

The most popular feed for ESA applications is the corrugated horn. The corrugated horn was first described by Simmons and Kay (41) and since then by many other authors (42-47). They have very good beam efficiency and have equal E and H beamwidth out to -25 to -35 dB. A corrugated horn with sufficient horn length would also have no visible sidelobes down to -40dB. Except for very narrow flare-angle horns ($<8^\circ$), a properly designed corrugated horn should have very wide beamwidth as well as low cross-polarization ($<30\text{dB}$).

Next in popularity is the multimode horn. Horns operated in the dominant mode (TE_{01} for rectangular and TE_{11} for circular) generally have unequal E and H-plane patterns and poor sidelobe performance. It is possible to improve the patterns by the use of higher order modes. The box horn (48) is an example for rectangular horns. Potter (49) in 1963 described a conical horn which used a step to generate the TM_{11} mode. This has low sidelobes and good cross-polarization. Versions of the Potter horn were used in some of the first earth station antennas. Foldes (50), Gruner (51) and Turrin (52), among others, have described versions of the circular multimode horn. Like the corrugated horn they have good beam efficiency.

The multimode horn depends for its operation on the combination at the aperture of two or more modes with exactly the required phase. For this reason it is more frequency sensitive than the corrugated horn. For operation over two bands, such as the 4/6 GHz and 12/14 GHz bands, a feed should ideally have the same beamwidth in both bands. The percentage change in the 10dB-Beamwidth of a feed over the two bands can be taken as a measure of the bandwidth performance of a given feed. Table 3.7.1 compares this for multimode and corrugated feeds over a frequency range of 1:1.563.

TABLE 3.7.1 FEED COMPARISON

| | Multimode Horn | | Corrugated Horn | | |
|--|----------------|----------------|-----------------|----------------|----------------|
| | Gruner (51) | Foldes (50) | Jeuken (42) | Andrew (53) | Andrew (54) |
| Low Band Frequency | 3.95GHz | 3.95GHz | 8.64GHz | 3.95GHz | 11.7GHz |
| 10dB Beamwidth H | 135 | 30.5 | 23 | 25 | 23.6 |
| (deg) E | 128 | 27 | 24 | 24 | 24.4 |
| High Band Frequency | 6.175GHz | 6.175GHz | 13.5GHz | 6.175GHz | 14.5GHz |
| 10dB Beamwidth H | 92 | 18 | 22 | 19 | 23.0 |
| (deg) E | 92 | 20 | 20 | 18 | 22.4 |
| Percentage change in 10dB beamwidth | 30% | 34% | 11% | 24% | 5%* |

*Change over 1:1.24 Frequency Band.

It can be seen that the corrugated feeds have smaller percentage change in beamwidth with frequency. It should also be noted that the corrugated feeds have good patterns over the entire 1:1.563 frequency band while the multimode feeds are only designed to operate over two relatively narrow bands.

3.7.2 Prime Focus Feeds

Requirements for prime focus feeds are to a great extent very similar to that given above for the two reflector systems. However, because the feed apertures required to produce the broad beamwidth for prime focus systems are generally much smaller a steep edge roll-off is much harder to achieve. This is why feed spillover is much harder to control. Also since the only feed phase error cannot be compensated by subreflector shaping a distinct phase centre becomes more important. One additional factor is introduced for prime focus systems. For dual-reflector systems, amplitude distribution within the 10dB beamwidth is not important, per se, since main aperture control can be provided by the subreflector. For prime focus systems the main aperture amplitude distribution is related directly to the feed distribution. Control of feed distribution becomes an important design tool for these systems. Thus higher efficiency can be achieved by introducing 'flat-top' distributions (see Figure 5.2.6 as an example)

The two most popular feeds used are wide angle corrugated feeds and circular waveguides with choke and other pattern improvement mechanisms added. The corrugated horn is already described for dual-reflector systems. The circular radiator finds wide applications in many off-the-shelf microwave antennas since it is relatively simple to fabricate. It can

be used only as prime focus feed in parabolic antennas of $f/d = < 0.35$. The aperture diameter can be chosen to give equal E and H plane patterns. The backlobe and beam efficiency can be improved by the use of quarter-wavelength chokes. The typical overall efficiency obtainable with this feed is about 50-65%. Cross-polarization performance is good. Cowan (55) reports maximum cross-polarization of -30 dB for a simple aperture with two chokes over the 12/14 GHz bands. Gruner (51) describes a circularly polarized 4/6 GHz prime focus feed with good VSWR (< 1.1) and a polarizer axial ratio of less than 1.65dB.

3.8 Environmental Effects

All the effects considered in the preceding sections form, in total, the actual antenna patterns as measured on an antenna pattern range. It is important to realize that the antenna pattern of an operational antenna can also be modified by environmental effects. The major effects are discussed in the Sub-Sections that follow.

3.8.1 Temperature Effects

A change in temperature may cause a change in antenna performance. Consider first the case of large ($> 5M$) antennas that are assembled from several panels. Each panel typically has an aluminum skin and a steel back-structure. The panels are aligned so that all the panel surfaces conform to the design profile. The first effect is that caused by a change in ambient temperature.

In order to assess the effect of temperature on an antenna structure it is necessary to resort to a computer simulation. As an example, such a simulation was carried out for the Andrew 8m antenna.

Appendix D describes in detail the computer model used. Two sets of results were obtained. The first predicted the deviations caused by a temperature decrease of $20^{\circ}C$. applied to the entire antenna structure^(case a). The second predicts the deviations when the antenna back structure is cooled by $10^{\circ}C$ when compared to the reflector panels (case b).

The actual computer predicted deviations are presented in Appendix D , however it is difficult to relate this directly to antenna performance. If a parabolic reflector is made of a single material which expands isotropically then a change in temperature would not affect antenna performance in any way because the paraboloid would still remain a true paraboloid except that it is a slightly smaller paraboloid. It is possible to use a computer ray-trace technique to calculate the RF path length from the new feed position to the aperture for this new slightly smaller paraboloid. If different points on the surface are taken it would be found that all the path lengths are slightly smaller than the original but are still equal in length to each other. The determination of the actual aperture phase using the method described above represents a very simple and direct way of assessing the effect of temperature on a reflector. Any departure from a uniform phase represents a departure of the reflector from the ideal one-metal reflector. The deviations given in Appendix D are used in a computer ray trace program to obtain the corresponding path lengths. These were in turn converted into actual electrical degrees assuming a frequency of 12 GHz. Figures 3.8.1 and 3.8.2 show the variation of aperture phase with aperture distance from the boresight axis. The aperture distance scale is drawn using a square law scale because the contribution to antenna performance from any element depends on the area (which in turn is directly proportional to the square of the radius). The use of a square law curve makes it easier to judge the effect of any phase variation on performance. Thus it is immediately obvious that a phase variation near the outside edge of the reflector has more weight than the same variation near the centre. It can be seen that the models predict very small phase variations. For the case of the 20°C decrease in temperature the phase remains relatively constant over most of the radiating area then increases sharply to a maximum of about 10 degrees near the

centre of the reflector. The behaviour for case (b) is also similar except the changes are smaller. To relate this to a mechanical deviation it is possible to use the EIA RS-411(27) definition of surface deviation. Surface deviation is equal to one half the change in RF path length. Using this definition and weighting the results by area represented by each point gives a weighted RMS deviation. The weighted RMS deviation for case (a) was found to be 0.003" while that for case (b) was 0.002". Thus the deviation predicted by the models represent a negligible effect on reflector performance. It should also be noted that temperature effects can be further minimized if necessary.

Temperature effects on the smaller (<5m) one-piece reflectors are generally less. As noted above a single material ideal antenna has no temperature effects at all. In practice the typical one-piece spun aluminum reflector would have a brass feed. The main error would therefore be that caused by a movement of the feed phase centre away from the reflector focus. For a 15' (4.5m) antenna the focal point displacement is less 0.002" for a 10°C change in ambient temperature. The effect on gain and sidelobe would therefore be very small.

The second temperature effect is that caused by the differential heating of the antenna surface. This can occur when the sun shines only on part of the antenna surface. The parts of the antenna surface in the shadow would then be cooler than those parts receiving solar insolation. A similar effect can occur if antenna surface heating elements are switched on only for part of the reflector surface. To avoid this effect the operational instructions should specify that all antenna heating elements must be switched on.

3.8.2 Gravitational Sag

An antenna which is a perfect paraboloid in the Zenith position will start to distort as the elevation angle is decreased. This gravitation sag of the antenna is maximum when the antenna boresight is horizontal. The distortion caused by gravitation sag can be reduced so that the largest error component is reflector astigmatism. The effect of reflector astigmatism is described in Section 3.6.2. Gravitation sag is a factor that must be considered in the design and operation of most earth station antennas.

The effect of gravitation sag is most severe for the very large antennas (>25m in diameter). The problem for very large reflectors has been studied by antenna designers. Von Hoerner and Wong (35) give details of an analysis for this problem using the Green Bank 140' (43m) radio telescope as an example. For very large antennas the ideal design is to have an antenna back-structure which deforms in a homologous fashion. That would be a reflector which deforms from one perfect paraboloid to another perfect paraboloid. Such a designs have been proposed and implemented (56) (57). For such a reflector it would only be necessary to move the feed system so that the phase centre is always at the focus of the reflector as it deforms. Such a reflector would not have any gain and sidelobe degradation due to gravitation sag. Figure 3.8.3 shows the measured gain loss for changes in elevation angle for the 140' (43m) Green Bank radio-telescope antenna (35) which is conventional in design. It can be seen that the antenna has a gain loss of more than 3dB at 10.7GHz as it is turned from the Zenith position to 18° from the horizon.

The problem is less for Intelsat type A stations (4/6 GHz from 25m to 30m) where the estimated losses are typically 0.3 to 1.dB.

For antennas of diameters ranging from 8m to 12m the problem is not as significant at the 4/6 GHz band. However for an antenna like the Andrew 8m antenna operating at 12/14 GHz the problem can be similar to a 25m antenna at 4/6GHz.

Fortunately a simple solution is available for antennas operating with geostationary satellites. Since movements of the antenna required to track the antenna are small the operating position remained almost constant. Gravitation sag can be kept small if the antenna panels are aligned with the antenna in the operating position. Alignment of an antenna in the operating position is more difficult than the traditional horizontal on-the-ground alignment. However once the special techniques required are developed the alignment time required is not excessive (about a day).

The problem is different for the small earth station antennas (<5m). Here the reflector used is manufactured as a single piece assembly either as a spinning or stamping or from a mold. In each case unlike the large antennas the reflector surface cannot be adjusted to correct for gravitational sag. It is therefore essential that the effect of gravitation sag must be considered. For successful operation, especially at the 12/14 GHz band, the reflector back structure and mounting supports must be designed to be rigid enough to resist gravitation sag. An example of a reflector (chosen for its flimsiness) which shows gravitation sag is shown in Figure 3.8.4. This shows the general nature of gravitation sag in small reflectors. The reflector is shown in the position of maximum sag (with the aperture plane vertical). The deflected shape is what one would expect from gravitational sag. The vertical section is "closing in" with maximum deflection at the top of the reflector. The horizontal section is "opening out" in a symmetrical fashion. The bumps in the vertical section show the effect of the support points. Figure 3.8.4 is obtained using computer model where the curved shell elements used conform very closely to the true profile. Similar elements are used for the support ring to ensure that the support geometry is accurately defined.

4 Upgrading of Existing Antennas

4.1 Large ESA's

4.1.1 Upgrade methods for 8m, 10m and 12m

Pattern envelopes for existing large Andrew earth station antennas are included in this section as Figures 4.1.1 through 4.1.10. These are peak envelopes for 8, 10 and 12 meter antennas. No weighting, averaging or 10% exceedence have been applied. The envelopes show that all antennas do not meet the 32-25 log θ curve. In order to lower sidelobe levels, under illumination of the main and subreflector is necessary. This under illumination will cause a decrease in antenna efficiency. Sidelobes produced by scattering off subreflector supports can be reduced by placing absorber on the struts. This was done on the TCTS ESA8-124.

4.1.2. 10m and 12m ESA's at 4 and 6 GHz

Andrew Antenna Co. Ltd. of Whitby designed and developed a 10M 4/6 GHz antenna during 1974 and 1975. Radiation patterns were measured on our Ashburn test range and the resulting peak pattern envelopes are presented in Figures 4.1.1 and 4.1.2. These envelopes show many areas where the patterns exceed the 32-25 log θ curve. Subsequent to these measurements, Andrew Corporation of the U.S. improved these envelopes to those shown in Figs. 4.1.3 and 4.1.4. This was accomplished by increasing the subreflector diameter and the corrugated feed horn aperture by approximately 10%. Comparing these four envelopes reveals improvements of up to 6dB in peak sidelobe levels with only a slight decrease in antenna gain. Even with the dramatic improvement, the modified antenna still does not

meet the $32-25\log\theta$ peak envelope. This same technique was applied to a 12M antenna and the applicable pattern envelopes are shown in Fig's 4.1.5 and 4.1.6. Again this antenna does not meet the peak $32-25\log\theta$ curve. Both antennas however meet this specification through FCC averaging. Some slight additional underillumination would probably improve these to the point of meeting the peak envelope however a slight decrease in gain would be expected.

4.1.3 8 Meter Antennas at 4/6 and 12/14 GHz

Andrew has manufactured two 8m antenna designs. The first, a 4/6 GHz version, was developed in the early 1970's for Telesat Canada. Peak radiation pattern envelopes for this antenna can be found in Fig's 4.1.7 and 4.1.8. This envelope is similar to the ESA10-46 with many areas exceeding the $32-25\log\theta$ curve. The antenna pattern could be improved by employing the same technique as used on the 10 meter. Again FCC averaging would still have to be used in order to meet the curve. Further improvement could be obtained by under illumination as in the 10 meter case.

The second 8 meter design was our most recent large ESA. This operates in the 12/14 GHz bands and also was developed for Telesat use. Figures 4.1.9 and 4.1.10 are it's pattern envelopes. Electrically this is a very large antenna with a diameter of over 300λ at 11.7 GHz. The efficiency is at least 73%. Subreflector and mainreflector spillovers have been kept to a minimum without under illumination and hence antenna efficiency is high. As stated previously in section 4.1.1, the antenna had absorber placed on the subreflector supports. With averaging of sidelobes this antenna will meet the following:

| | |
|-------------------|--|
| $29-25\log\theta$ | dBi for $\theta \leq 10^\circ$ |
| $26-25\log\theta$ | dBi for $10^\circ \leq \theta \leq 27.5^\circ$ |
| -10 | dBi for $\theta \geq 27.5^\circ$ |

Additional improvement in antenna performance could be obtained by the under illumination technique previously discussed. This would likely result in the antenna meeting the $32-25\log\theta$ peak envelope.

4.2 Small ESA's

4.2.1 Upgrade Methods for Small ESA's

Pattern envelopes for some existing small Andrew Earth Station antennas are shown in Figures 4.1.11 through 4.1.16. Again all envelopes are peak with no weighting, averaging or 10 % exceedence. Techniques for lowering sidelobe levels are the same as those described in para. 4.1.1.

4.2.2. J Hook Feed Antennas

Peak PE's for a 15ft dual band "J Hook" 4/6 GHz antenna are shown in figures 4.1.11 and 4.1.12. The nominal efficiency of this antenna is 40% at 6 GHz and 56% at 4 GHz. The low efficiency of 6 GHz is due to under illumination of the main reflector. This has improved main reflector spillover levels by as much as 8 dB. However, peak values still exceed $32-25\log\theta$. Near in lobes generally are at a higher level than those at 4 GHz. This is probably due to the blockage which has become more significant because of the increased energy levels at the center of the reflector. Further evidence of this effect can be seen by examining the computer calculated Figs 4.1.17, 4.1.18 and 4.1.19. Fig. 4.1.17 is a pattern for a 10ft antenna at 6.175 GHz with a .3 F/D ratio and 64% efficiency. The under illuminated case of $F/D = .25$ and 51% efficiency is shown in Fig. 4.1.18. Near in sidelobe levels out to 18° show very little improvement with this 13% decrease in efficiency. Fig. 4.1.19 displays the affect of reducing blockage by 60% for the under illuminated case. Sidelobe levels are up to 5dB lower with the reduced blockage.

4.2.3 Cassegrain Antennas at 4/6 GHz

Pattern envelopes for a 15 foot cassegrainian are shown in Figs. 4.1.13 and 4.1.14. Efficiencies for the two bands are 64% at 4 GHz and 51% at 6 GHz. Near in lobes out to 15° are generally 1 to 3dB lower in the under illuminated 6 GHz band when compared to 4 GHz. Main reflector spillover levels are as much as 8dB lower at 6 GHz. Note that the near in lobes at 6 GHz still do not meet $32-25\log\theta$.

4.2.4 Cassegrain Antennas at 12/14 GHz

Pattern envelopes for a 12/14 GHz 15 foot ESA can be seen in Figs. 4.1.15 and 4.1.16. Again this antenna with an electrically large aperture ($D=180\lambda$) does not come close to meeting the $32-25\log\theta$ curve.

Efficiencies of this antenna are 62% at 11.95 GHz and 56.5% at 14.25 GHz. Further under illumination employed on this antenna would likely only tend to reduce spillover levels since the 14 GHz PE for near in lobes is approximately the same as the 12 GHz PE even though the efficiency is about 6% less. Blockage affects previously discussed probably account for this.

4.3 Summary of Upgrade Costs.

In section 4.1 (LARGE ESA'S) we saw that it was possible to reduce sidelobe levels significantly by keeping spillover levels to a minimum with very little under illumination and thereby to some extent reduce near in sidelobes somewhat as well. Modification of the ESA's would require field replacement of the horn-subreflector assembly at a cost of \$9K or \$10K plus installation costs which would vary greatly depending upon location.

The pattern performance of small ESA's cannot be improved effectively and therefore no proposed upgrading cost is given.

New Antenna Designs

Section 4 has given a general review of how low sidelobe techniques can be applied to existing Andrew ESA designs. It showed that while improvements are possible new designs are necessary to meet the much stricter specifications proposed (Proposed Envelopes (1)-(4) - See Section 1). This Section describes the antenna configurations that are proposed to meet future low sidelobe requirements. Section 5.2 covers design configurations suitable only for small antennas (<5m in diameter). Section 5.1 covers antenna configurations that can be applied to large antennas. In the case of the offset and horn antennas the designs are also suitable for small antennas.

5.1 Large ESA Designs

The Sub-Sections that follow describe three different antenna configurations that are suitable for large earth station antennas. Section 5.1.1 describes a proposed 8-12m near-field Cassegrain with foam subreflector support designed to attempt to meet envelopes (1) to (4) on an averaged basis. Sections 5.1.2 and 5.1.3 describe the offset and the horn reflector antennas which can be used for both large and small ESA designs. These two configurations should meet envelopes (1) to (4) on an averaged basis.

5.1.1. New 8-12m ESA Antennas

Section 4.1 has shown that the existing Andrew antenna designs for the 8m to 12m size at 4/6 GHz cannot be upgraded to meet the more severe pattern envelopes proposed.

To meet the more stringent sidelobe requirements a new design approach is required. The two main problems with the existing designs are feed spillover and scattering and blockage by the struts. The new design configuration proposed here avoids these problems.

Figure 5.1.1 shows the proposed foam-supported near field Cassegrain which was described briefly in Section 3.4.1.3. The basic near-field Cassegrain antenna was first described by Hogg and Semplak (58) in 1964. Near-field Gregorian and Cassegrainian systems were also described by Dragone and Hogg (59) in their review of near field symmetrical and offset systems. The basic principle of the system is the use of a parallel beam from behind the main reflector to illuminate the subreflector (a convex paraboloid). This eliminates the feed (with its attendant blockage and multiple reflection effects) from the reflector/subreflector region. Because this is a near-field effect there is very little energy outside the beam. This means practically no spillover pass the subreflector. This parallel beam can be generated where convenient and then guided to the subreflector by a series of reflecting mirrors. This has been done in several beam waveguide antenna systems.

Figure 5.1.1 shows the system that is most easy to implement for this requirement. The parallel beam is generated by a horn reflector (small and therefore easy to manufacture for this particular application) mounted behind the dish.

The hollow foam cone support shown is used to provide an electrically transparent means of supporting the subreflector. This is not the only transparent support available.

Studies of other transparent supports (such as the fibre glass tube support) would form part of the new design implementation. In addition a prototype can be fitted with different supports including conventional struts to study the cost/sidelobe tradeoff.

No attempt is made here to indicate any kind of optimised design for this system since a full design study cannot be undertaken in the time frame available. Figure 5.1.1 represents the results of a short conceptual study for the proposed design. A deep reflector ($F/D=0.2$) is used so that the spillover of the subreflector past the main reflector can easily be controlled. It also has the advantage that the subreflector is very near the main reflector. This means the foam cone support can be kept as small as possible. The size of the transparent support is one of the major problems with this proposed design. Obviously a normal shallow dish of $F/D=0.35$ would almost double the support size and may make the design unattractive. For normal Cassegrain designs it is advantageous to place the subreflector as far away from the feed source as possible. For a near field design the opposite is true to some extent. The subreflector should be well within the near-field of the source aperture to ensure that the feed edge-taper is kept as low as possible. The 3.5' (1.1m) subreflector shown provides a reasonable compromise between the requirement for low blockage and that for high spillover efficiency. Figure 5.1.2 (a) shows the subreflector patterns designed to produce uniform aperture distribution at the main reflector (feed edge taper = 19.5dB). Figure 5.1.2(b) shows the calculated far field pattern of the system for the distribution of Figure 5.1.2(a). Figure 5.1.3 shows the patterns for tapered illuminations.

Figure 5.1.2 (b) shows the effects expected from the use of a pattern shaped solely for maximum efficiency (Gain = 51.8dB with efficiency = 83%).

The near-in sidelobes are relatively high and come close to touching the FCC curve. Some aperture taper should help here. From 6 to 15 degrees the intrinsic curve is quite good with more than 6dB of margin. From 15 degrees onwards the curve tends to show the effect of the high back-lobe of the subreflector. Because of the high edge illumination the back lobe energy is correspondingly high (-10dBi at the peaks). This high backlobe added to the intrinsic pattern is enough to push some peaks above the -10dBi line. This, almost constant -10dBi back-lobe dominated, region can be reduced substantially by introducing a lower edge taper on the subreflector pattern. This should also decrease the high pattern "bump" starting at about 70° which is caused by subreflector energy that just miss the main reflector. This again emphasize the importance of introducing a sharp roll-off at the edge of the main reflector. With such a taper it should be possible to meet the current CCIR specification. With some addition gradual aperture taper it should be possible to meet proposed envelopes (1) and (3) with averaging. If one allows a design margin of 3dB over this calculated pattern it becomes difficult to predict how much tapering would be needed to meet proposed curves (2) and (4).

To try to see if proposed envelopes (2) and (4) can be achieved with this system two cases of under-illumination are given here as examples. The first is an attempt to drastically under-illuminate the dish to see if this will

produce much lower sidelobes. The subreflector pattern shown in Figure 5.1.3(a) is used for the reflector to produce the pattern shown in Figure 5.1.3(b). the gain is now only 37.7dB and efficiency is down to a miserable 32.4%. The pattern is certainly better than that for high efficiency case with a pronounced absence of the feed backlobe effects. However the pattern within the 30° region shows the effect of under illumination and blockage with the normal sidelobe structure almost hidden by a much coarser pattern. The sidelobe levels below the 6° point begins to degrade and starts to approach the CCIR curve. This curve still cannot meet the proposed envelopes (2) to (4). The improvement in pattern is not really worth the 3dB loss of gain due to under-illumination. Figure 5.1.3 (c) shows the antenna pattern using the modified Taylor distribution shown in Figure 3.2.2. This subreflector pattern would produce a Taylor distribution at the main reflector. However as shown in Figure 3.2.2 unlike an idealized subreflector pattern the energy from the subreflector does not stop abruptly at the main reflector edge. The gradual roll-off produces main reflector spillover which must be considered in the pattern calculations.

The Taylor distribution has its most dramatic effect on the first sidelobe reducing it to 26.3dB from 16dB in the uniform illumination case. The near-in sidelobe still suffer from the blockage effects. However they are all at least 3 to 4dB below the FCC curve. The pattern gets better beyond 4° with the improvement maintained up into the subreflector backlobe region. Because of the lower edge illumination the backlobe is now well below the -10dBi line. This again proves the point about high edge illumination. The subreflector edge taper at the rim of the main reflector is lower than that for the uniform illumination. However it is still not low enough

to bring the main reflector spillover below the required -10dBi. Obviously like the case for uniform illumination a fast roll-off near the edge must also be introduced for a practical Taylor distribution. The gain of the Taylor distribution was 51.4dB (77%) showing that the slight gain loss is well worth the improvement in pattern.

Figure 5.1.3 (d) shows the antenna with exactly the same Taylor illumination as Figure 5.1.3(c) without any sub-reflector blockage. This shows very clearly how the subreflector blockage is limiting the amount of sidelobe reduction within the amount of sidelobe reduction within the region of the first few sidelobes. This unblocked Taylor distribution meets proposed envelopes (1) to (4) except again in the region of the spillover pass the main reflector) and illustrate what is possible with an unblocked aperture. To meet the proposed envelopes (2) and (4) even on an averaged basis with subreflector blockage some form of blockage compensation (see Section 3.4.2.2) would probably be necessary. This is because the 10% averaging allowed cannot reduce the RPE levels caused blockage which raises much more than 10% of the sidelobes within an affected region.

Except for the spillover pass the main reflector (which can be easily corrected) the predicted pattern meets proposed envelopes (1) and (2). A full optimization study would be required to produce an antenna that can meet the above envelopes with a comfortable design margin. It should be noted that these are calculated patterns which take subreflector blockage into account. In practice the sidelobe peaks may be much higher for conventional systems due to effects (ie struts etc) which are not considered here. Because support struts have been eliminated it is expected that an actual measured pattern would be much closer to the calculated

results. Spillover, of the feed pass the subreflector, and associated diffraction effects which can be a problem with conventional dual reflector systems is also greatly reduced because of the near-field configuration. However subreflector/horn-reflector interactions can exist and may contribute the odd unexpected peak. The reflector surface error may also have an effect at these low sidelobe levels. If a peak envelope is required the design should allow an additional 4 to 6dB margins over that for an envelope for which averaging is allowed.

The new design would involve additional cost over that of a conventional system since the horn reflector and foam support would be more expensive to fabricate than the scalar horn and conventional strut support. It is estimated that for a 8-12m antenna overall cost would be increased by 15 to 20% for such a design compared with a conventional design.

5.1.2 Offset Antenna

Andrew has researched the possibility of using this type of antenna to lower sidelobes in the typical problem areas. A very small model (equivalent to a 15ft at 4GHz) has been measured. The peak pattern envelope is shown in Fig. 5.1.4. together with the 29-25log θ and 26-25log θ curves. The antenna easily meets 26-25log θ for angles greater than two degrees. The cost of such a 15 ft antenna would approach 25-30% above a conventional cassegrain. The price of a large 8m antenna of this design has been estimated at approx 40% higher than a conventional cassegrain 8m design.

5.1.3 Horn Reflector Antenna

Peak Pattern envelopes for the Andrew 10ft. horn reflector antenna are shown in Figs 5.1.5 and 5.1.6. The near in lobes of this antenna (out to approx 5°) exceed 29-25log θ . However beyond this point the envelope meets this specification. Sidelobe levels have been reduced in this antenna with microwave absorber and therefore a higher than normal noise temperature can be expected. The cost of this antenna with mount is estimated at \$30,000. A 15ft horn antenna would meet the following peak envelope at 4GHz.

| | | |
|-------------------|-------------|-----------------------------|
| 32-25log θ | dB θ | 1.5° $\leq \theta \leq$ 5° |
| 29-25log θ | dB θ | 5° $\leq \theta \leq$ 8° |
| 26-25log θ | dB θ | 8° $\leq \theta \leq$ 27.5° |
| -10 | dB θ | $\theta \geq$ 27.5° |

An estimated cost of \$60,000 for this antenna would probably prohibit its use.

This Section describes designs for small diameter earth stations. Typical sizes would be 10' to 15' (3-4.5m) reflector at 4/6 GHz and 3' to 5' (1 - 1.5m) reflectors at 12/14 GHz. The requirement here is different from that for the large ESA designs described previously. These reflectors must generally be designed to be cost effective since they are usually sold in large quantities.

Three designs specifically suitable for small earth station antennas are given in the Sub-Sections that follow. It should be noted that none of these designs will be as good as similar designs using either the offset or horn-reflector antenna. Both these configurations have already been described in Sections 5.1.2 and 5.1.3 respectively under the category of large antennas. However they are equally suitable for the small sizes as well since they do not have struts or other blockage problems. Their cost disadvantage referred to for large antennas also apply for small antennas. Conventional paraboloids using off-the-shelf dishes do not incur any addition reflector tooling cost. In contrast the reflector tooling cost is very high for even a 10' offset reflector. In addition the feed and support structure is generally also more expensive for an offset system. As an example of relative cost, the 10' foot horn reflector costs twice as much as conventional 10 foot high performance microwave antenna. An exception would be a small diameter (3 to 5 ft) offset reflector which can be die-formed out as a single piece reflector. Such an application must have a volume large enough to justify the high tooling cost involved.

For small antennas struts and central aperture blockage become all important. The advantages in performance of the three configurations over conventional systems have been described in Sections 3.4.1.2 to 3.4.2.2.

The Sub-Sections that follow give details of existing systems as well as explore the performance that can be expected from the new designs. Sections 5.2.3 and 5.2.4 describe the Dielguide and Fibreglass tube-supported antennas which are both Cassegrainian antennas that use electrically transparent subreflector supports. Both antennas can use a shaped subreflector to optimise gain and sidelobe performance. Their main problem is the blockage caused by the subreflector. The smallest subreflector which can give reasonable patterns control is about 8 wavelengths in diameter. For a 40-wavelengths reflector this represents 4% blockage which has a very significant effect on sidelobes (see Sections 3.2 and 3.4.2). This is why dual reflector systems can^{not} be used for very small antennas. The axially supported feed described in Section 5.2.1 overcomes the blockage problem by reducing the central blocked region to that of a small diameter feed. However without the subreflector the degree of aperture control has become much more limited. This problem can be minimized to a limited extent by a careful feed design using the various techniques of feed pattern control available. As an example efficiencies of about 70 % is achieved for the 15' 4/6 GHz antenna described in Section 2.3.

One of the problems common to all three systems is the spillover of energy pass the main reflector. This feed (or in the case of Cassegrainian system - subreflector) spillover generally causes a significant increase sidelobe level within the 40° to 140° region of a typical reflector pattern. This spillover is normally above the -10dBi level required. This -10dBi level can be achieved either by significantly under illuminating the reflector or by the use of a deep dish with a shield. These solutions lead to loss of efficiency (to 35% to 45%) gain as well as an increased cost.

A shielded antenna generally cost twice as much as a non-shielded antenna. The increase in antenna size required to compensate for under-illumination can increase cost by 25%-35%. A relaxation of the envelope level (for antennas less than 100 wavelengths in diameter) within this region to allow for a single spillover peak region of -5 to -7dBi would serve to make small antenna designs more cost effective. The actual method of allowing for feed spillover should be the subject of further discussions and study. One possible approach would be to retain the -10dBi region in the envelope but allow 20% of all the peaks in that region to exceed the envelope.

5.2.1 Antenna with Axially Supported Feed

While the horn-reflector and off-set antennas described in Sections 5.1.2 and 5.1.3 do have the best sidelobe performance a very strong case can be made for the use of a standard paraboloid with an axially supported feed. The cost of new tooling necessary for an offset system is difficult to justify for any performance gain, except for the case of very small antennas sizes (<5 ft Diameter).

Section 3.4.1.4 has already described the antenna using an axially supported feed. (See Figure 3.4.6(b)). Figure 5.2.1 shows how such a feed is implemented for a single polarized system. The feed consists of a radiating cavity which is both supported and excited by a rectangular waveguide. Since this waveguide is along the paraboloid axis blockage is reduced to a minimum. The cavity alone does not provide very good patterns since the backlobe (0° to 90° region of the antenna) is quite high. This is the reason why such feeds have not found wide application in the past. However by the use of the efficiency plate shown as well as by carefully matching the radiating cavity it is possible to greatly improve the radiation characteristics of such feeds.

Figure 5.2.2 shows the measured radiation pattern envelope for a 15' (4.5m) antenna with such a feed in the 12 GHz band. It can be seen that the radiation pattern is well below the current CCIR curve up to 40°. Except for a few strong peaks within the 20 to 24 degrees region it can also meet proposed envelopes (1) and (3) in this region. The strong peaks illustrate one of the difficulties of meeting peak pattern envelopes without averaging. In any practical design these are always present.

If averaging is not allowed an additional design margin of 3 to 6dB has to be included to meet peak specifications. For the very stringent specifications such as the proposed envelopes (2) and (4) the design often becomes impossible. The region from 40° to 120° shows the effect of reflector edge illumination and feed spillover. It is typical for such small antennas. One solution is to greatly under illuminate the reflector to reduce the spillover. However efficiencies of 15 to 30% do not make such antennas very desirable. An alternative solution is to use a reflector shield to reduce the spillover and eliminate some of the edge effects. Figure 5.2.3 (a) and (b) show H and E planes for a shielded antenna. This is a 6' (2m' $D/\lambda = 73$) antenna at 12 GHz. The measured efficiency is still a respectable 56% minimum. The measured patterns illustrate very clearly the desirable effects of a shield (estimated noise temperature with shield = 13.6°K). The backlobe is well below -20dBi with no sign of any edge or spillover effects present. It can be seen that the antenna can satisfy proposed envelopes (1) and (3) (again with averaging) over the entire range. Except for the near-in sidelobe even proposed envelopes (2) and (4) can be satisfied. It is expected that the sidelobe can be reduced further in any new design. However the one disadvantage of this existing design is the fact that the feed is suitable only for single-polarized operations. This can be a severe limitation for a high performance antenna.

Figure 5.2.4 shows a dual-polarized version of the axially supported feed that was proposed by the author in 1977. Here, a circular instead of a rectangular waveguide is used as the feed support. The waveguide is then tapered so that it can be used to excite the cavity. To raise the tapered section above cutoff a dielectric rod is inserted within the tapered section. This rod, which is tapered as shown, is also used to support and match the radiating cavity. The radiation properties of the cavity are again improved by the use of an efficiency plate as shown.

The feed radome serves to protect the feed, maintain pressurization as well as support the radiating structure. Figure 5.2.4 shows the details necessary to produce a pressurized version of the feed. A foam filled version of the feed with all radiating parts molded from plastic can also be implemented at a greatly reduced cost. Another alternative method of feed support would be to use a much smaller diameter tube which would present even less blockage to the radiating cavity. In this case the low loss co-axial waveguide mode can be used instead of the normal TE_{11} mode which would be below cut-off.

A study of the comparative cost of this system (TVR0 15' unshielded ESA at 12 GHz) shows that it is 16% more expensive than a comparable ESA antenna with a J-hook type of feed. A similar Cassegrainian system would cost 26% more than the J-hook system. Thus it can be seen that the axially supported feed can offer a better performance without too significant an increase in cost.

5.2.2. Dielguide Antennas

Section 3.4.1.3 describes the advantages of antennas that use dielguides. The use of low permittivity dielectric cones (called dielguides) as feeds for paraboloid antennas (Figure

3.4.5) was first described by Bartlett and Moseley (60) in 1966. They presented experimental results to show that a dielguide can be used to enhance antenna performance but did not present any design theory. Since then the radiating characteristics of dielguides have been studied by Selema (61). The use of dielguides in microwave antenna has been described by Clarricoats et. al (62) (63). The dielectric foam support provides a completely blockage-free support for the subreflector. Thus like the tube support antenna of Section 5.2.3 the only aperture blockage is that due to the subreflector. The dielguide support has two main advantages over the tube support antenna. The dielguide acts as guiding structure which converts the feed fields into hybrid modes closely bounded to the guiding surface. This means that the size of the feed aperture can be smaller than that for an equivalent conventional feed/subreflector system. Because the modes propagating in the dielguide are similar to those in a corrugated horn, the fields at the dielguide aperture have the same desirable characteristics. (see Section 3.7.1).

Figure 5.2.5 shows the design details of a typical dielguide antenna. To keep the cost low a simple conical horn is used to excite the dielguide. The dielguide cone is made from an inexpensive low density foam. Figure 5.2.6 shows the field distribution at the aperture of the dielguide (ie. the field at the subreflector position). The field shows the "flat-top" characteristic that is typical of a well designed dielguide. As in the case of many wide-angle corrugated horns this "flat-top" region can be shown to be due mainly to the presence of a second order mode. This field behaviour contributes to a good efficiency (>60% typical) and low subreflector edge tapers.

As shown in Figure 5.2.5 the rays from the subreflector are deviated as they pass out of the dielguide. This means that a true hyperboloid cannot be used as the subreflector. Appendix E shows how the profile of a subreflector can be calculated. Figure 5.2.7 shows the main beam and near-in sidelobe H plane pattern for a 4' dielguide antenna at 11.2GHz. The far outside lobe behaviour H-plane pattern is shown in Figure 5.2.8.

Again the spillover past the main reflector and rim illumination effects can be seen in the pattern.

This antenna cannot meet the current FCC specification. It must be realized that this design was produced more than 10 years ago. The designers did not have access to many of the design tools and techniques now available. A new antenna specifically designed to produce low sidelobe would use a larger subreflector, a more uniform foam and a different horn design. The new design should meet the current FCC curve and may meet proposed envelope (1) and (3) on an averaged basis.

5.2.3 Fiberglass Tube Supportted Antenna

The effects of subreflector supporting struts in a Cassegrain type antenna can be eliminated if the antenna assembly as shown in Figure 3.4.4 is used. This type of Cassegrain antenna was designed in 1973 with the objective of attaining high gain, high efficiency, equal E and H plane beamwidths and excellent VSWR characteristics.

The subreflector supporting struts are eliminated by supporting the subreflector on a truncated fiberglass cone. The cone is made from a fiberglass sheet by laying out a plane development of a truncated cone in two pieces and bonding the pieces together. One end of the cone is attached to a hollow extension mounted on the hub of the main reflector. The feed horn assembly, consisting of a circular waveguide ended on a stepped horn is placed along the axis of the cone and the extension. A radome is used to protect the feed and cone assembly from the environment.

A typical RPE for this type of antenna is shown in figure 3. This RPE was constructed by using the peak envelope method. It is the RPE of a 12 foot dual polarized Cassegrain ESA operating at 5.925-6-425 GHz. The gain of the antenna is 45.8 dBi at 6.175 GHz which is slightly above the design goal. Also plotted in figure 5.2.9 is the reference RPE. It can be seen that the RPE of the antenna exceeds the reference RPE by an average of 5dB. This is mainly due to two factors. The major design goal was to attain high gain and efficiency. Not much effort was done to lower the sidelobe levels. The RPE was constructed by using the "Peak Envelope" method. This is the most conservative method which represents the worst case of all sidelobe levels. Although details are not included here, this antenna meets the FCC performance Standard A.

This method of supporting the subreflector is also used in the 8ft and 10ft. ESA. An example of the E and H plane radiation patterns of a 10 foot ESA designed in 1973 are shown in Figure 5.2.10(a), 5.2.10(b), 5.2.11(a) and 5.2.11(b).

It can be seen that the 3dB beamwidth of the E and H plane patterns are exactly the same. The high sidelobe levels in the 60° to 120° region is due to the over-illumination around the edge of the subreflector in order to attain high gain and efficiency. Modern computerized diffraction analysis has since been developed to design optimal subreflectors to achieve VSWR characteristics and low sidelobes, without very significant loss of efficiency.

The cost of this antenna is the same as the Andrews' Ultra High Performance (UHX) shielded antenna which uses a centrally-mounted J-hook feed. However the gain of this antenna is one dB higher than the UHX antenna.

The study into the causes of sidelobe degradation show that many different factors must be considered in an antenna designed to meet the more restrictive pattern envelopes proposed. Many of these factors such as reflector aberrations and aperture distributions can be effectively controlled in a design. However the study also shows that certain sidelobe degradation mechanism such as diffraction and blockage do limit the sidelobe performance achievable. An example is the effect of support struts and subreflectors:

For the low near-in sidelobes required by the proposed envelopes it was shown that aperture blockage becomes a very important factor in a design. For the cases considered (4.5m at both 4/6 GHz and 12 GHz and 10m at 4/6 GHz) central aperture blockage (by a feed or subreflector) limits the lowest RPE achievable in the near-in sidelobe region. For a paraboloid this places a severe constraint on the use of a conventional dual-reflector configuration for small antennas and make the use an axially supported prime focus feed very attractive. An alternative solution is to use offset reflectors or horn reflectors that have unblocked apertures.

The study shows that the CCIR method of presentation, while good in concept, suffer from ambiguities and defects if it is to be applied to the actual specification of the performance of individual antennas. It is also shown that a relative level method of presentation (See Sections 2.4.1.4 and 2.4.1.5) makes the judgement of envelope compliance much easier than the current CCIR method.

The upgrading of existing ESA's was considered in Section 4 with upgrade cost summarized in Section 4.3. The pattern performance of the existing small ESA (<5m) cannot be improved significantly. It was shown that the existing large ESA (8 and 10m) at 4/6 GHz can be upgraded (approximate hardware cost = \$10000) to meet the 32-25 log θ curve with averaging. The envelope of the new high performance 8m ESA at 12/14 GHz meets and in most regions exceeds by more than 3dB the 29-25log θ curve with averaging. However due to just a few stray peaks it will not meet the 32-25log θ curve without averaging. This serves to highlight one of the reasons why envelopes with averaging are strongly recommended in preference to envelopes without averaging.

The study concludes that it would be possible to meet a 29-25 log θ curve with averaging for new designs. For the large earth stations a new near-field cassegrainian design is proposed (Section 5.1.1). For small earth station antennas (<5m), configurations such as the axially support feed as well as offset reflectors and horn reflectors can be used. For very small ESA in large quantities (<1.5m) the best configuration would be an offset antenna using a die-formed reflector. It is therefore concluded that the envelope given below can be specified for new Earth Station Antennas.

$$G_1 = 29 - 25 \log \theta \text{ dBi} \quad \theta_{\min} < \theta < 36.3^\circ$$

$$G_2 = -10 \text{ dBi} \quad \theta > 36.3^\circ$$

where

G_1 represents the level exceeded by 10% of the antenna peaks.

G_2 represents the level exceeded by 10% of the antenna peaks.

θ_{\min} = The greater of 1° or the region beyond the 1st sidelobe peak (at or beyond $\theta \approx 100 \lambda/D$ degrees.)

The optimum envelopes for small antennas (<5m) deserve further study. In particular the problem of feed spillover past the main reflector (see Section 5.2) should be considered in the envelope specifications. A significant savings in cost can be achieved if the envelope is adjusted to allow for spillover lobes. For example G_2 above can be redefined to be:-

G_2 represents the level exceeded by 20% of all peaks of the antenna above 36.3° .

Appendix A.

A method of producing any aperture distribution

This appendix describes briefly a method that can be used to shape an antenna system to produce any given aperture distribution. This allows the antenna designer the maximum freedom in the choice of an aperture distribution to obtain a desired far-field behaviour.

A.1 The general equation for a Shaped-System

The aperture distribution $P(x)$ at any point x can be related to the feed pattern $F(\theta)$ by considering the conservation of power.

$$P(x) \, dx = F(\theta) \, \sin \theta \, d\theta \quad (A.1)$$

Also since total power across the aperture is equal to power of the feed,

$$\int_0^\theta F(\theta) \, \sin \theta \, d\theta = \int_0^{x_{\max}} P(x) \, dx \quad (A.2)$$

Combining (A.1) and (A.2) gives

$$\frac{dx}{d\theta} = \frac{F(\theta) \, \sin \theta \int_0^{x_{\max}} P(x) \, dx}{\int_0^{\theta_{\max}} F(\theta) \, \sin \theta \, d\theta} \quad (A.3)$$

Equation (A.3) can be used in cases when an entirely general aperture is required. However in most of the cases of interest the distribution can be described by simple functions (linear or quadratic equations). In such cases the analysis can be simplified by considering them as an extension of the case of uniform illumination.

For the case of uniform illumination equation (A.3) reduces (by differentiating) to

$$\frac{dx}{d\theta} = \frac{x_{\max}^2 F(\theta) \sin \theta}{2\pi \int_0^{\theta_{\max}} F(\theta) \sin \theta d\theta} = Q(\theta, x) \quad (\text{A.4})$$

All other aperture distributions can be regarded as $Q(\theta, x)$ multiplied by additional factors of the general form

$$\frac{dx}{d\theta} = \frac{Q(\theta, x) [S(x) - P(x)]}{R(x)} \quad (\text{A.5})$$

Two groups of distribution are given as examples in tables A.1 and A.2.

Two groups of distributions are considered. The first group (A) affects the distribution near the centre of the aperture from $x = 0$ and the second group (B) affects the illumination near the edge $x = x_{\max}$. It is possible to combine any member of one group with any member of another group to produce a composite distribution.

TABLE A.1 (a)

GROUP A

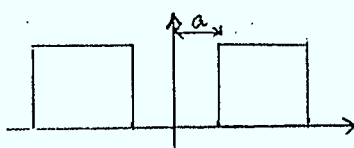
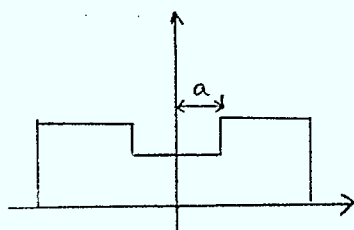
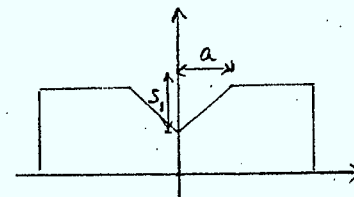
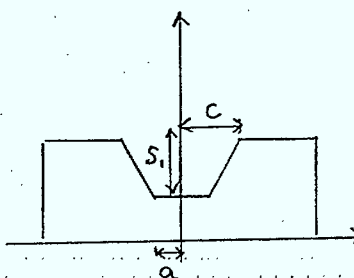
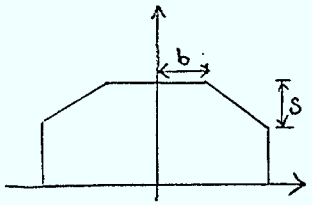
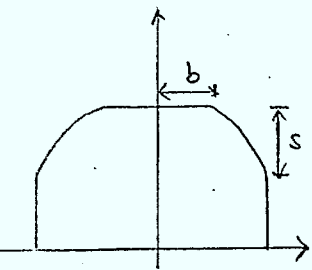
| TYPE | $S(x)$ | $P(x)$ | $R(x)$ |
|---|--------|--|---|
|  | 1 | $\frac{a^2}{x_{\max}^2}$ | 1 |
|  | 1 | $\frac{S_1 a^2}{x_{\max}^2}$ | $(1 - S_1)$ for $x < a$ 1 for $x \geq a$ |
|  | 1 | $\frac{S_1 a^2}{x_{\max}^2}$ | $1 - S_1 + \frac{S_1 x}{c}$ for $x < c$ 1 for $x > c$ |
|  | 1 | $\frac{S_1 c^2}{3x_{\max}^2} + \frac{2S_1 a^2}{3x_{\max}^2}$ | $1 - S_1$ for $x \leq a$ $1 - S_1 + \frac{S_1 x}{c}$ for $a < x < c$ 1 for $x \geq c$ |

TABLE A.1(b)

| GROUP B | | | |
|--|--|--------|---|
| TYPE | $S(x)$ | $P(x)$ | $R(x)$ |
|  | $S(x) = \frac{(x_{\max} - b + sb)}{3} - \frac{2s}{3} \frac{x_{\max}^3}{b^2}$ | 0 | $R(x) = \begin{cases} 1 & \text{for } x \leq b \\ \frac{x_{\max} - b + sb - sx}{x_{\max}} & \text{for } x > b \end{cases}$ |
|  | $S(x) = (x_{\max} - b)^2 - sb^2 - 2sbx - sx^2$ | | $R(x) = \begin{cases} 1 & \text{for } x \leq b \\ \frac{(x_{\max} - b)^2 - sb^2 + \frac{2sb}{3} - \frac{sx_{\max}^2}{4} + \frac{sb^4}{x_{\max}}}{x_{\max}} & \text{for } x > b \end{cases}$ |

APPENDIX B

This appendix gives the tabulated results of the maximum and minimum isolation between two circular polarized antennas for both the co-polarized and cross-polarized cases.

The following equations were used:

$$I_{\min}^{\max} = \frac{(AR+1)^2(ARa+1)^2 + (AR-1)^2(ARa-1)^2 \pm 2(AR^2-1)(ARa^2-1)}{4(AR^2+1)(ARa^2+1)}$$

$$\text{Co-polarized Power Transfer}_{\min}^{\max} = 10 \log (I_{\min}^{\max}) \text{dB}$$

$$\text{Cross polarized Power Transfer}_{\max}^{\min} = 10 \log (1 - I_{\min}^{\max}) \text{dB}$$

where AR is the voltage axial ratio of the transmit signal and ARa is the voltage axial ratio of the receive antenna.

| AXIAL RATIO (TRANSMIT)= .5 dB | | | | |
|-------------------------------|----------------------------|------|-------------------------------|-------|
| AXIAL RATIO (REC) | CO-POLARIZATION POWER (dB) | | CROSS POLARIZATION POWER (dB) | |
| | MAX. | MIN. | MIN. | MAX. |
| .25 | 0 | 0 | 36.83 | 27.3 |
| .5 | 0 | .01 | 61.45 | 24.8 |
| .75 | 0 | .02 | 36.85 | 22.87 |
| 1 | 0 | .03 | 30.84 | 21.29 |
| 1.25 | 0 | .04 | 27.34 | 19.97 |
| 1.5 | .01 | .05 | 24.86 | 18.82 |
| 2 | .03 | .08 | 21.38 | 16.92 |
| 2.5 | .05 | .12 | 18.94 | 15.39 |
| 3 | .08 | .17 | 17.06 | 14.11 |
| 4 | .16 | .27 | 14.3 | 12.08 |
| 5 | .26 | .4 | 12.32 | 10.53 |
| 6 | .37 | .54 | 10.81 | 9.3 |
| 8 | .63 | .85 | 8.66 | 7.5 |
| 10 | .91 | 1.17 | 7.22 | 6.26 |

| AXIAL RATIO (TRANSMIT)= 1 dB | | | | |
|------------------------------|----------------------------|------|-------------------------------|-------|
| AXIAL RATIO (REC) | CO-POLARIZATION POWER (dB) | | CROSS POLARIZATION POWER (dB) | |
| | MAX. | MIN. | MIN. | MAX. |
| .25 | 0 | .02 | 27.32 | 22.88 |
| .5 | 0 | .03 | 30.84 | 21.29 |
| .75 | 0 | .04 | 36.87 | 19.96 |
| 1 | 0 | .05 | 62.24 | 18.81 |
| 1.25 | 0 | .07 | 36.89 | 17.8 |
| 1.5 | 0 | .08 | 30.9 | 16.9 |
| 2 | .01 | .12 | 24.93 | 15.35 |
| 2.5 | .03 | .17 | 21.47 | 14.06 |
| 3 | .05 | .22 | 19.03 | 12.96 |
| 4 | .11 | .34 | 15.68 | 11.17 |
| 5 | .2 | .48 | 13.39 | 9.77 |
| 6 | .3 | .63 | 11.68 | 8.65 |
| 8 | .54 | .97 | 9.31 | 6.98 |
| 10 | .79 | 1.31 | 7.75 | 5.82 |

| AXIAL RATIO (TRANSMIT)= 1.5 dB | | | | |
|--------------------------------|----------------------------|------|-------------------------------|-------|
| AXIAL RATIO (REC) | CO-POLARIZATION POWER (dB) | | CROSS POLARIZATION POWER (dB) | |
| | MAX. | MIN. | MIN. | MAX. |
| .25 | .02 | .04 | 22.91 | 19.98 |
| .5 | .01 | .05 | 24.86 | 18.82 |
| .75 | 0 | .07 | 27.37 | 17.8 |
| 1 | 0 | .08 | 30.9 | 16.9 |
| 1.25 | 0 | .1 | 36.93 | 16.08 |
| 1.5 | 0 | .12 | 63.21 | 15.33 |
| 2 | 0 | .17 | 30.99 | 14.03 |
| 2.5 | .01 | .22 | 25.03 | 12.92 |
| 3 | .03 | .28 | 21.58 | 11.95 |
| 4 | .08 | .41 | 17.31 | 10.35 |
| 5 | .15 | .57 | 14.6 | 9.08 |
| 6 | .24 | .73 | 12.66 | 8.05 |
| 8 | .45 | 1.09 | 10.02 | 6.5 |
| 10 | .68 | 1.46 | 8.33 | 5.42 |

| AXIAL RATIO (TRANSMIT)= 2 dB | | | | |
|------------------------------|----------------------------|------|-------------------------------|-------|
| AXIAL RATIO (REC) | CO-POLARIZATION POWER (dB) | | CROSS POLARIZATION POWER (dB) | |
| | MAX. | MIN. | MIN. | MAX. |
| .25 | .04 | .07 | 20.03 | 17.84 |
| .5 | .03 | .08 | 21.38 | 16.92 |
| .75 | .02 | .1 | 22.98 | 16.1 |
| 1 | .01 | .12 | 24.93 | 15.35 |
| 1.25 | 0 | .15 | 27.45 | 14.66 |
| 1.5 | 0 | .17 | 30.99 | 14.03 |
| 2 | 0 | .22 | 34.46 | 12.9 |
| 2.5 | 0 | .28 | 31.1 | 11.92 |
| 3 | .01 | .35 | 25.16 | 11.06 |
| 4 | .05 | .5 | 19.31 | 9.62 |
| 5 | .11 | .66 | 16 | 8.45 |
| 6 | .18 | .84 | 13.75 | 7.5 |
| 8 | .37 | 1.23 | 10.8 | 6.06 |
| 10 | .59 | 1.62 | 8.94 | 5.05 |

| AXIAL RATIO (TRANSMIT)= 3 dB | | | | |
|------------------------------|----------------------------|------|-------------------------------|-------|
| AXIAL RATIO (REC) | CO-POLARIZATION POWER (dB) | | CROSS POLARIZATION POWER (dB) | |
| | MAX. | MIN. | MIN. | MAX. |
| .25 | .1 | .14 | 16.22 | 14.76 |
| .5 | .08 | .17 | 17.06 | 14.11 |
| .75 | .06 | .19 | 17.99 | 13.51 |
| 1 | .05 | .22 | 19.03 | 12.96 |
| 1.25 | .04 | .25 | 20.22 | 12.44 |
| 1.5 | .03 | .28 | 21.58 | 11.95 |
| 2 | .01 | .35 | 25.16 | 11.06 |
| 2.5 | 0 | .42 | 31.25 | 10.27 |
| 3 | -.01 | .5 | - | 9.56 |
| 4 | .01 | .68 | 25.49 | 8.36 |
| 5 | .04 | .87 | 19.69 | 7.36 |
| 6 | .09 | 1.08 | 16.42 | 6.54 |
| 8 | .24 | 1.52 | 12.58 | 5.27 |
| 10 | .42 | 1.97 | 10.31 | 4.37 |

| AXIAL RATIO (TRANSMIT)= 4 dB | | | | |
|------------------------------|----------------------------|------|-------------------------------|-------|
| AXIAL RATIO (REC) | CO-POLARIZATION POWER (dB) | | CROSS POLARIZATION POWER (dB) | |
| | MAX. | MIN. | MIN. | MAX. |
| .25 | .18 | .24 | 13.69 | 12.58 |
| .5 | .16 | .27 | 14.3 | 12.08 |
| .75 | .14 | .31 | 14.96 | 11.61 |
| 1 | .11 | .34 | 15.68 | 11.17 |
| 1.25 | .09 | .38 | 16.46 | 10.75 |
| 1.5 | .08 | .41 | 17.31 | 10.35 |
| 2 | .05 | .5 | 19.31 | 9.62 |
| 2.5 | .02 | .59 | 21.88 | 8.95 |
| 3 | .01 | .68 | 25.49 | 8.36 |
| 4 | 0 | .89 | 32.24 | 7.32 |
| 5 | .01 | 1.11 | 25.91 | 6.45 |
| 6 | .04 | 1.35 | 20.16 | 5.73 |
| 8 | .14 | 1.84 | 14.75 | 4.6 |
| 10 | .28 | 2.34 | 11.91 | 3.8 |

| AXIAL RATIO (TRANSMIT)= 5 dB | | | | |
|------------------------------|----------------------------|------|-------------------------------|-------|
| AXIAL RATIO (REC) | CO-POLARIZATION POWER (dB) | | CROSS POLARIZATION POWER (dB) | |
| | MAX. | MIN. | MIN. | MAX. |
| .25 | .29 | .36 | 11.83 | 10.94 |
| .5 | .26 | .4 | 12.32 | 10.53 |
| .75 | .23 | .44 | 12.84 | 10.14 |
| 1 | .2 | .48 | 13.39 | 9.77 |
| 1.25 | .17 | .52 | 13.97 | 9.42 |
| 1.5 | .15 | .57 | 14.6 | 9.08 |
| 2 | .11 | .66 | 16 | 8.45 |
| 2.5 | .07 | .77 | 17.66 | 7.88 |
| 3 | .04 | .87 | 19.69 | 7.36 |
| 4 | .01 | 1.11 | 25.91 | 6.45 |
| 5 | 0 | 1.36 | 61.45 | 5.68 |
| 6 | 0 | 1.63 | 26.43 | 5.04 |
| 8 | .07 | 2.18 | 17.52 | 4.03 |
| 10 | .18 | 2.73 | 13.78 | 3.3 |

| AXIAL RATIO (TRANSMIT)= 6 dB | | | | |
|------------------------------|----------------------------|------|-------------------------------|------|
| AXIAL RATIO (REC) | CO-POLARIZATION POWER (dB) | | CROSS POLARIZATION POWER (dB) | |
| | MAX. | MIN. | MIN. | MAX. |
| .25 | .41 | .49 | 10.41 | 9.65 |
| .5 | .37 | .54 | 10.81 | 9.3 |
| .75 | .33 | .58 | 11.24 | 8.97 |
| 1 | .3 | .63 | 11.68 | 8.65 |
| 1.25 | .27 | .68 | 12.16 | 8.34 |
| 1.5 | .24 | .73 | 12.66 | 8.05 |
| 2 | .18 | .84 | 13.75 | 7.5 |
| 2.5 | .13 | .96 | 14.99 | 7 |
| 3 | .09 | 1.08 | 16.42 | 6.54 |
| 4 | .04 | 1.35 | 20.16 | 5.73 |
| 5 | 0 | 1.63 | 26.43 | 5.04 |
| 6 | 0 | 1.92 | 66.22 | 4.45 |
| 8 | .03 | 2.53 | 21.34 | 3.54 |
| 10 | .1 | 3.13 | 16.04 | 2.88 |

| AXIAL RATIO (TRANSMIT)= 8 dB | | | | |
|------------------------------|----------------------------|------|-------------------------------|------|
| AXIAL RATIO (REC) | CO-POLARIZATION POWER (dB) | | CROSS POLARIZATION POWER (dB) | |
| | MAX. | MIN. | MIN. | MAX. |
| .25 | .68 | .79 | 8.35 | 7.77 |
| .5 | .63 | .85 | 8.66 | 7.5 |
| .75 | .58 | .9 | 8.98 | 7.23 |
| 1 | .54 | .97 | 9.31 | 6.98 |
| 1.25 | .49 | 1.03 | 9.66 | 6.74 |
| 1.5 | .45 | 1.09 | 10.02 | 6.5 |
| 2 | .37 | 1.23 | 10.8 | 6.06 |
| 2.5 | .3 | 1.37 | 11.65 | 5.65 |
| 3 | .24 | 1.52 | 12.58 | 5.27 |
| 4 | .14 | 1.84 | 14.75 | 4.6 |
| 5 | .07 | 2.18 | 17.52 | 4.03 |
| 6 | .03 | 2.53 | 21.34 | 3.54 |
| 8 | -.01 | 3.25 | - | 2.77 |
| 10 | .02 | 3.97 | 22.78 | 2.22 |

Appendix C

Scattered Field from a Reflector.

The far field of a reflector can also be obtained by considering the scattered field of the reflector. One method which is not too difficult to implement numerically is to calculate the currents induced on the surface of a reflector by an incident field. The reflector can be considered as being replaced by this pattern of induced currents and a far field for this calculated by integrating the induced current density over the current sheet. The far field of the system is obtained by considering the above far field together with that of any other sources, such as the feed and other reflectors in the system. The induced currents are obtained on the basis of geometrical optics. The incident field is assumed to have a poynting vector in the direction predicted by geometrical optics. It is assumed to be reflected as though an infinite plane wave is incident on an infinite plane. Because of this assumption the method is only true for a surface with a radius of curvature that is large compared to the wave length. It is also assumed that the reflector is in the far field of the feed and does not affect the radiation pattern of the feed. Currents behind the reflector are assumed to be zero. This method has been described by Silver (64), who applied it to point-source feeds and a line source with a cylindrical reflector. Rusch (65) (11) has applied the method to a hyperboloidal subreflector and has obtained good agreement with measurements.

Phillips (66) has used the method to obtain the scattered field of a Gregorian corrector for a spherical reflector. The formulations referred to above are each for one particular surface profile and describes the surface explicitly by using its equation. However, in general, shaped profiles which are of interest here cannot be described explicitly. What is required is a more general formulation where the reflector can be any arbitrary surface of revolution. In practice the solution of this on a computer is no more difficult than the previous cases as it is possible to describe any function numerically by interpolating between a given set of points.

Equations giving the scattered far field of such an arbitrarily shaped symmetrical reflector have been given by Claydon (24) and also by Rusch (54). Fig. C.1 shows the geometry of a feed-reflector system. The reflector is assumed to be a surface of revolution about the axis. Its profile can be described by the general polar equation,

$$P(\theta) = -\frac{1}{kq(\theta')} \text{ for } \theta_0 \leq \theta' \leq \pi \quad (C.1)$$

where $k = 2\pi/\lambda$

Rusch and Potter (11) have shown that if the field of the feed incident on the reflector is represented by the Fourier series

$$E_{inc} = \frac{e^{-jk\rho}}{\rho} \left\{ \sum_{m=1}^{\infty} (a_m(\theta') \sin m\phi' + b_m(\theta') \cos m\phi') a_{\theta'} + \sum_{m=1}^{\infty} (c_m(\theta') \sin m\phi' + d_m(\theta') \cos m\phi') a_{\phi'} \right\} \quad (C.2a)$$

$$H_{inc} = \frac{-1}{j\omega\mu} \nabla \times E_{inc} \quad (C.2b)$$

then the scattered field is given by

$$E_s = \frac{e^{-jkR}}{R} \left\{ \sum_m [f_m(\theta) \sin m\phi + g_m(\theta) \cos m\phi] a_{\theta} + \sum_m [h_m(\theta) \sin m\phi + k_m(\theta) \cos m\phi] a_{\phi} \right\} \quad (C.3)$$

where

$$f_m(\theta) = \left(-\frac{1}{2}\right)(j)^m \int_{\theta_0}^{\pi} \frac{d\theta' e^{-j\alpha \sin \theta'}}{[q(\theta')]^2} \left\{ a_m(\theta') [\cos \theta [g'(\theta') \sin \theta' - g(\theta') \cos \theta'] [J_{m-1}(\beta) - J_{m+1}(\beta)] - 2j [g'(\theta') \cos \theta' + g(\theta') \sin \theta'] \sin \theta J_m(\beta) \right. \\ \left. + d_m(\theta') [-g(\theta')] \cos \theta [J_{m-1}(\beta) + J_{m+1}(\beta)] \right\} \quad (C.4)$$

$$g_m(\theta) = -\left(\frac{1}{2}\right)(j)^m \int_{\theta_0}^{\pi} \frac{d\theta' e^{-j\alpha \sin \theta'}}{[q(\theta')]^2} \left\{ b_m(\theta') [\cos \theta [g'(\theta') \sin \theta' - g(\theta') \cos \theta'] [J_{m-1}(\beta) - J_{m+1}(\beta)] - 2j [g'(\theta') \cos \theta' + g(\theta') \sin \theta'] \sin \theta J_m(\beta) \right. \\ \left. + c_m(\theta') g(\theta') \cos \theta [J_{m-1}(\beta) + J_{m+1}(\beta)] \right\} \quad (C.5)$$

$$h_m(\theta) = \left(\frac{1}{2}\right) (j)^m \int_{\theta_0}^{\pi} \frac{d\theta' e^{-j\alpha \sin \theta'}}{g(\theta')^2} \left\{ b_m(\theta') \right.$$

$$\left[g'(\theta') \sin \theta' - g(\theta') \cos \theta' \right] \left[J_{m-1}(\beta) + J_{m+1}(\beta) \right] + c_m(\theta') - \cancel{(\theta') g(\theta')} \left[J_{m-1}(\beta) - J_{m+1}(\beta) \right] \} \quad (C.6)$$

$$k_m(\theta) = - \left(\frac{1}{2}\right) (j)^m \int_{\theta_0}^{\pi} \frac{d\theta' e^{-j\alpha \sin \theta'}}{g(\theta')^2} \left\{ a_m(\theta') \right.$$

$$\left[g'(\theta') \sin \theta' - g(\theta') \cos \theta' \right] \left[J_{m-1}(\beta) + J_{m+1}(\beta) \right] - d_m(\theta') g(\theta') \left[J_{m-1}(\beta) - J_{m+1}(\beta) \right] \} \quad (C.7)$$

In the case of a linearly polarized feed the azimuthal dependence is $m = 1$. If the feed is circularly symmetric it can be represented by

$$E_{inc}(\theta', \phi') = A(\theta') \frac{e^{ikR}}{R} E(\theta', \phi') \quad (C.8)$$

In this case the scattered H-plane and E-plane fields are given respectively by:

$$\sqrt{(R_\phi^2 + I_\phi^2)} \quad \text{and} \quad \sqrt{(R_\theta^2 + I_\theta^2)}$$

where

$$R_\phi = 1/2 \int_{\theta_1}^{\theta_2} I_1 \sin \alpha d\theta' \quad (C.9)$$

$$I_\phi = A(\theta') + 1/2 \int_{\theta_1}^{\theta_2} I_1 \cos \alpha d\theta' \quad (C.10)$$

$$R_\theta = 1/2 \int_{\theta_1}^{\theta_2} (I_2 \cos \alpha - I_3 \sin \alpha) d\theta' \quad (C.11)$$

$$I_\theta = A(\theta') + 1/2 \int_{\theta_1}^{\theta_2} (I_2 \sin \alpha + I_3 \cos \alpha) d\theta' \quad (C.12)$$

and

$$I_1 = \frac{A(\theta') \sin \theta'}{[g(\theta')]^2} \left\{ g(\theta') [J_0(\beta) - J_2(\beta)] \right. \\ \left. + [g'(\theta') \sin \theta' - g(\theta') \cos \theta'] [J_2(\beta) + J_2'(\beta)] \right\} \quad (C.13)$$

$$I_2 = \frac{A(\theta') \sin \theta'}{[g(\theta')]^2} \left\{ \cos \theta [(1 + \cos \theta') g(\theta') - \sin \theta' g'(\theta')] \right. \\ \left. \times [J_0(\beta) - J_2(\beta)] - 2 \cos \theta g(\theta') J_0(\beta) \right\} \quad (C.14)$$

$$I_3 = \frac{A(\theta') \sin \theta'}{[g(\theta')]^2} \left\{ 2 \sin \theta [\sin \theta' g(\theta') \right. \\ \left. + \cos \theta' g'(\theta')] \times J_1(\beta) \right\} \quad (C.15)$$

$$\alpha = \frac{\cos \theta' \cos \theta - 1}{g(\theta')} \quad (C.16)$$

$$\beta = - \frac{\sin \theta \sin \theta'}{g(\theta')} \quad (C.17)$$

For arbitrary surfaces of revolution such as those of sub-reflectors of shaped systems, $\rho(\theta)$ is specified by points. This is related to $g(\theta')$ by equation (C.1) and a numerical interpolation was used to specify $g(\theta')$. Many surfaces can of course be specified in close form.

For a paraboloid of focal length f

$$g(\theta') = \frac{1 - \cos \theta'}{2kf} \quad (\text{C.18})$$

For a hyperboloid or ellipsoid of eccentricity e and distance p between the foci

$$g(\theta') = \frac{(1 + e \cos \theta')}{kep} \quad (\text{C.19})$$

For a cone of external half-angle β and distance b between feed phase centre and vertex

$$g(\theta') = \frac{\cos \theta' + \cot \beta \sin \theta'}{kb} \quad (\text{C.20})$$

APPENDIX D TEMPERATURE EFFECTS OF 8m ANTENNA

In order to assess the effect of temperature on the Andrew 8m antenna the thermal deformation analysis given below was performed.

D.1 Thermal Deformation Analysis- Model Description

A quarter symmetry structural model is shown in Figure D.1. The model comprises three 30° petals (each made up of 3 curved shell elements). Connected to a web of steel trusses by short beams which represent the connecting/adjusting bolts.

The petal structure includes the stiffening members and is representative in cross sectional area and bending stiffness of the actual petal.

The shell and truss geometry accurately represents the actual antenna in sectional view. A few diagonal members present in practice, would not permit 1/4 symmetry and since these would have little additional effect, have been omitted.

Each petal is constrained by six beams connecting it to the back structure, the beams having a stiffness representative of the adjusting bolts. This is important since it governs the interaction between the steel and aluminum masses. Two members of the quadrupod supporting the sub-reflector, complete the structure. Constraints necessary to create 1/4 symmetry are added to the radial boundaries.

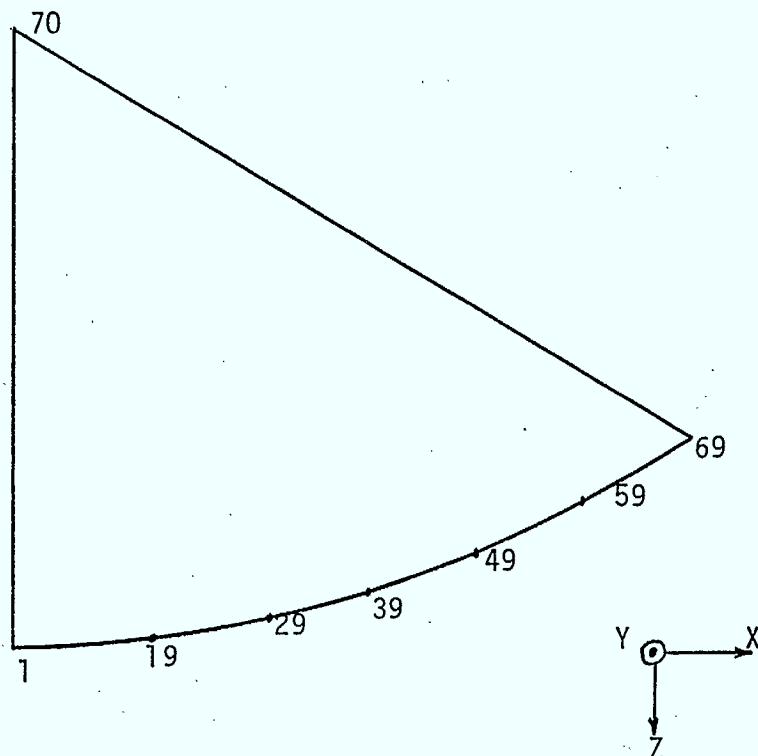
D.2 Load Cases

Two load cases have been examined.

- a) Air temperature cooling of 20°C
- b) Temperature differential between reflector and back-structure. The backstructure was cooled 10°C.

The computer model was run using the ASAS finite element program which gives displacements or reactions at each node and stresses in each element.

GEOMETRY OF A SECTION



| Node | X | Z |
|------|-------|--------|
| 1 | 0 | 0 |
| 19 | 32.5 | -2.35 |
| 29 | 65.0 | -9.39 |
| 39 | 85.0 | -16.05 |
| 49 | 105.0 | -24.49 |
| 59 | 126.0 | -35.27 |
| 69 | 147.0 | -48.0 |
| 70 | 0 | -131.5 |

Load Case Results

DISPLACEMENTS:

| NODE | ALL NODES -20°C | | STEEL -10°C | |
|------|-----------------|--------|-------------|---------|
| | X | Z | X | Z |
| 1 | 0 | 0 | 0 | 0 |
| 19 | -.01446 | .00264 | -.00041 | -.00092 |
| 29 | -.02715 | .01496 | -.00177 | -.00571 |
| 39 | -.03561 | .01951 | -.00219 | -.00646 |
| 49 | -.04384 | .02512 | -.00275 | -.00739 |
| 59 | -.05159 | .03387 | -.00368 | -.00906 |
| 69 | -.06090 | .03997 | -.00416 | -.00969 |
| 70 | 0 | .04280 | 0 | -.01017 |

APPENDIX E DIELGUIDE PARABOLOID SYSTEM

The profile of the subreflector can be obtained by using a ray optics analysis. In Fig. E.1 a spherical wave represented by AB is assumed to emerge from the cone apex.

It is reflected by the subreflector at B and suffers refraction at the dielguide surface at C. The subreflector is shaped to ensure that it emerges as a spherical wave (CD) that appears to originate from the paraboloid focus. Equations E.1 to E.3 are obtained by applying Snell's laws of reflection and refraction at the two reflector surfaces and at the dielguide-air interface while applying the conditions given above. The geometry and symbols are given by Fig. E.1

$$\frac{dr}{d\beta} = r \tan \frac{(\theta + \beta + \delta)}{2} \cdot \frac{d\theta}{d\beta} \quad (E.1)$$

$$(\theta + \beta + \delta) = \sin^{-1} \left[\frac{P}{r} \left(\frac{\tan \beta}{\sec(\beta + \delta)} \right) \times \left(\frac{\tan(\beta + \delta) + \tan \theta_{dmax}}{\tan \delta + \tan \theta_{dmax}} \right) \right] \quad (E.2)$$

$$= \cos^{-1} \left\{ \frac{\cos(\theta_{dmax} + \beta)}{e^{\frac{1}{2}}} \right\} \quad (E.3)$$

From power considerations it is possible to obtain the paraboloidal aperture distribution $P(\beta)$ in terms of the dielguide-feed distribution $F(\theta)$ which is given in equation below,

$$P(\beta) = \frac{F(\theta) \sin \theta \sin^3 \beta}{(1 - \cos \beta)^2} \cdot \frac{d\theta}{d\beta} \quad (E.4)$$

Reference

- (1) CCIR Recommendations 465-1 (Rev. 1974),
"Reference Earth Station Radiation Pattern for use in
Co-ordination and Interference assessment in the Frequency
Range from 2 to about 10 GHz"
- (2) CCIR Report 391-3 (Rev. 1978),
"Radiation Diagrams of Antenna for Earth Stations in the Fixed
Satellite Service for use in interference studies and for the
determination of a Design Objective."
- (3) Intelsat Documents BG-28-72 (Standard A Stations); BG-28-73
(Standard C Stations); BG-28-74 (Standard B Stations).
- (4) FCC Rules and Regulations, paragraphs 25-209
"Antenna Performance Standards",
- (5) CCIR Document 4/308-E, Intelsat, "Draft Reports 391-3
(MODI) and 555-1 (MODI)." June 1981.
- (6) Green, K.A. "Modified Cassegrain
Antenna For Arbitrary Aperture
Illumination"-AP-11 September 1963,
pp. 589-590.
- (7) Galindo, V. "Design of Dual-Reflector Antenna with
Arbitrary Phase and Amplitude
Distributions", IEEE Transactions on
Antennas and Propagation, Vol. AP-12,
No.4 (July 1964), pp. 403-408.
- (8) Dunbar, A.S. "Calculations of doubly curved
Reflectors for shaped Beams" Proc IRE
Vol 36 pp 1280-1296 Oct 1948.
- (9) Williams, W.F. "High Efficiency Antenna Reflector",
The Microwave Journal Vol. 8, No. 7,
(July 1965), pp. 79-82.

- (10) Wood, P.J. "Spherical Waves in Antenna Problems", Marconi Review, (1971), 182, pp. 149-172.
- (11) Rusch, W.V.T. and Potter, P.D., "Analysis of Reflector Antennas", Academic Press, 1970
- (12) Elliot and Poulton "Diffraction Optimised Shaped-Beam Reflector Antenna", Electronics Letters, Vol. 13 No 11 May 1977.
- (13) Dolph, C.L. "A current Distribution for broadside arrays which optimizes the relationship between beamwidth and sidelobe level", Proc IRE Vol 34 p 335-345 June 1946.
- (14) Taylor, T.T. (1955). "Design of line-source antennas for narrow beamwidth and low side-lobes." IRE Trans. Antennas Propagation 3, 16-28.
- (15) Wheeler, H.A. "Antenna patterns which retain shape with beam defocussing" IRE Trans AP10 pp 573-580 1962.
- (16) Rudduck, R.C. "Directive Gain of Circular Taylor Patterns", NASA-CR-66850, Aug. 1979.
- (17) Taylor, T.T. "Design of Circular Apertures for Narrow Beamwidth and Low Sidelobes", IRE Trans. AP-8 pp. 17-48 January '60.
- (18) A.C. Ludwig. "The definition of cross-polarization," "IEEE Trans. Antennas Propagat, vol. AP-21, pp.116-119, Jan. 1973.

- (19) Safak, M and Delogne P.P. "Cross polarization in Cassegrainian and front-fed paraboloidal antennas" IEE Trans. Ap-24 p 497-501 July 1976.
- (20) P.J. Wood, Depolarisation with Cassegrainian and front-fed reflectors, "Electronics Letters, vol. 3. pp. 181-183, 3rd May 1973.
- (21) Thomas, B., "Cross-polarization Characteristics of axially symmetric Reflectors", Electron Lett. Vol 12 pp. 218-219 Apr 1976.
- (22) Watson and Ghobrial, "Off-axis polarisation characteristics of Cassegrainian and front-fed paraboloidal antennas," IEEE Trans. Antennas Propagat., vol. AP-20 pp. 691-698, 1972.
- (23) Chn, T, Turrin, R.H. "Depolarization Properties of Offset Reflector Antennas", Ap-21 pp. 309-345, May 1973.
- (24) Dijk, J et al, "The polarization losses of offset Paraboloid Antennas", AP-22 pp. 513-520 July 1974.
- (25) Rusch, W.T, "Double Aperture Blocking by Two Wavelength-sized Feed-support Struts", Elect Lett. Vol 10, No 15, pp. 295-6 July 74.
- (26) Janky, J.M. et al "New Sidelobe Envelopes for small aperture Earth Stations", IEEE Trans. BC-22, No. 2, pp. 39-44, June '76.

- (27) EIA. The electrical and mechanical characteristics of antennas for satellite earth stations" EIA standard RS-411, 1973.
- (28) Poutlon G.T., Lim., S.H. and Masterman, P.H. "Calculation of Input-Voltage Standing-Wave Ratio for a Reflector Antenna", Electronics Letters, Vol. 8 No. 25 (14th Dec. 1972).
- (29) Hu, YY "A method of Determining Phase Centres and its Application to electromagnetic Horns", Franklin Inst. Journal pp31-39 Jan 1961.
- (30) Ohtera, I and Hiroshi,U "Nomographs for Phase Centres of Conical Corrugated and TE₁₁ Mode Horns", AP-23 pp 858-9 Nov. 1975.
- (31) Cheng, D.K. "Effect of Arbitrary Phase Errors on Gain and Beamwidth Characteristics of Radiation Pattern "IRE Trans AP3 pp 145-147 July 1955.
- (32) Ingerson, P.G. and Rusch, W.T. "Radiation from a paraboloid with an axially defocus Feed", IEEE Trans AP21 pp 104-105 Jan. 1973.

- (33) M. Landry and Y.Chasse "Measurement of electromagnetic field intensity in focal region of wide-angle paraboloid reflector." IEEE Trans. AP-19, pp. 539-543, July 1971.
- (34) Cogdell, J.R. and Davis, J.H. "Astigmatism in Reflector Antennas", IEEE Trans AP21 pp 565-567 July 1973.
- (35) Von Hoerner, S and Wong W.Y. "Gravitational Deformation and Astigmatism of Tilttable Radio Telescopes" IEEE Trans AP23 pp 689-695 Sept. 1975.
- (36) Jones, R.T. "Coma of modified Gregorian and Cassegrainian mirror systems" -J. Opt. Soc. Am. 44 p630-633, 1954.
- (37) Kelleher, K.S. and Coleman, H.P. "Off axis characteristics of paraboloid reflectors" Navel Research Labs Rp 4088 Dec. 1952.
- (38) Imbraile, W.A. et.al "Large lateral feed displacements in a parabolic reflector", IEE Trans. AP-22 p 742-745 Nov. 1974.

- (39) Ruze, J. "Lateral feed Displacement in a paraboloid" - IEE Tran Ap-13, p 660-665, 1965.
- (40) Ruze, J. "Antenna Tolerance Theory - A. Review", Proc. IEEE, Vol. 54, No. 4, April 1966.
- (41) Simmons, A.J. and Kay, A.F. "The Scalar Feed - A High Performance Feed for Large Paraboloid Antenna", IEE Conference Publication, 21, (1968), pp. 213-217.
- (42) Jansen, J.K.M. et al "The Scalar Feed" A.E.C. Band 26 (1972), Helt I, pp. 22-30
- (43) Clarricoats, P.J.B., and Saha, P.K. "Propagation and Radiation Behaviour of Corrugated Feeds", Parts 1 and 11, Proceedings of the IEEE, Vol. 118, No. 9 (October 1971), pp. 1167-1177 and 1178-1186.
- (44) Clarricoats, P.J.B. and Seng, L.M. "Influence of Horn Length on Radiation Pattern of Obligue-flare-angle Corrugated Horn; Electronics Letters Vol. 9, No. 1 (11/Jan. 1973) pp. 15-16.

- (45) Hockham, G.A. "Investigation of a 90° Corrugated Horn", Electronics Letters Vol. 12, No. 8 (15/April, 1976), pp. 199-200.
- (46) Dragone, C. "Reflection, Transmission and Mode conversion in a Corrugated Feed", BSTJ Vol 56 No6 pp 835-867 Aug. 1977.
- (47) Terzuoli, A.J. et al "Shielding Effectiveness of Corrugations in Corrugated Feeds", IEEE Trans. AP26 No 5 pp. 654-8 Sept. 1978.
- (48) Silver, S. "Microwave Antenna Theory and Design", Vol. 12 MIT Radiation Lab. Series, McGraw Hill, New York 1949.
- (49) Potter, P.D. "New Horn Antenna with Suppressed Sidelobes" - Microwave J. Vol. 6 June 1963, pp. 71-78.
- (50) Foldes, P. "A New Earth Station Antenna for Domestic Satellite Communications RCA Review Vol. 33 pp. 695-727, Dec. 1972.
- (51) Gruner, R.W. "A 4 and 6 GHz. Prime Focus, CP Feed with Circular Pattern Symetry" -AP-S 1975 Symp.
- (52) Turrin, R.H. "Dual Mode Small-Aperture Antenna", AP-15, March '67, pp. 307-308.

- (53) Andrew Antenna Co.Ltd. Corrugated Feed used on a 4/6 GHz 26' ESA.
- (54) Andrew Antenna Co.Ltd. Corrugated Feed used on 12/14 GHz 8m ESA.
- (55) Cowan, J.H. 'Dual-Band Reflector-feed Element for Frequency Re-use Applications', Electronics Letters, Vol. 9, No. 25 (13/Dec, 1973), pp. 596-597.
- (56) S. von Hoerner J. Struct Div. Proc. Amer. Soc. Civil Eng., vol. 93, pp. 461-485, 1967
- (57) J.W. Findlay and S. von Hoerner, "A 65-m telescope for millimeter wavelength, "National Radio Astron. Obs., Charlottesville, VA., 1972.
- (58) Hogg, D.C. and Semplak, R.A. "An Experimental Study of Near-Field Cassegrainian Antennas;" Bell Sys. Tech. Jour., Vol. 43, 2677-2704. 1964.
- (59) Dragone C. and Hogg D.C. "The Radiation Pattern and Impedance of Offset and Symmetrical Near-Field Cassegrainian and Gregorian Antennas", IEEE Trans AP 22 pp 472-475 May 1974.

- (60) Bartlett, H.E., and Moseley, R.E. "Dielguides.- Highly Efficient Low Noise Antenna Feeds", Microwave Journal, Vol. 9, (1966), pp. 53-58
- (61) Salema, C.E.R.C. "Theory and Design of Dielectric Cone Antennas", Ph. D. Thesis, University of London, (Sept. 1972).
- (62) Clarricoats, P.J.B. and Salema, C.E.R.C. "Propagation and Radiation Characteristics of Low Permittivity Dielectric Cones", Electronics Letters, Vol. 7, No. 17, (26th August 1971), pp. 483-485.
- (63) Clarricoats, P.J.B., Salema, C.E.R.C., and Lim S.H. "Design of Cassegrain Antennas employing Dielectric Cone Feeds", Electronics Letters, Vol. 8, No. 15, (27th July 1972), pp. 384-385.
- (64) Silver, S. "Microwave Antenna Theory and Design", Vol. 12 MIT Radiation Lab. Series, McGraw Hill New York 1949.
- (65) Rusch, W.V.T "Scattering from a Hyperboloid Reflector in A Cassegrainian feed system", PTGAP Transactions July 1963.
- (66) Phillips, C.J.E. "The Theoretical Performance of Spherical Reflectors with Gregorian Correctors and Scalar Feeds", Queen Mary College (London), Research Report No. 006/1969.



ANDREW

PE

Approved

PATTERN ENVELOPE

ANTENNA TYPE NUMBER

Gain: GHz
dBi at GHz
15 dB BEAMWIDTH: DEGREES

ANTENNA DIRECTIVITY - dBi

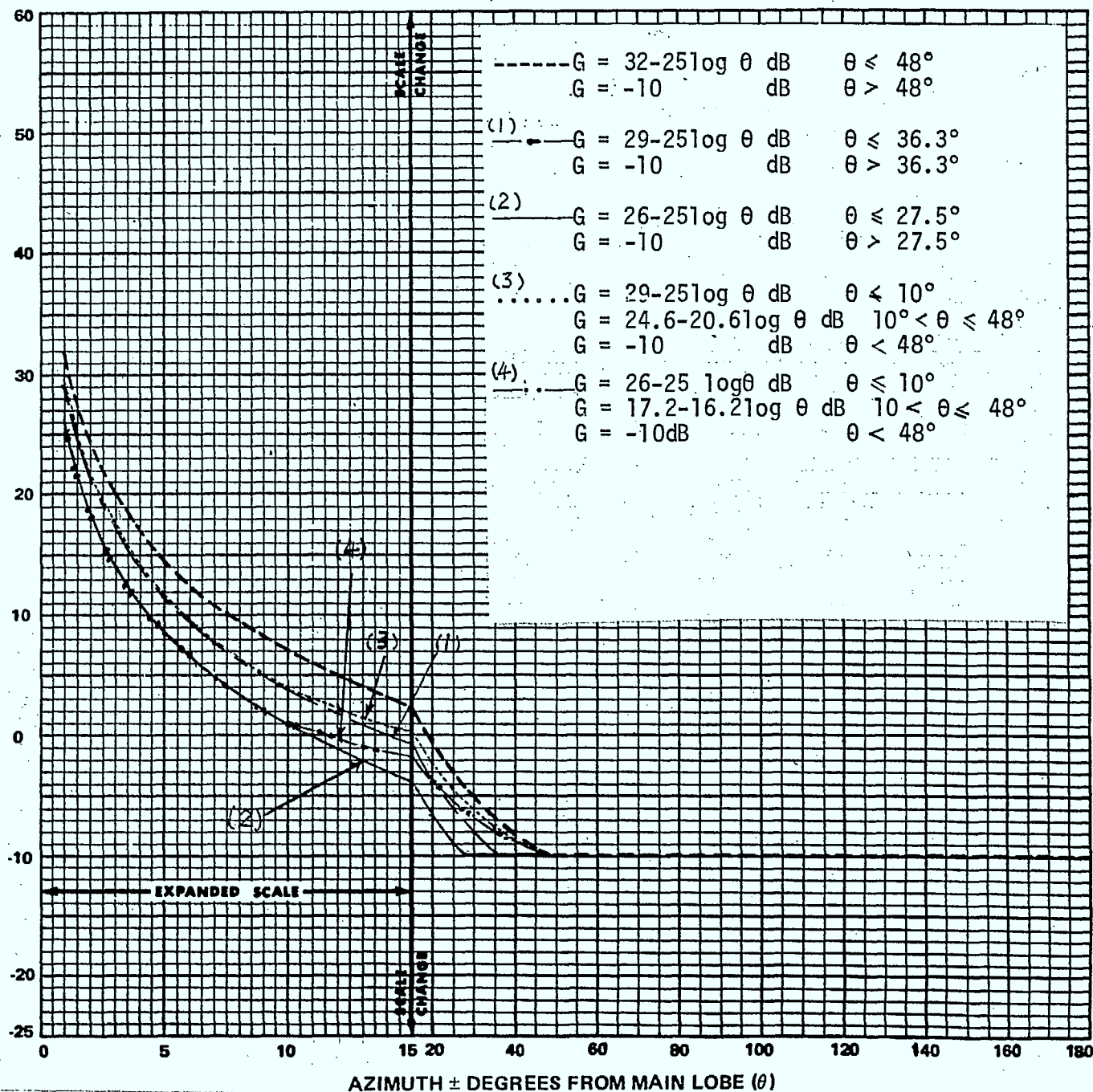
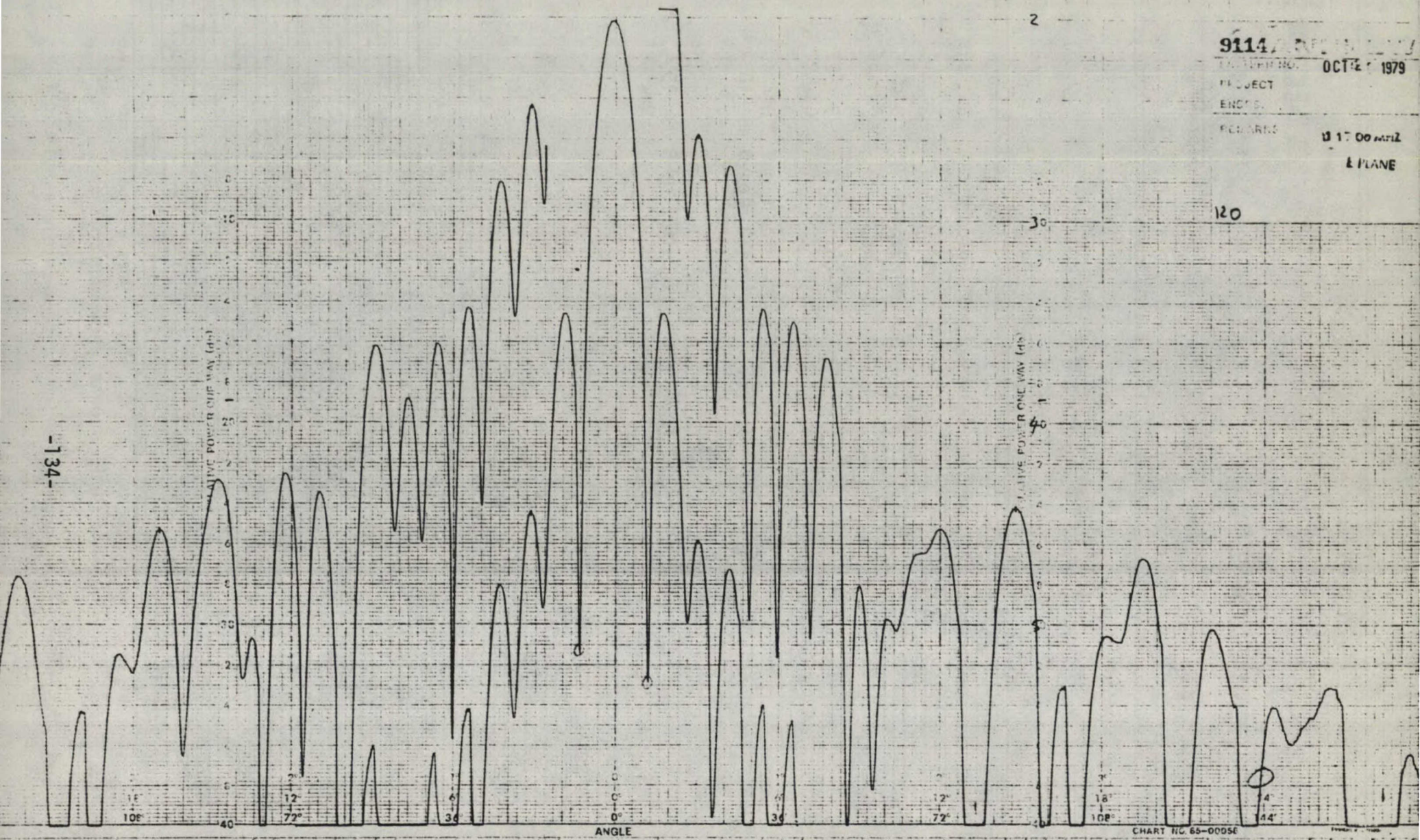
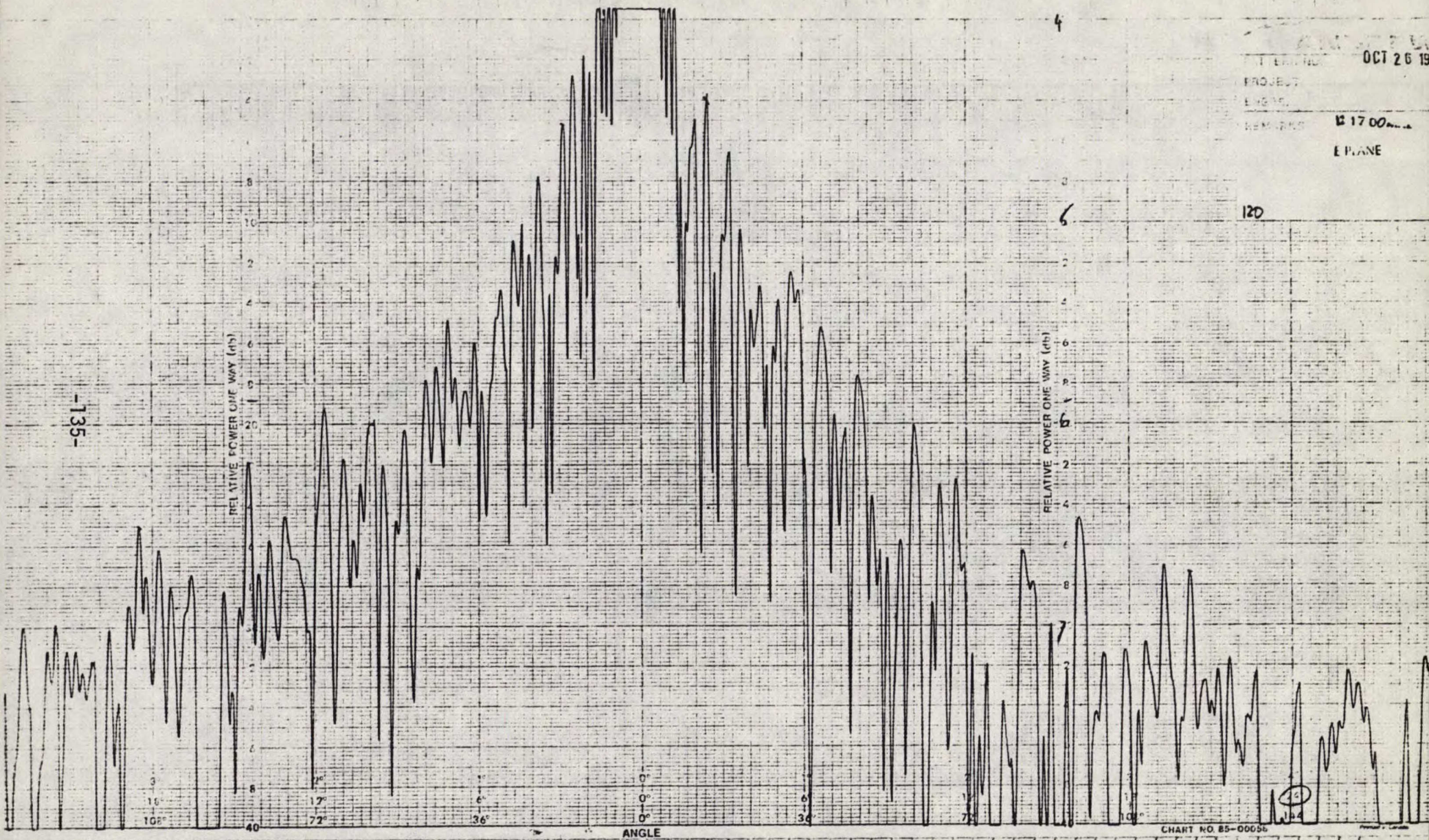


Figure 1.1

Proposed Radiation Pattern Envelopes (1) to (4)





-136-

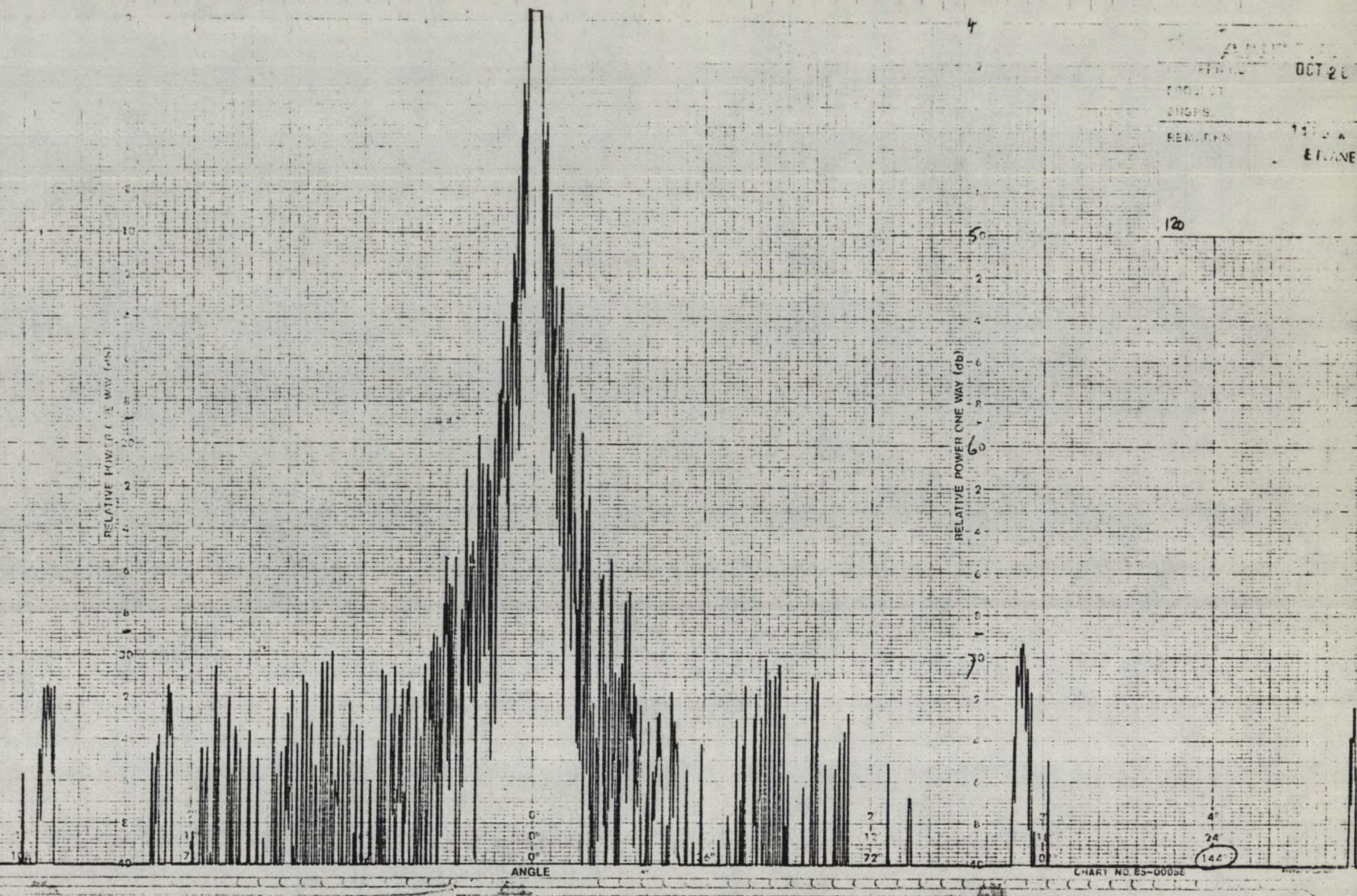


Figure 2.1(c) Typical radiation pattern for $-180^\circ < \theta < 180^\circ$

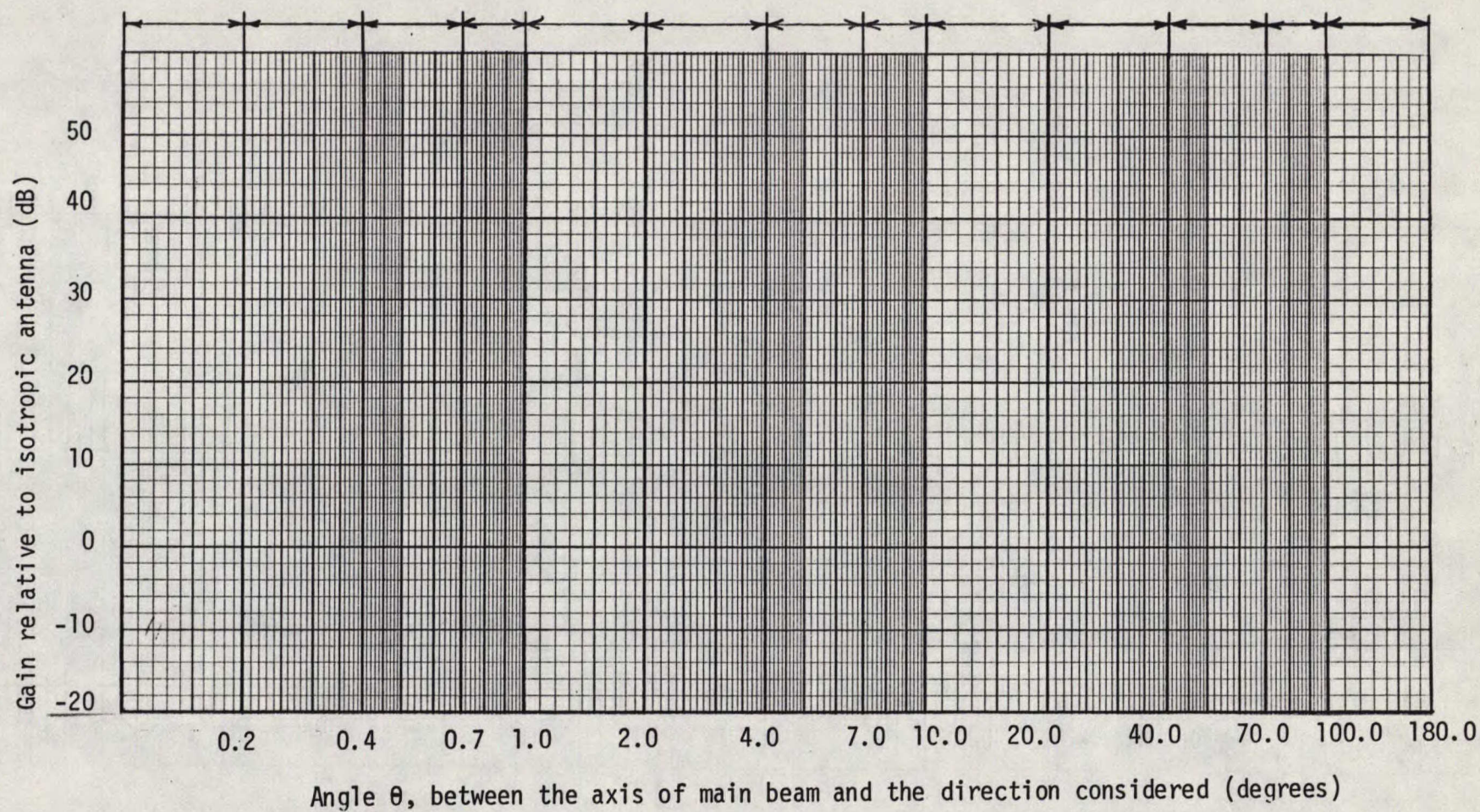


Figure 2.2 An example of the CCIR window boundaries

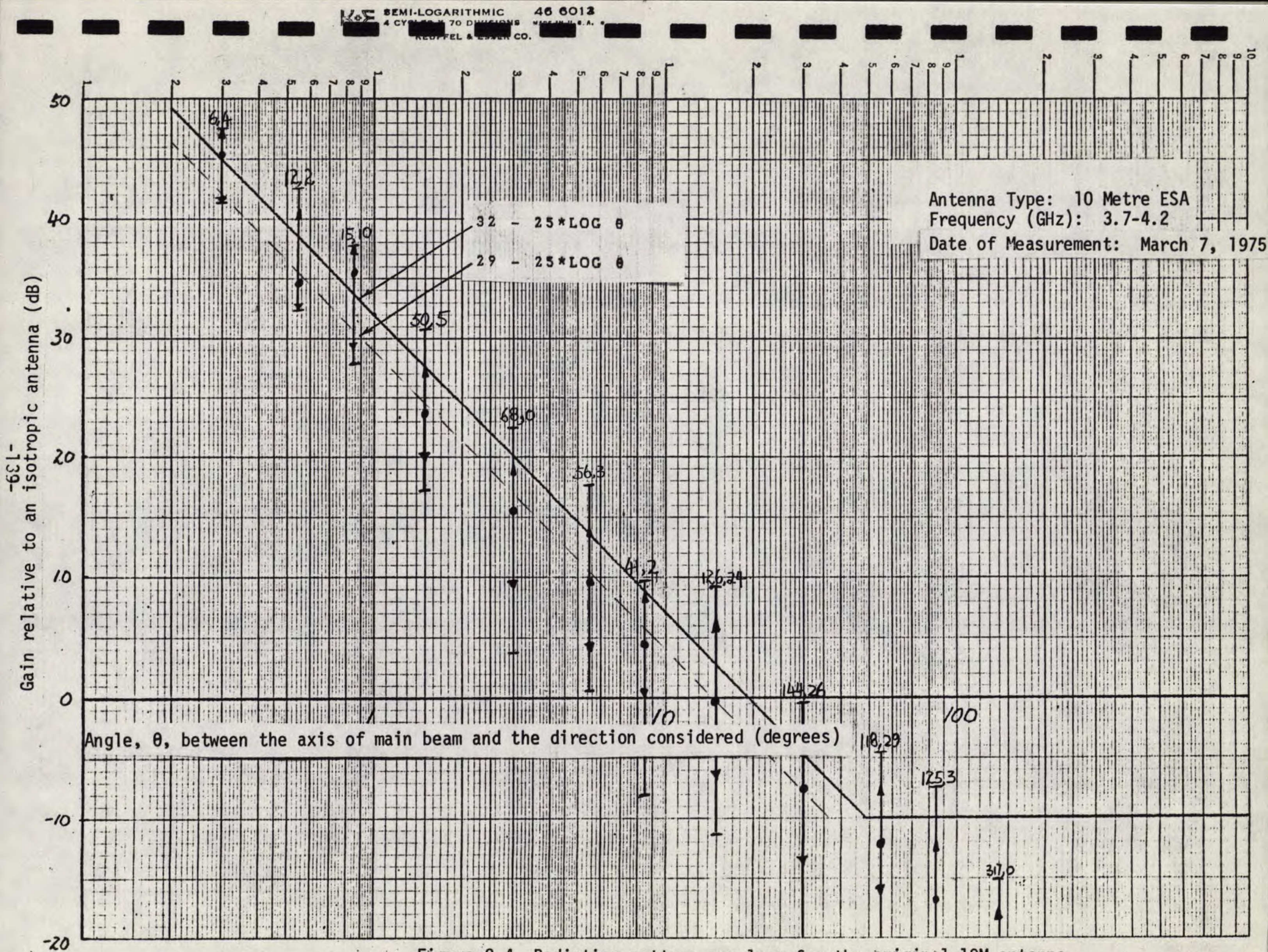


Figure 2.4 Radiation pattern envelope for the original 10M antenna

Gain relative to the 32-25logθ level (dB)

-140-

-10

-20

Antenna Type: 10 Metre ESA
Frequency (GHz): 3.7-4.2
Date of Measurement: March 7, 1975

Angle, θ , between the axis of main beam and the direction considered (degrees)

6.4

12.2

15.10

52.5

63.0

56.3

46.2

126.24

144.26

118.29

125.3

37.0

10

100

Figure 2.5 Radiation pattern envelope for the original 10M antenna with reference to the 32-25 logθ level

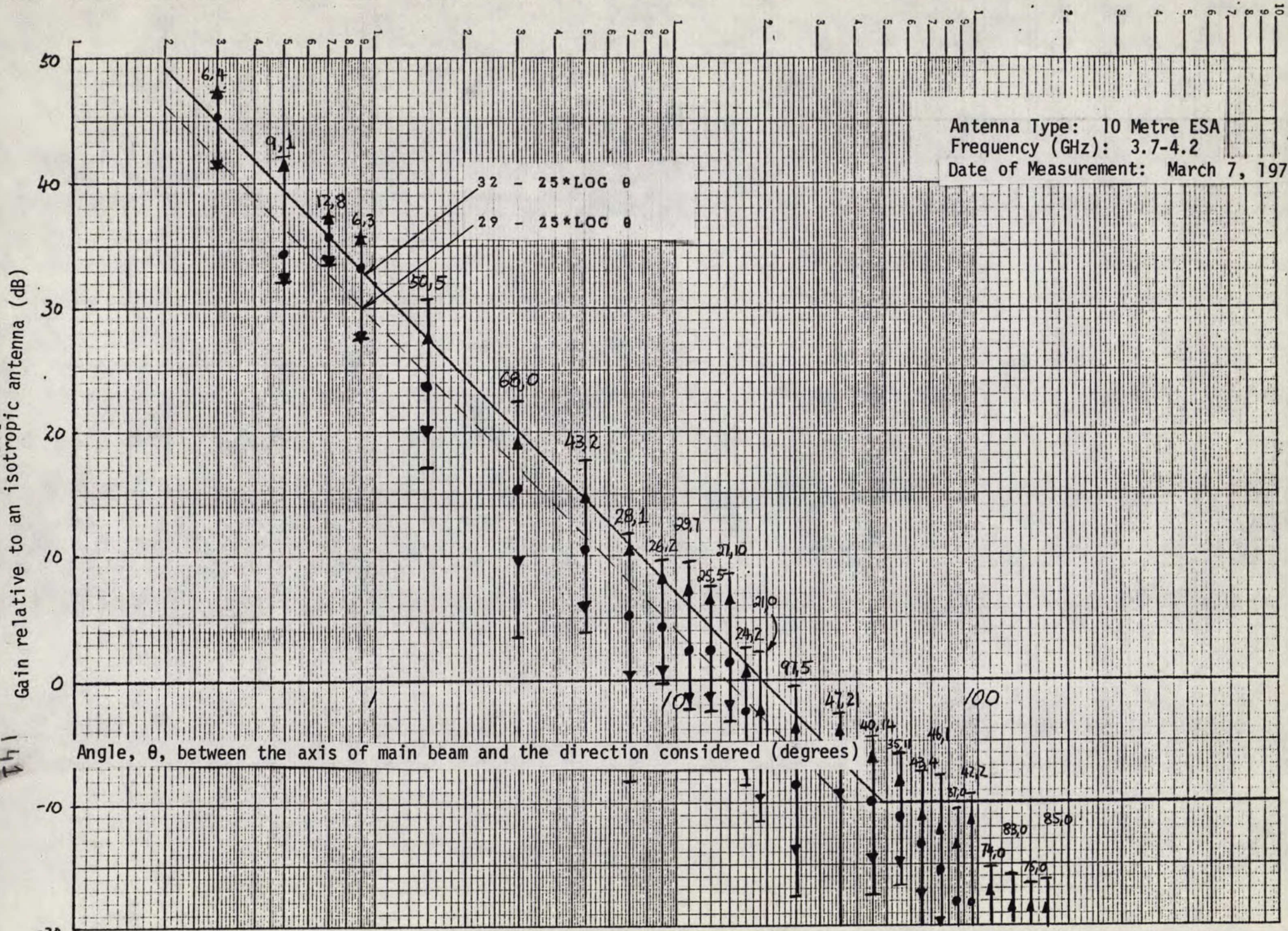


Figure 2.6 Radiation pattern envelope for the original 10M antenna

Gain relative to an isotropic antenna (dB)

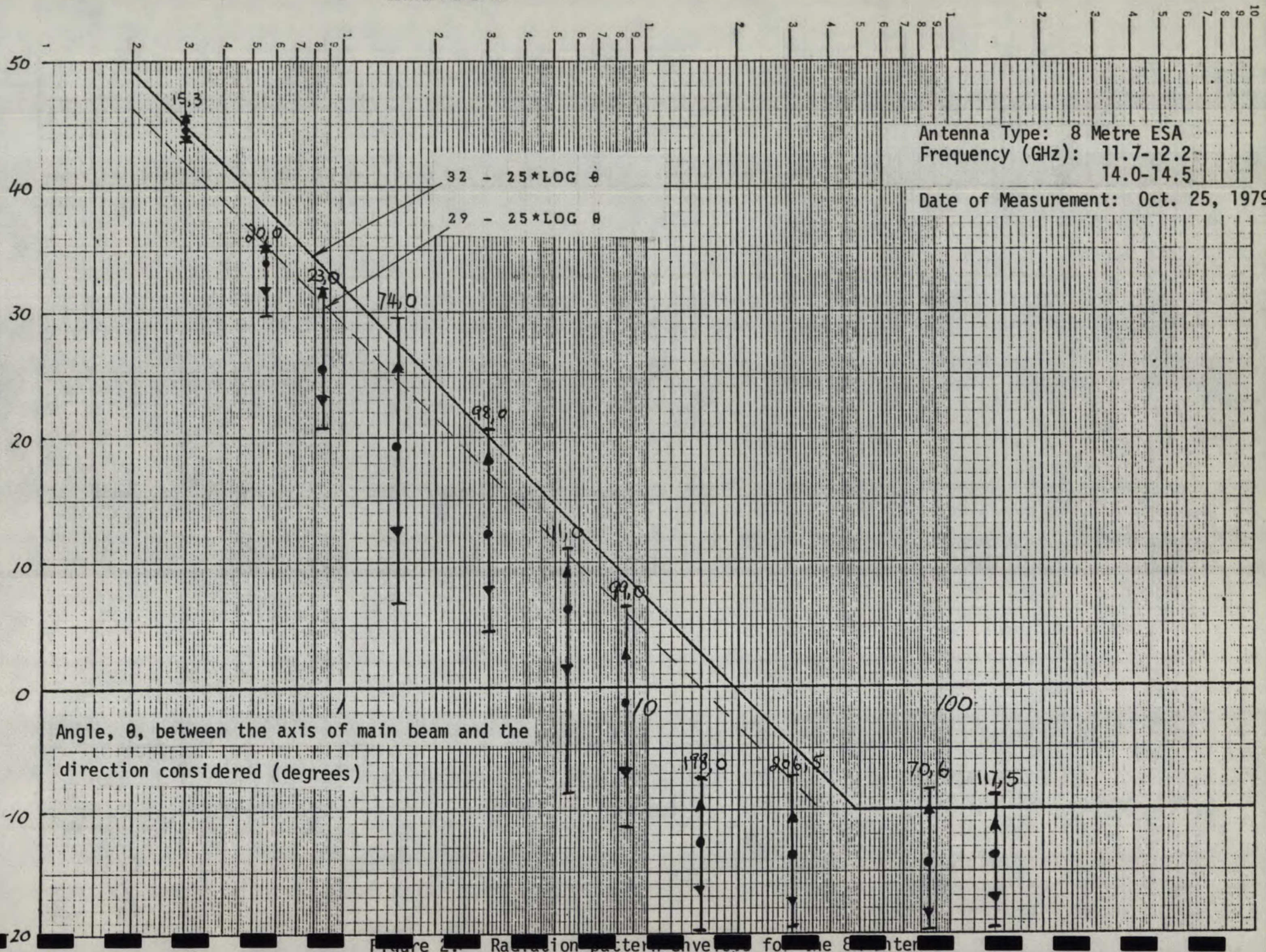


Figure 2. Radiation pattern envelope for the 8 Metre antenna

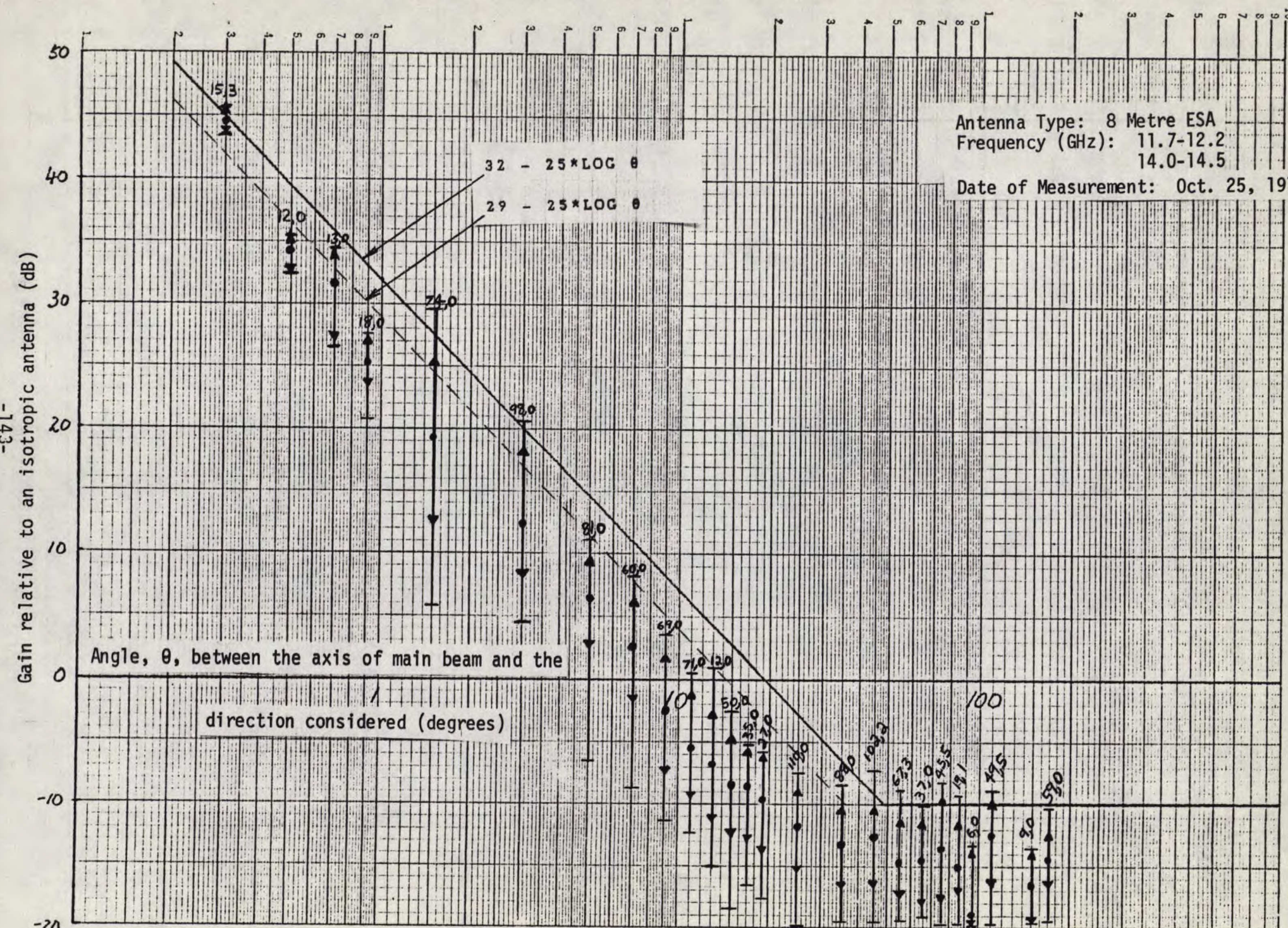


Figure 2.8 Radiation pattern envelope for the 8M antenna

Gain relative to an isotropic antenna (dB)

Antenna Type: 8 Metre ESA
 Frequency (GHz): 11.7, 12.2
 Date of Measurement: Oct. 25, 1979

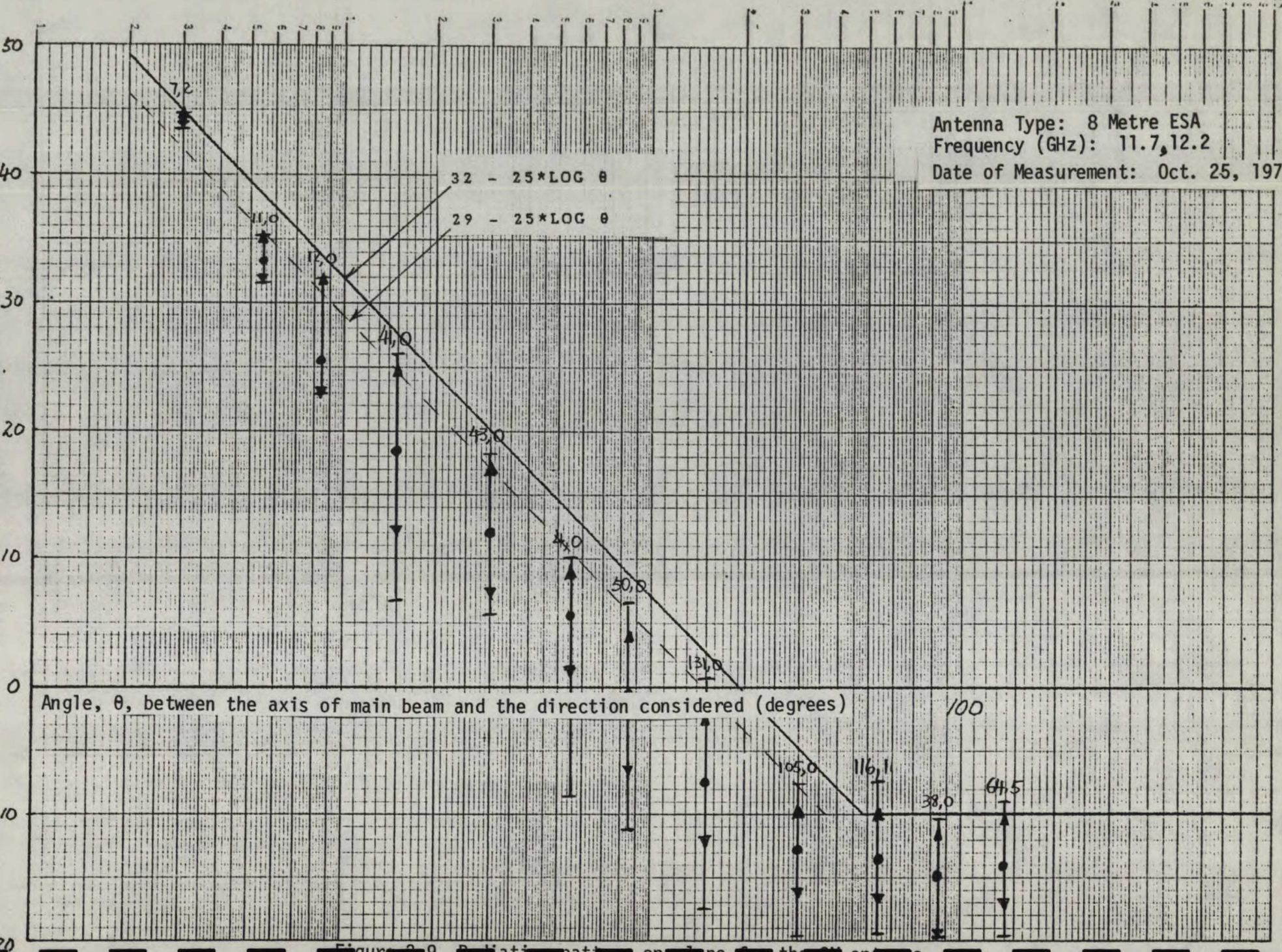


Figure 2.9 Radiation pattern envelope of the antenna

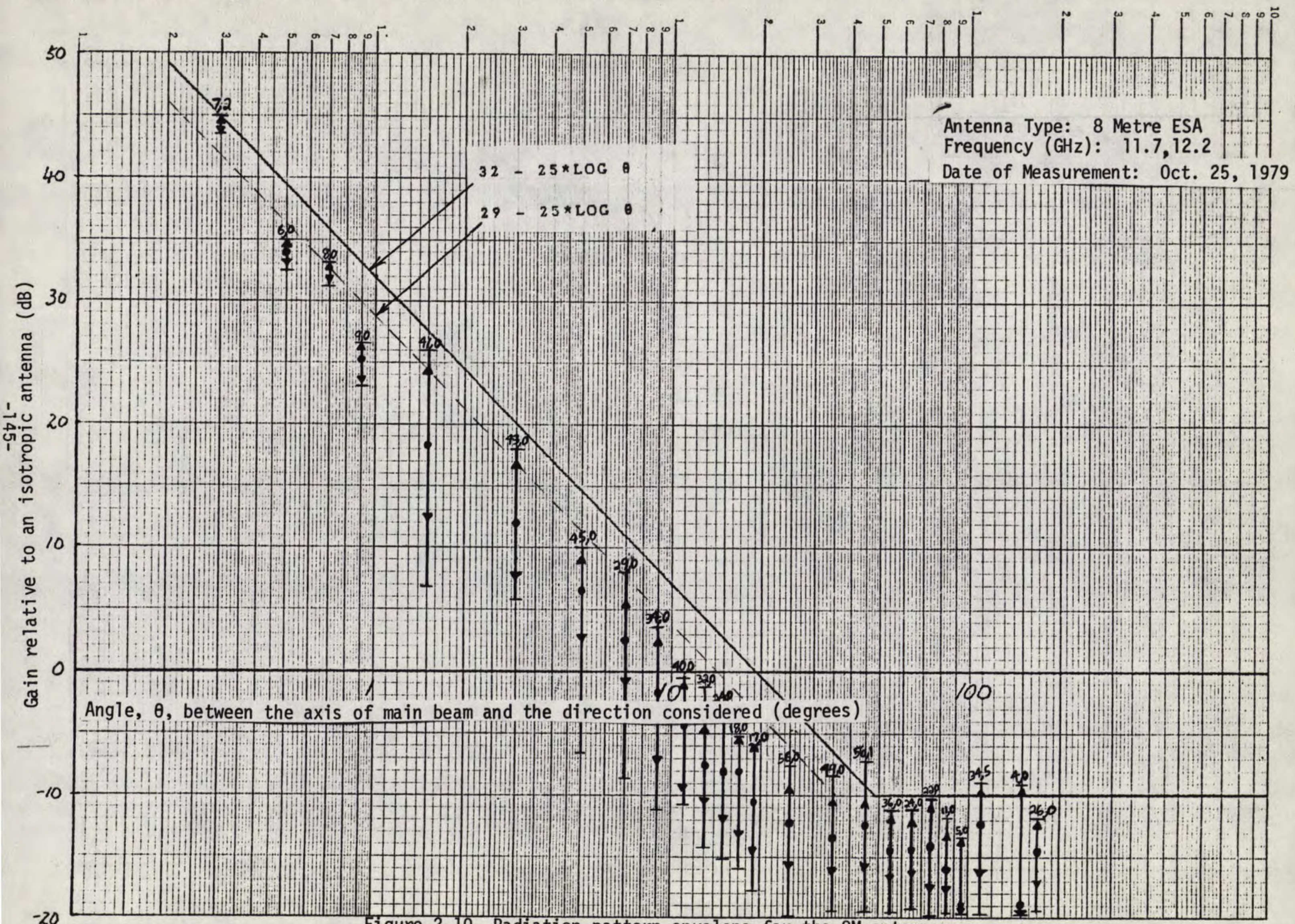


Figure 2.10 Radiation pattern envelope for the 8M antenna

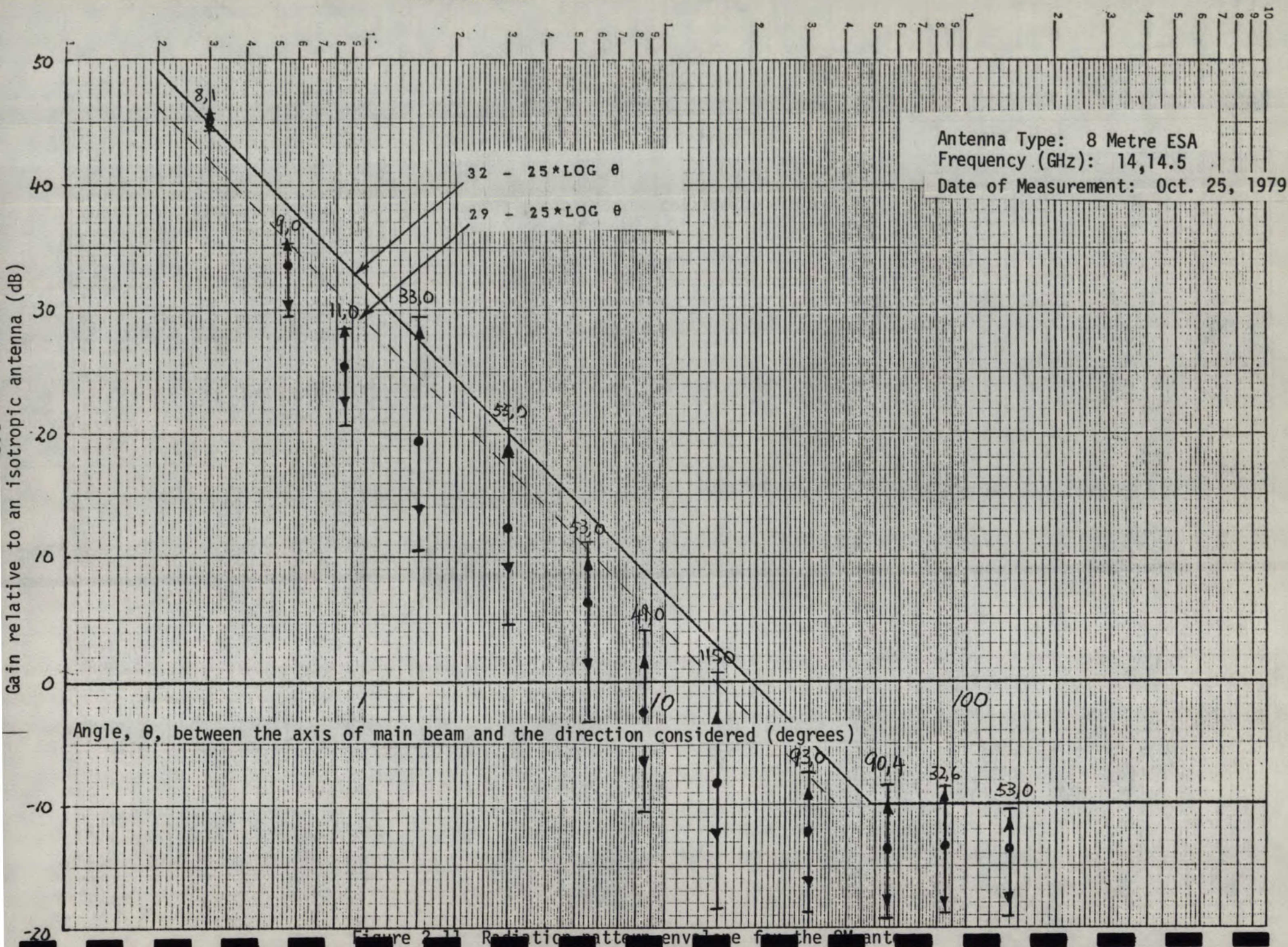


Figure 2-11 Radiation pattern envelope for the 8M ant

Antenna Type: 8 Metre ESA
Frequency (GHz): 14, 14.5
Date of Measurement: Oct. 25, 1979

Gain relative to an isotropic antenna (dB)

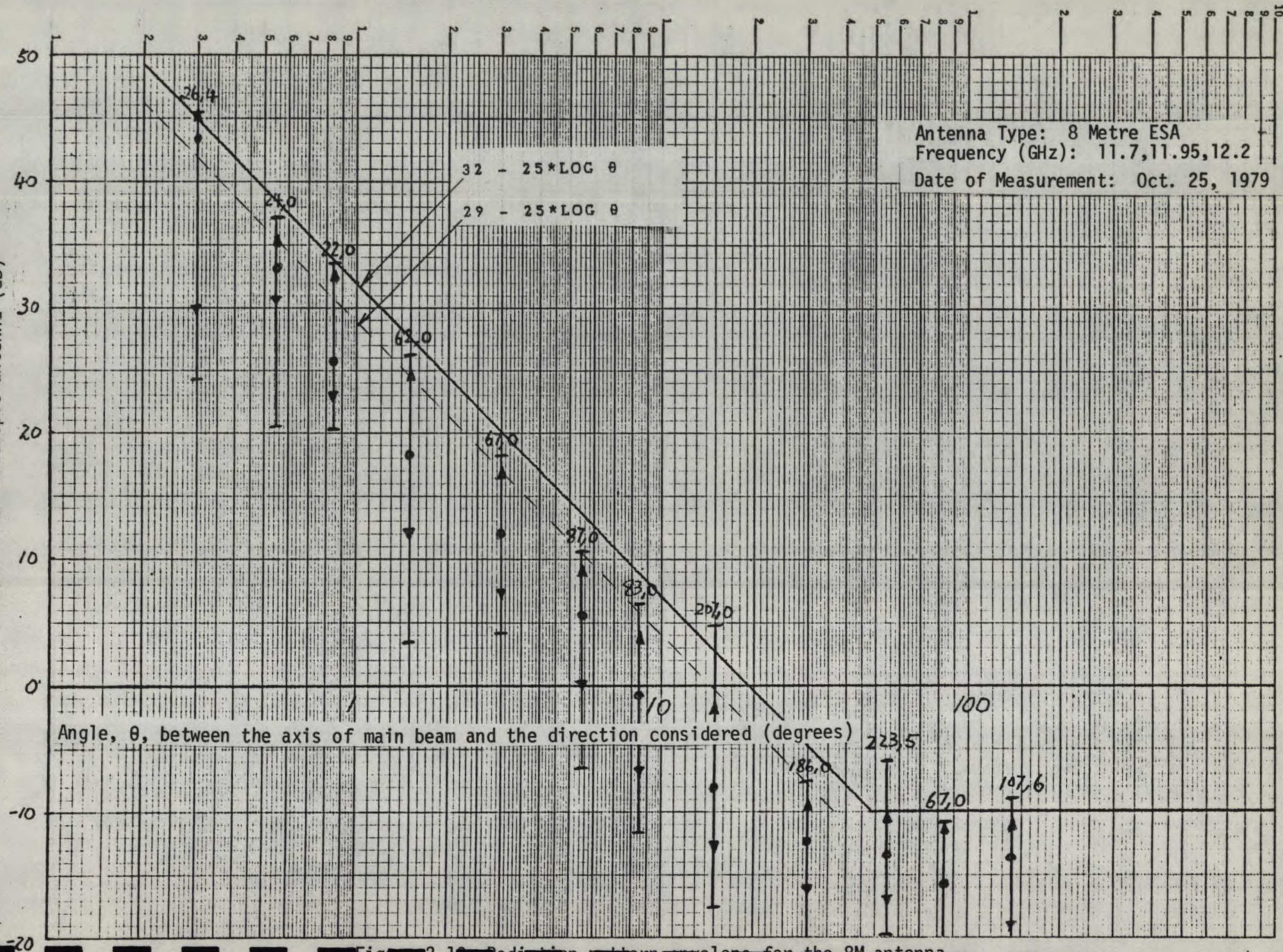


Fig. 2.10 Radiation pattern envelope for the 8M antenna

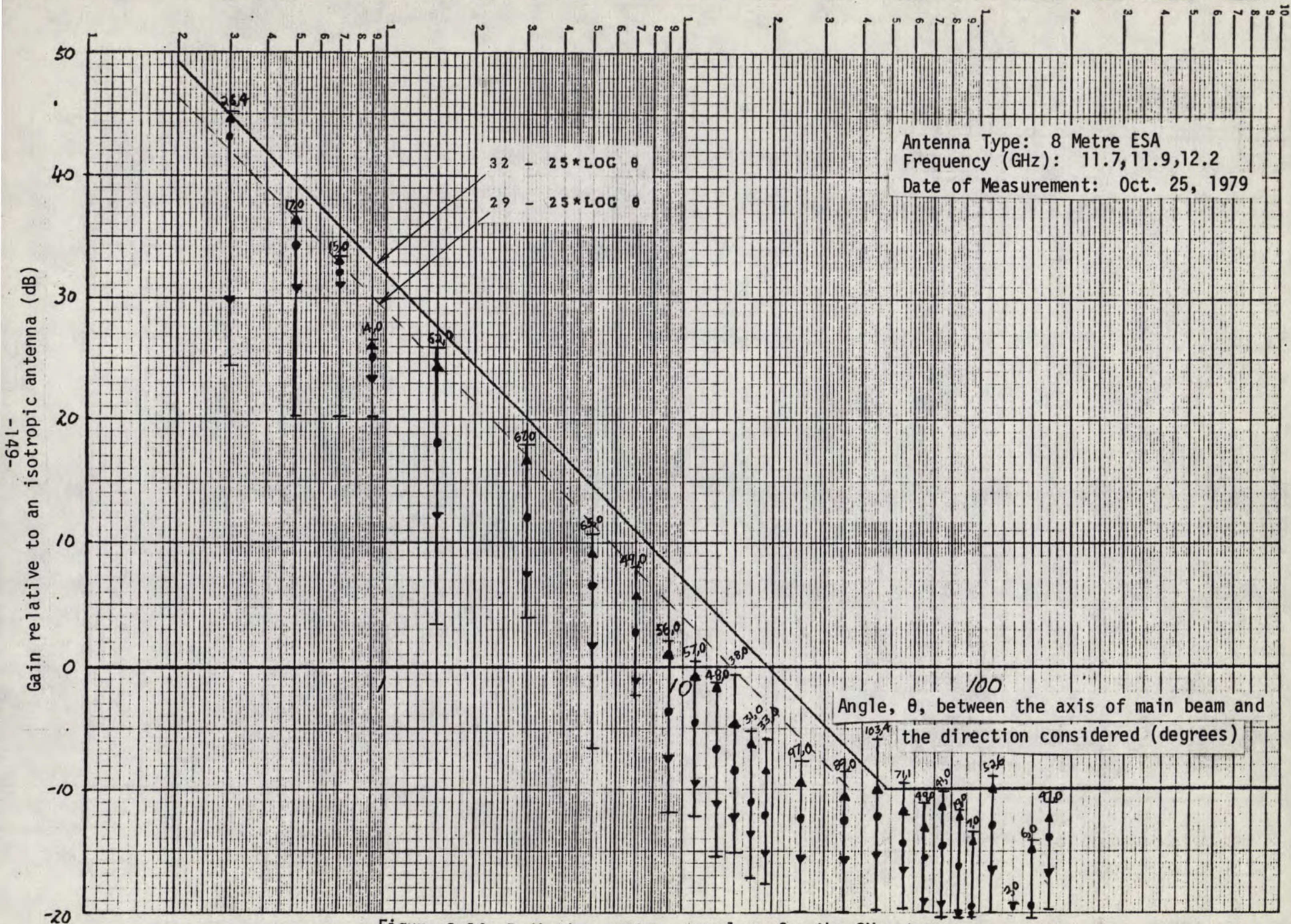
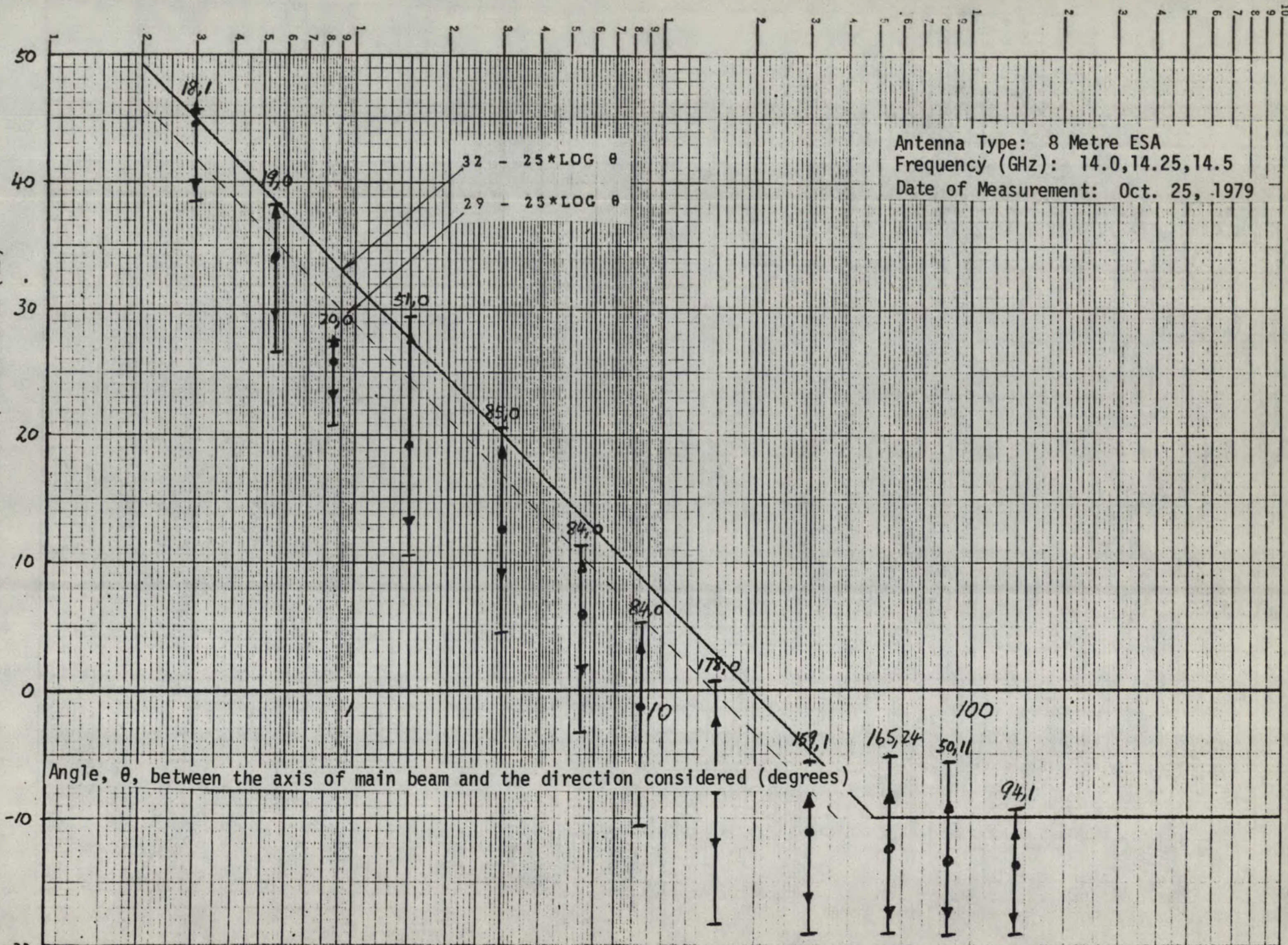
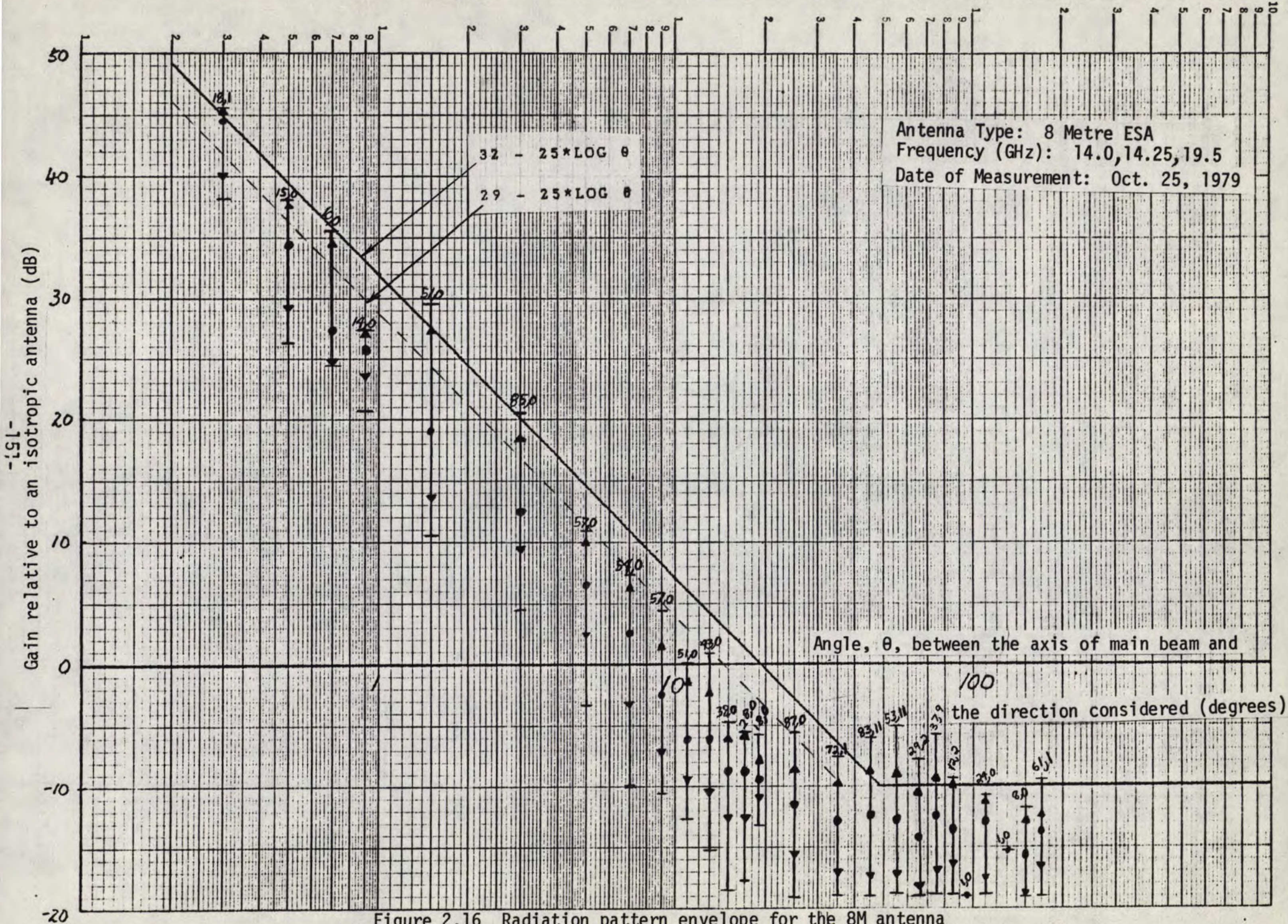


Figure 2.14 Radiation pattern envelope for the 8M antenna

Gain relative to an isotropic antenna (dB)





gain relative to an isotropic antenna (db)

-20

-10

0

10

20

30

40

50

direction considered (degrees)

Angle, θ , between the axis of main beam and the

188.11 581.55

10

13.0

51, 12

100

91.0

20.0

21.0

18.2

85.7

29 - 25 * LOG θ

32 - 25 * LOG θ

15.15

12.12

10

Antenna Type: 15'

Frequency (GHz): 3.7-4.2

Date of Measurement: Sept. 19, 19

Figure 2.17 Radiation pattern envelope for the 15' antenna

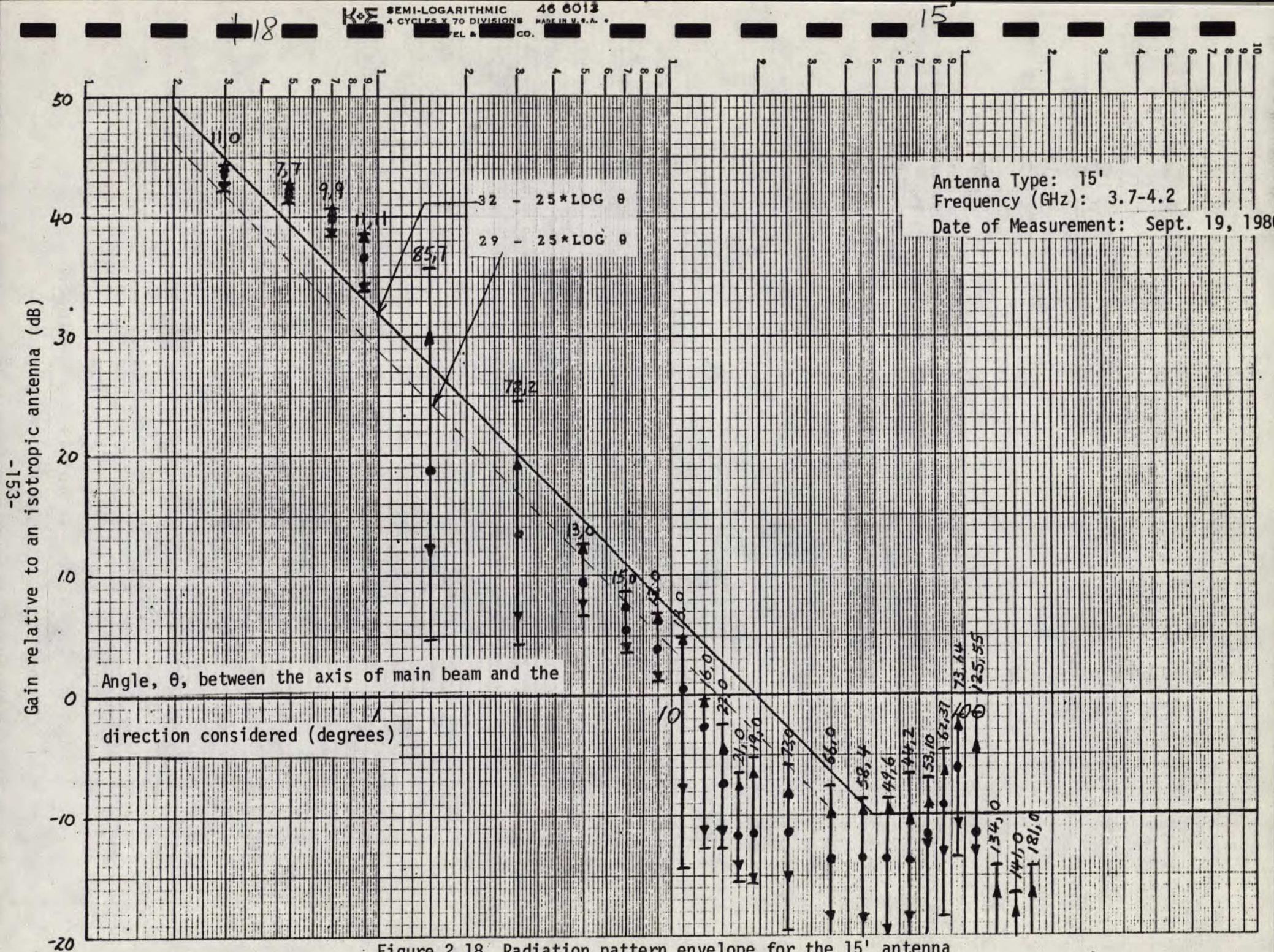


Figure 2.18 Radiation pattern envelope for the 15' antenna



ANDREW

PATTERN ENVELOPE

ANTENNA TYPE 10 METRE EARTH STATION

PE 3321

R Boyle
Approved

June 27, 1975

3.7-4.2 GHz

Gain: 51.0 \pm .2 dBi at 3.95 GHz

15 dB BEAMWIDTH: .96 DEGREES

(Curve A) defined as:

$32 - 25 \log_{10} (\theta)$ dBi, $1^\circ \leq \theta \leq 48^\circ$

-10 dBi, $48^\circ \leq \theta \leq 180^\circ$

Pattern Envelope of worst case sidelobes across the band for horizontal and vertical polarizations, right and left sides. Envelope is smoothed such that peak gain of an individual sidelobe has been reduced by averaging its peak level with the peaks of the nearest sidelobes on either side, with the peaks of two nearest sidelobes on either side, provided that no individual sidelobe exceeds Curve A by more than 6 dB.

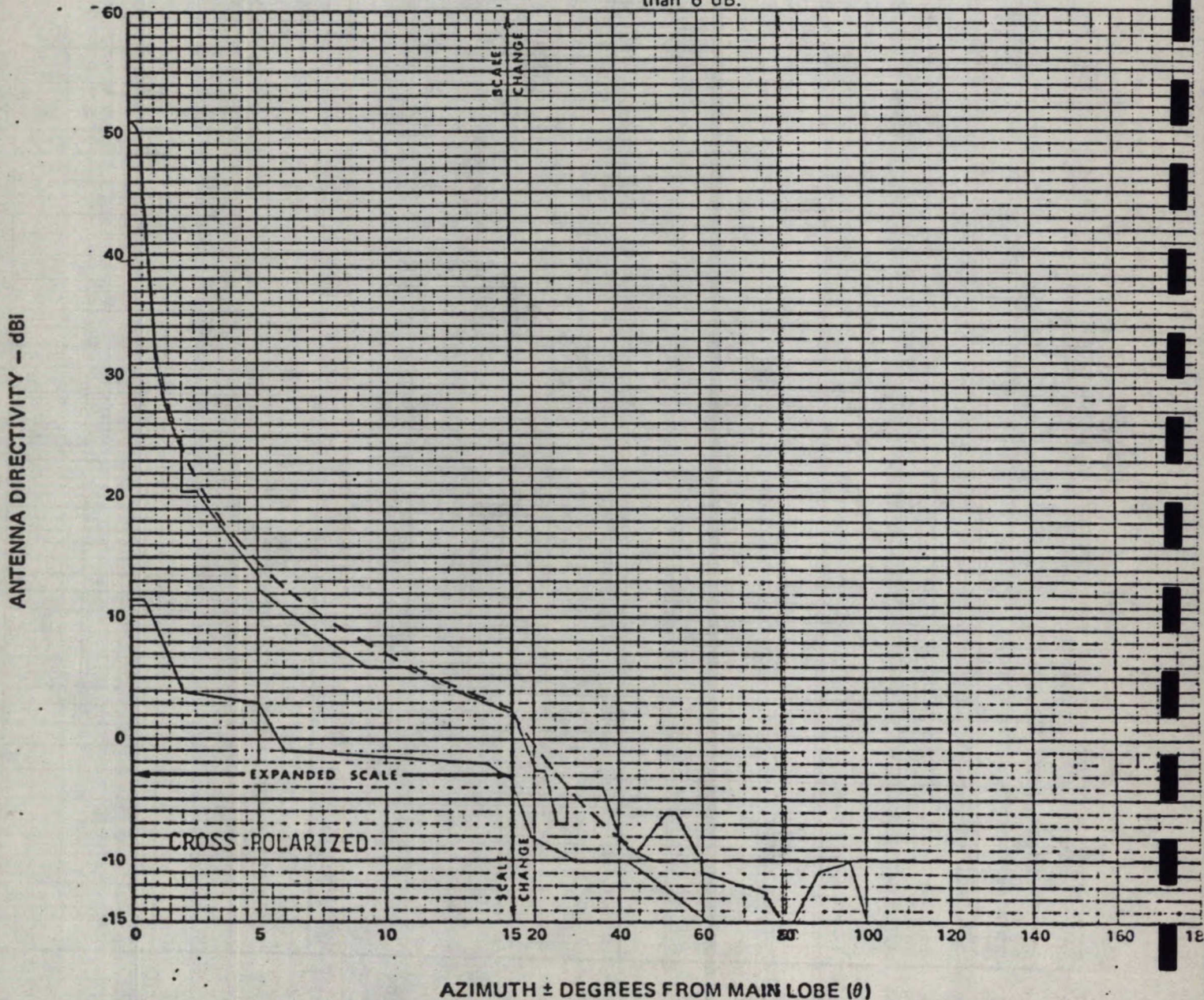


Figure 2.19 Radiation pattern envelope for the original 10i antenna

PATTERN ENVELOPE

ANTENNA TYPE NUMBER ESAB-124



ANDREW

PE 3316

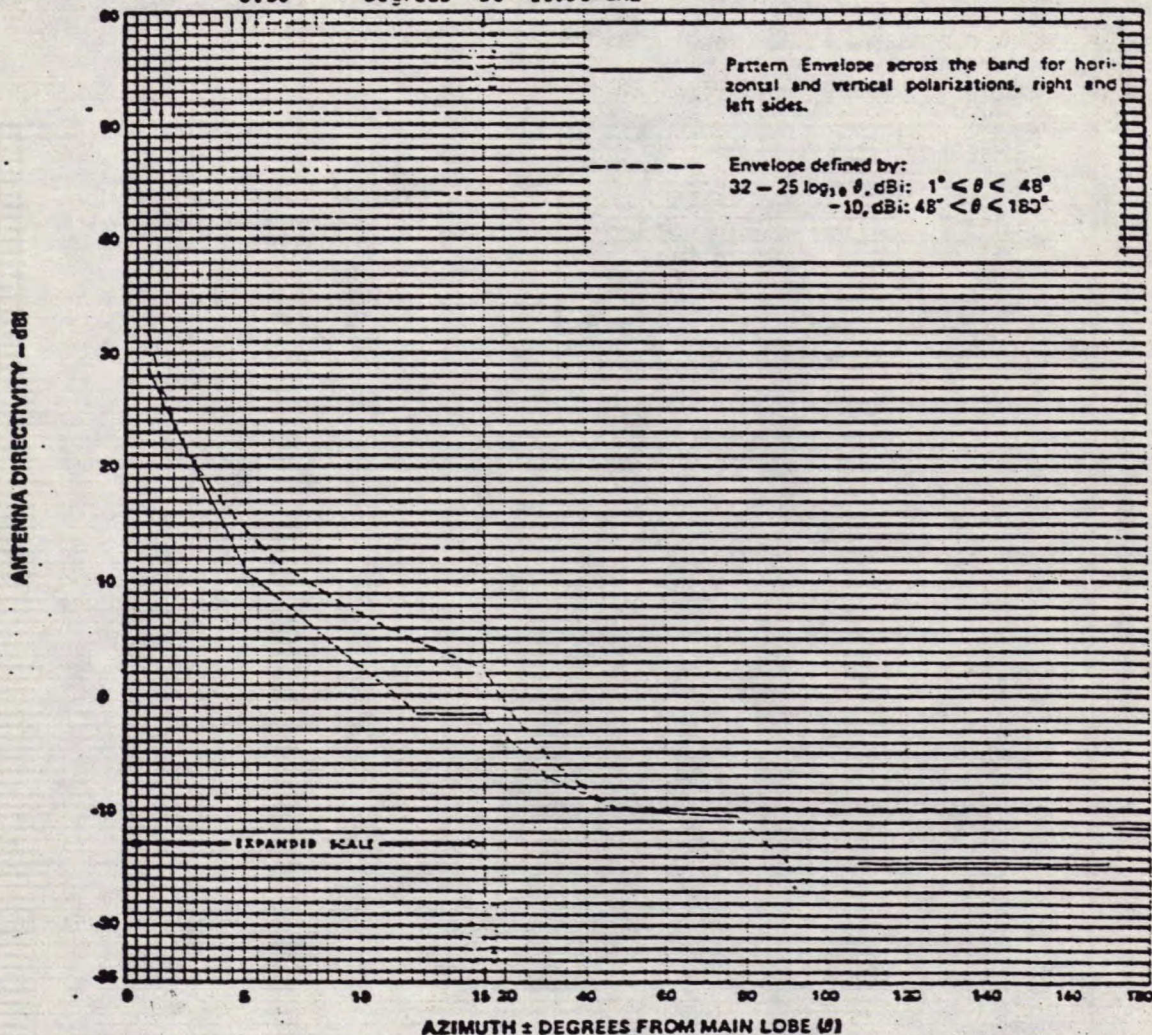
GTW

Approved

16 February 1981 -

10.95 - 11.80 GHz
11.70 - 12.20 GHz
Gain: 58.7 ± 0.2 dBi at 11.35 GHz
59.2 ± 0.2 dBi at 11.95 GHz
15 dB BEAMWIDTH: 0.38 DEGREES at 11.35 GHz
0.35 DEGREES at 11.95 GHz

This is a transmit and receive antenna. See PE 3318 for transmit band.



Andrew Corporation 10500 W. 153rd St.
Orland Park, IL U.S.A. 60462
Andrew Antenna Company Ltd.
Whitby, Ontario, Canada
FORM 4016D (11/79)

Andrew Antennas
Lechelly, File, Great Britain
Andrew Antennas
Reservoir, Victoria, Australia

Andrew Antenas Limitada
Sorocaba, SP, Brazil
Antenas Y Perforajes
Mexico, D.F. Mexico

Antennas Andrew S.A.R.L.
Nogent-le-Rotrou, France
Andrew S.R.L.
Milano, Italy



Figure 2.20 (a) Radiation pattern envelope for the 8M antenna

ANDREW

ANDREW CORPORATION
10500 W. 153rd Street
Orland Park, Illinois U.S.A. 60462

NO. SP08-01
REV. Orig. 16 Feb. 1981 SHEET 8 of 9

PATTERN ENVELOPE

ANTENNA TYPE NUMBER ESAB-124



ANDREW

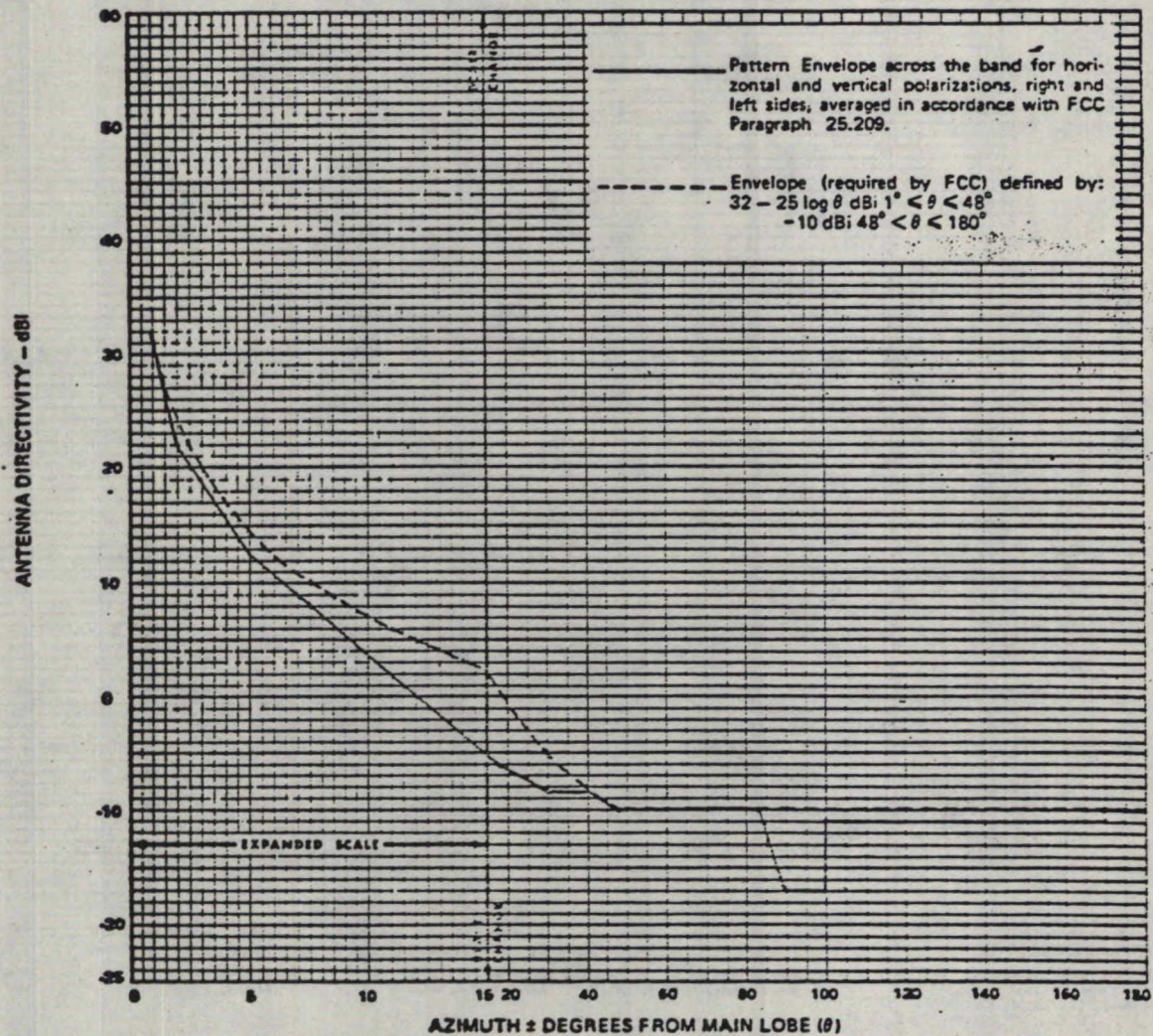
PE 3318

G. J. W.
Approved

16 February 1981

14.0 - 14.50 GHz
Gain: 60.4 ± 0.2 dBi at 14.25 GHz
15 dB BEAMWIDTH: 0.32 DEGREES

This is a transmit and receive antenna.
See PE3316 for receive band.



Andrew Corporation 10500 W. 153rd St.
Orland Park, IL U.S.A. 60462
Andrew Antenna Company Ltd.
Whitby, Ontario, Canada
FORM 4016C (9/78)

Andrew Antennas
Lochgelly, Fife, Great Britain
Andrew Antennas
Reservoir, Victoria, Australia

Andrew Antennas Limitada
Sorocaba, SP, Brazil
Antenas Y Perforajes
Mexico, D.F. Mexico

Antennas Andrew S.A.R.L.
Nogent-le-Rotrou, France
Andrew S.R.L.
Milano, Italy



Figure 2.20 (b) Radiation pattern envelope for the 8M antenna



ANDREW

ANDREW CORPORATION
10500 W. 153rd Street
Orland Park, Illinois U.S.A. 60462

NO. SP08-01

REV. Orig. 16 Feb. 1981 SHEET 9 of 9

PATTERN ENVELOPE

ANTENNA TYPE NUMBER ESAC5-4B

4.5 M Receive Only Earth Station Antenna

3.7 - 4.2 GHz

Gain: 44.2 ± 0.2 dBi at 4 GHz

15 dB BEAMWIDTH: 2.5 DEGREES



ANDREW

PE 3370

R Bayko
Approved

September 29/80

ANTENNA DIRECTIVITY - dBi

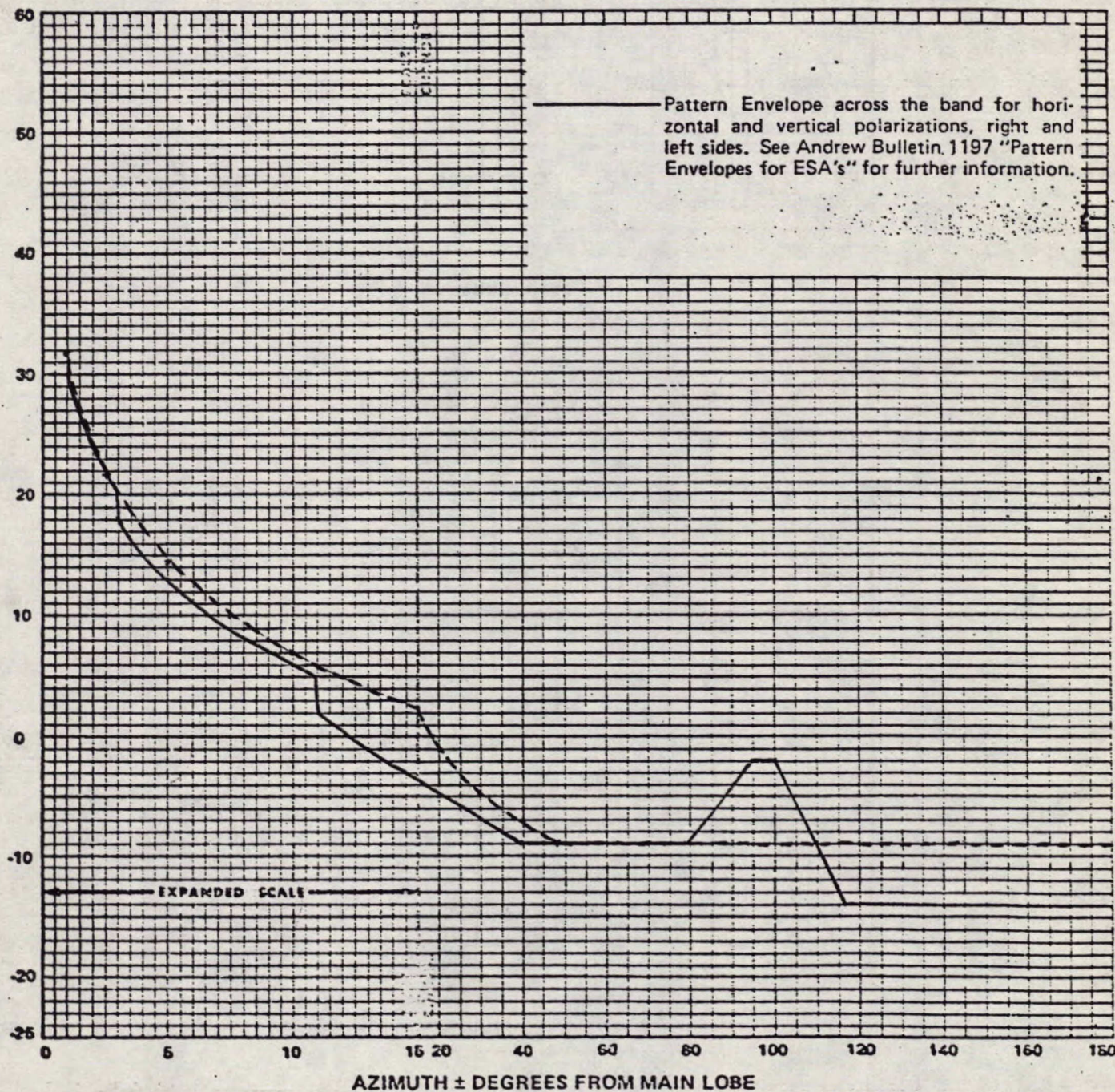


Figure 2.21 Radiation pattern envelope for the 15' antenna

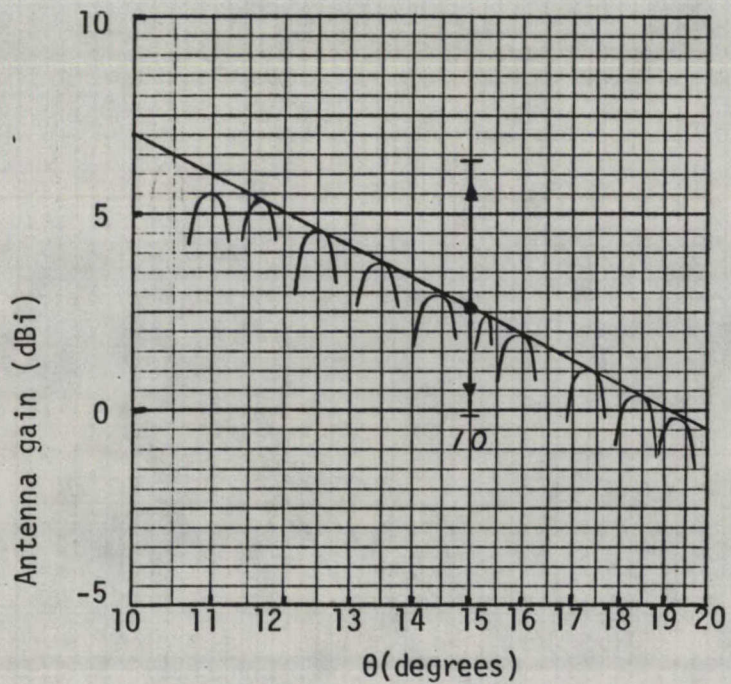


Figure 2.22(a)

Example of a distribution following the CCIR curve (calculated using the dBi method)

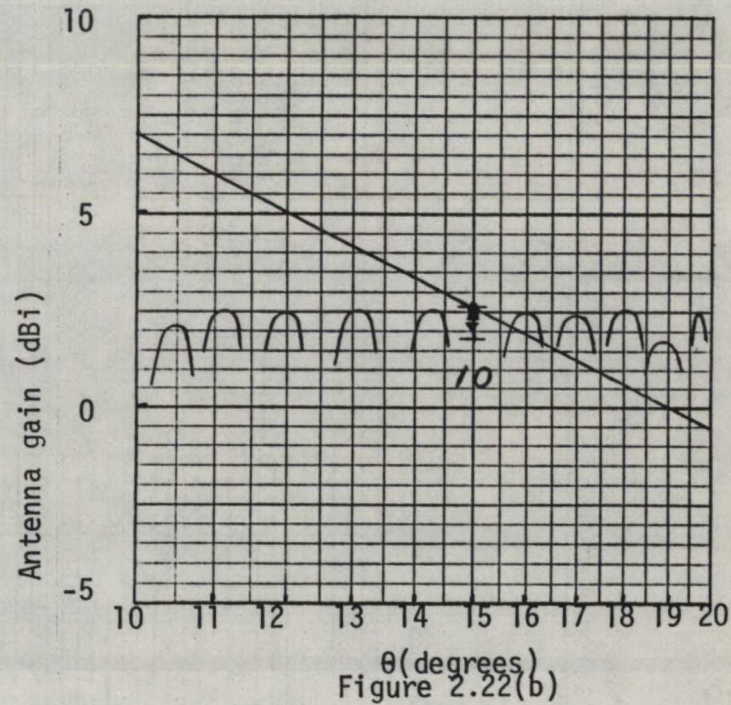


Figure 2.22(b)

Example of a flat distribution (calculated using the dBi method)

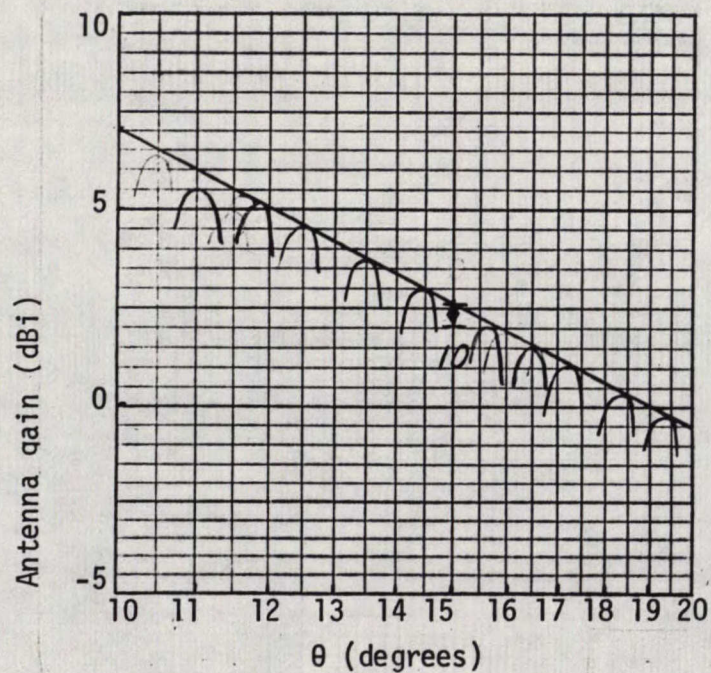


Figure 2.22(c)

Example of a distribution following the CCIR curve (calculated using relative level method)

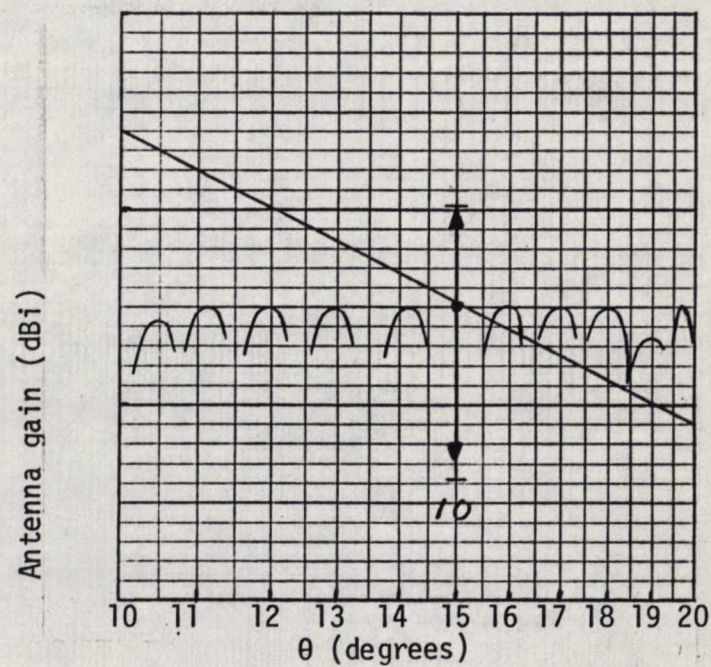


Figure 2.22(d)

Example of a flat distribution (calculated using relative level method)

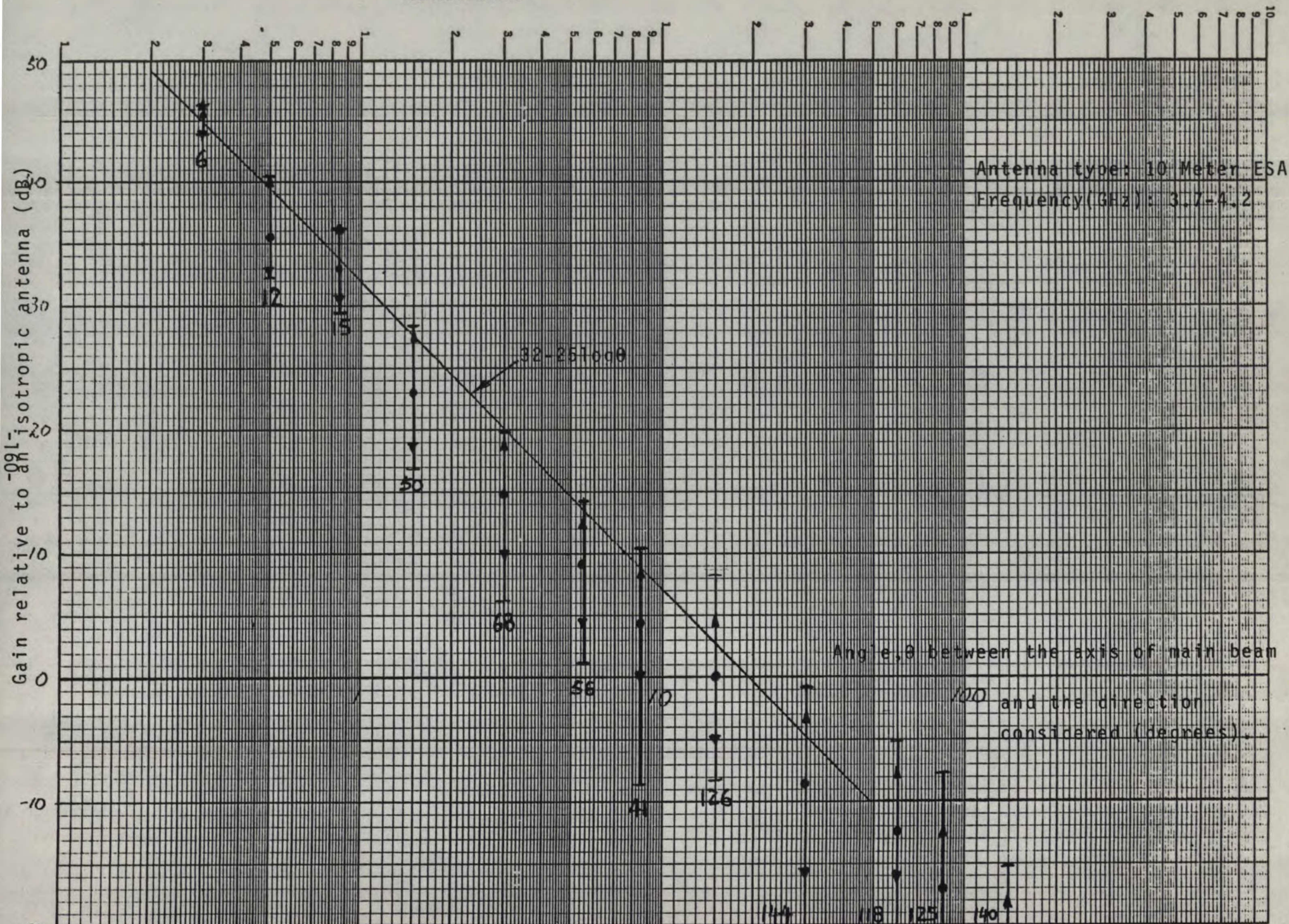


Figure 23 for rig 10 inter plotted using relative method

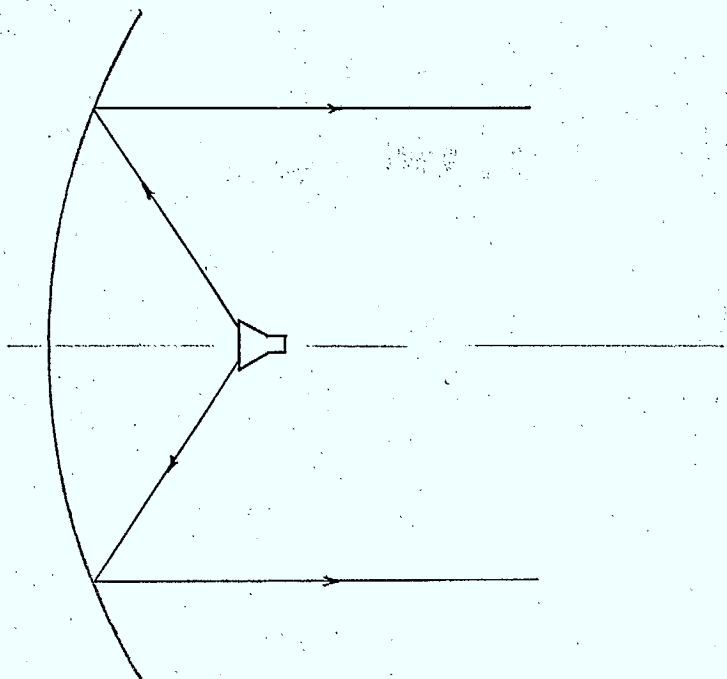


Figure 3.1.1(a) Prime focus paraboloid antenna

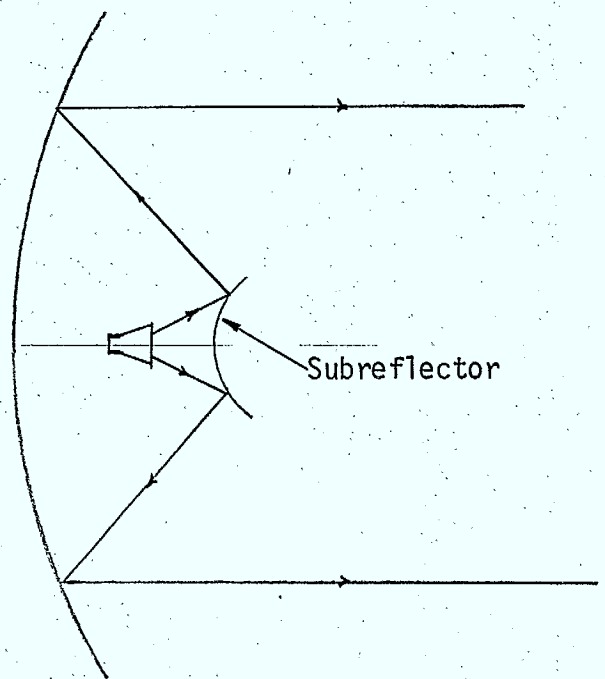


Figure 3.1.1(b) Paraboloid - dual reflector antenna

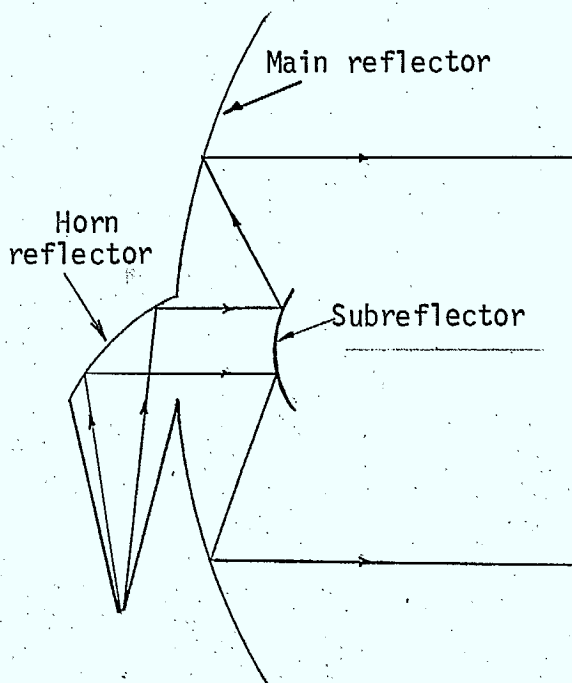


Figure 3.1.1(c) Near-field Cassegrain antenna

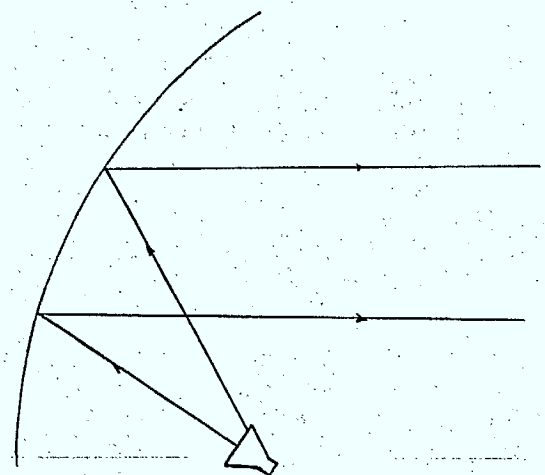


Figure 3.1.1(d) Single reflector offset antenna

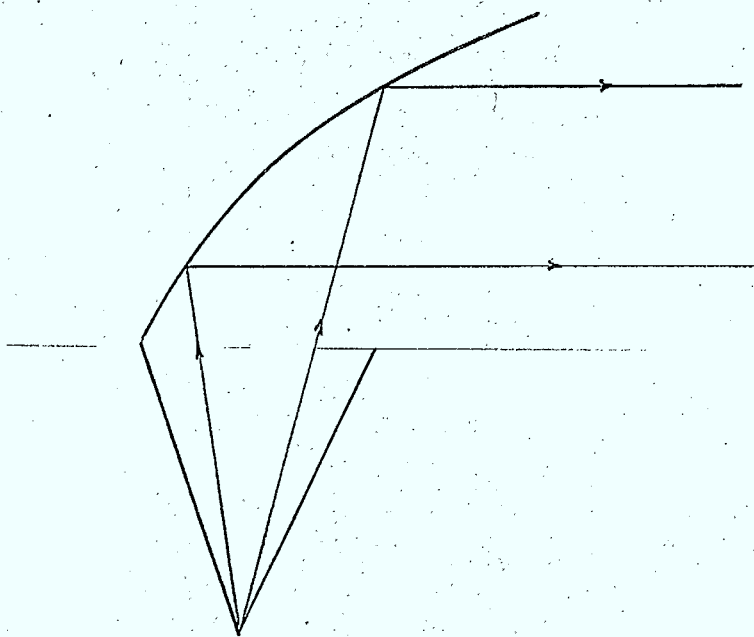


Figure 3.1.1(e) Horn reflector antenna

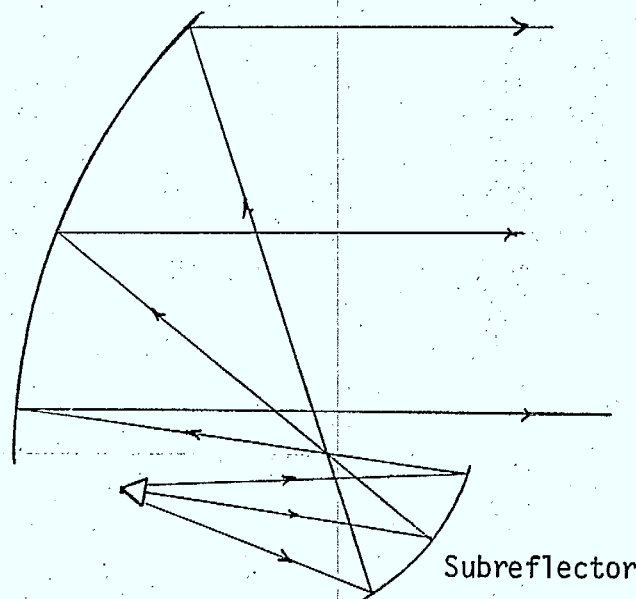


Figure 3.1.1(f) Offset dual reflector antenna

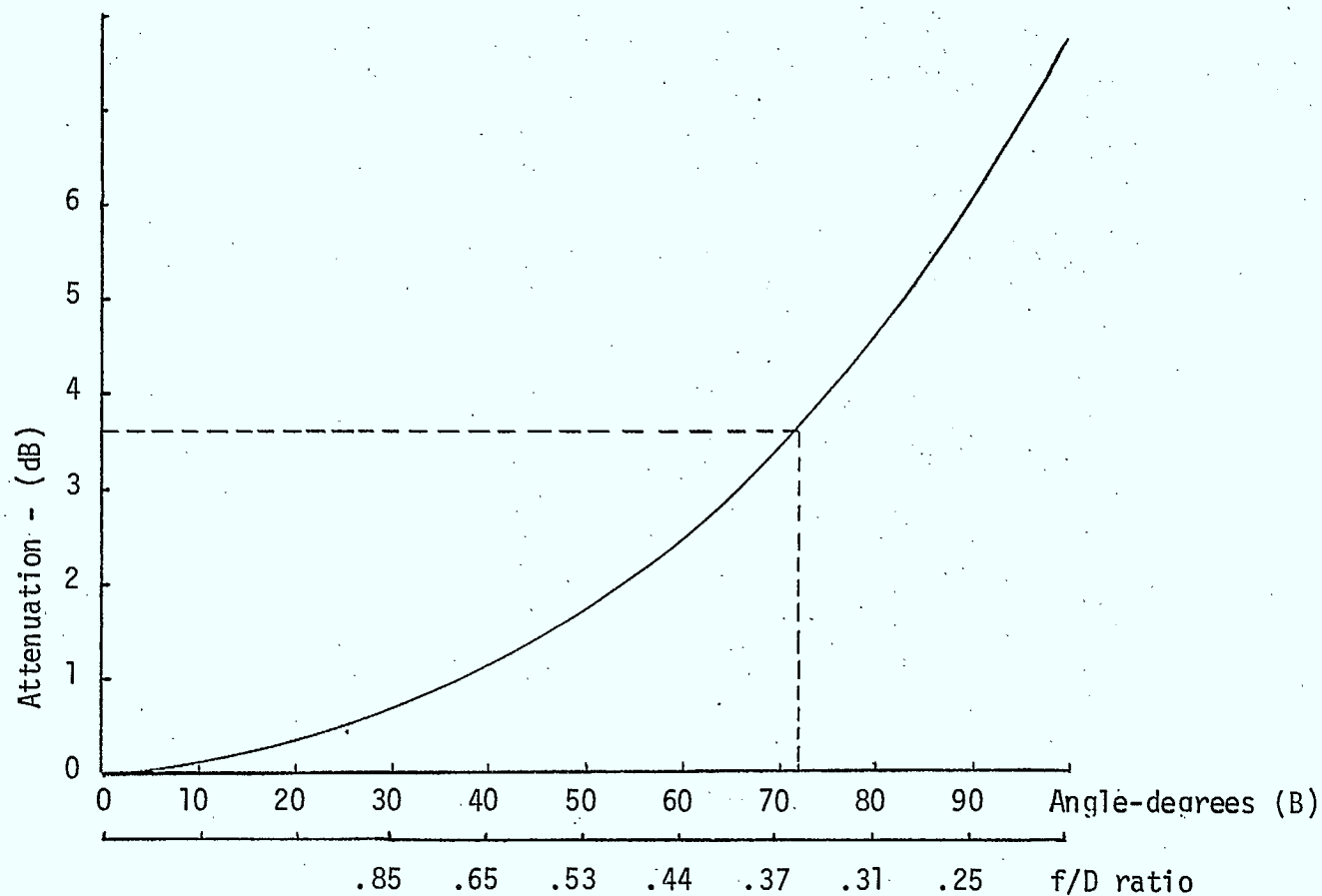


Figure 3.1.2(a) Space attenuation vs feed angle for a prime feed paraboloid

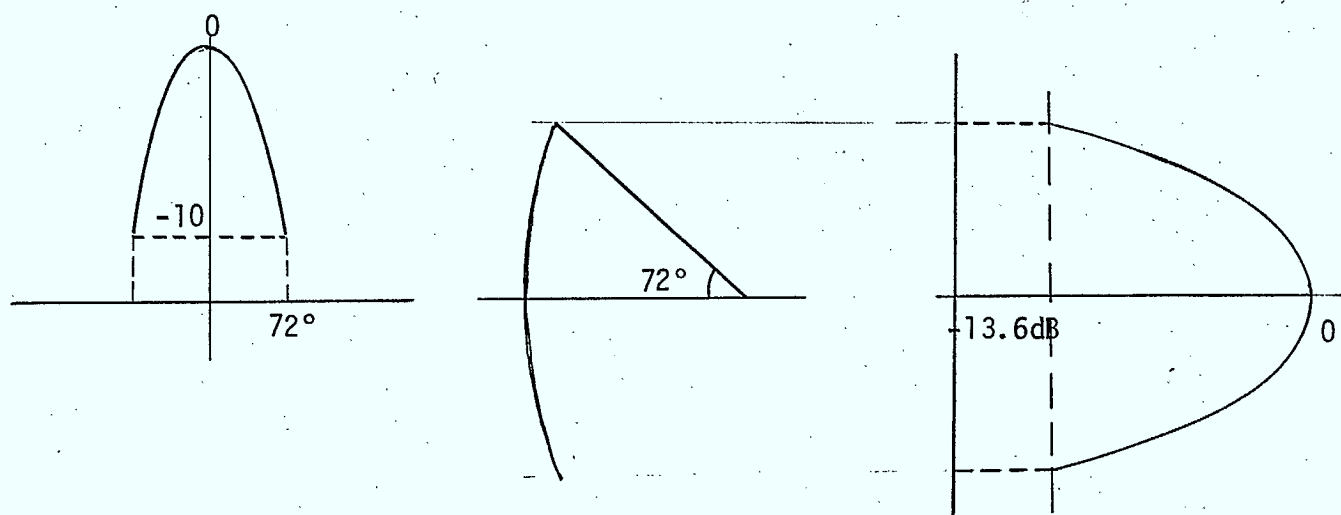


Figure 3.1.2(b) Example of aperture distribution calculation

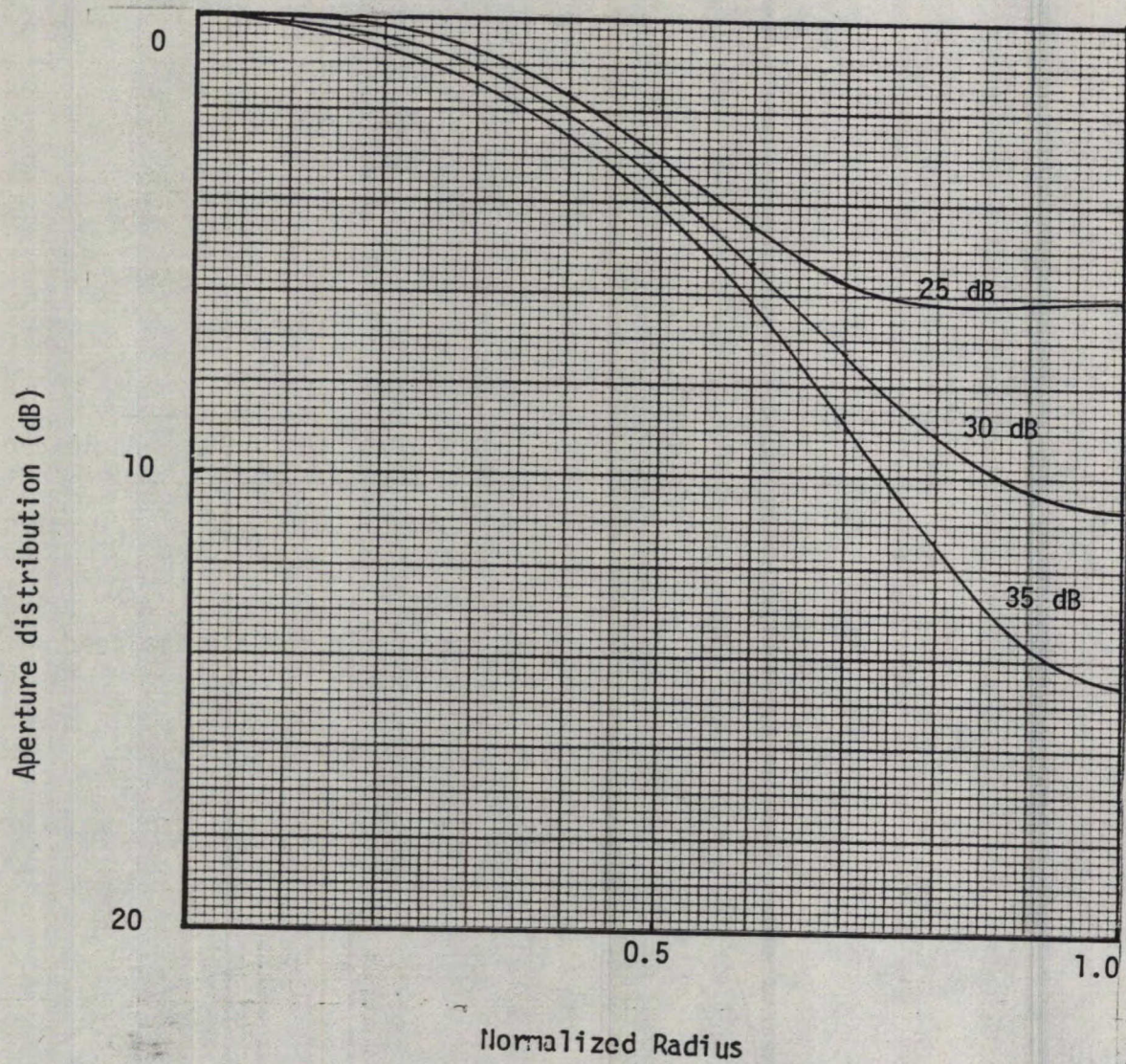


Figure 3.2.1 Taylor aperture distribution for circular aperture ($n=4$)

Relative power, dB

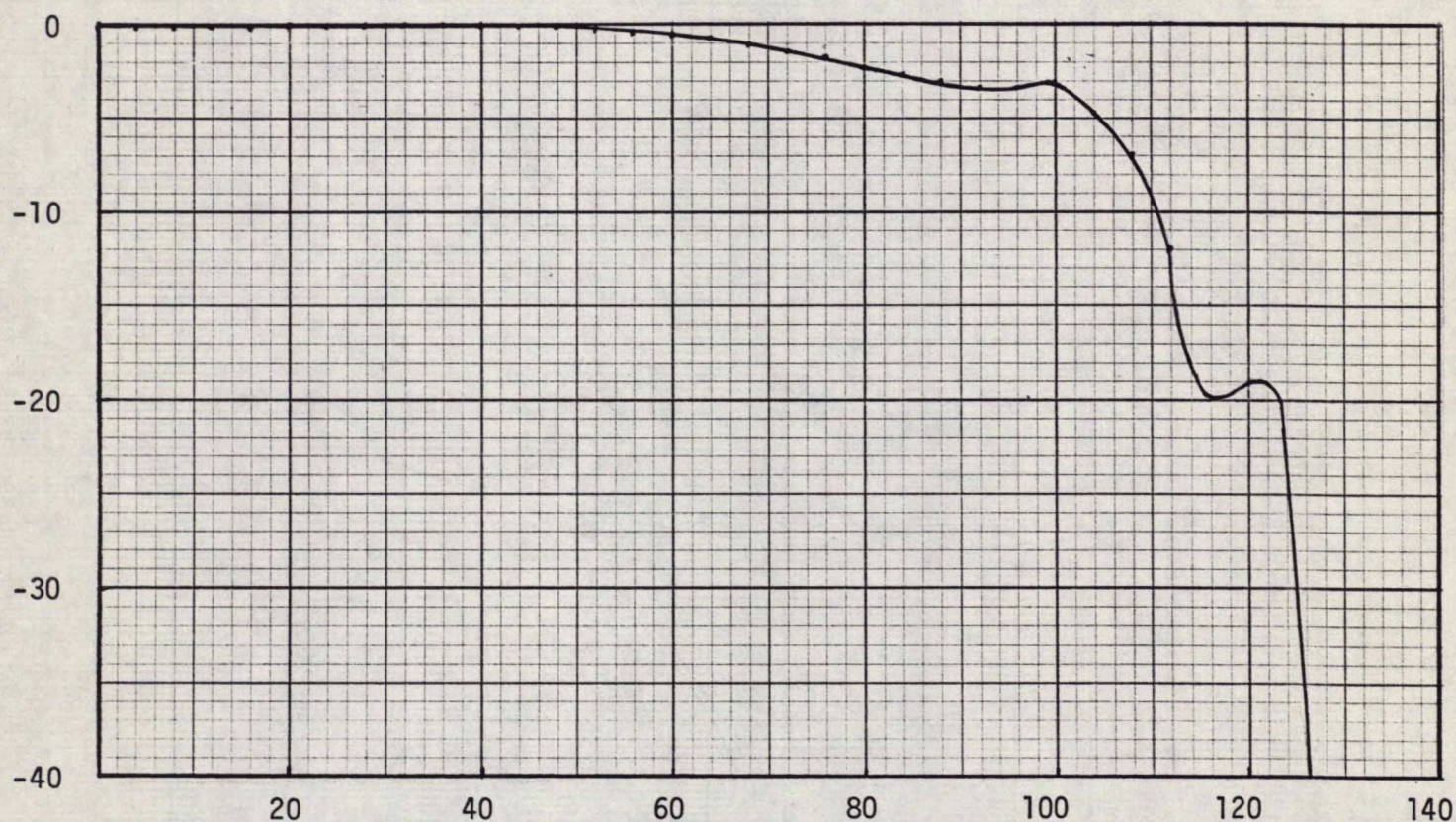


Figure 3.2.2 Subreflector pattern required to produce Taylor Distribution for 30dB sidelobes (dish $F/D = 0.2$)

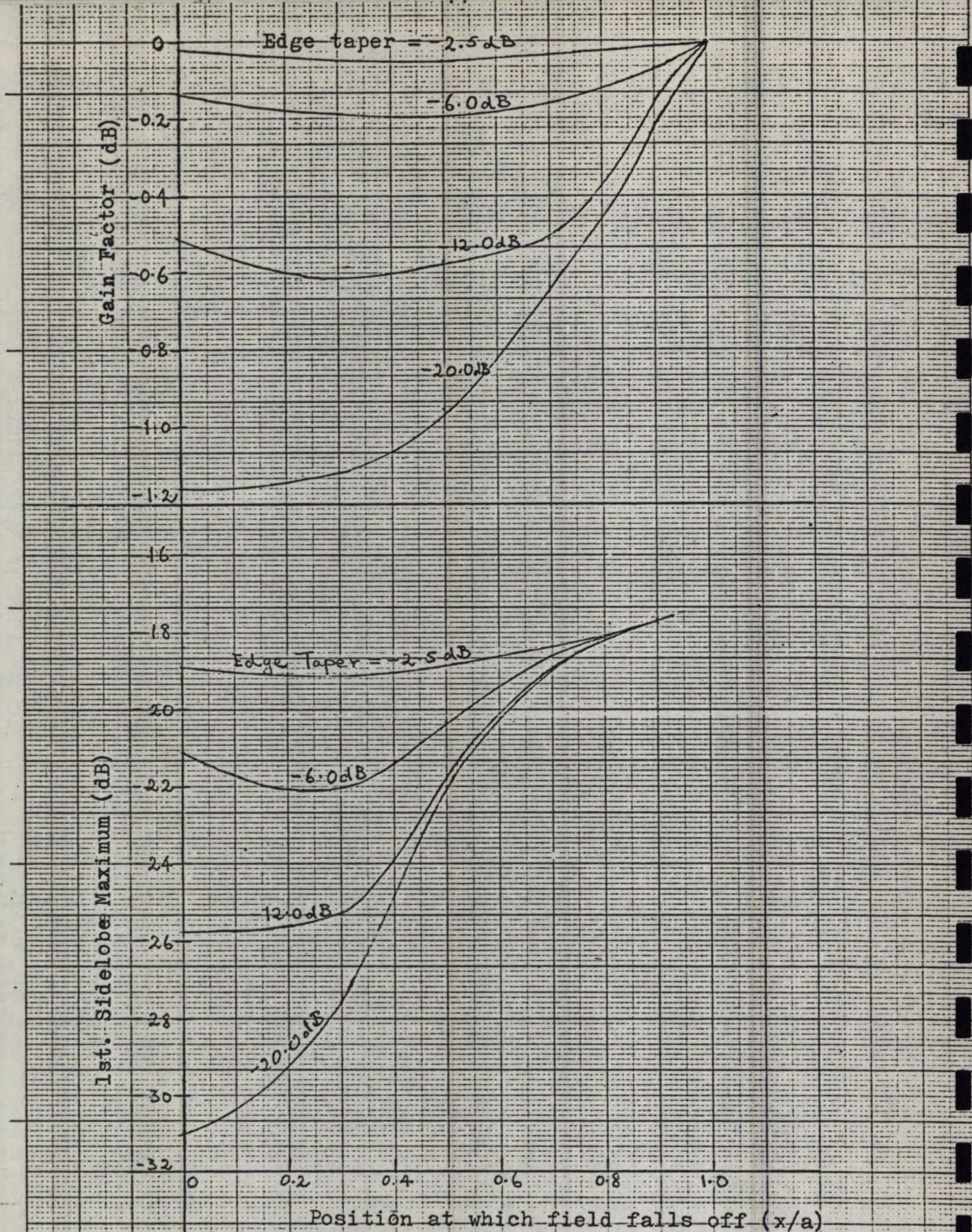


Fig. 3.2.3 Effect on gain and sidelobe level of aperture distribution where blockage = 0%

Linear Taper

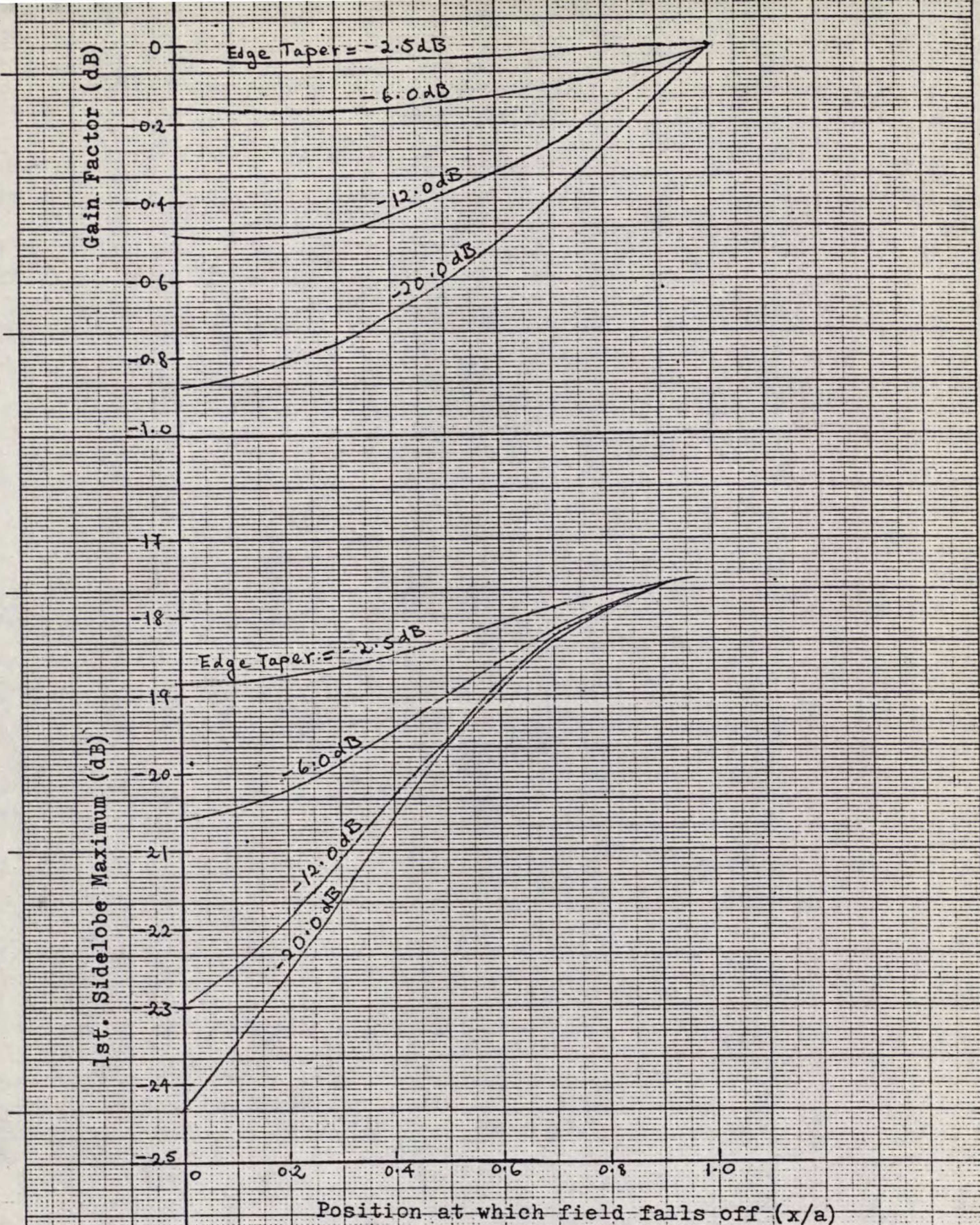


Fig 3.2.4 Effect on gain and sidelobe level of aperture distribution where Blockage = 0%
Square Law Taper

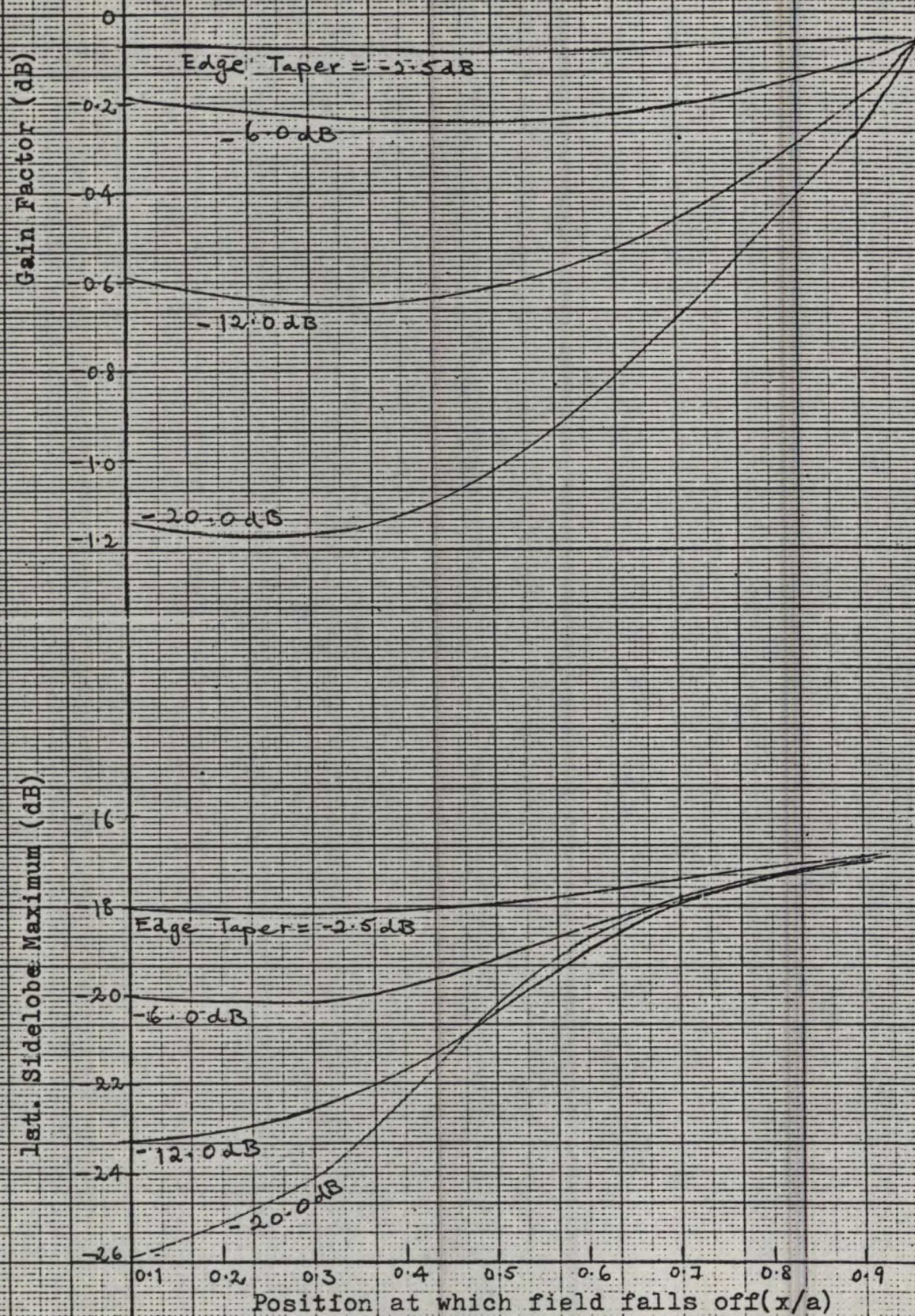


Fig 3.2.5 Effect on gain and sidelobe level of aperture distribution where blockage=1% Linear taper

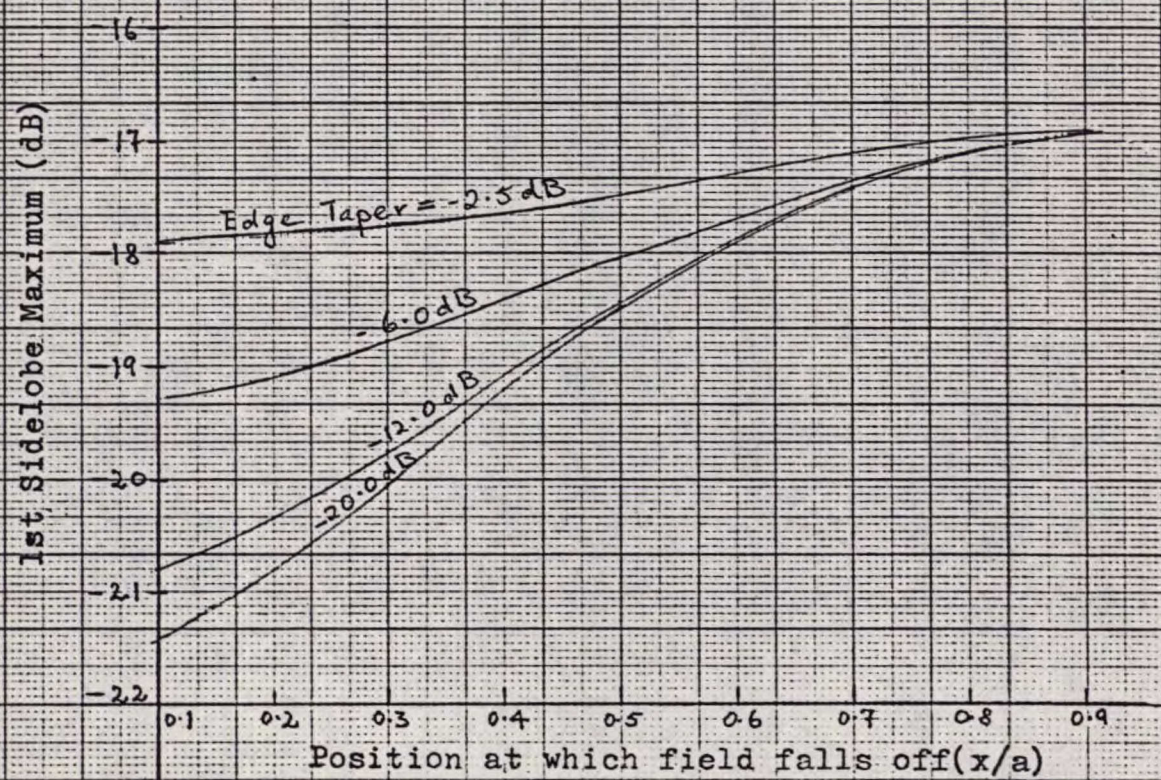
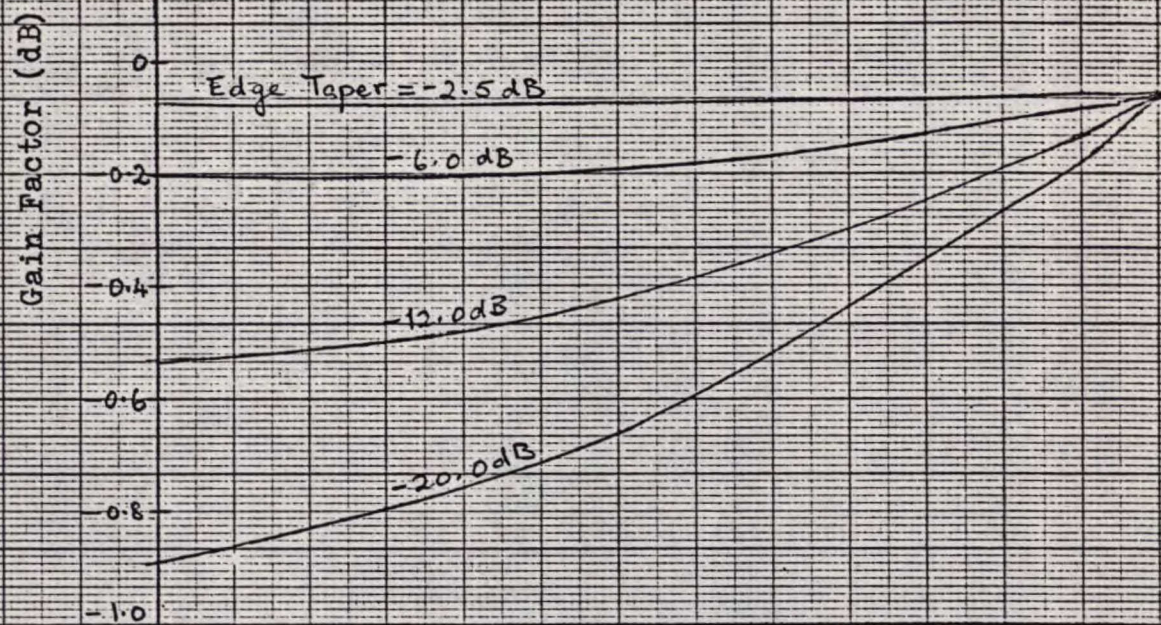


Fig 3.2.6 Effect on gain and sidelobe level of aperture distribution where blockage=1%
-169- Square law taper

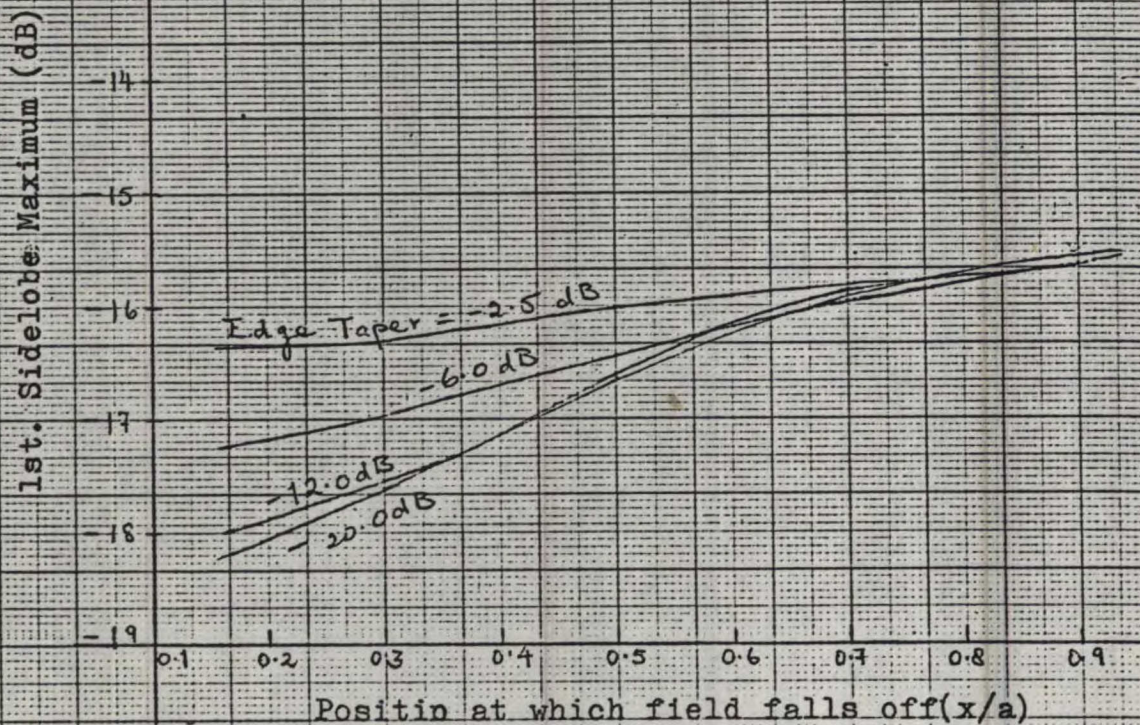
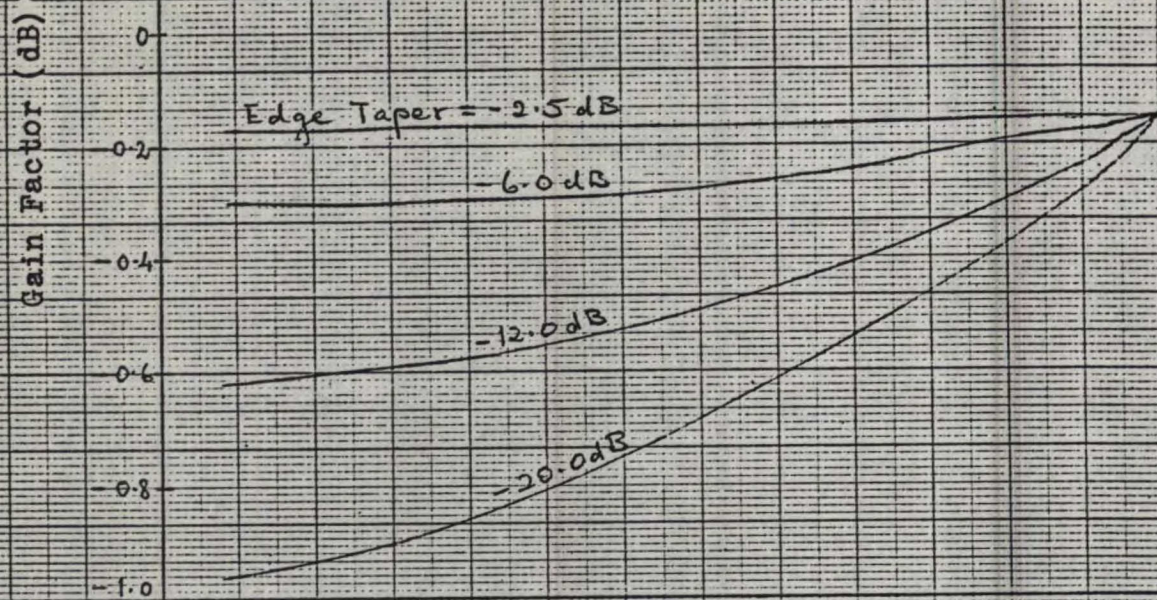


Fig 3.2.7 Effect on gain and sidelobe level of aperture distribution where blockage=3% Square law taper

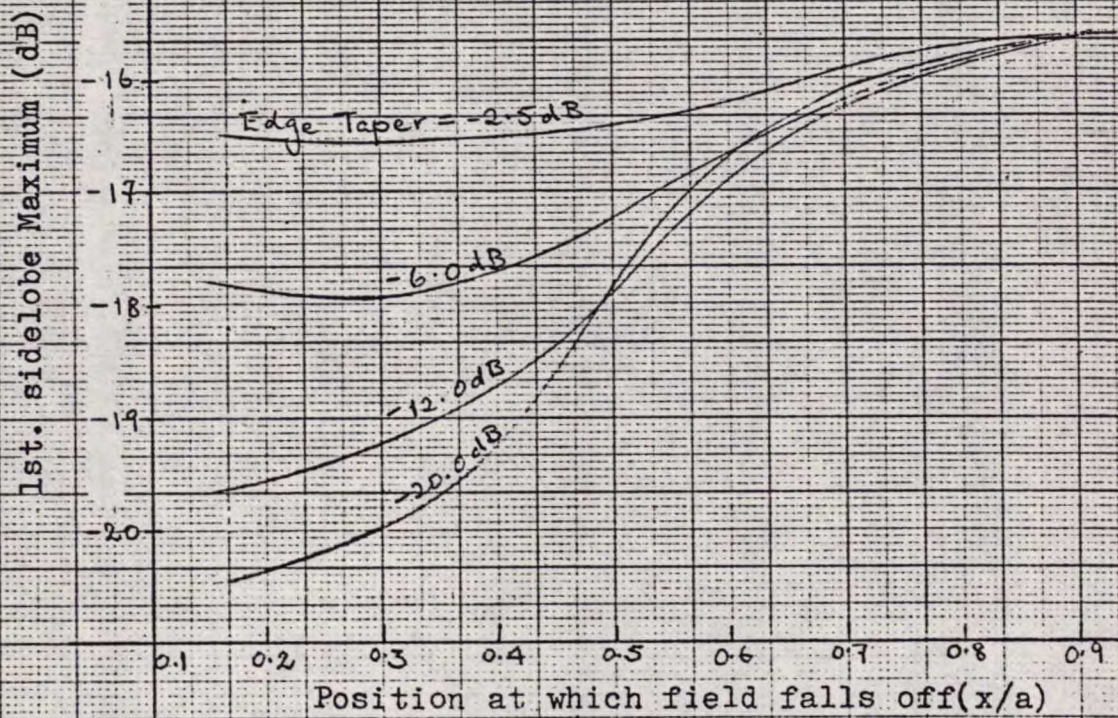
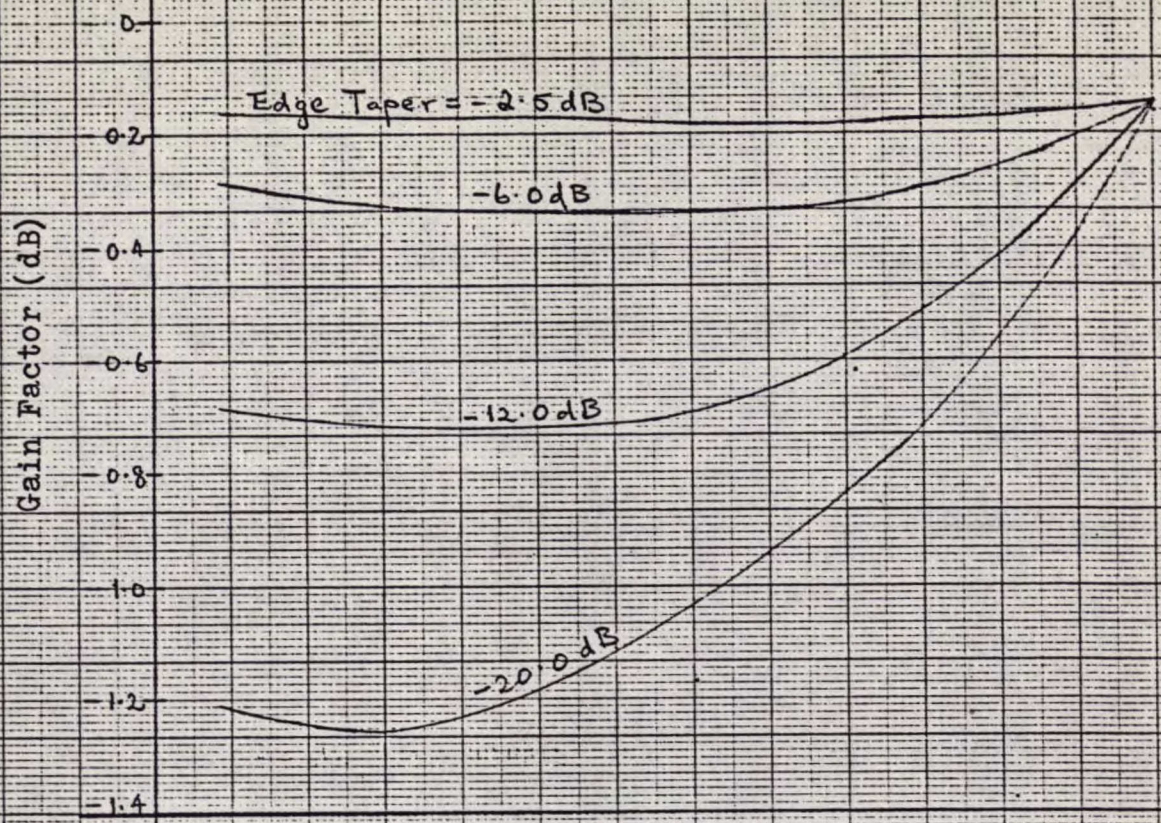


Fig 3.2.8 Effect on gain and sidelobe level of aperture distribution where blockage=3%
Linear taper

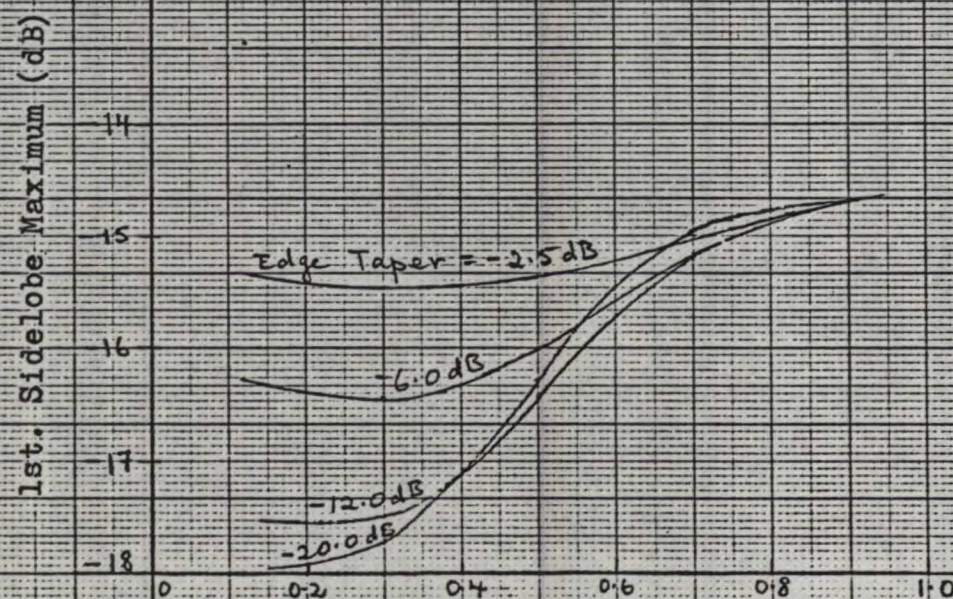
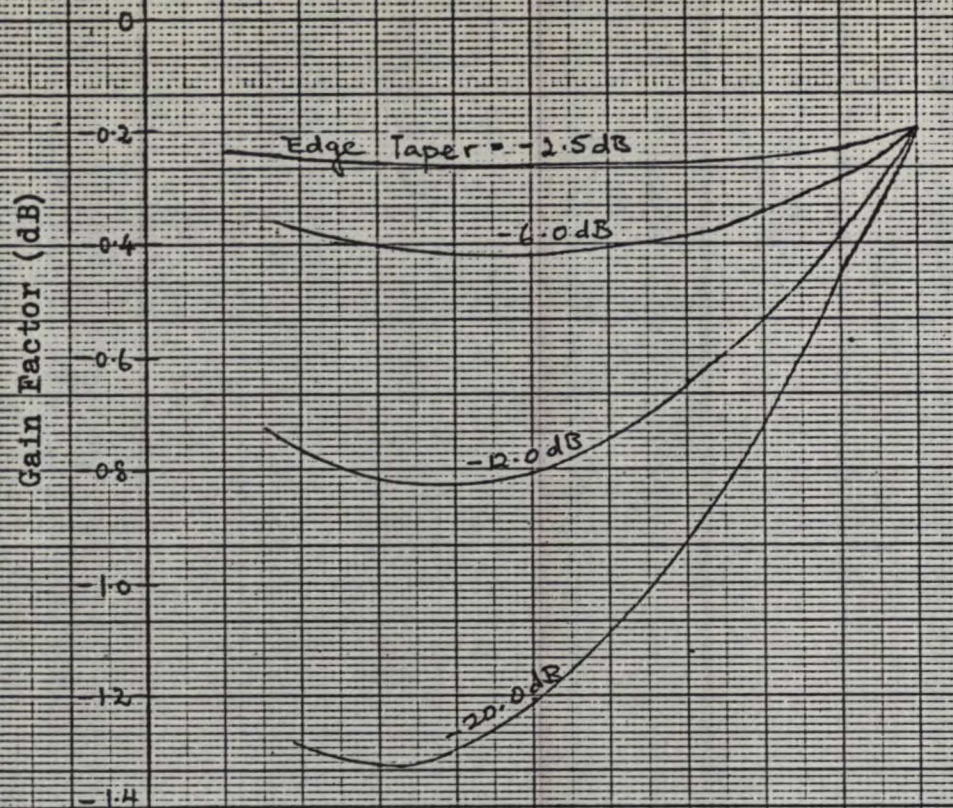
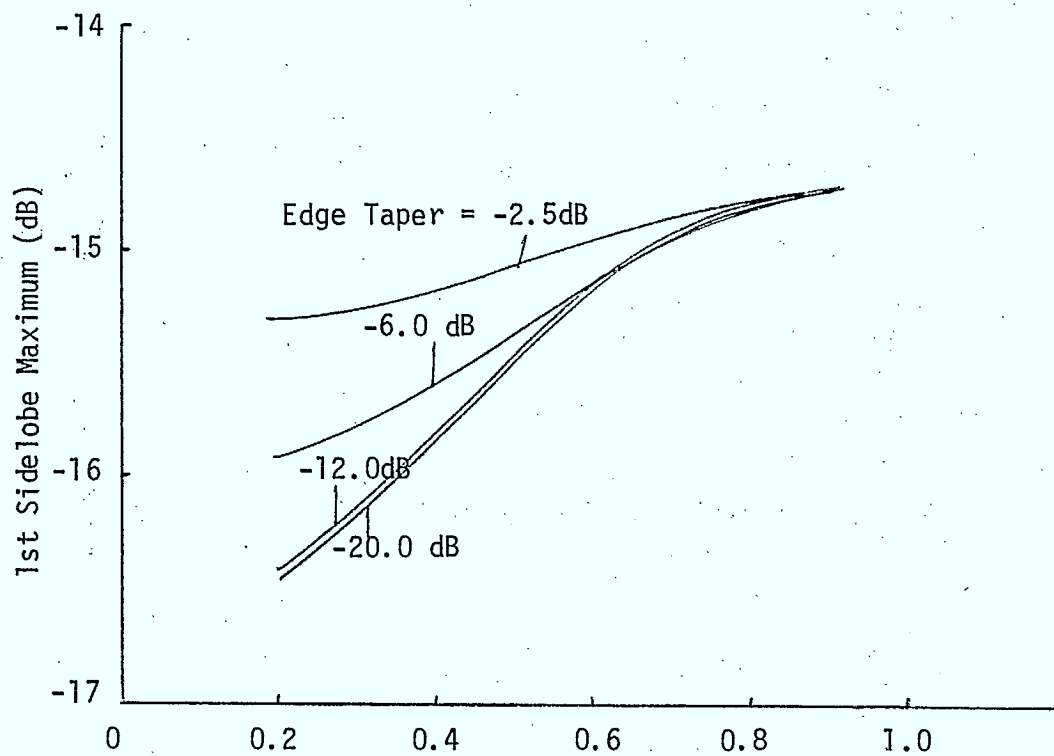
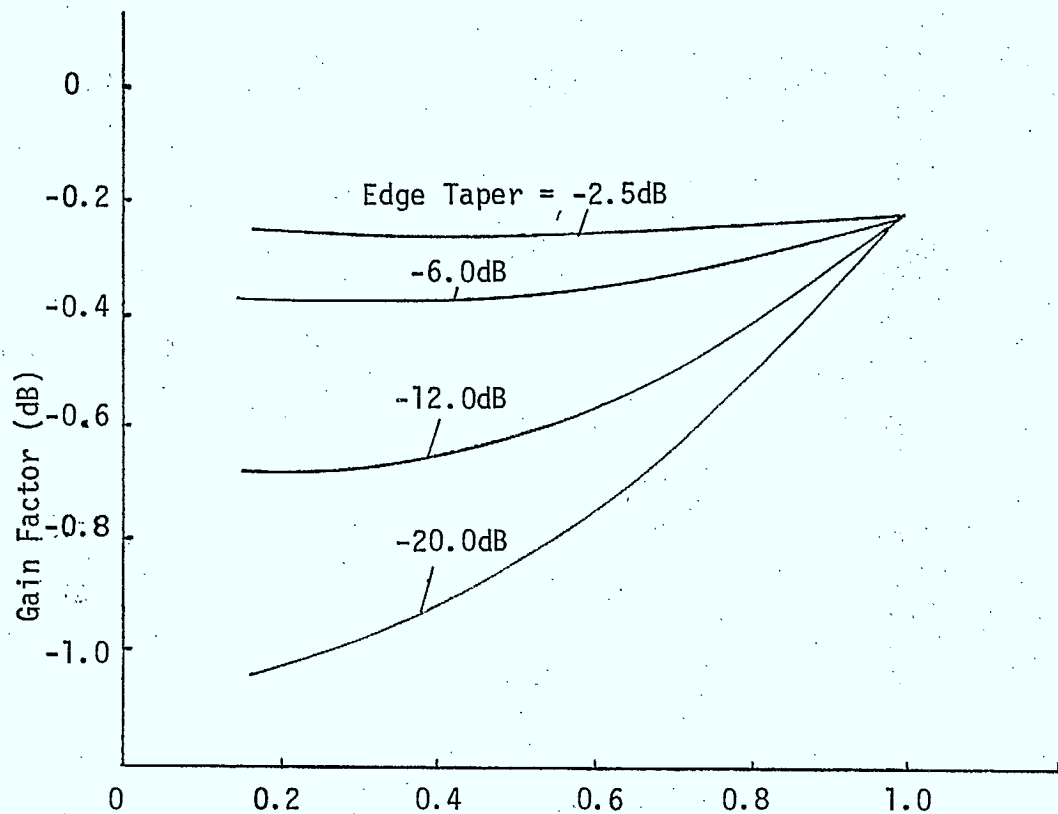


Fig. 3.2.9 Effect on gain and sidelobe level of aperture distribution where blockage=5%
Linear taper



Position at which field falls off (x/a)

Figure 3.2.10 Effect on gain and sidelobe level of aperture distribution where blockage = 5%
Square-law Taper

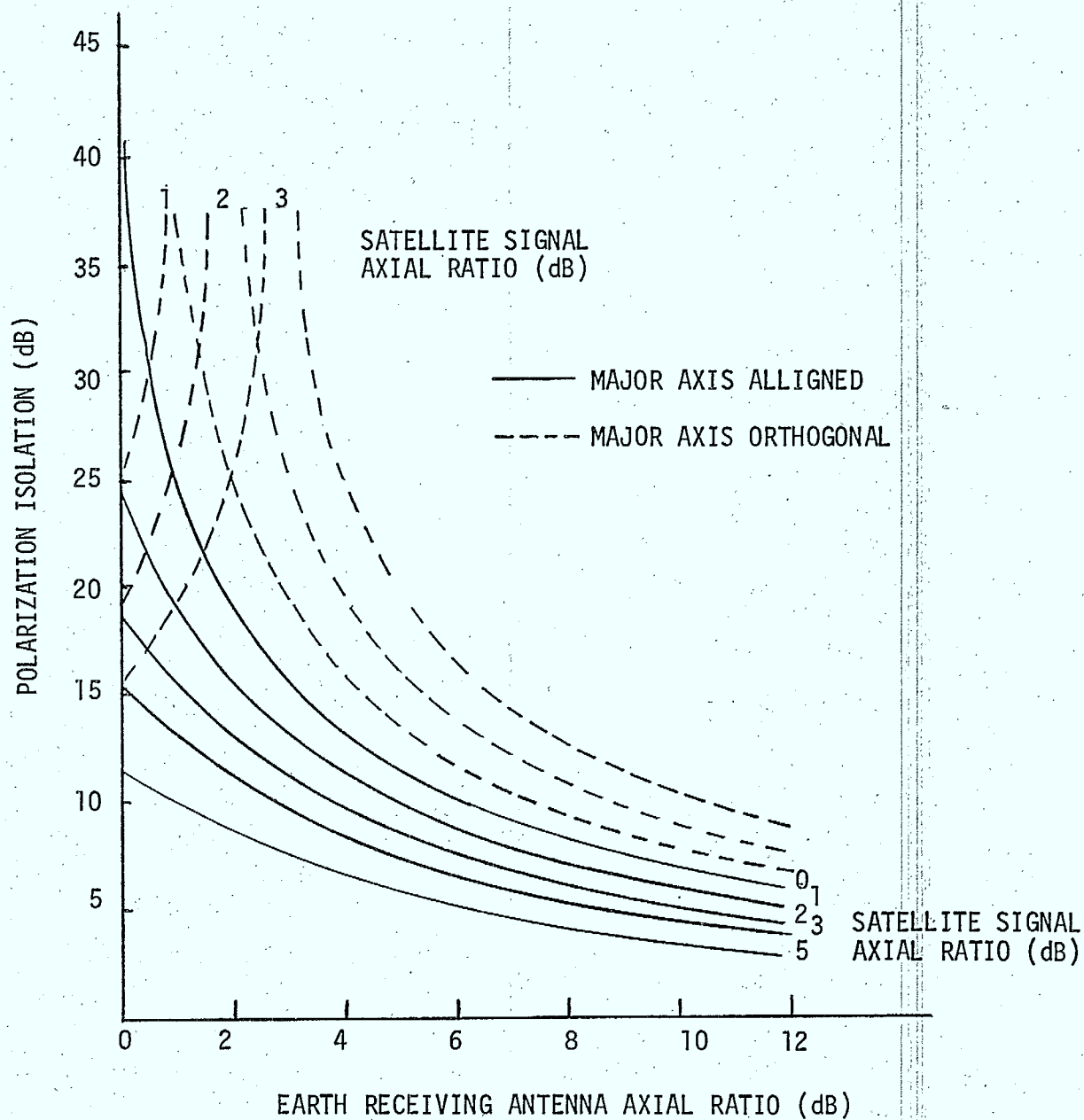


Figure 3.3.1. Polarization isolation between circularly polarized waves

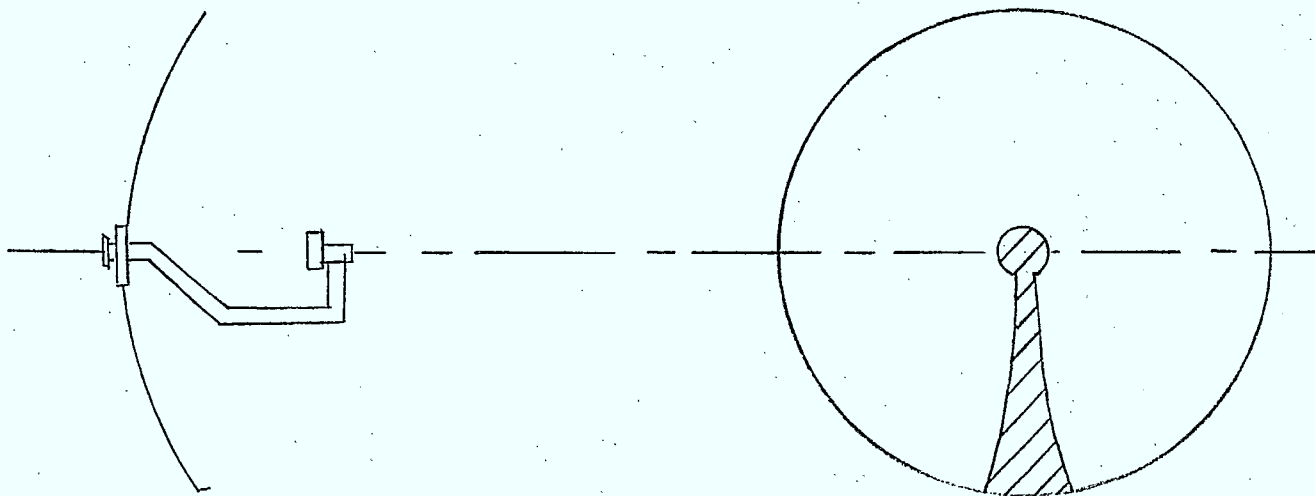


Figure 3.4.1(a) Centrally-mounted J-hook feed.

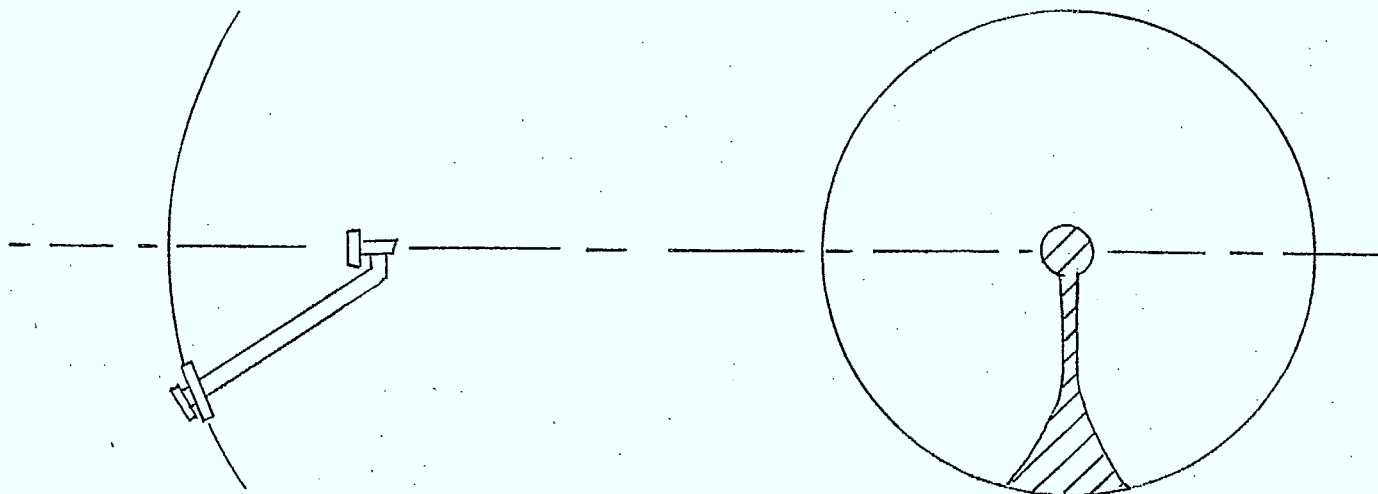


Figure 3.4.1(b) Side-mounted J-hook feed.

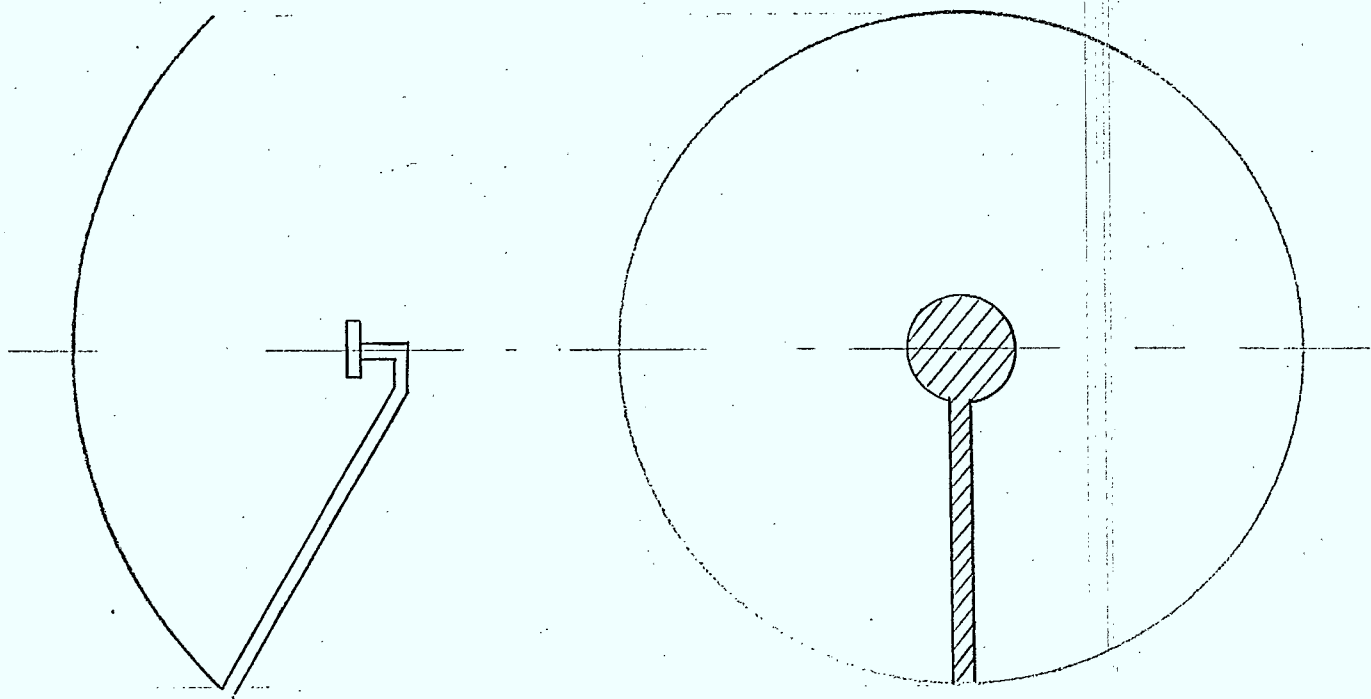


Figure 3.4.1(c) Rim mounted J-hook feed

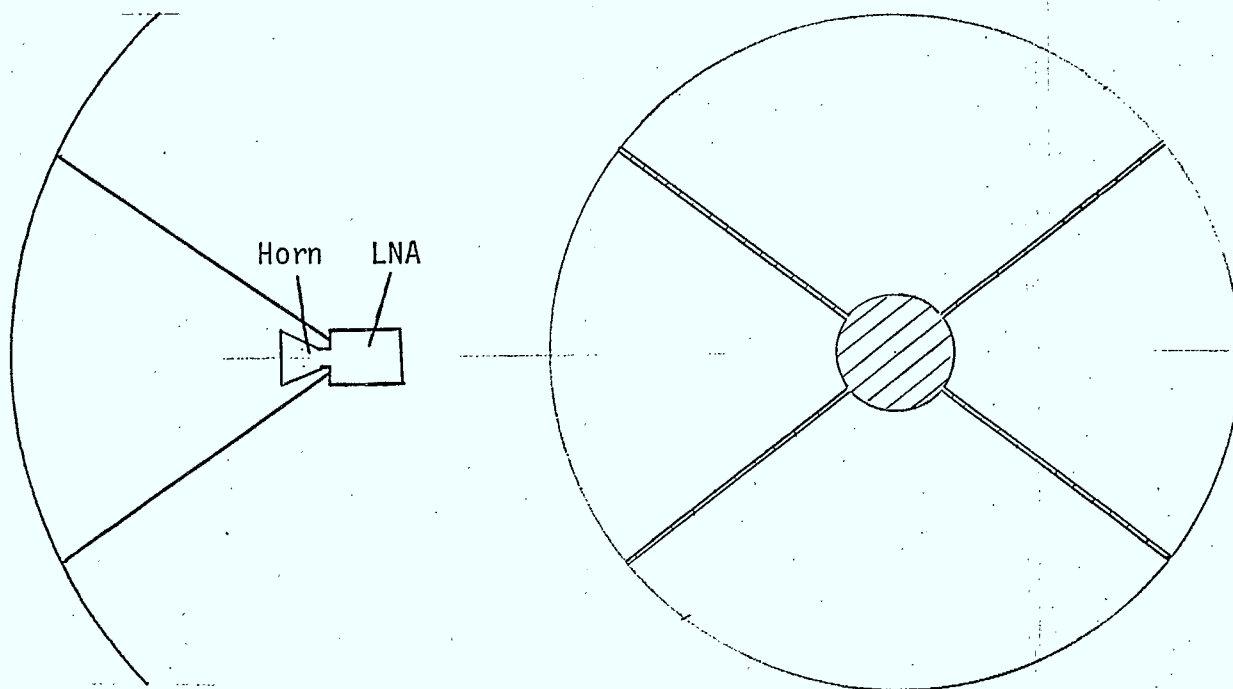


Figure 3.4.1(d) Strut supported feed

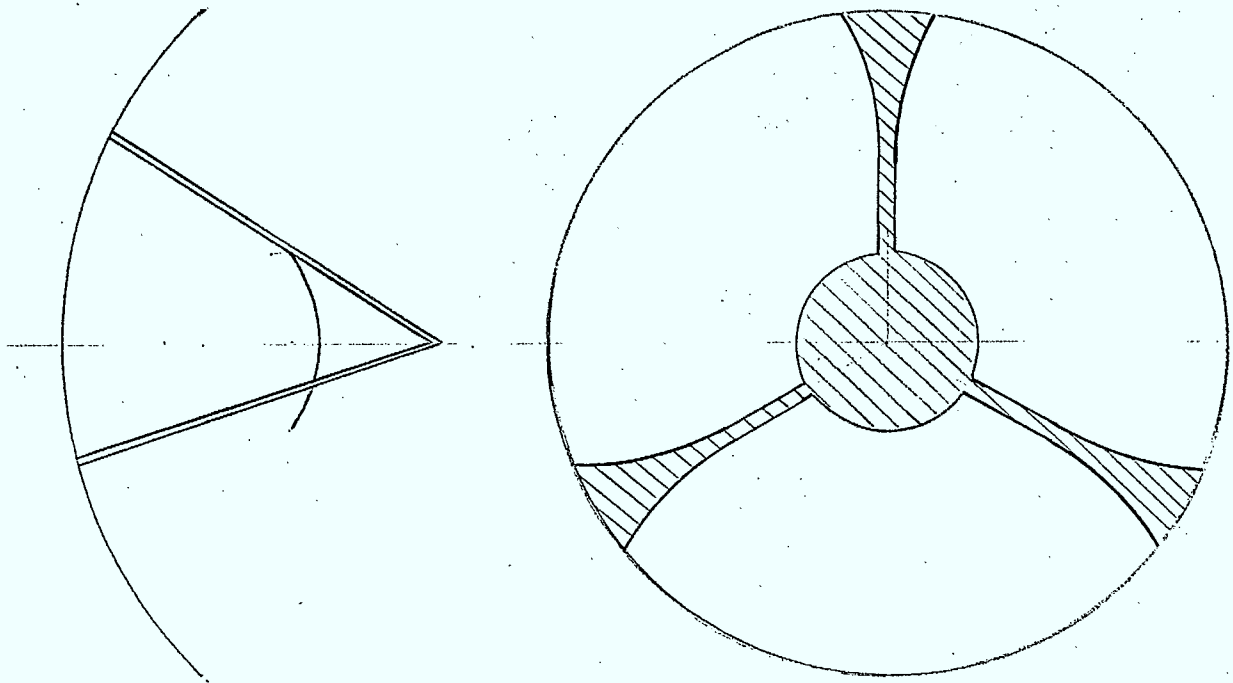


Figure 3.4.1(e) Tripod supported sub-reflector

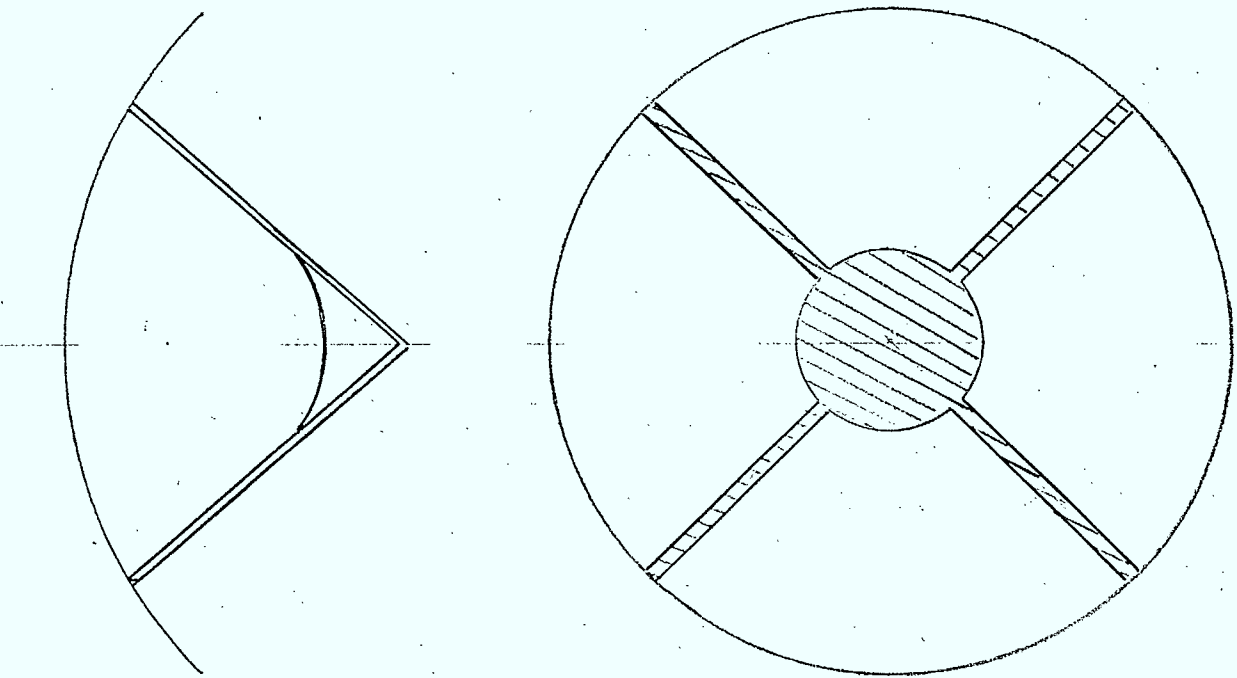


Figure 3.4.1(f) Quadripod supported sub-reflector

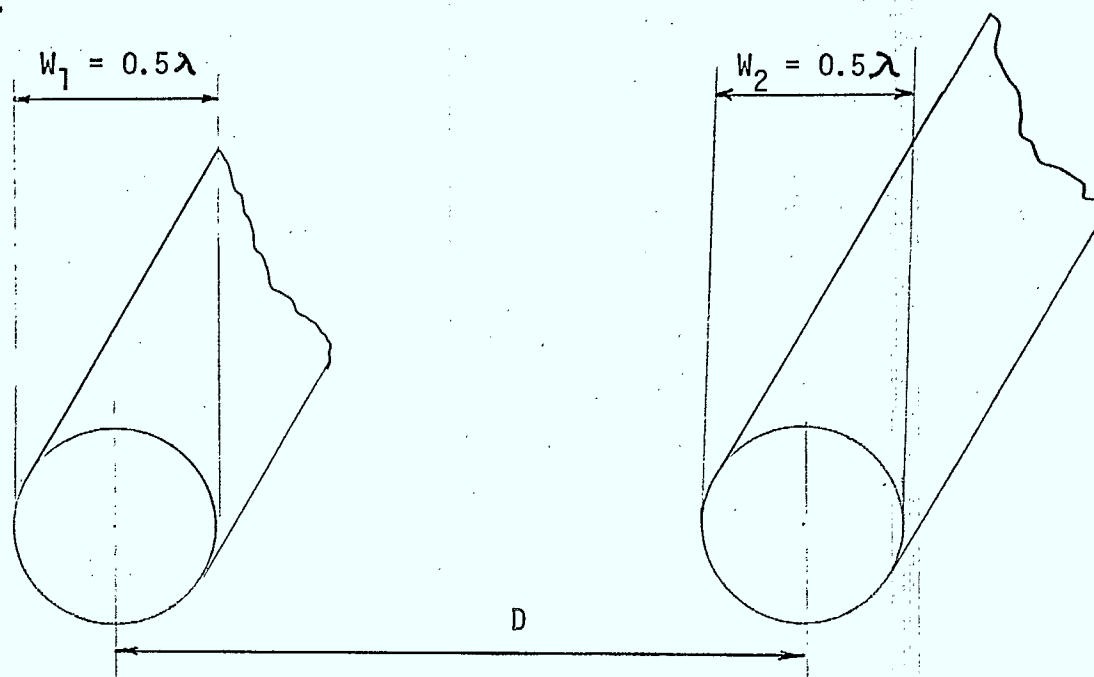


Figure 3.4.2(a)

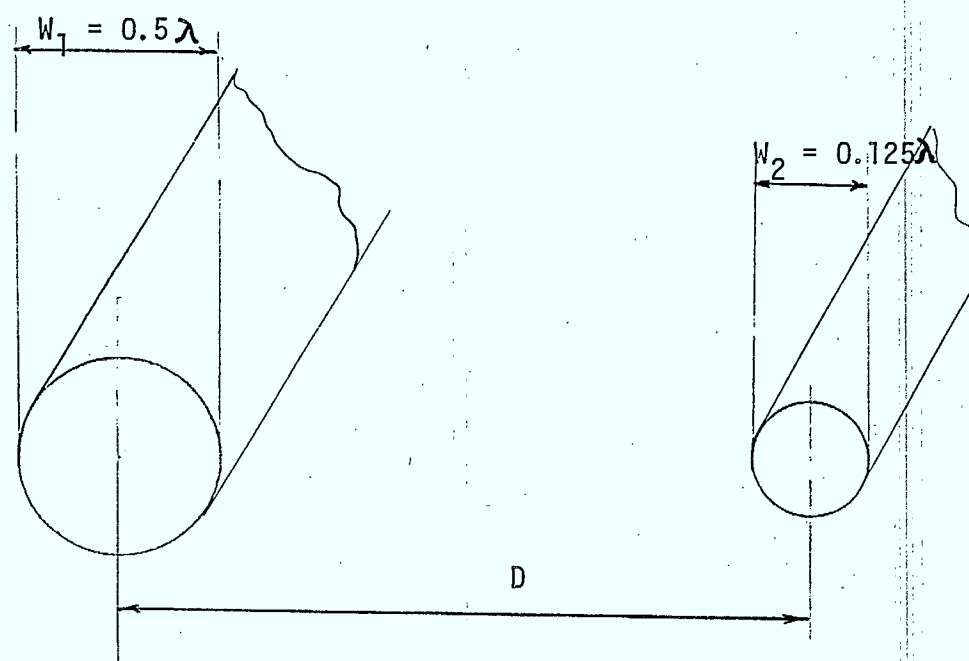


Figure 3.4.2(b)

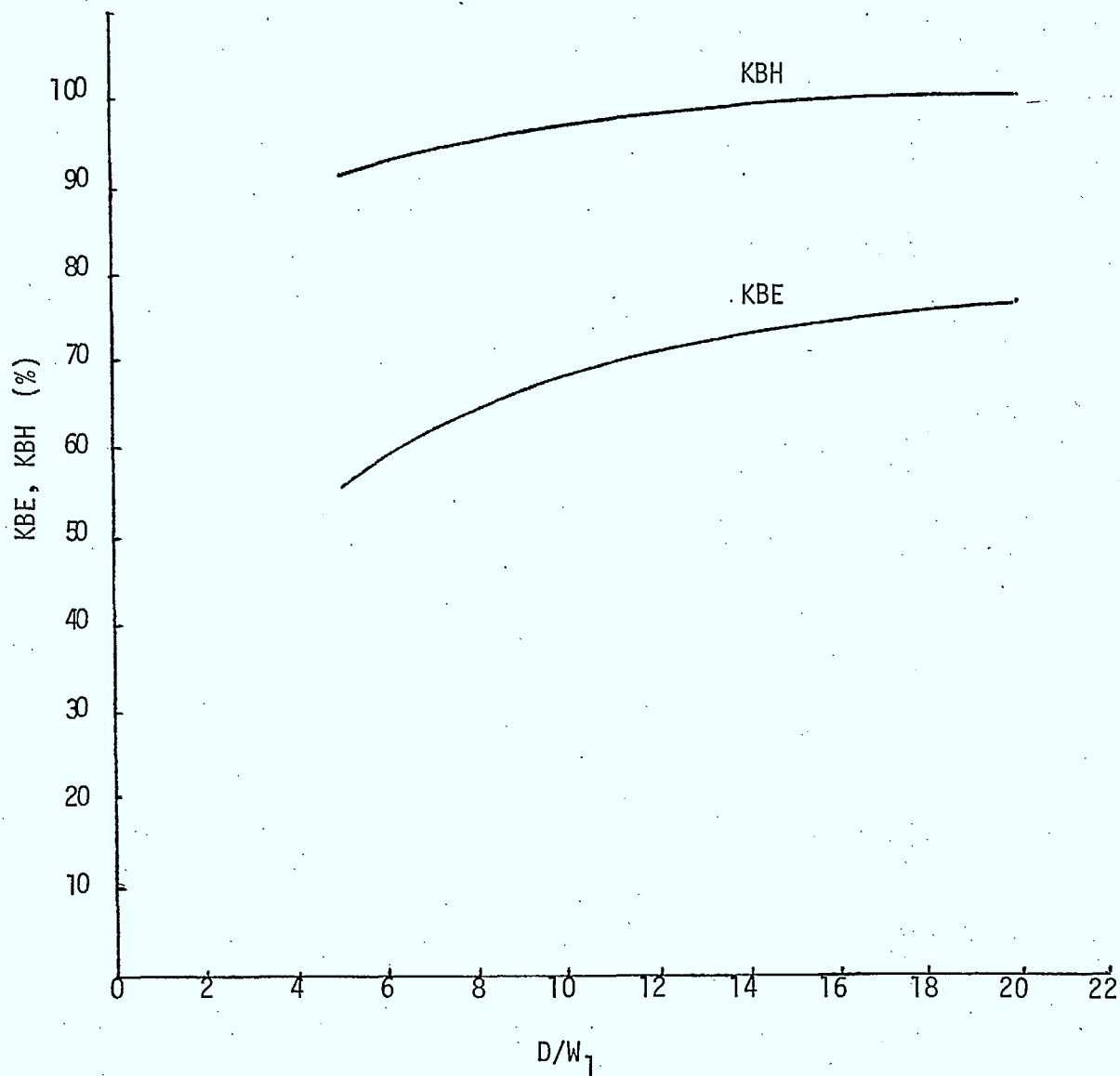


Figure 3.4.3(a) Composite KBE and KBH for right-circular cylinders as function of separation/larger-diameter

$$W_1 = 0.5\lambda \quad W_2 = 0.5\lambda$$

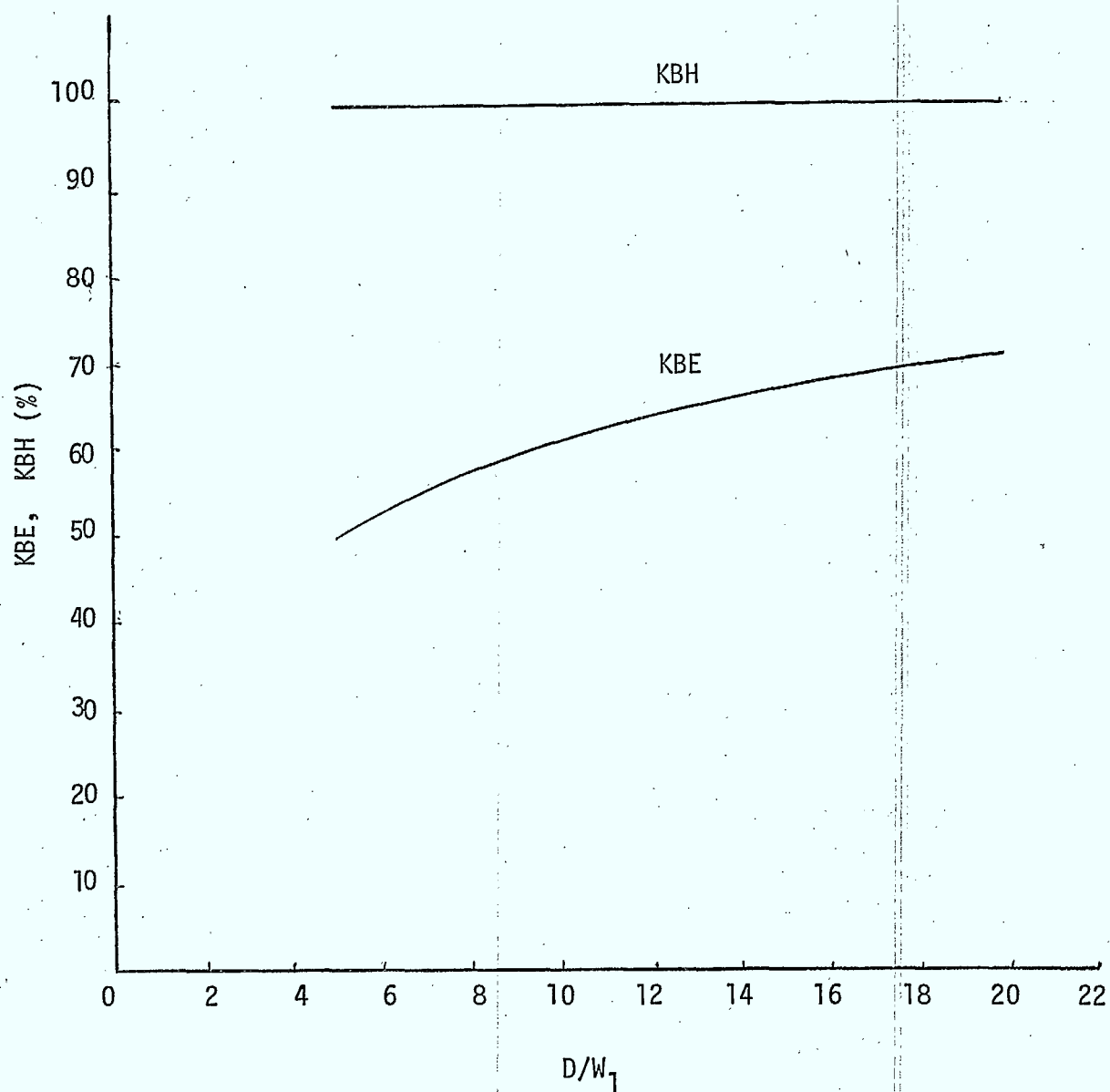


Figure 3.4.3(b) Composite KBE and KBH for right-circular cylinders as function of separation/larger-diameter

$$W_1 = 0.5\lambda \quad W_2 = 0.125\lambda$$

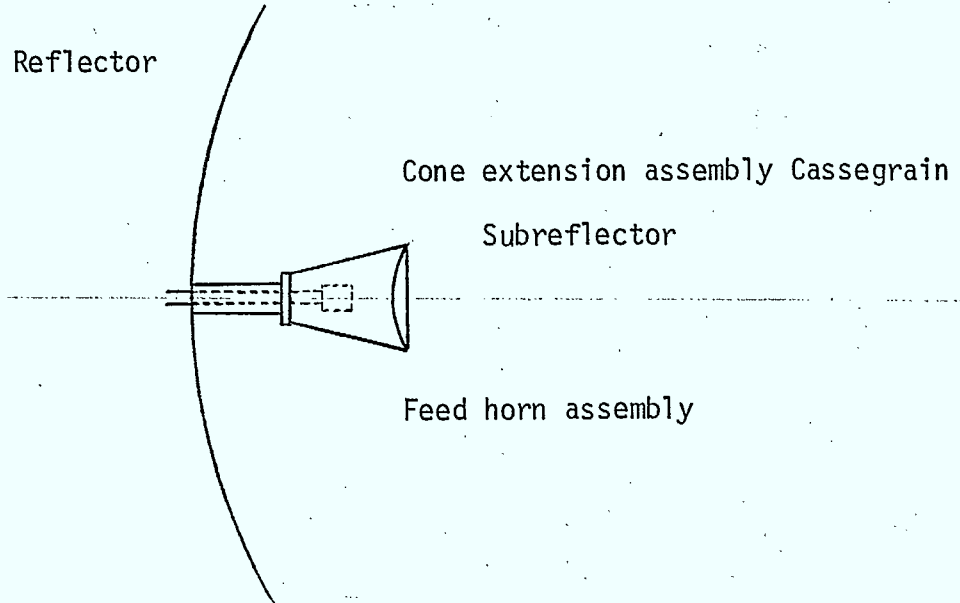


Figure 3.4.4 Conical tube support

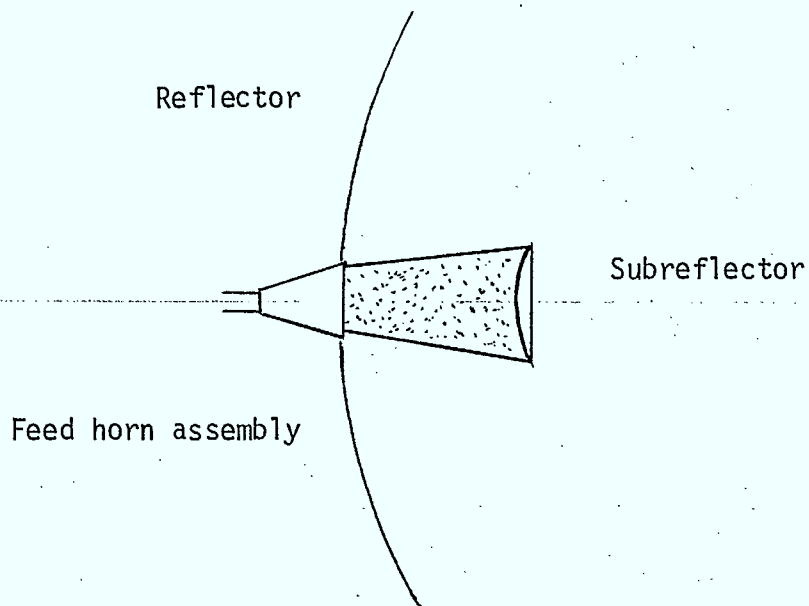


Figure 3.4.5(a) Dielectric guide support

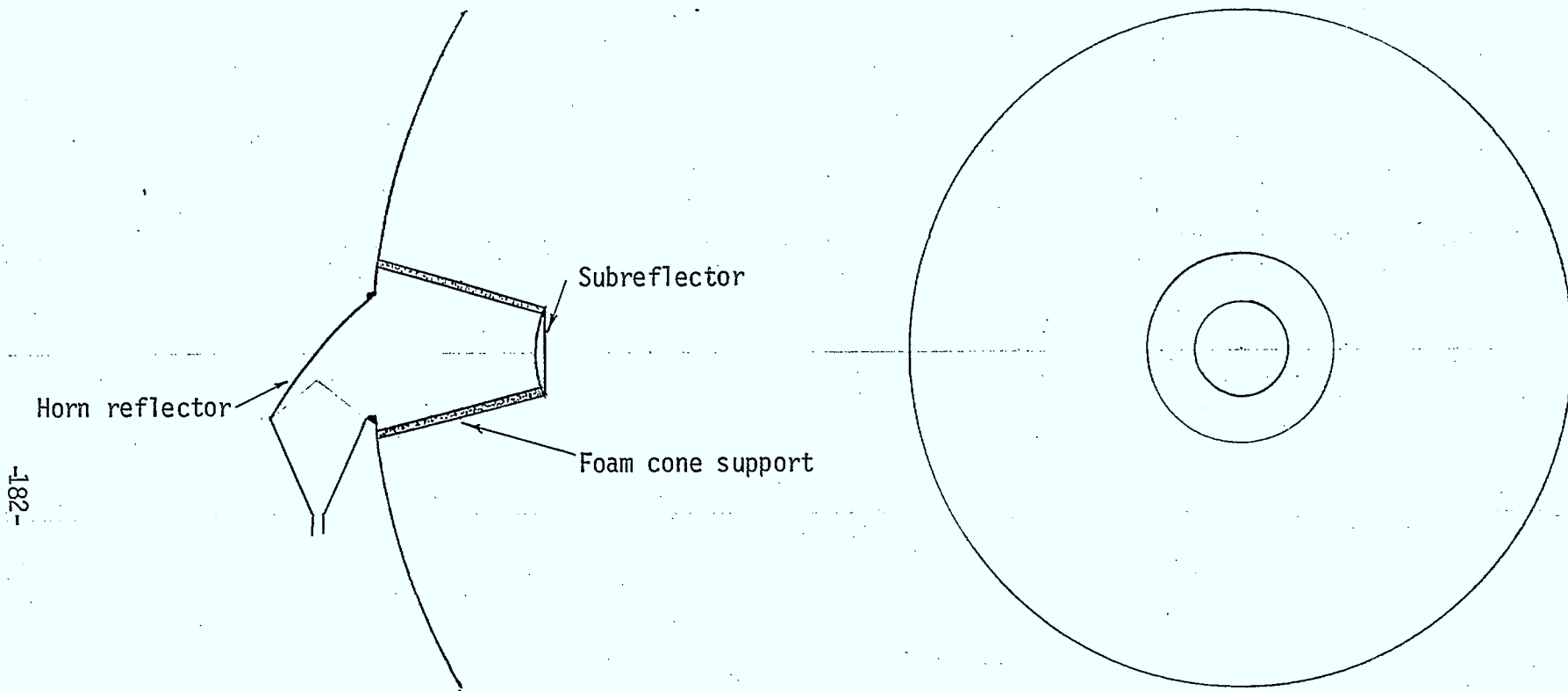


Figure 3.4.5(b) Foam cone subreflector support used in a Near Field Cassegrain

Paraboloid
Reflector

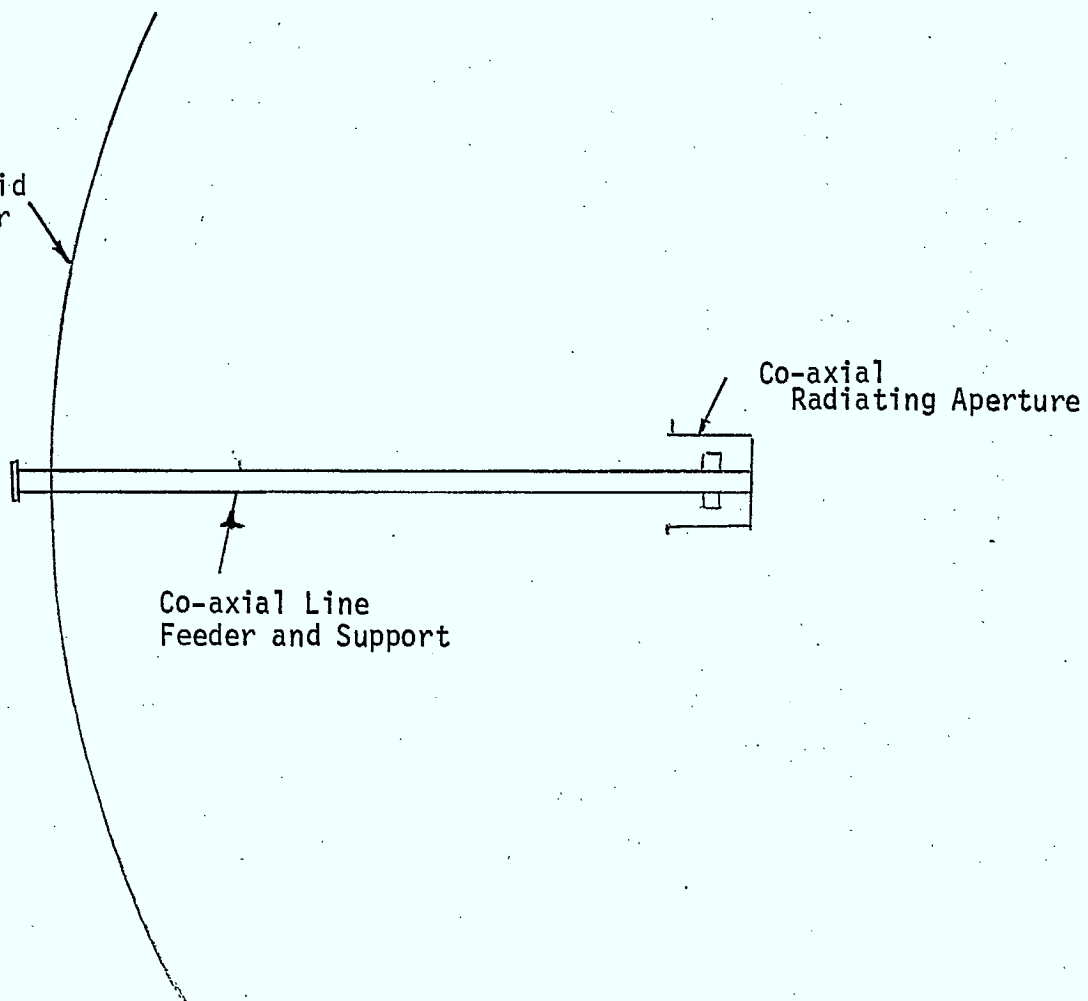


Figure 3.4.6(a) Co-axial line feed.

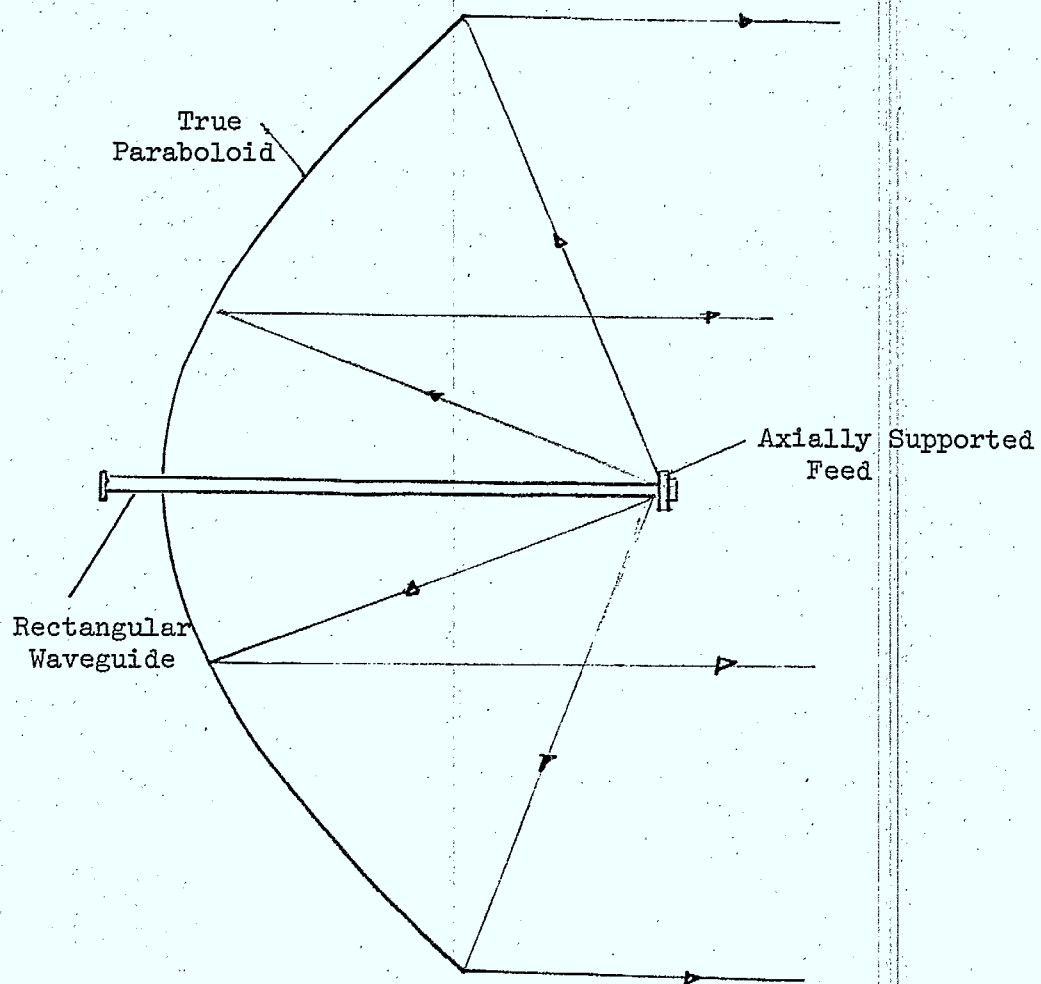


Figure 3.4.6(b) Paraboloid with an axially supported waveguide feed.

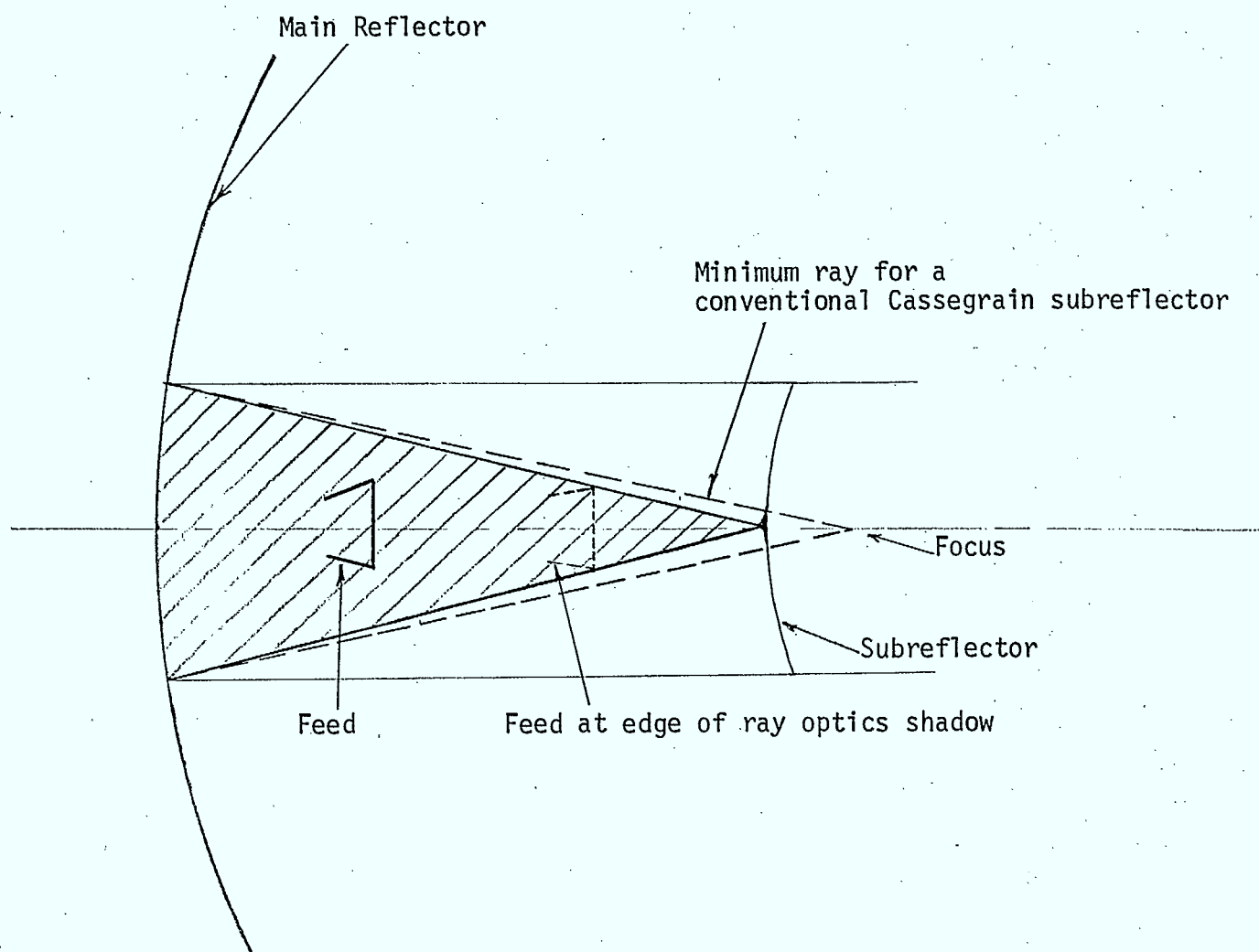


Figure 3.4.7 Shaped Cassegrain showing region where a feed can be placed without introducing an additional blockage.

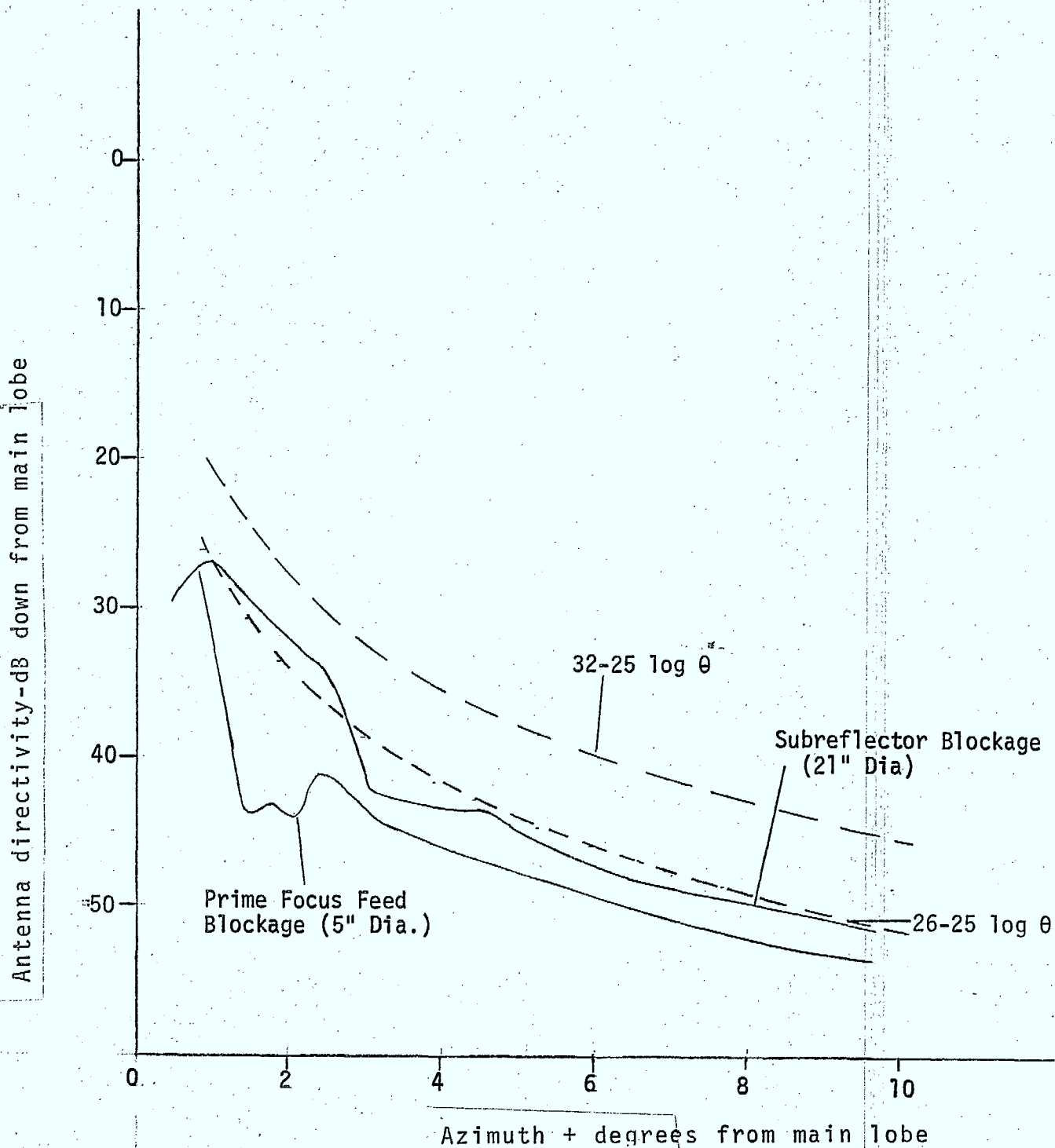


figure 3.4.8 Radiation pattern envelope of 15' reflector
at 11.95 GHz.

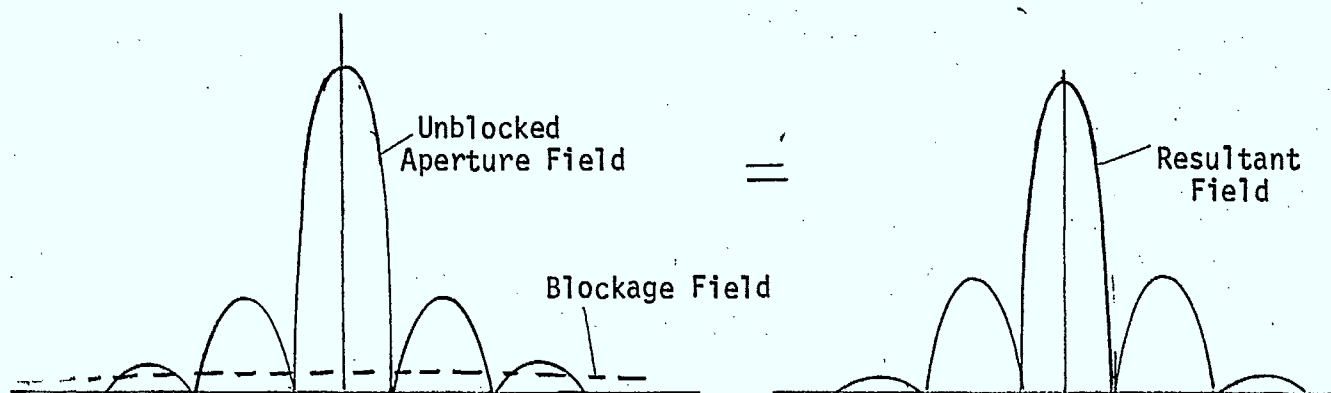


Figure 3.4.9(a) Effect of blockage.

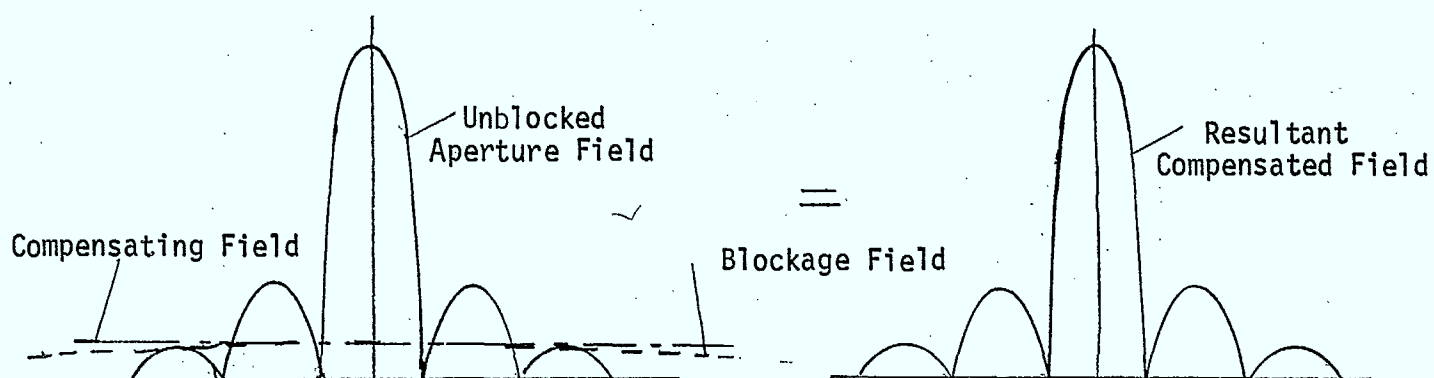


Figure 3.4.9(b) Effect of compensation.

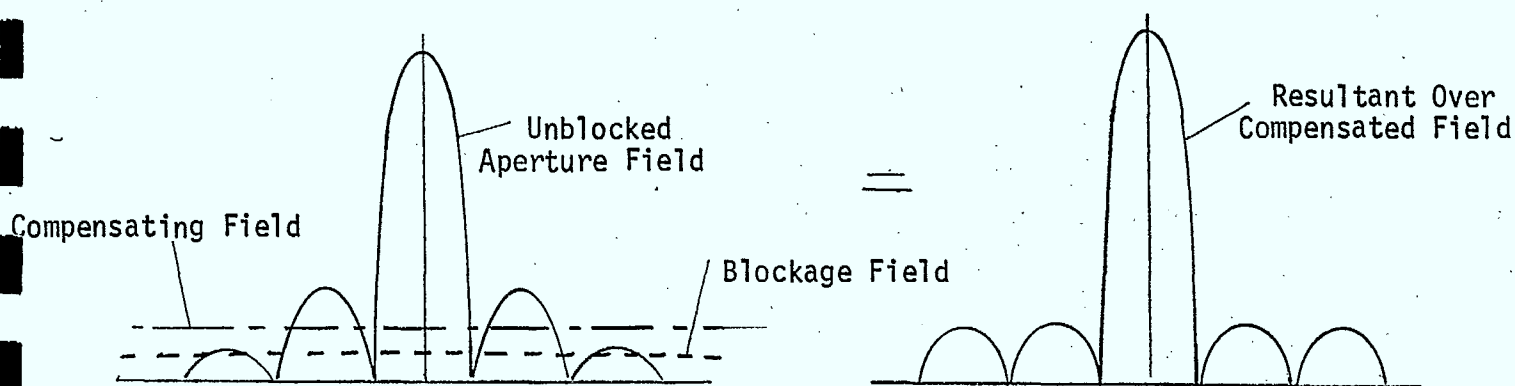


Figure 3.4.9(c) Effect of over compensation.

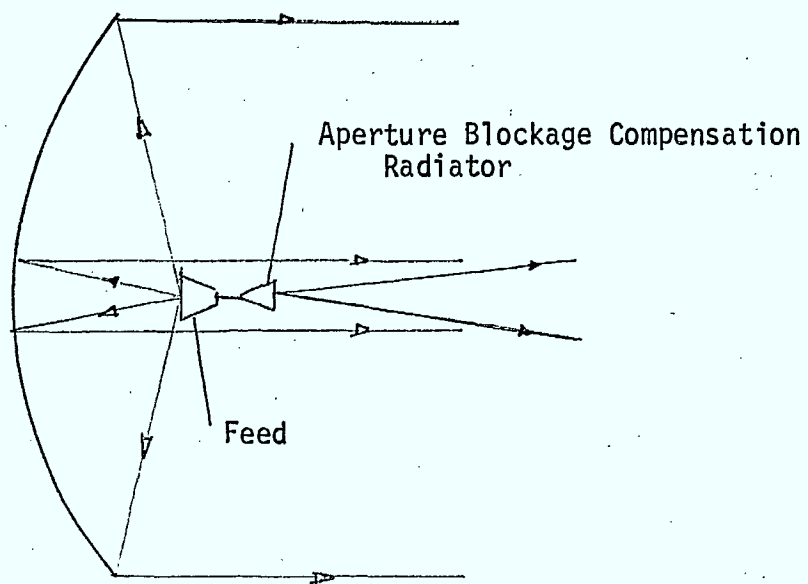


Figure 3.4.10(a) Aperture blockage compensation.

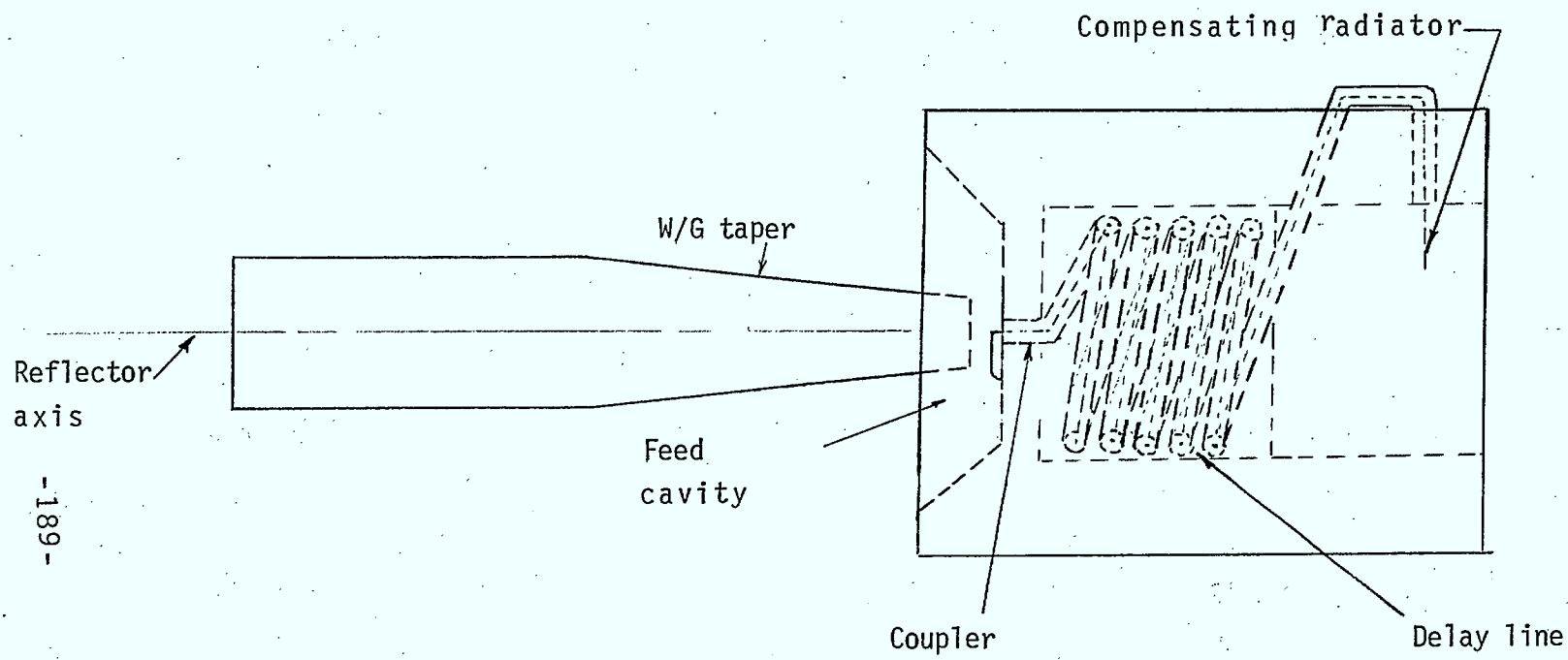


Figure 3.4.10(b) Aperture blockage compensation with an axial supported feed.

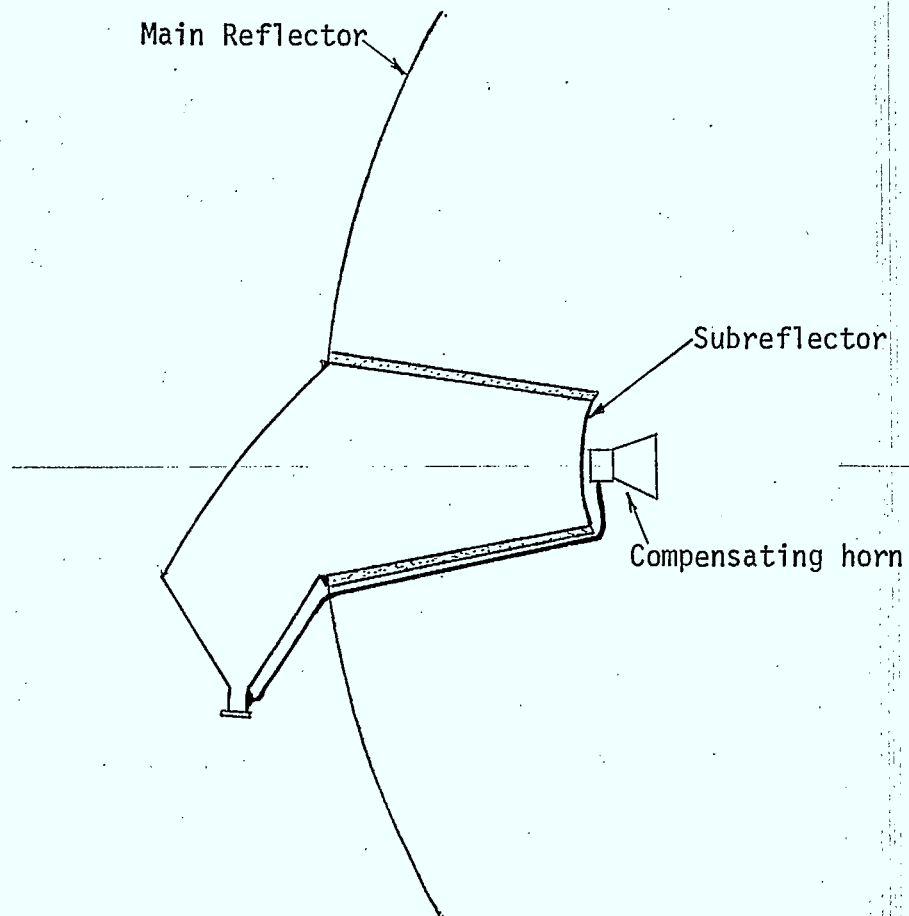


Figure 3.4.10(c) Aperture blockage compensation for a subreflector.

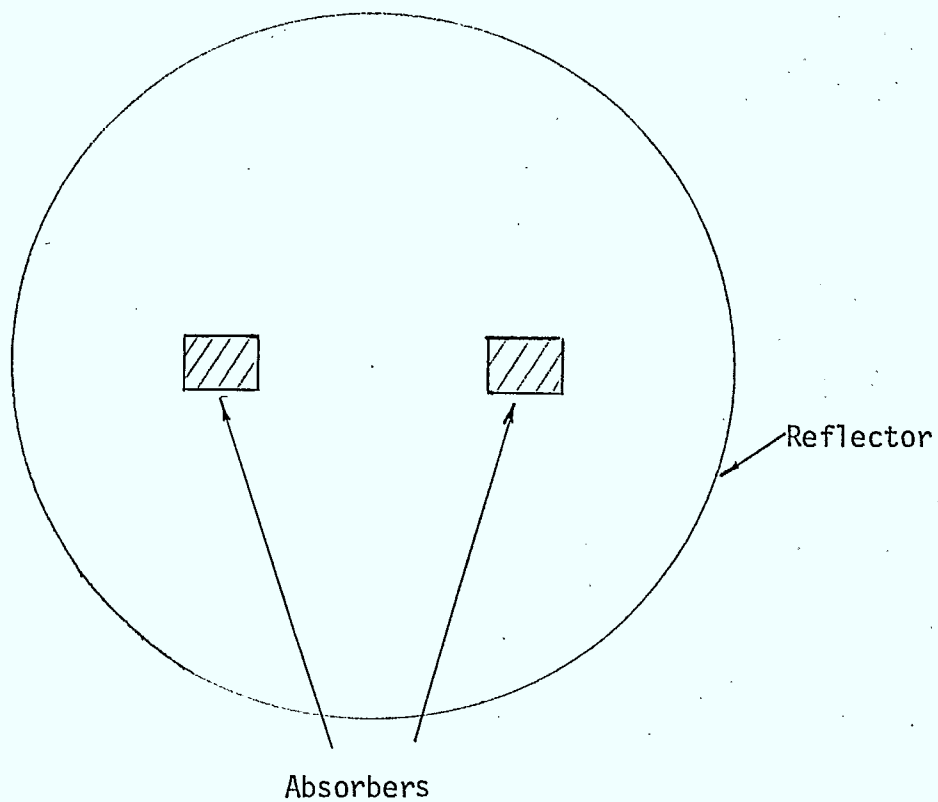


Figure 3.4.11 The use of absorbers for selective compensation of Antenna Sidelobes.

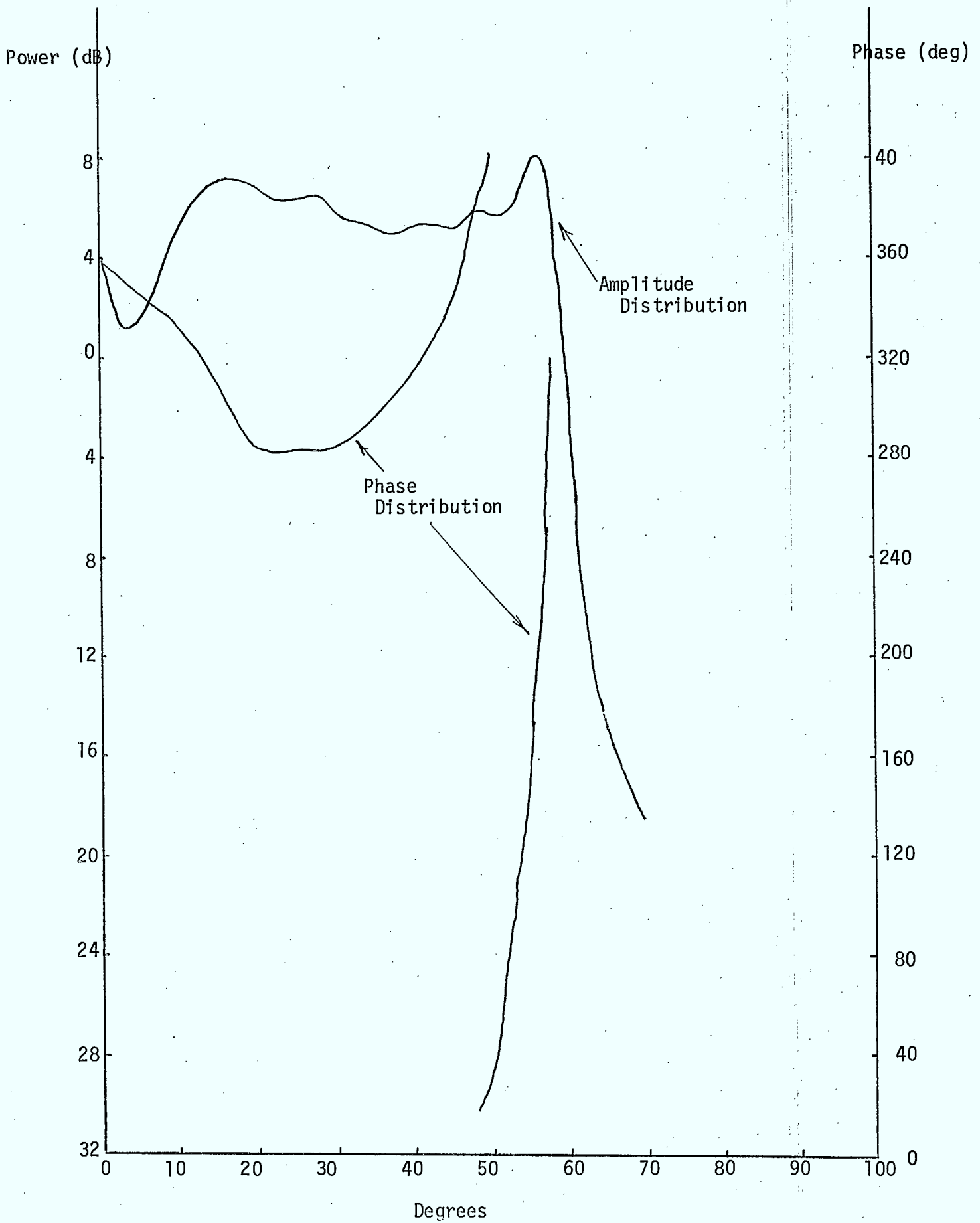


Figure 3.5.1 Diffraction Pattern from a 69 Subreflector

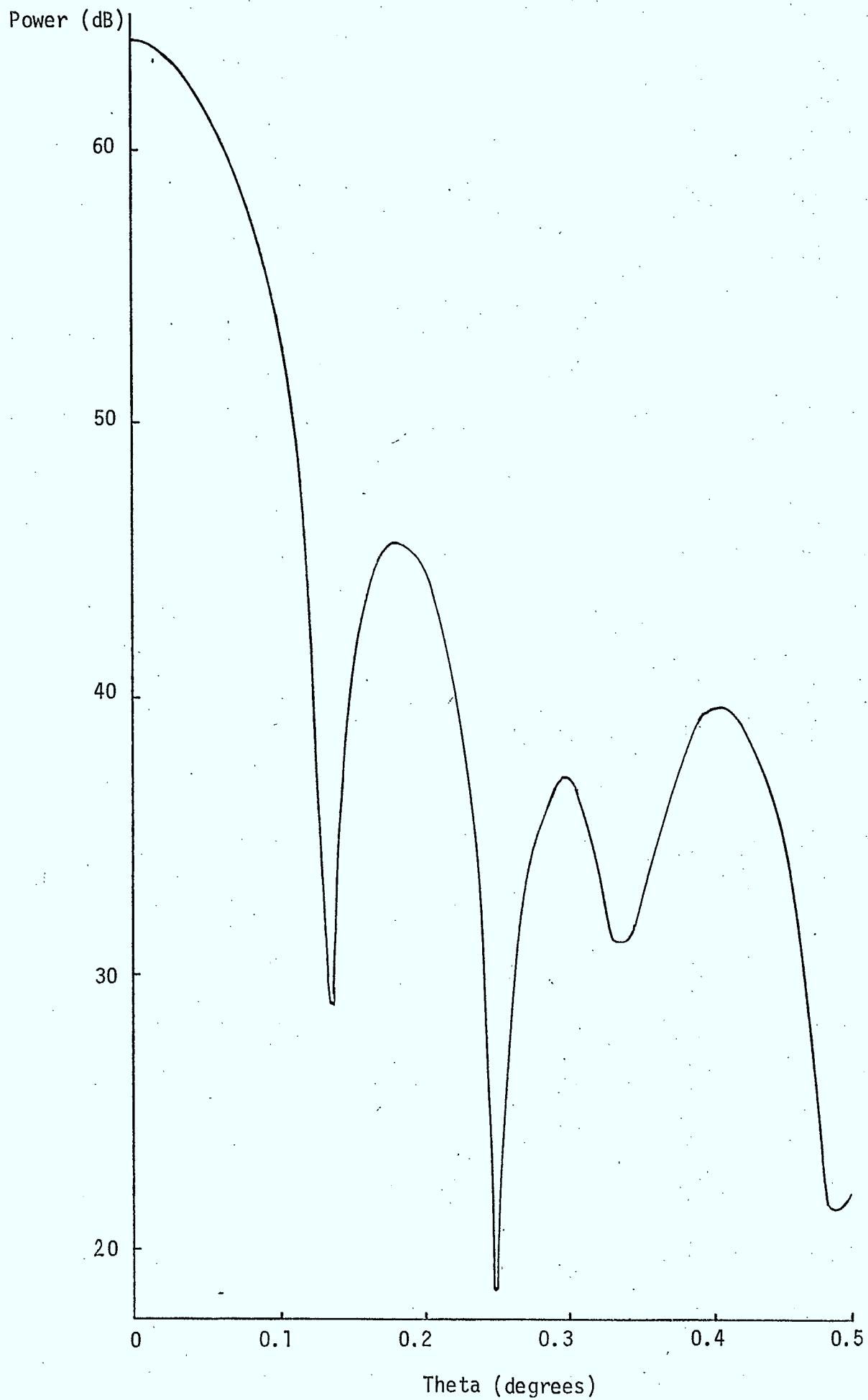


Figure 3.5.2 Far field diffraction pattern of a 529λ antenna

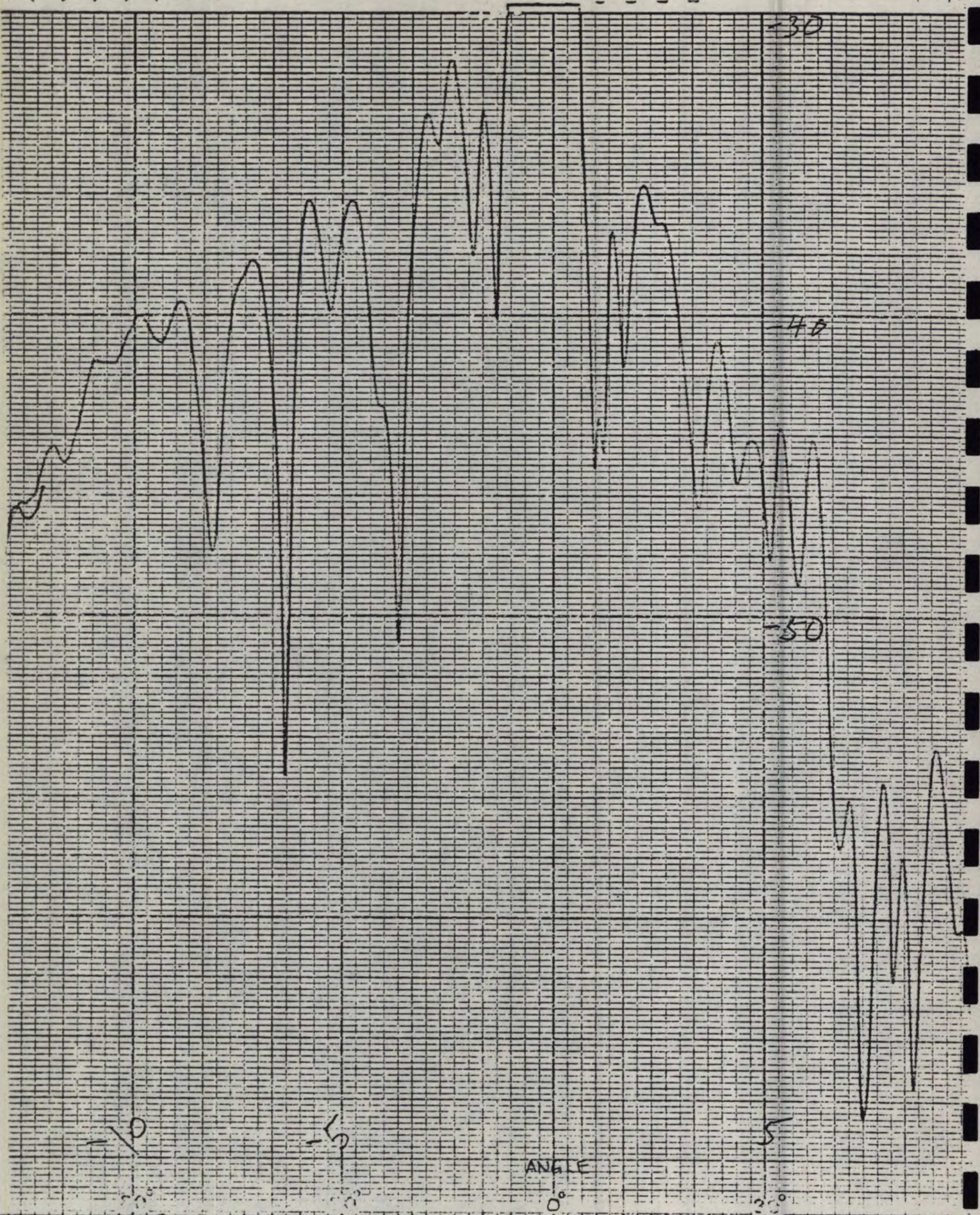


Figure 3.5.3(a) 12' J-hook supported antenna at 11.7GHz - no absorber.

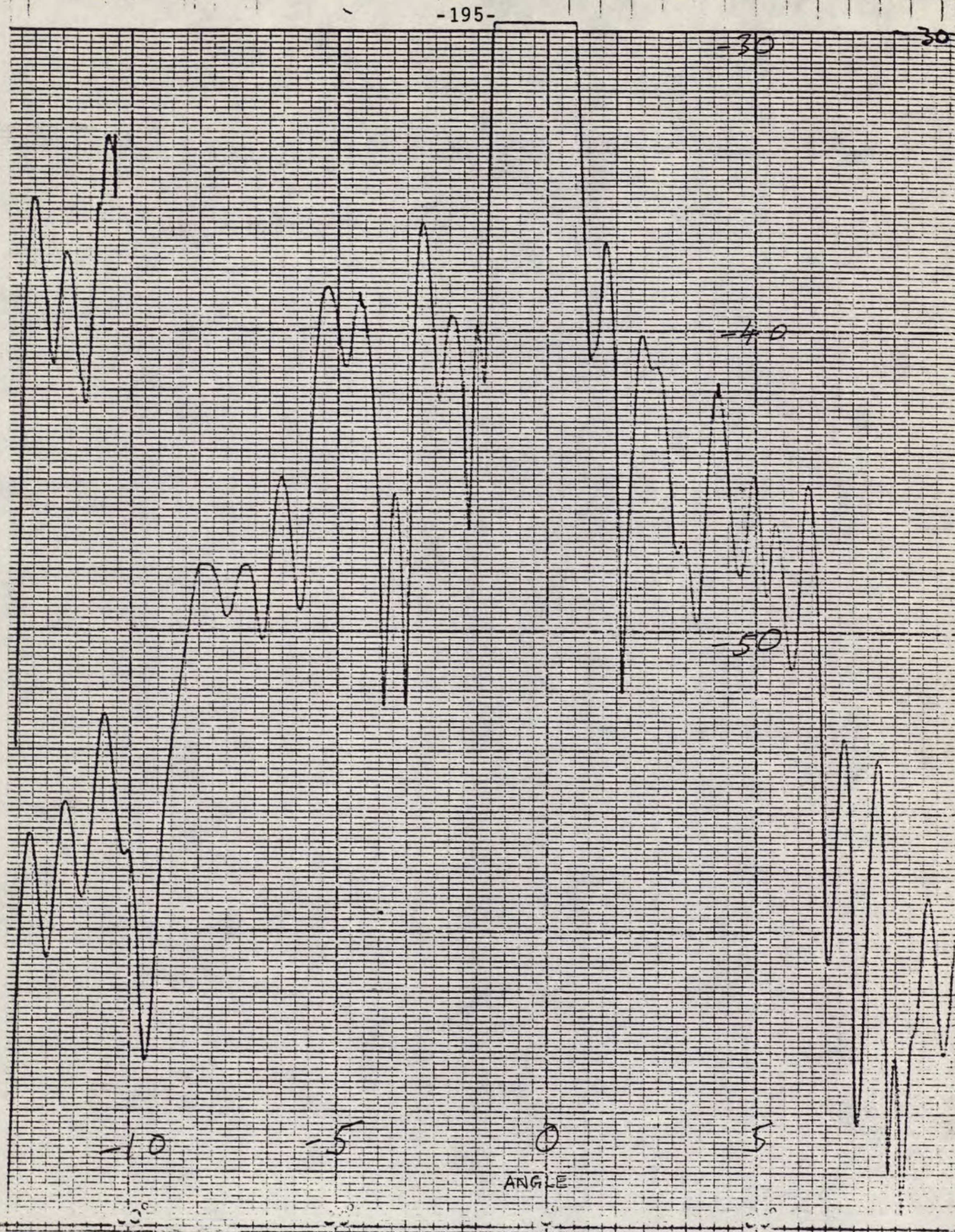


Figure 3.5.3(b) 12' J-hook supported antenna at 11.7 GHz - with absorber on J-hook.

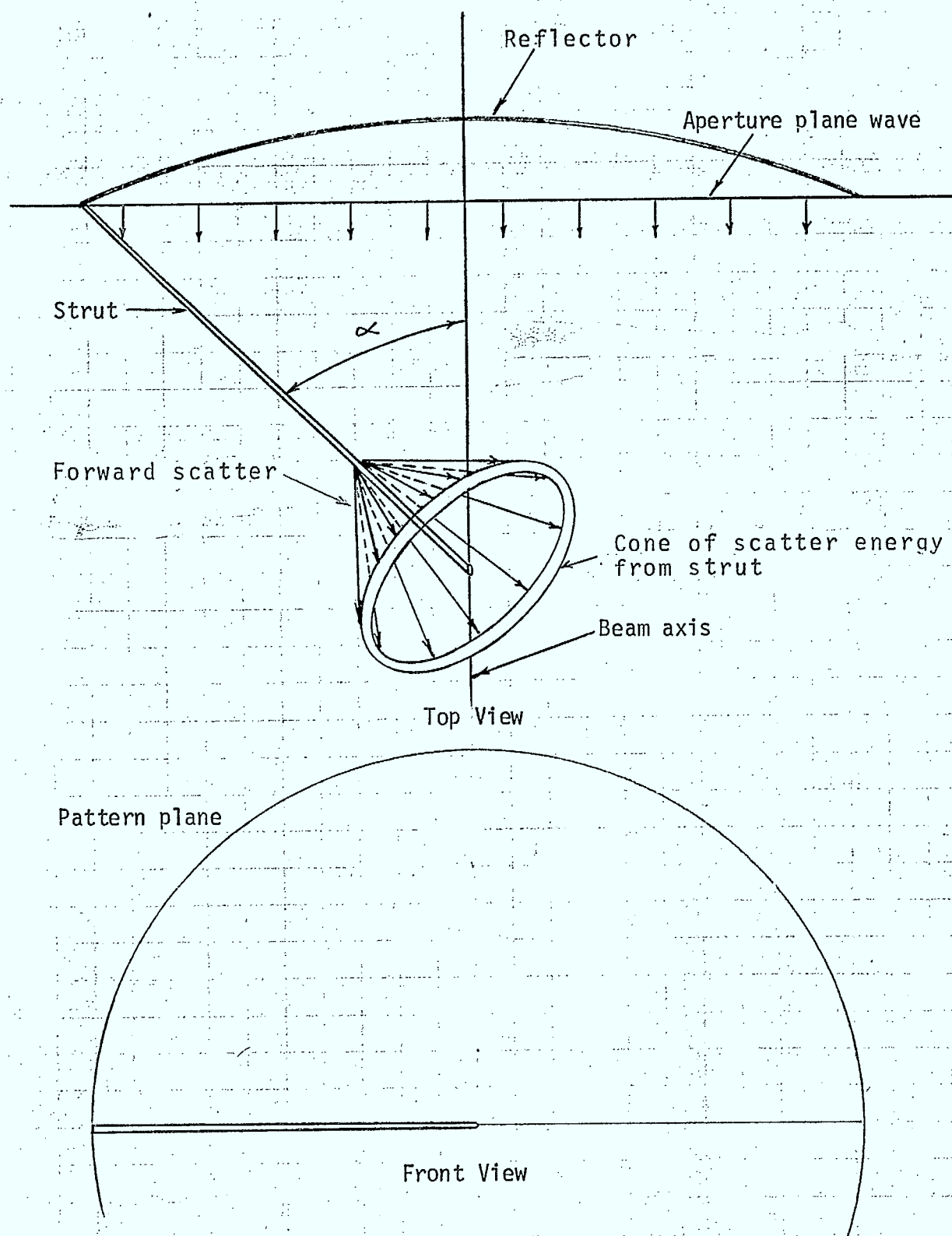


Figure 3.5.4 Scatter pattern of a strut

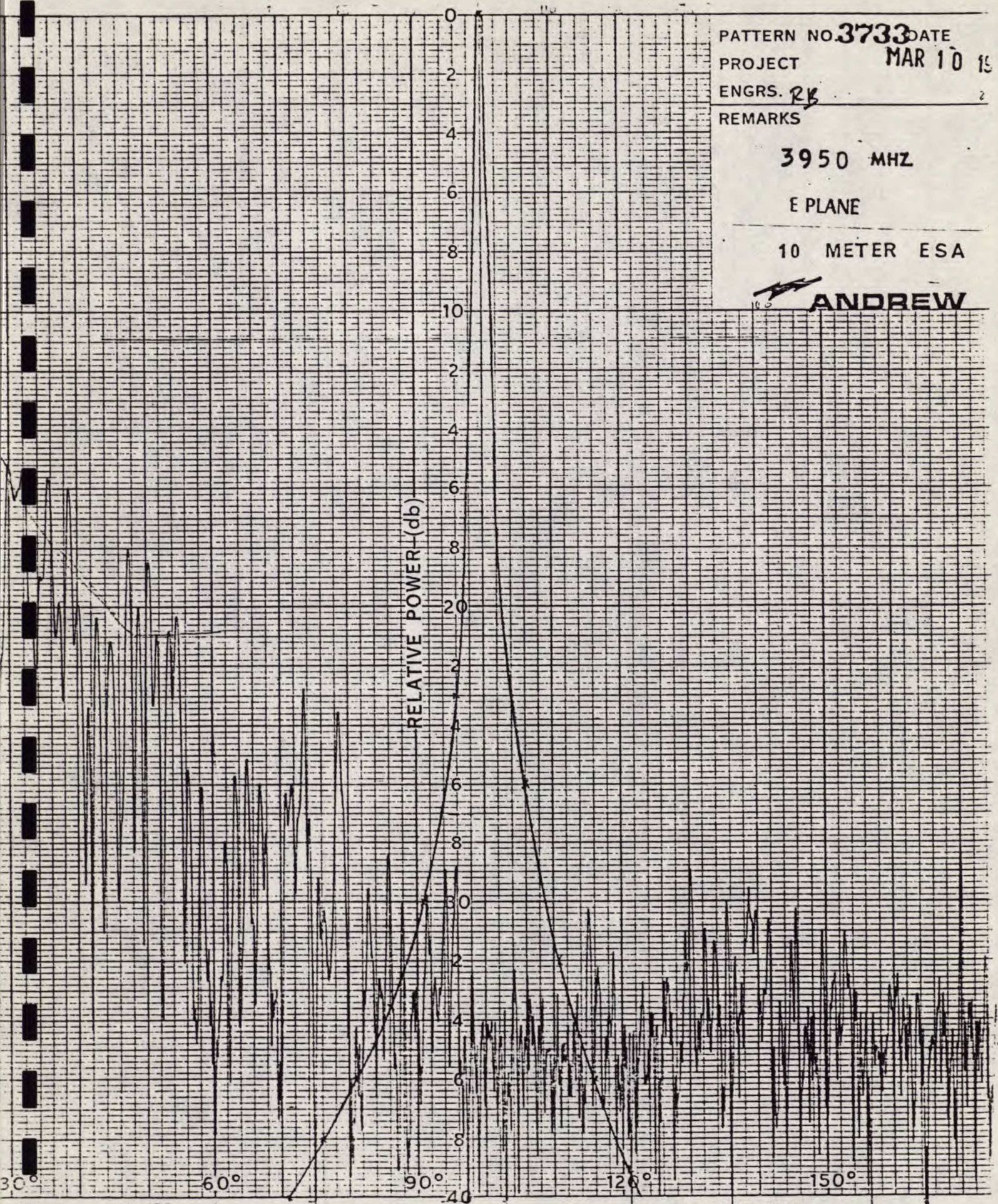
PATTERN NO. **3733** DATE
PROJECT **MAR 10 19**
ENGRS. **RB**
REMARKS

3950 MHZ

E PLANE

10 METER ESA

ANDREW



No. 153 Figure 3.5.5 Calculated RPE of scatter from 1 strut

PRINTED IN U.S.A.

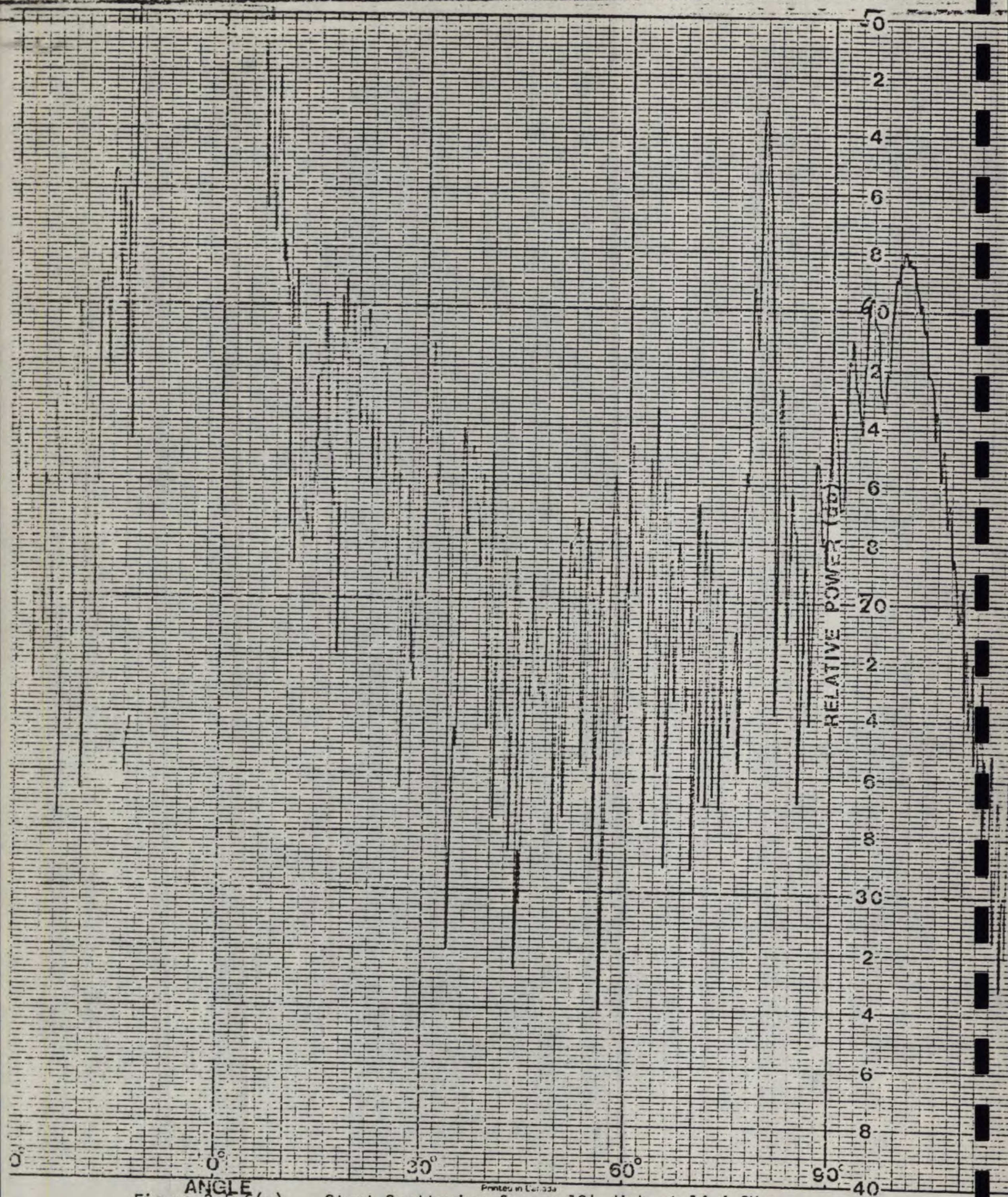


Figure 3.5.6(a)

Strut Scattering from a 12' dish at 14.4 GHz

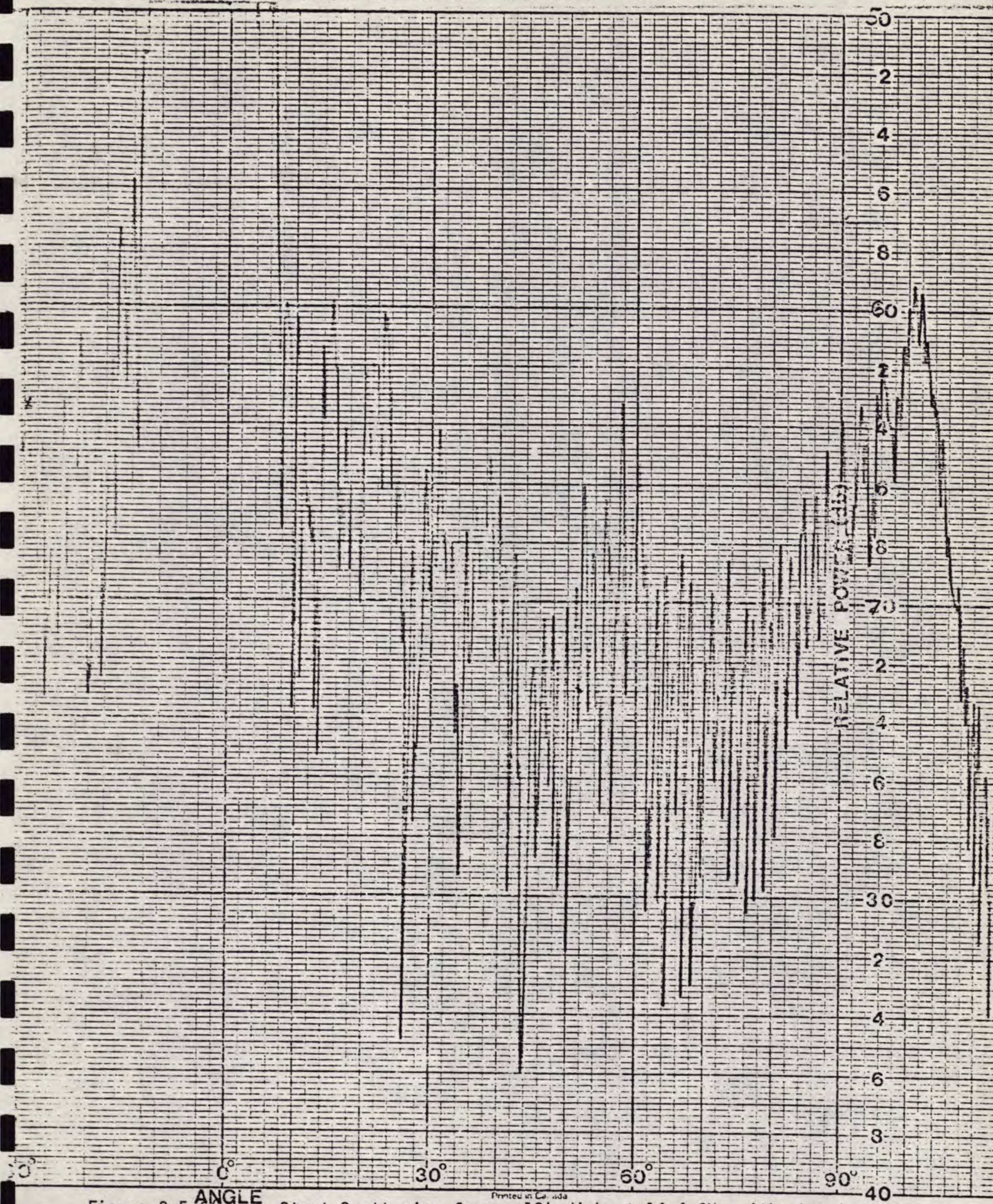


Figure 3.5.6(b) Strut Scattering from a 12' dish at 14.4 GHz with absorber

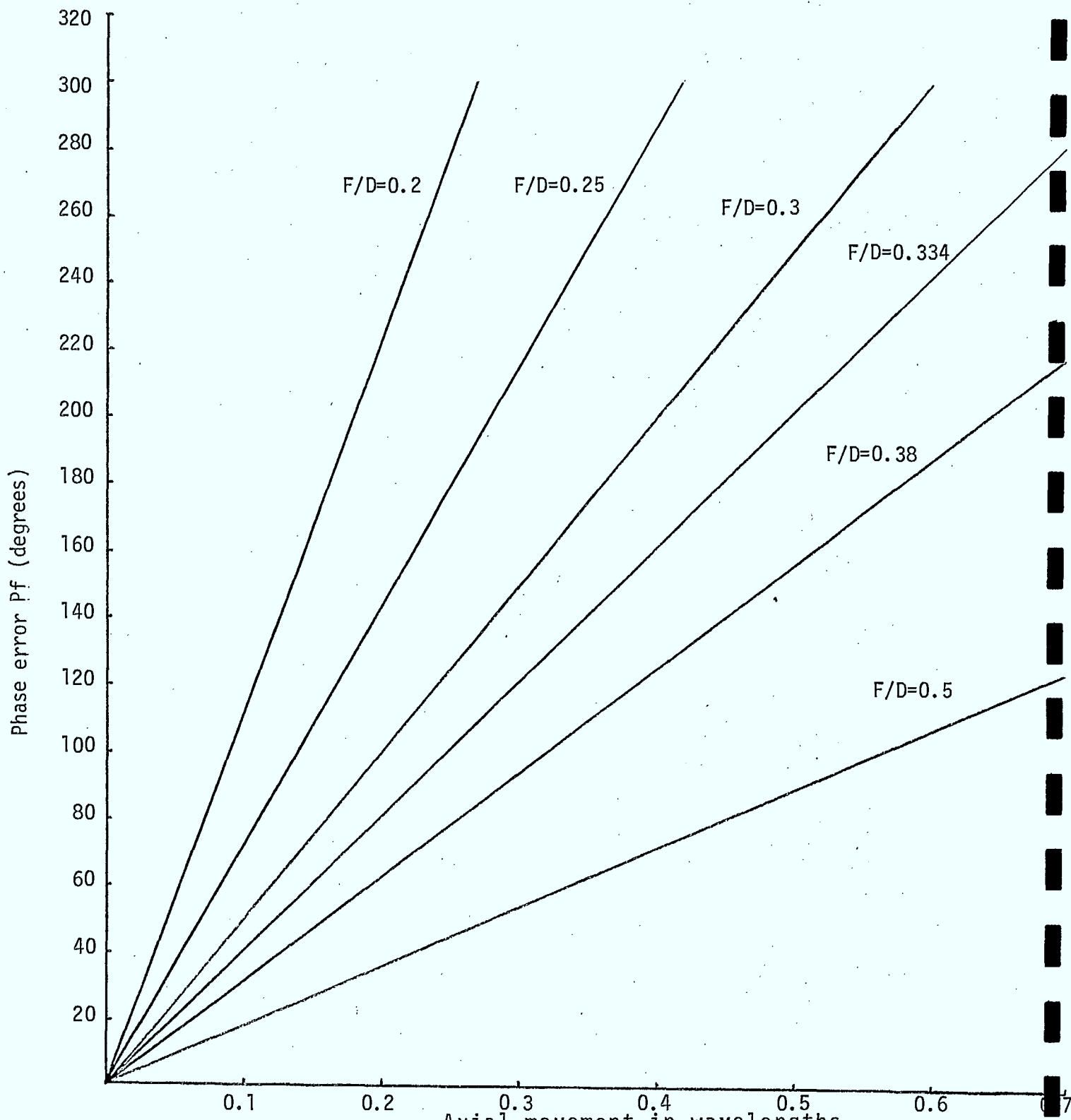


Figure 3.6.1

Axial movement in wavelengths
Phase error vs feed axial movement
for parabolic reflector.

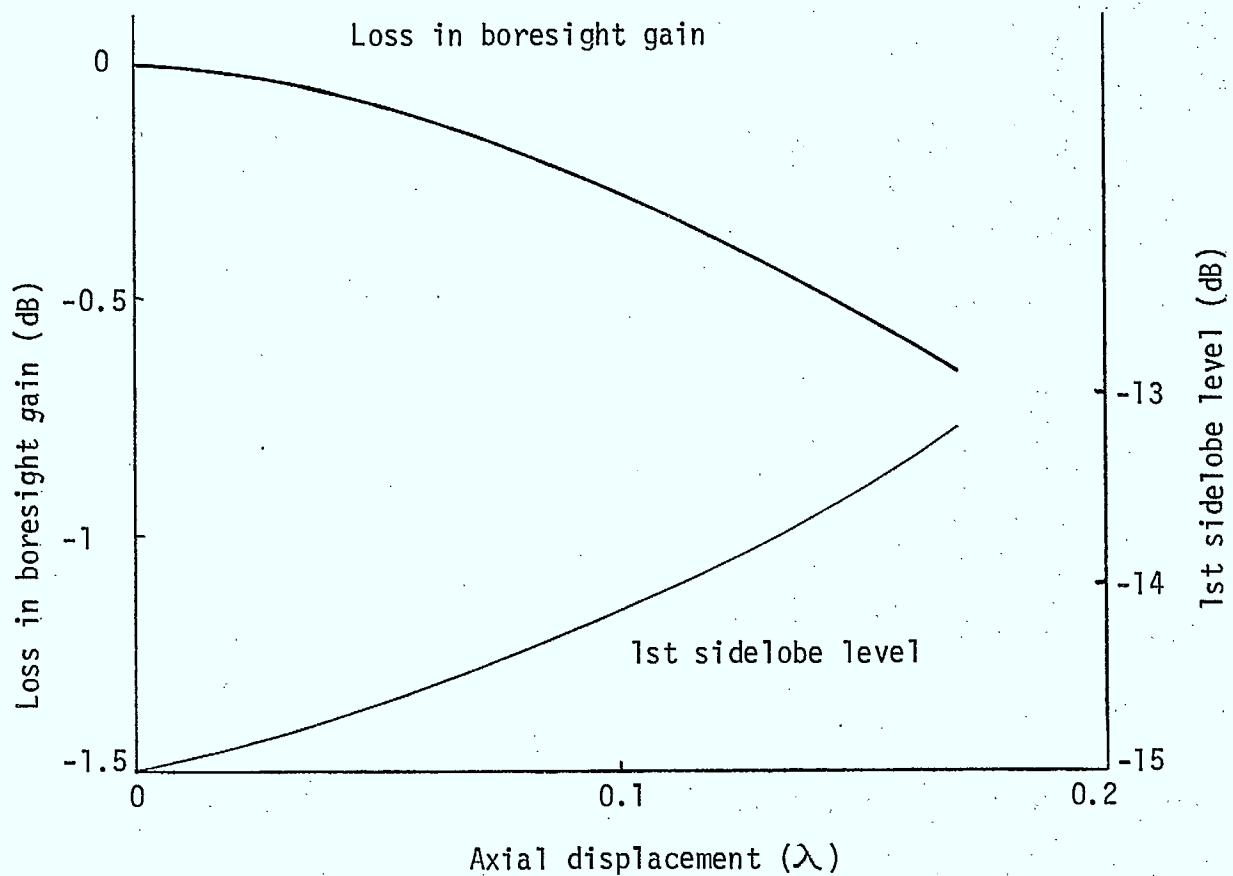


Figure 3.6.2(a)

Effect of the displacement from the designed position of the feed-subreflector combination of a shaped cassegrain (main reflector = 84λ ; subreflector = 14.2λ)
 $F/D = 0.2$

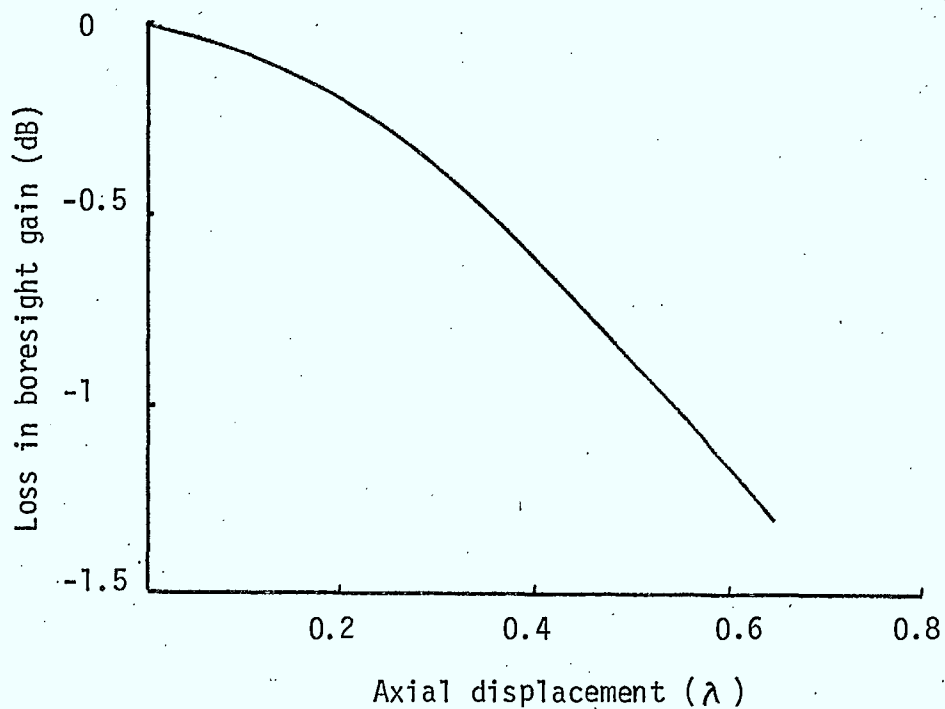


Figure 3.6.2(b) Effect of the displacement from the designed position of the feed-subreflector combination of a Shaped Cassegrain
 (Main reflector = 529λ ; subreflector = 68λ)
 $F/D = 0.44$

Gain loss (dB) for a typical reflector (R.M.S. = 0.014") at 13.2 GHz

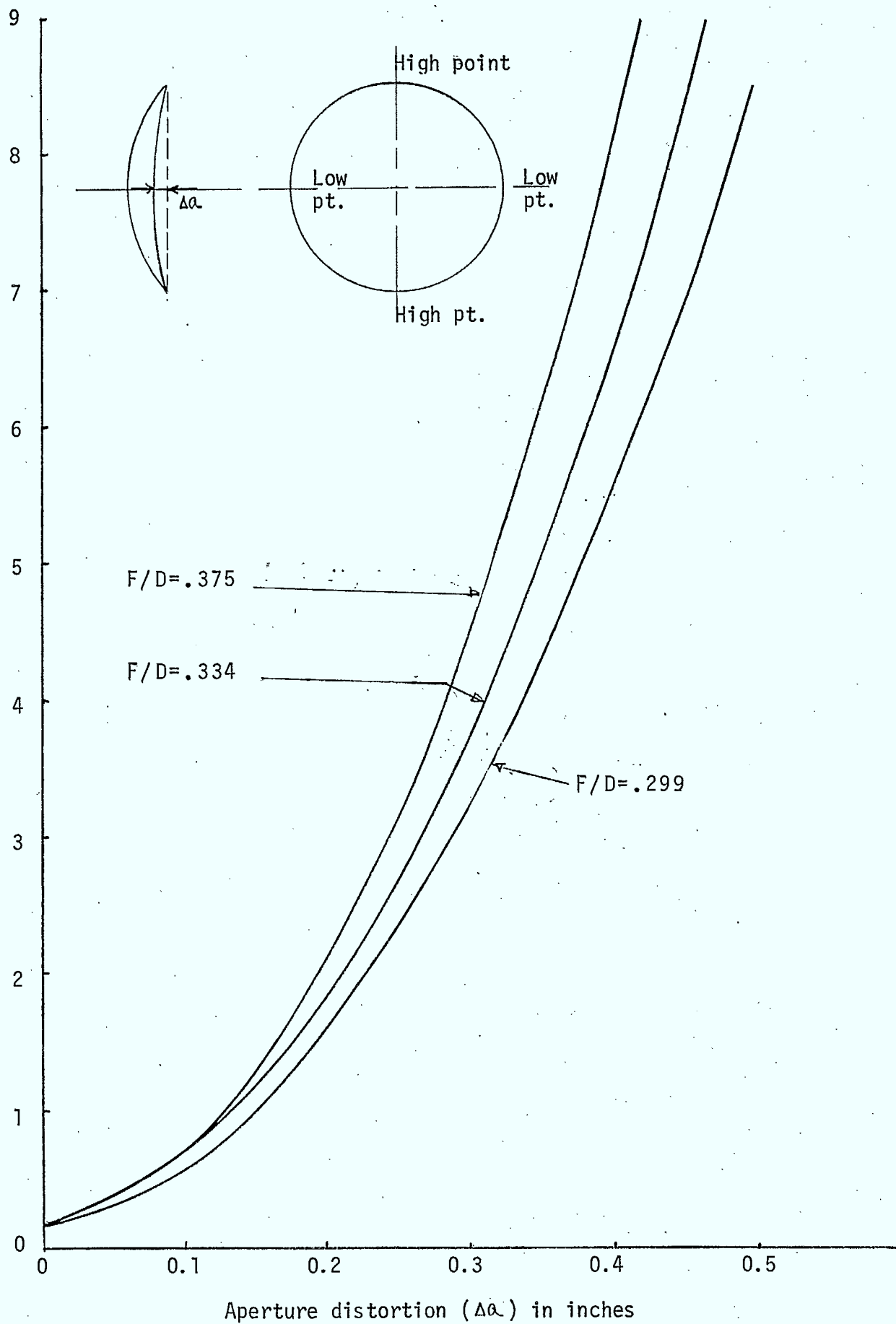


Figure 3.6.3 Gain loss vs. aperture distortion.

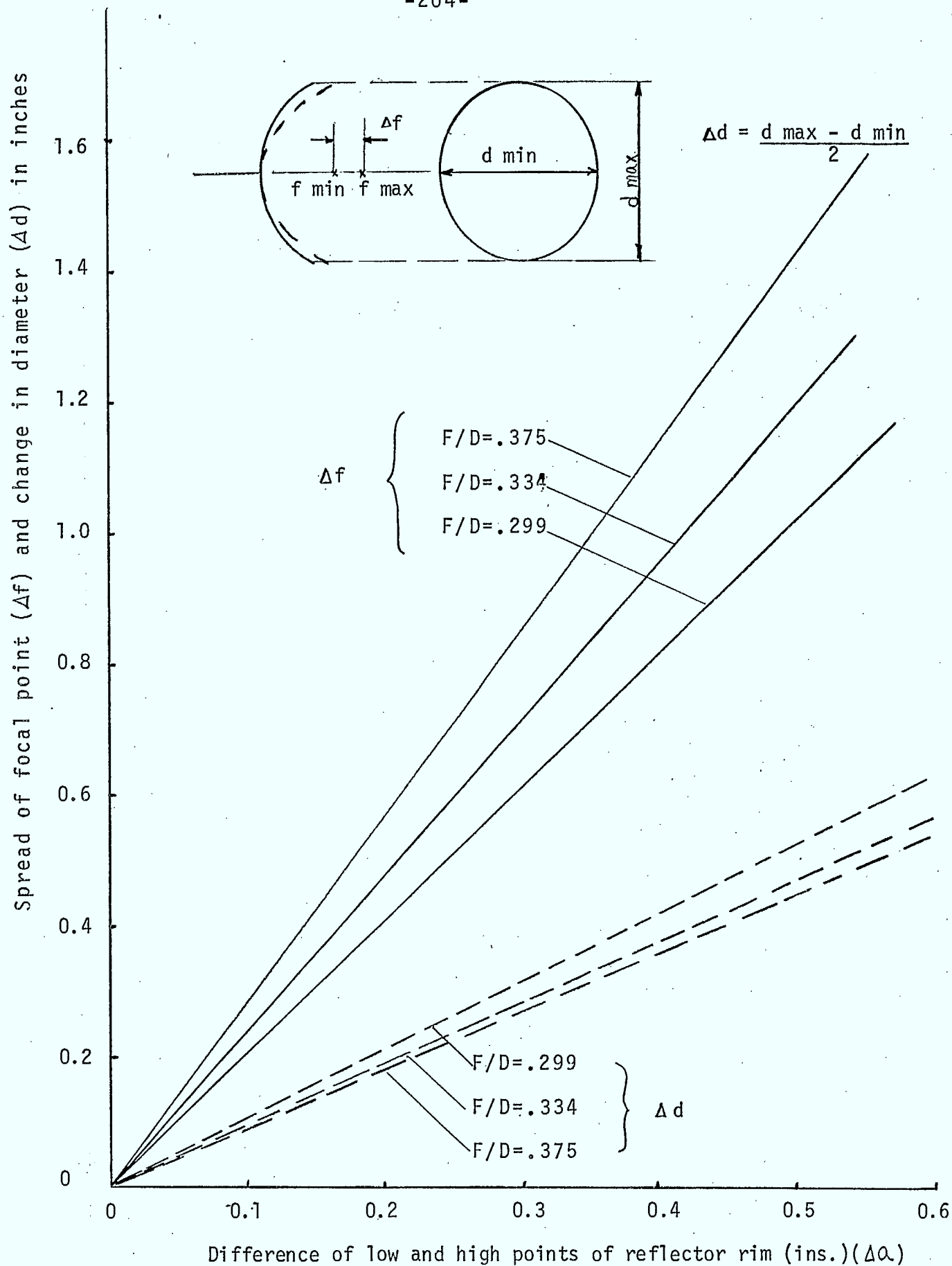


Figure 3.6.4 Focal point spread - vs. aperture distortion,

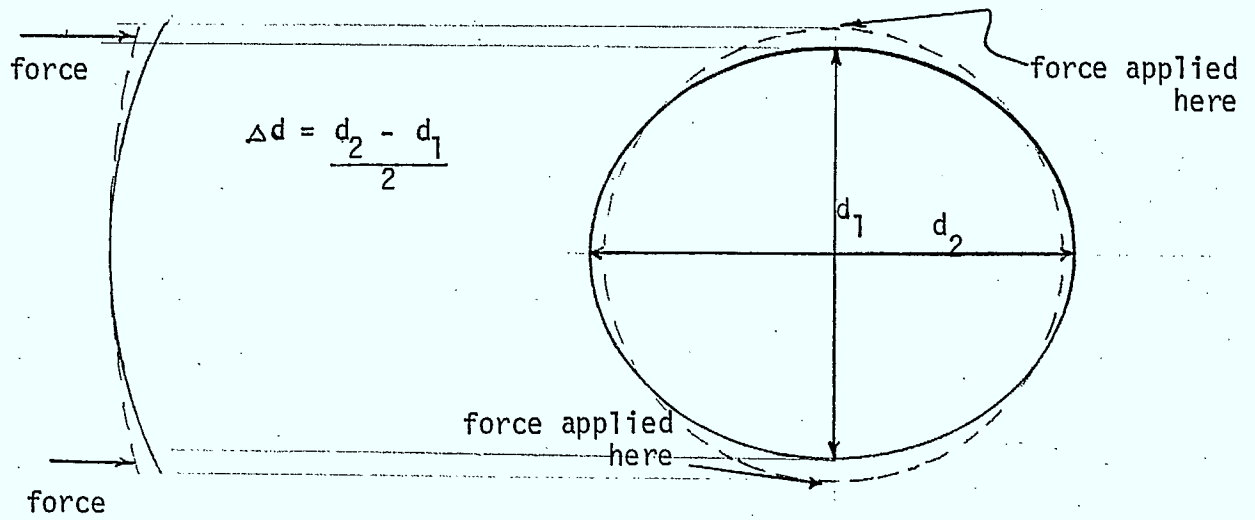


Figure 3.6.5 Experimental distortion of dish to produce astigmatism

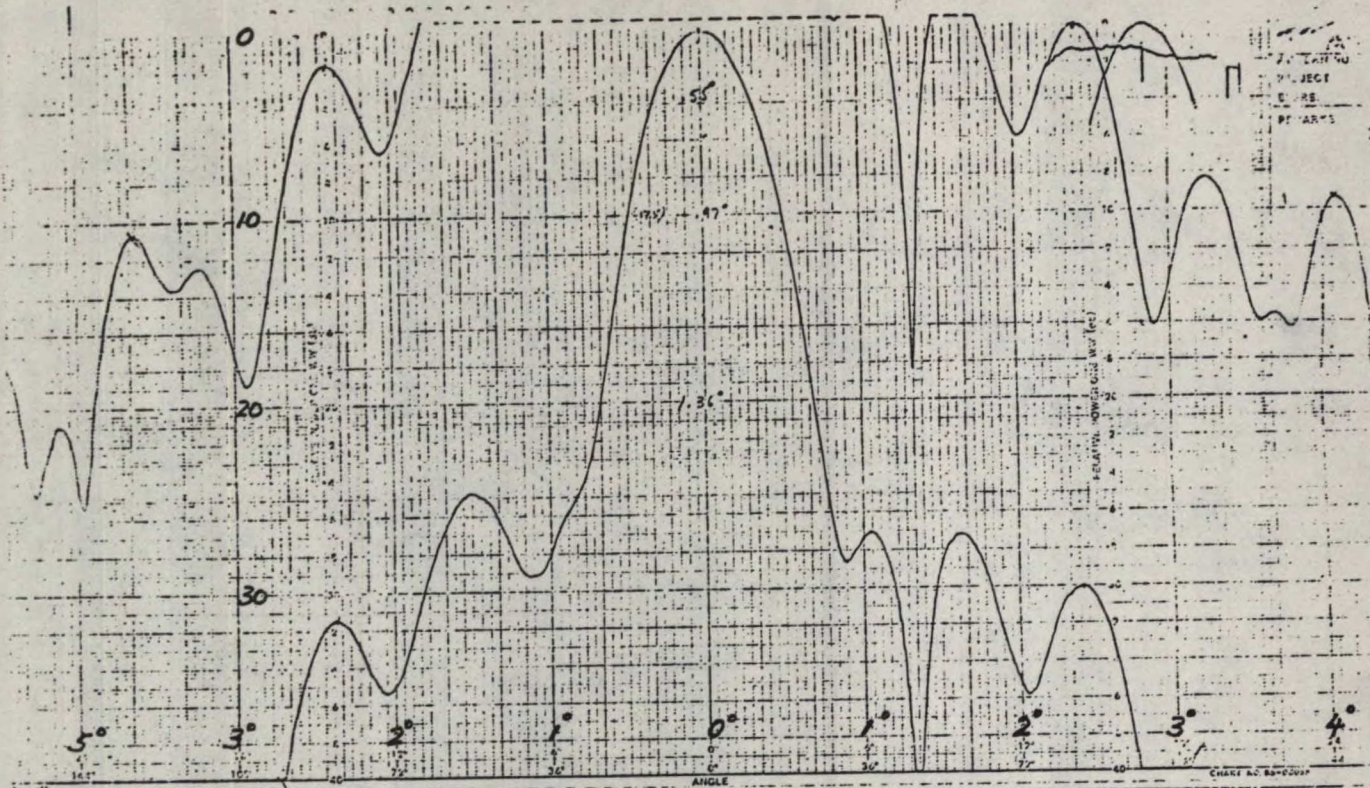


Figure 3.6.6 (a) 10' Antenna at 13.2 GHz E plane

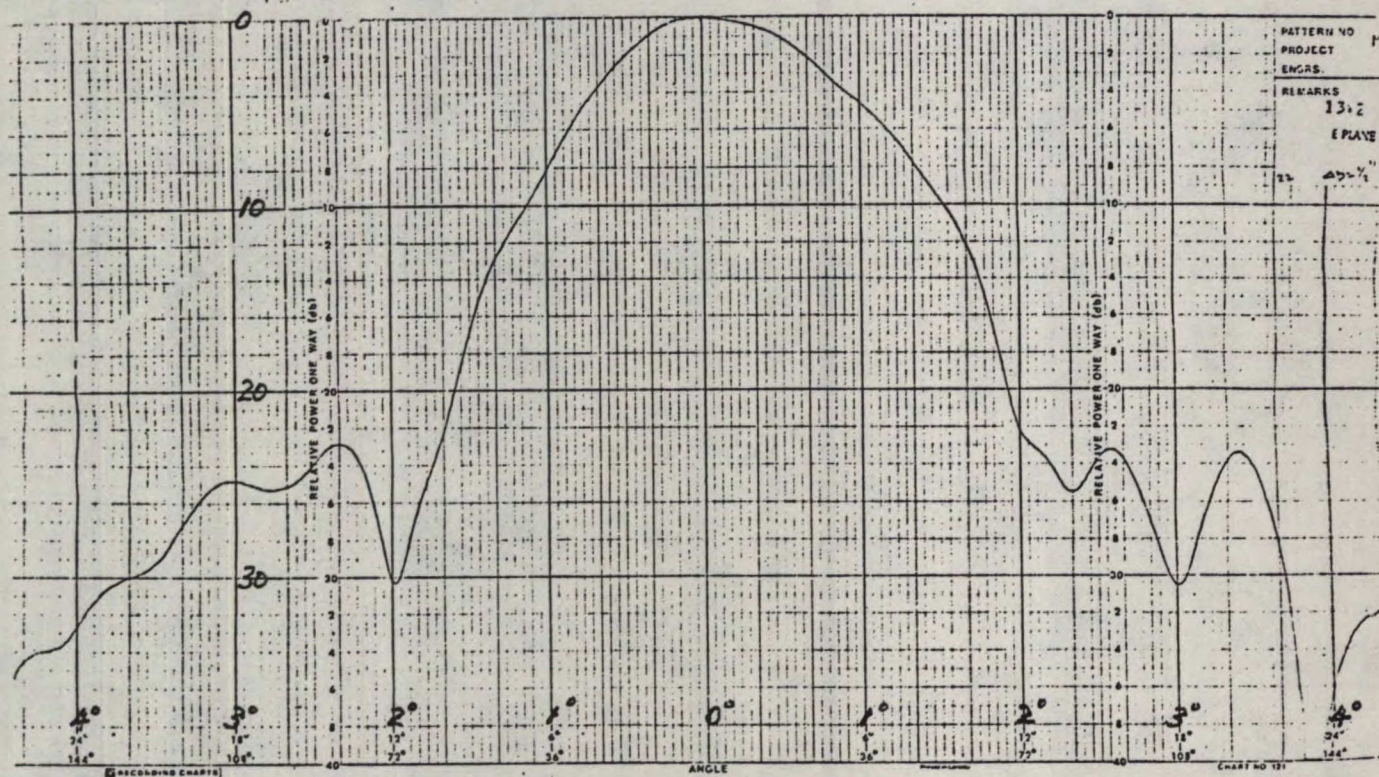


Figure 3.6.6 (b) 10' Antenna at 13.2 GHz E plane ($\Delta d = 1/2$ ")

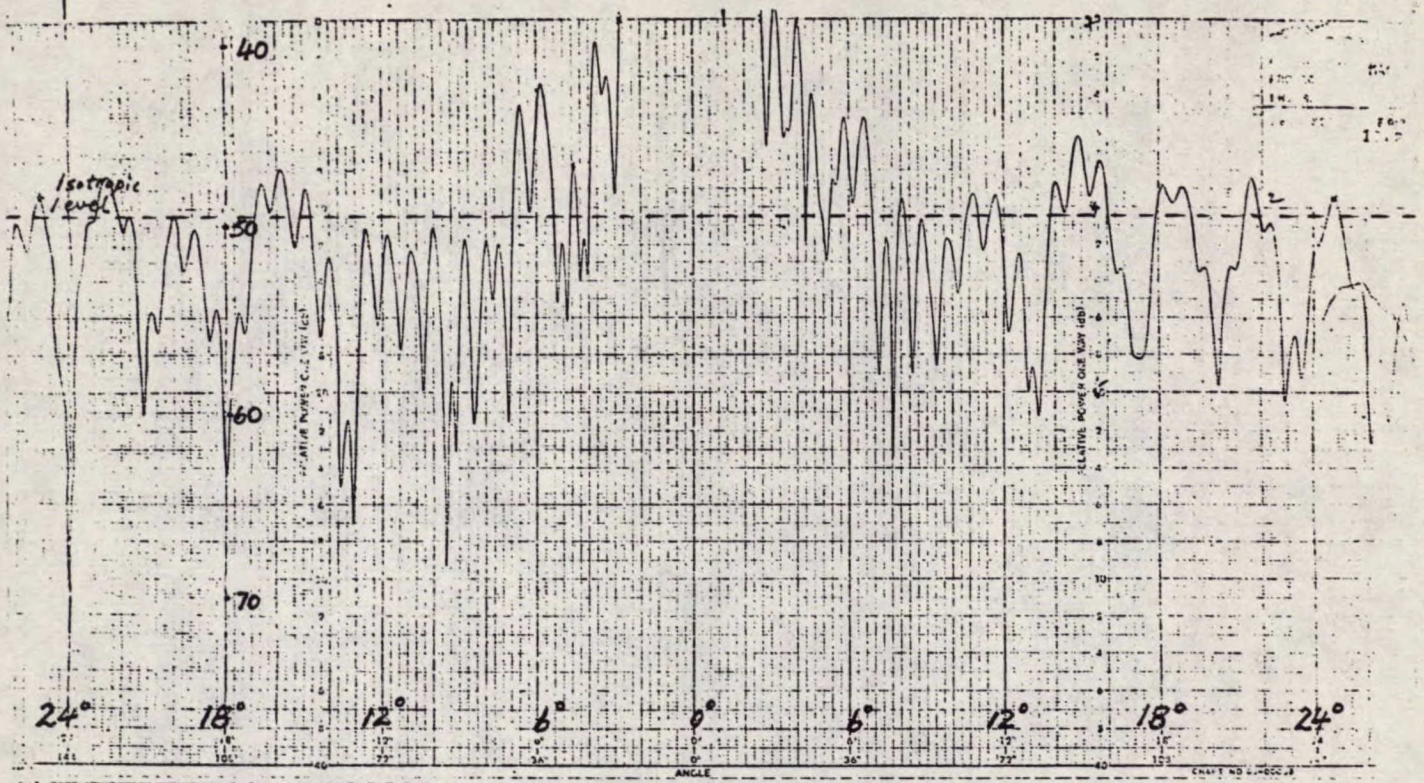


Figure 3.6.7 (a) 10' Antenna at 13.2 GHz E plane

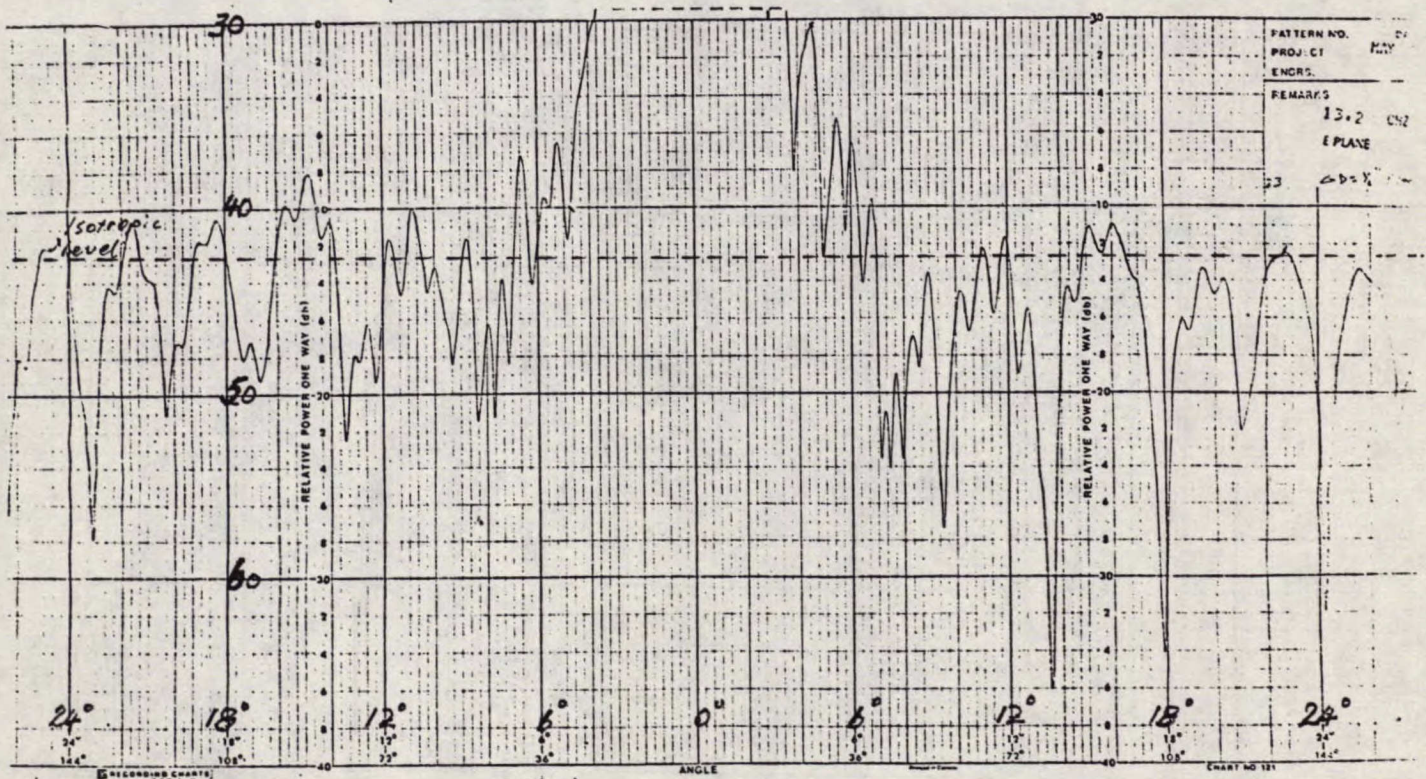


Figure 3.6.7 (b) 10' Antenna at 13.2 GHz E plane ($\Delta d = 1/2''$)

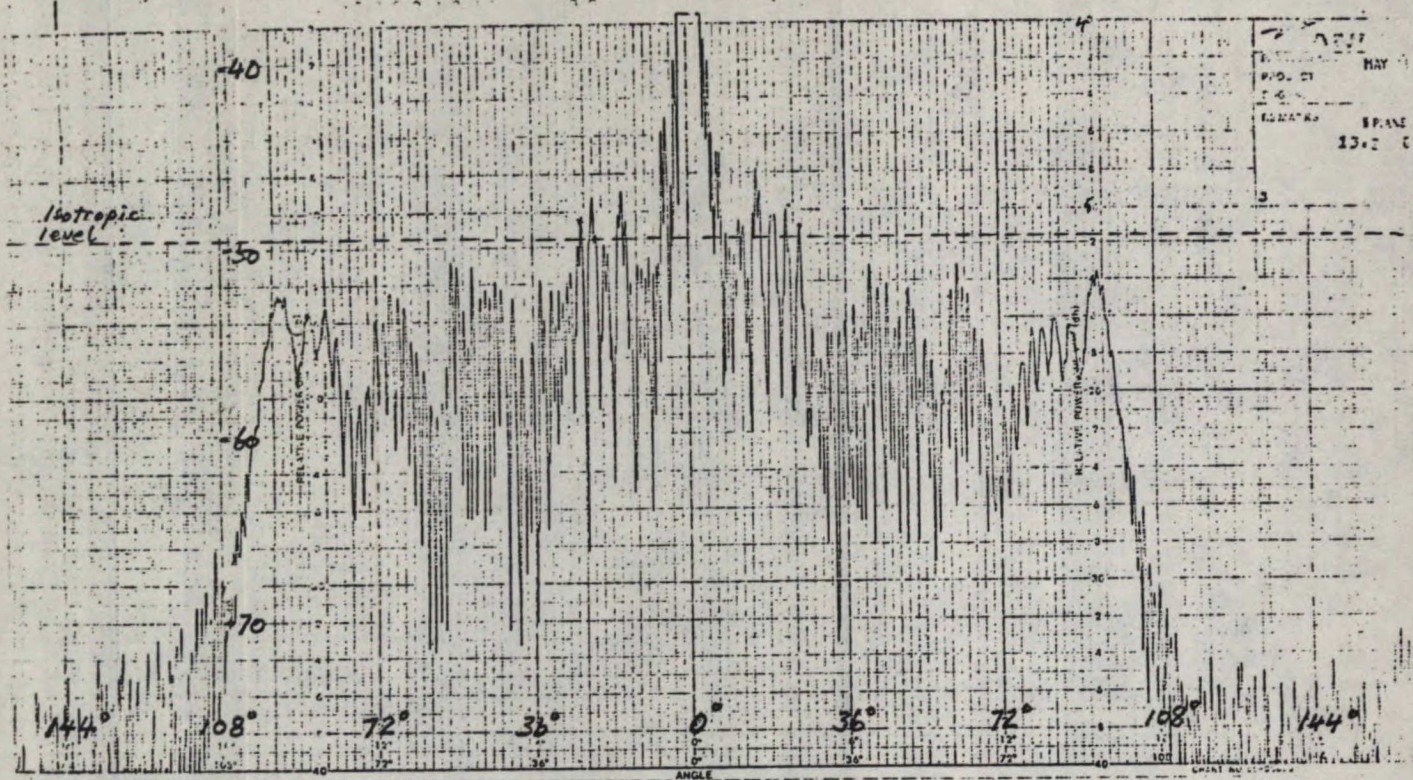


Figure 3.6.8 (a) 10' Antenna at 13.2 GHz E plane

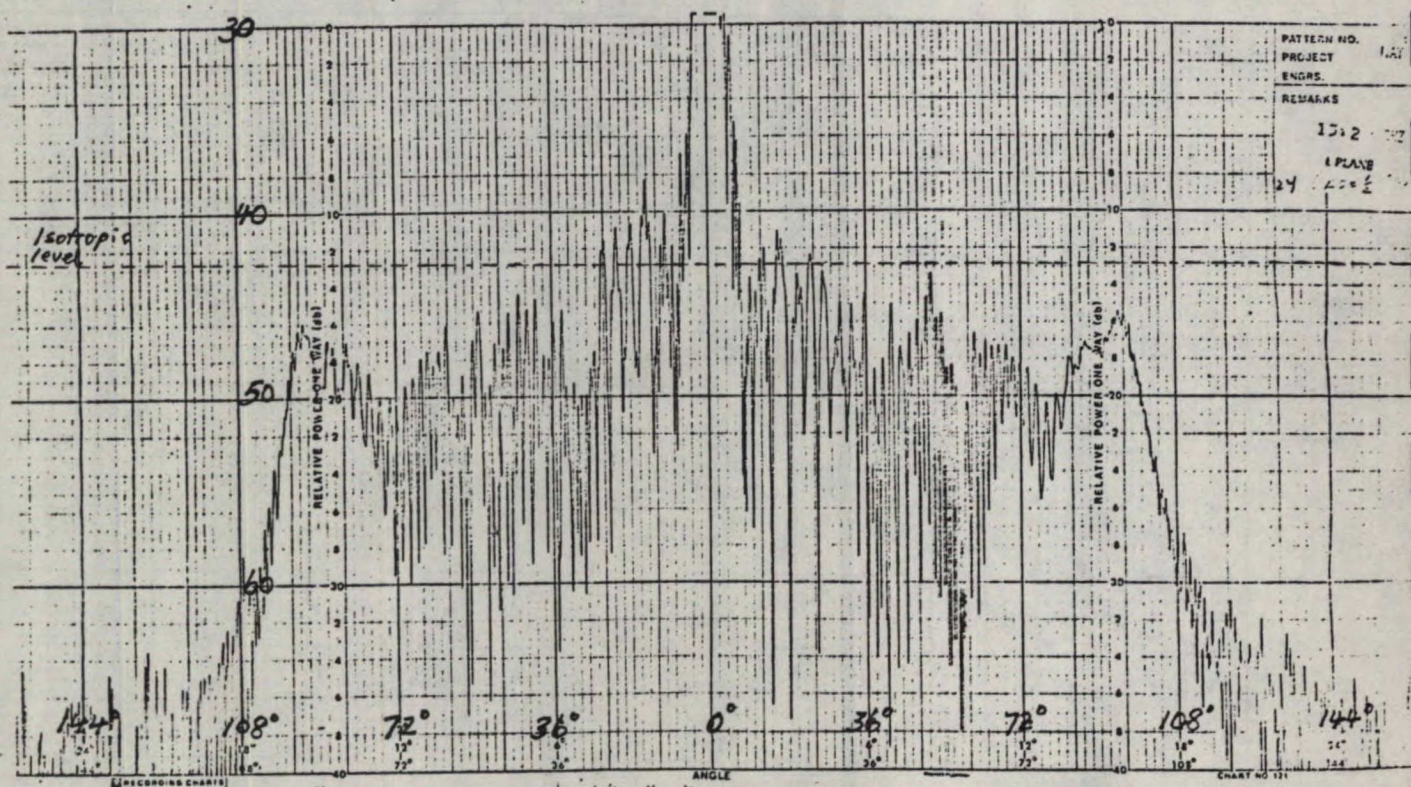


Figure 3.6.8 (b) 10' Antenna at 13.2 GHz E plane ($\Delta d = 1/2''$)

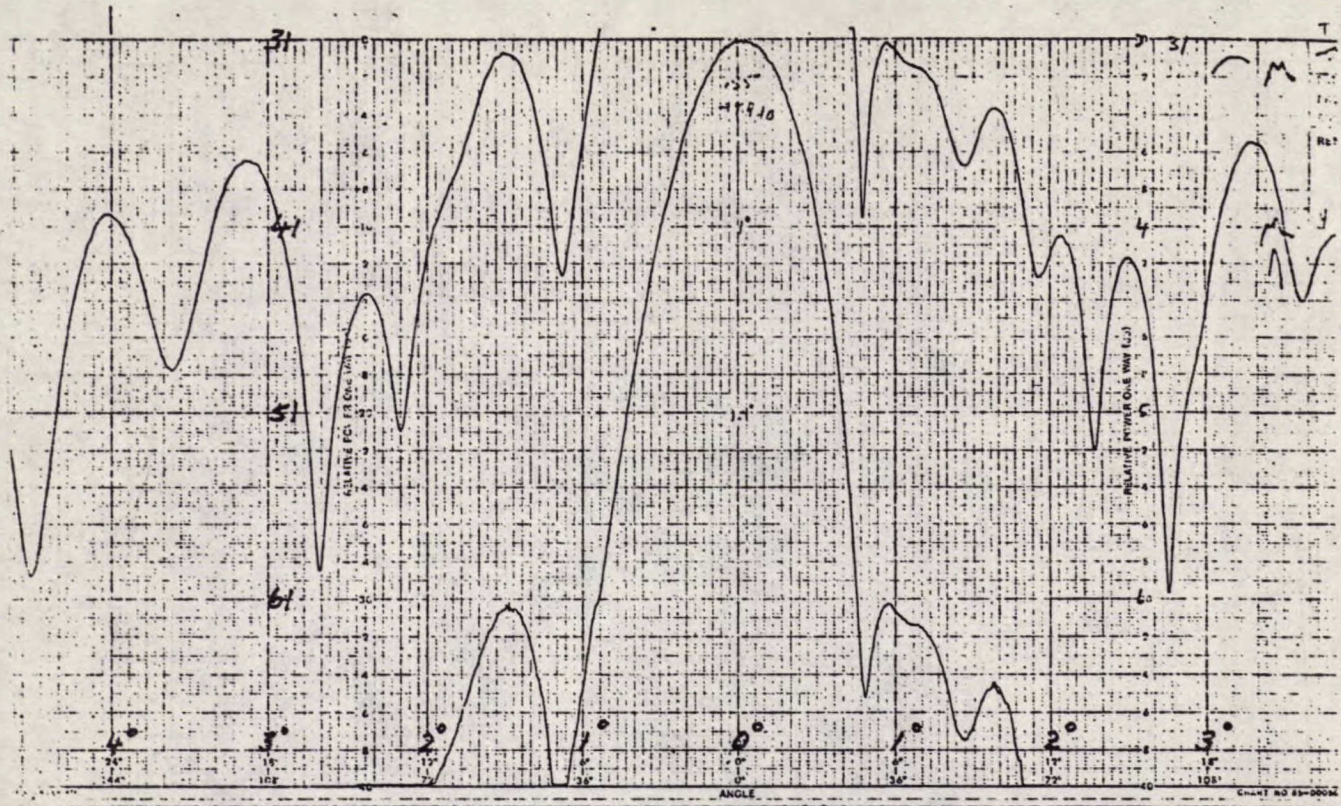


Figure 3.6.9 (a) 10' Antenna at 13.2 GHz H plane

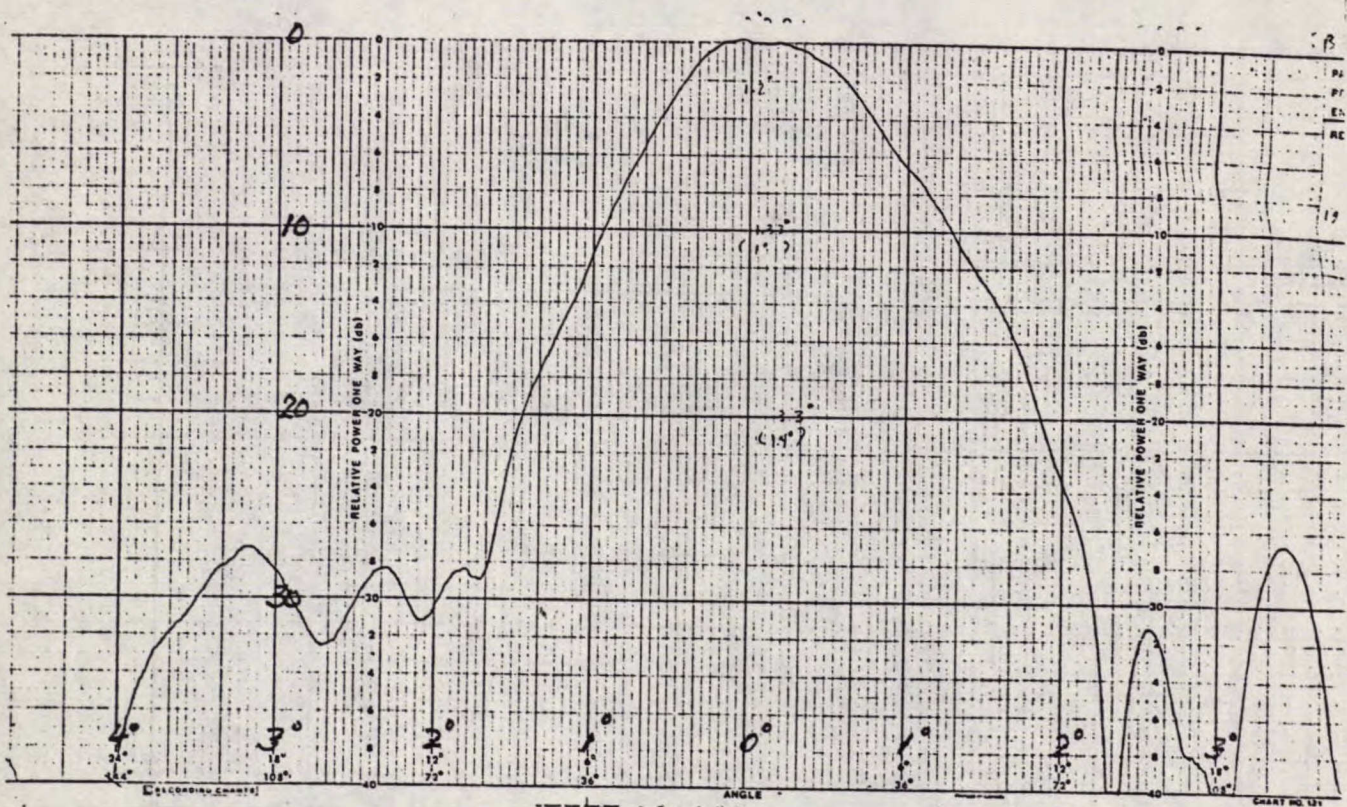


Figure 3.6.9 (b) 10' Antenna at 13.2 GHz H plane ($\Delta d = 1/2''$)

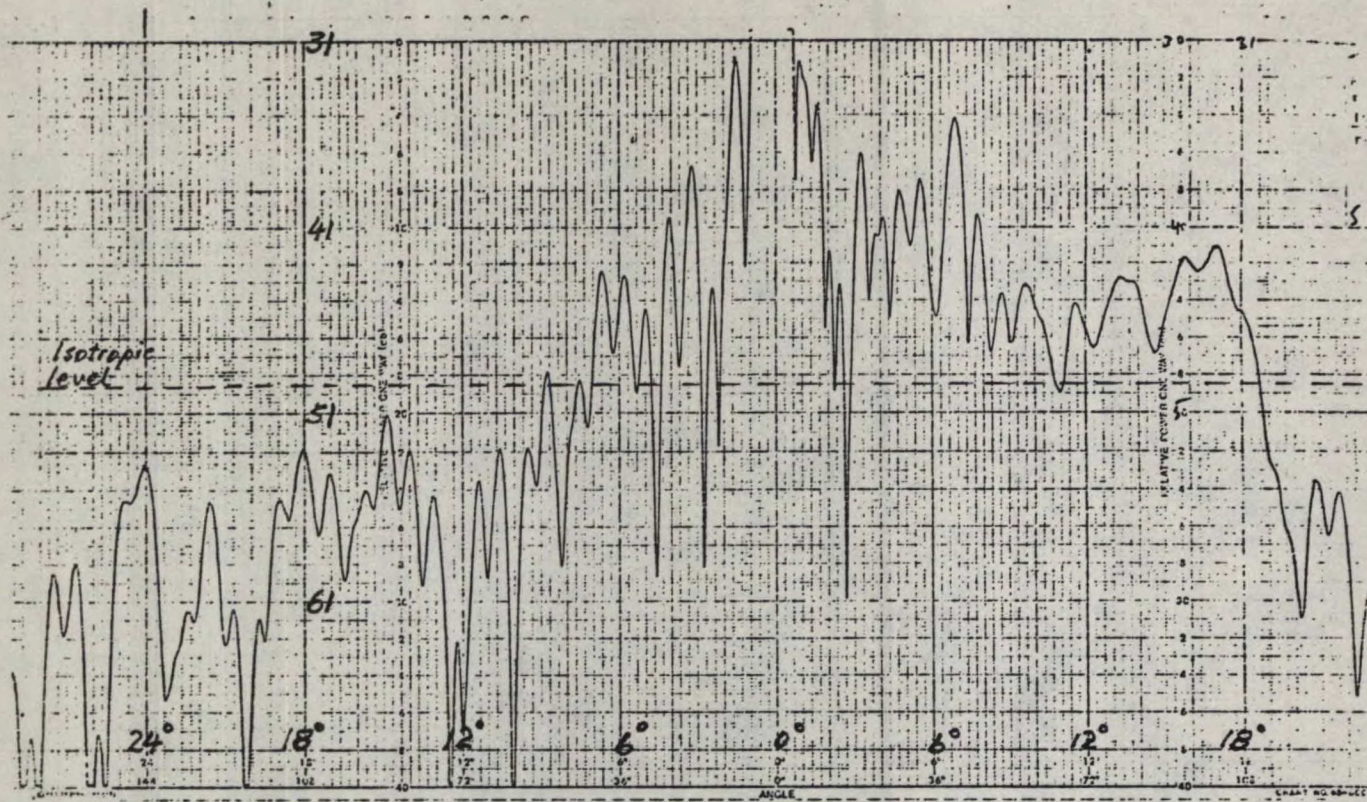


Figure 3.6.10 (a) 10' Antenna at 13.2 GHz H plane

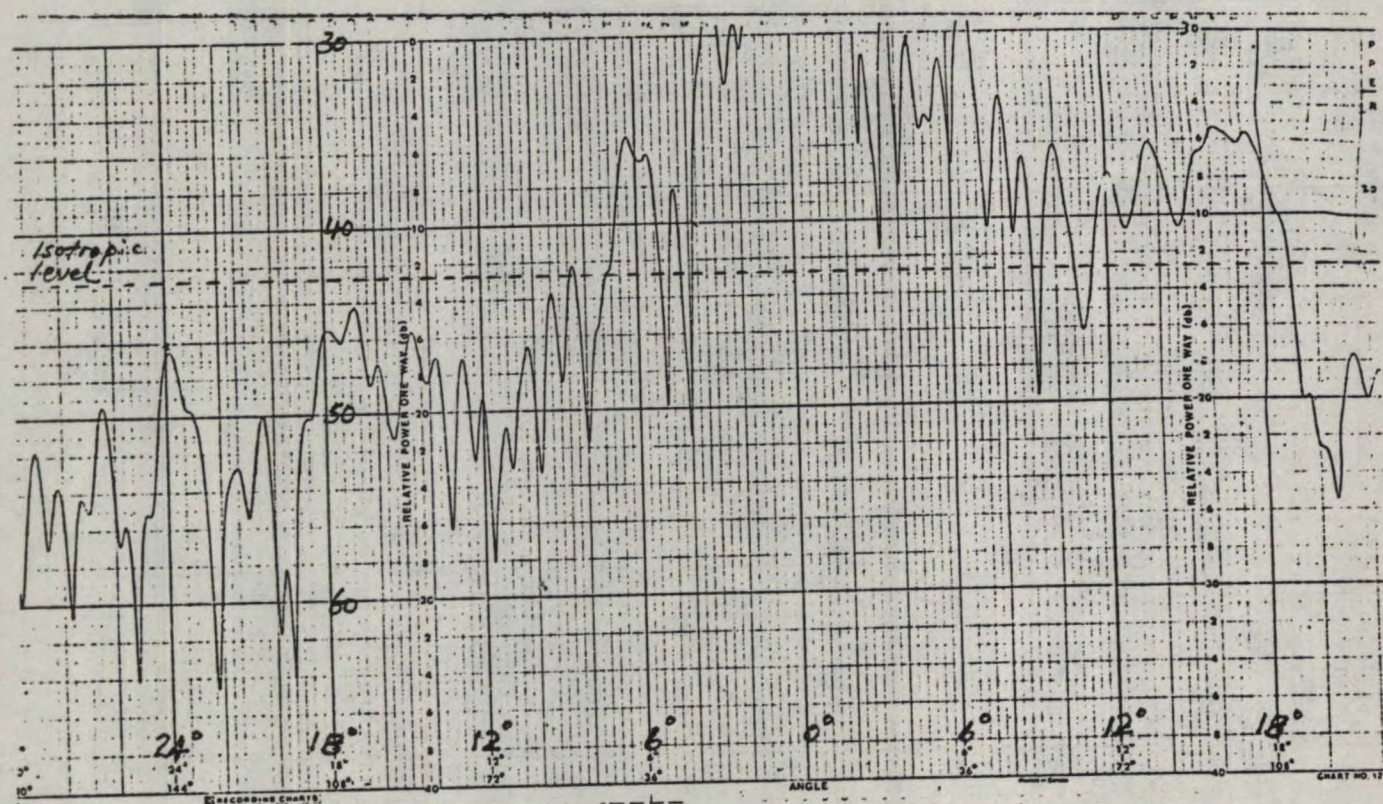


Figure 3.6.10 (b). 10' Antenna at 13.2 GHz H plane ($\Delta d = 1/2''$)

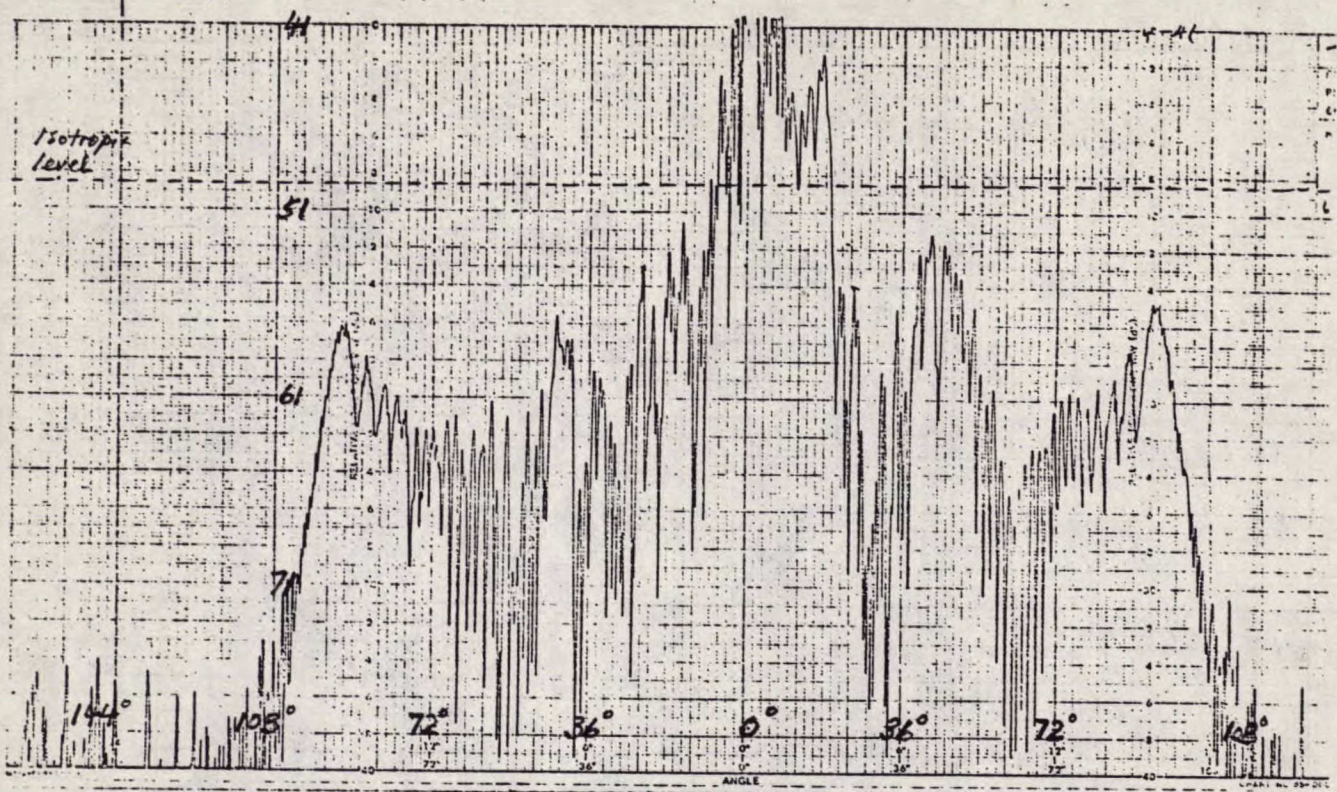


Figure 3.6.11 (a) 10' Antenna at 13.2 GHz H plane

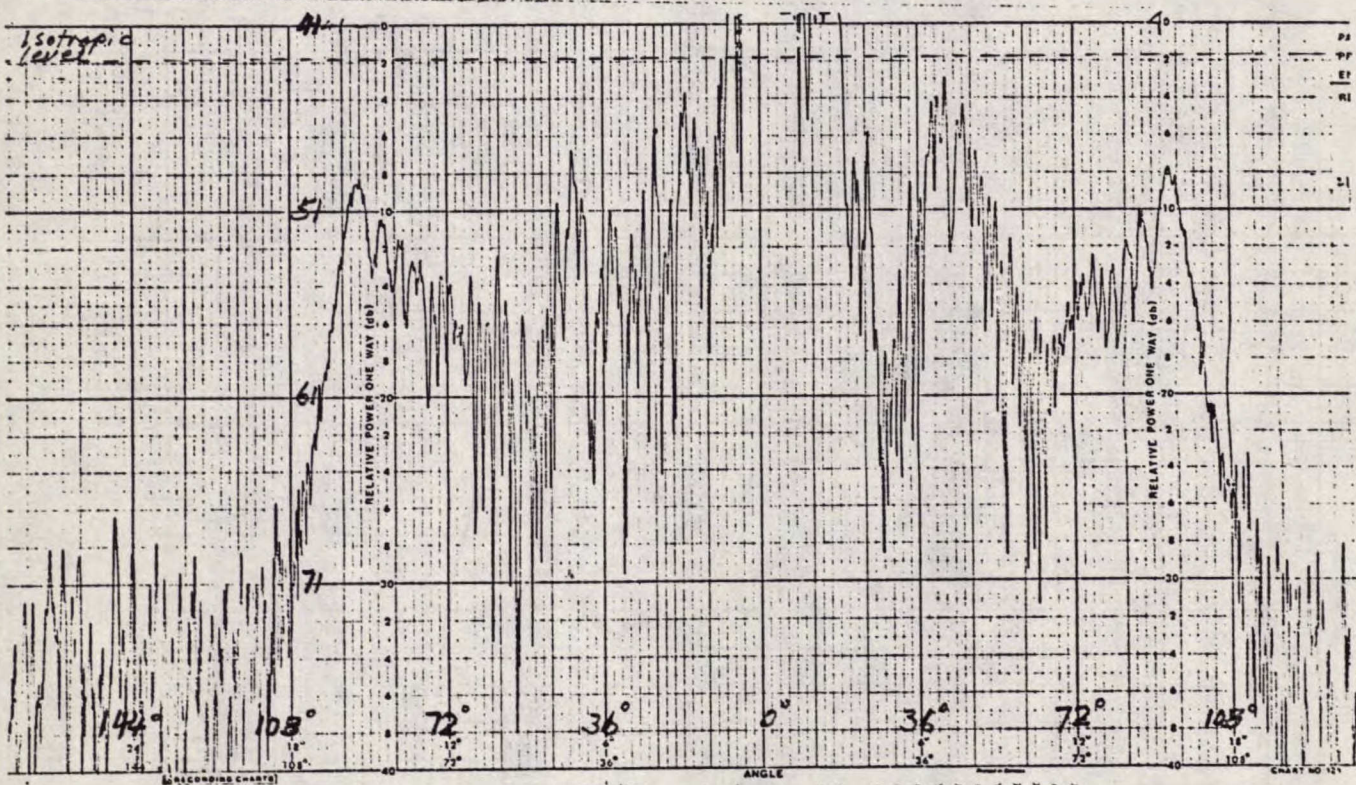


Figure 3.6.11 (b) 10' Antenna at 13.2 GHz H plane ($\Delta d=1/2''$)

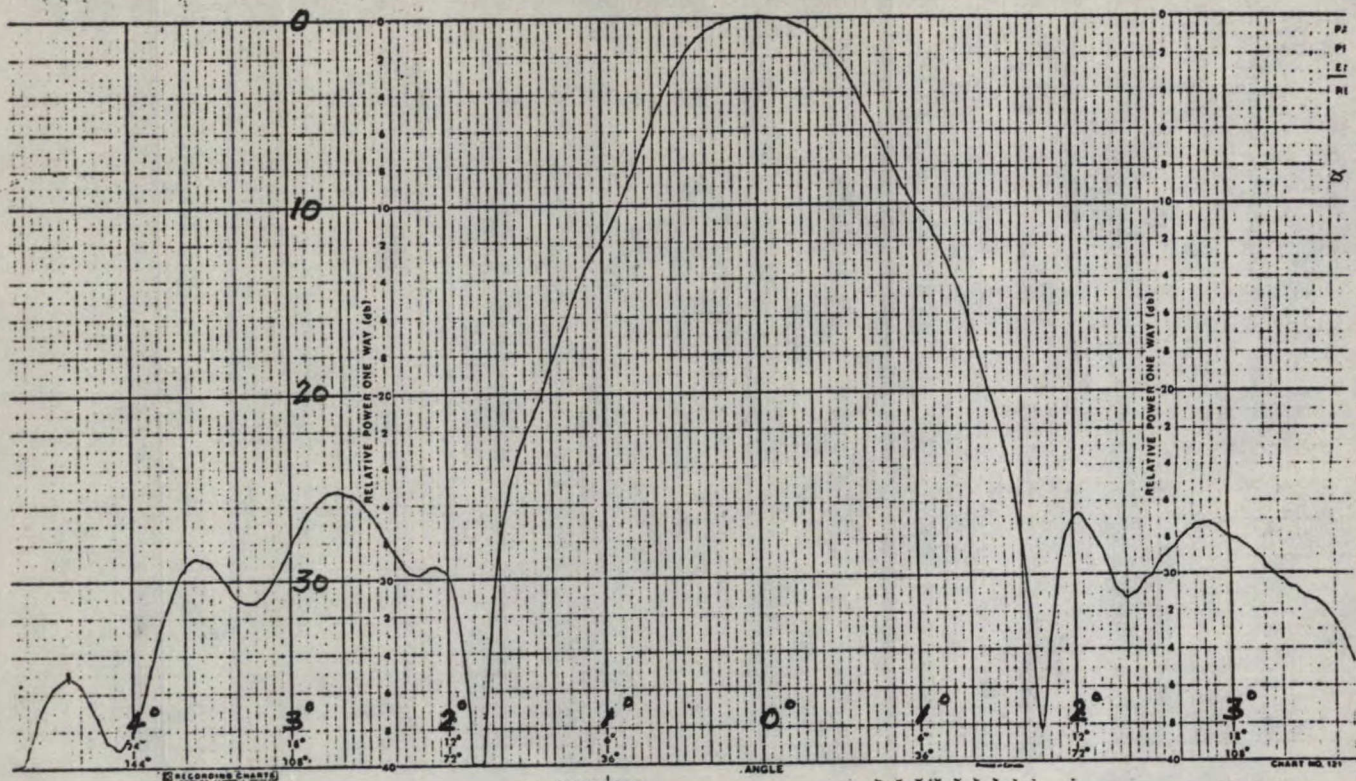


Figure 3.6.12 (a) 10' Antenna at 13.2 GHz E plane ($\Delta d=1/4"$)

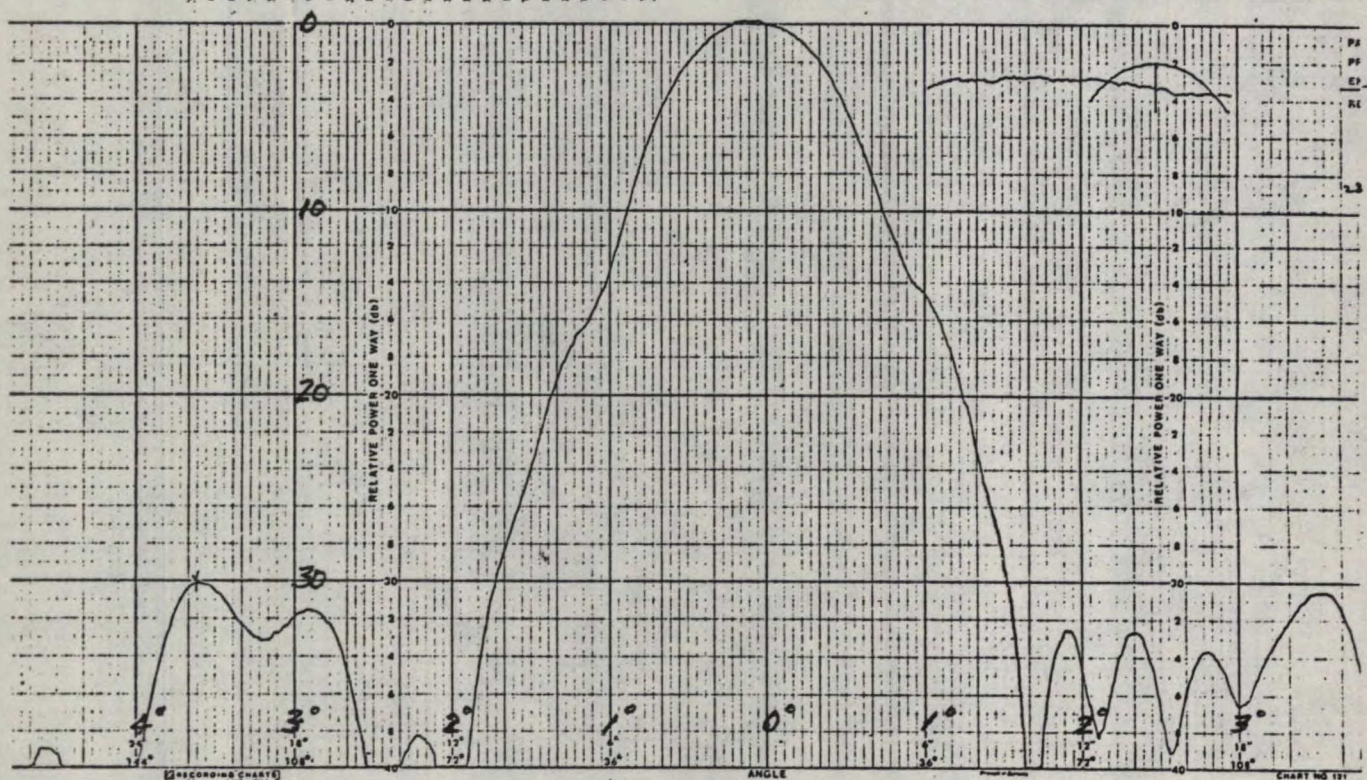


Figure 3.6.12 (b) 10' Antenna at 13.2 GHz H plane ($\Delta d=1/4"$)

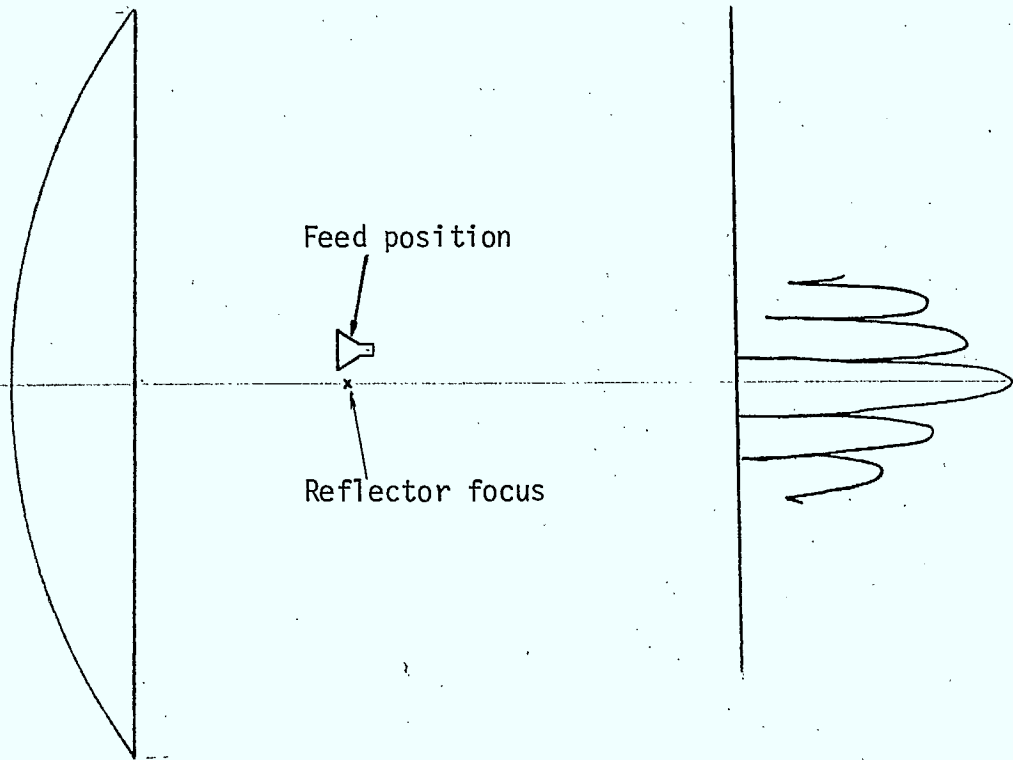


Figure 3.6.13 (a) Front-Fed Paraboloid with coma distortion.

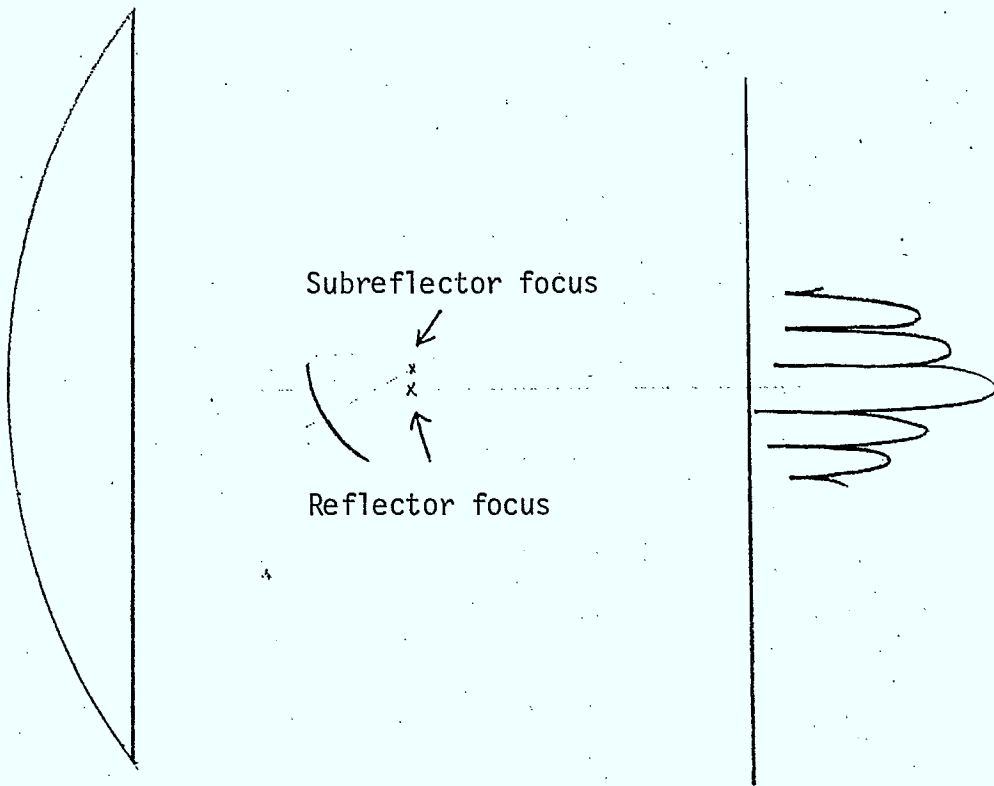


Figure 3.6.13 (b) Cassegrainian Subreflector System with coma distortion.

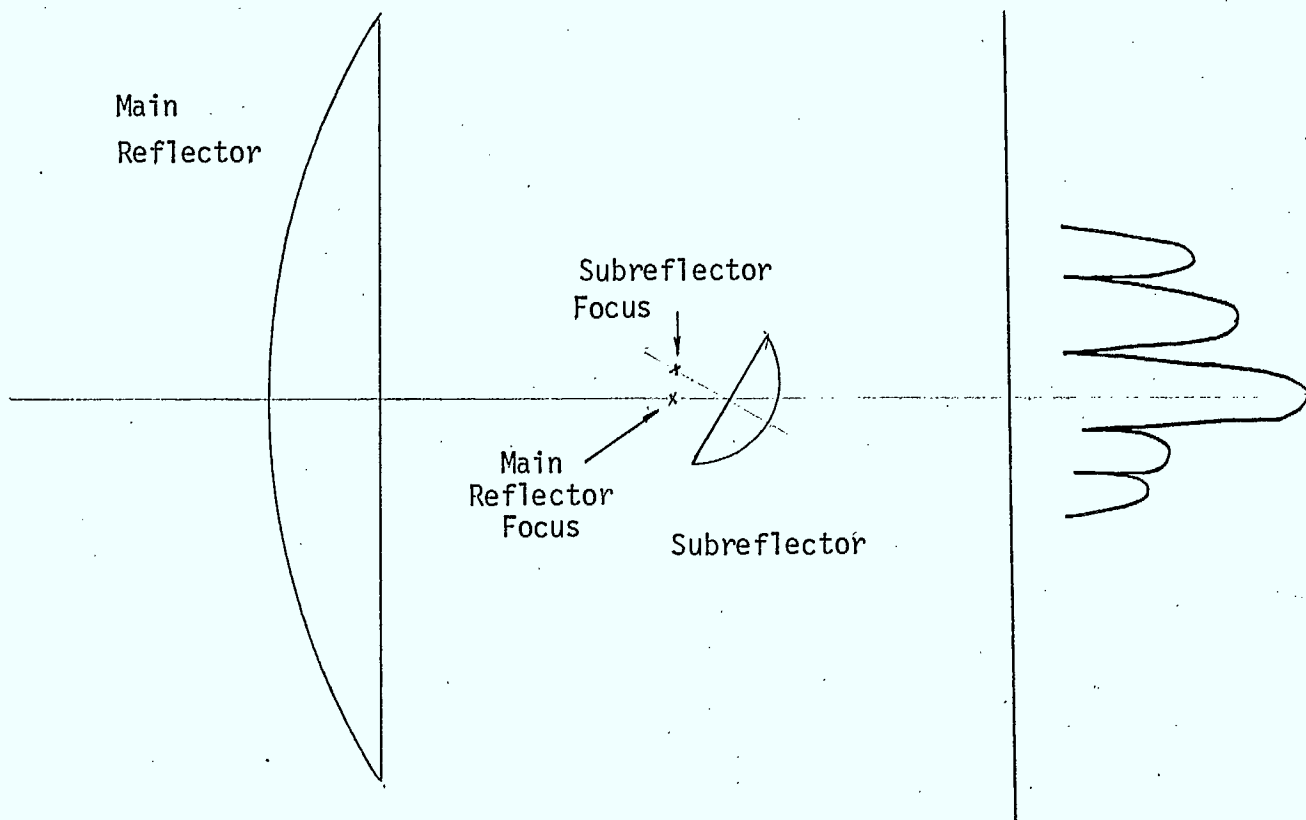


Figure 3.6.13(c) Gregorian Subreflector system with coma lobes,

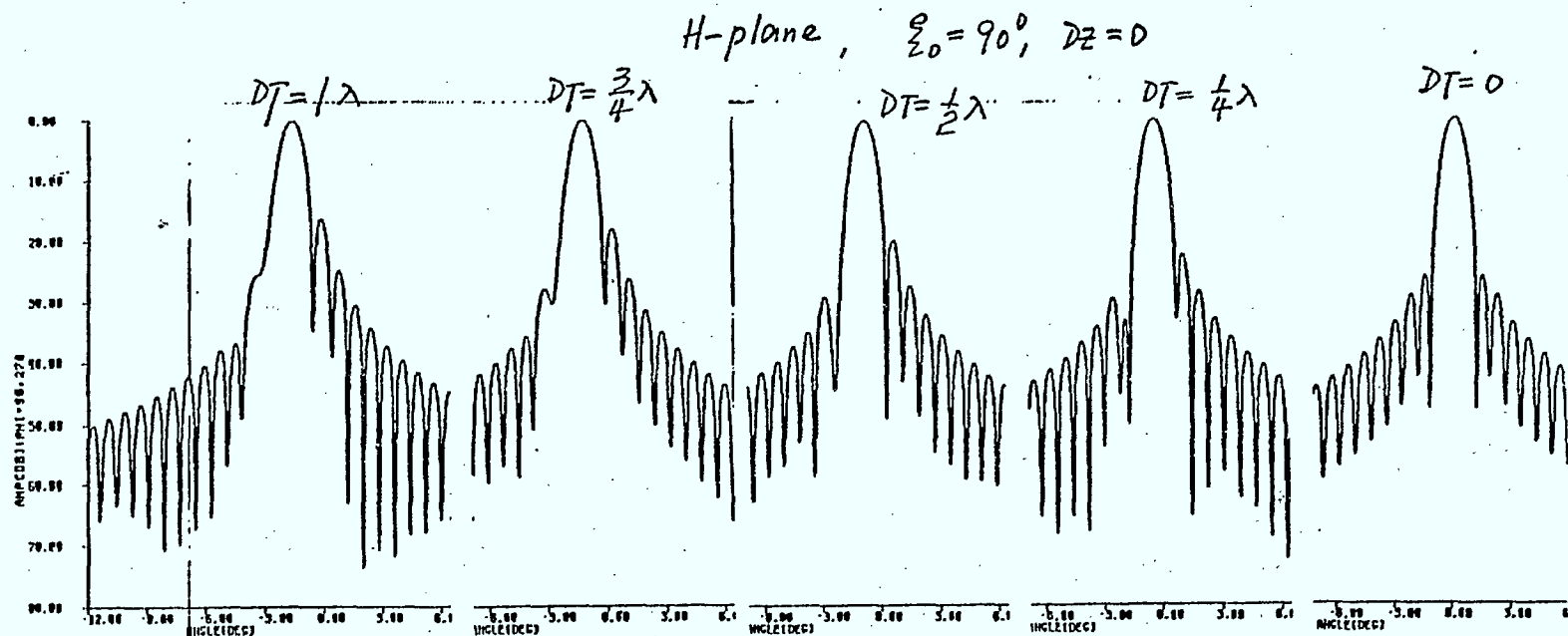


Figure 3.6.14(a) Example of coma lobes caused by lateral Feed Displacement
(9 ft. parabolic reflector at 7.9 GHz)

DEFOCUSING PROPERTIES
DEFOHG 6 / 30 / 80

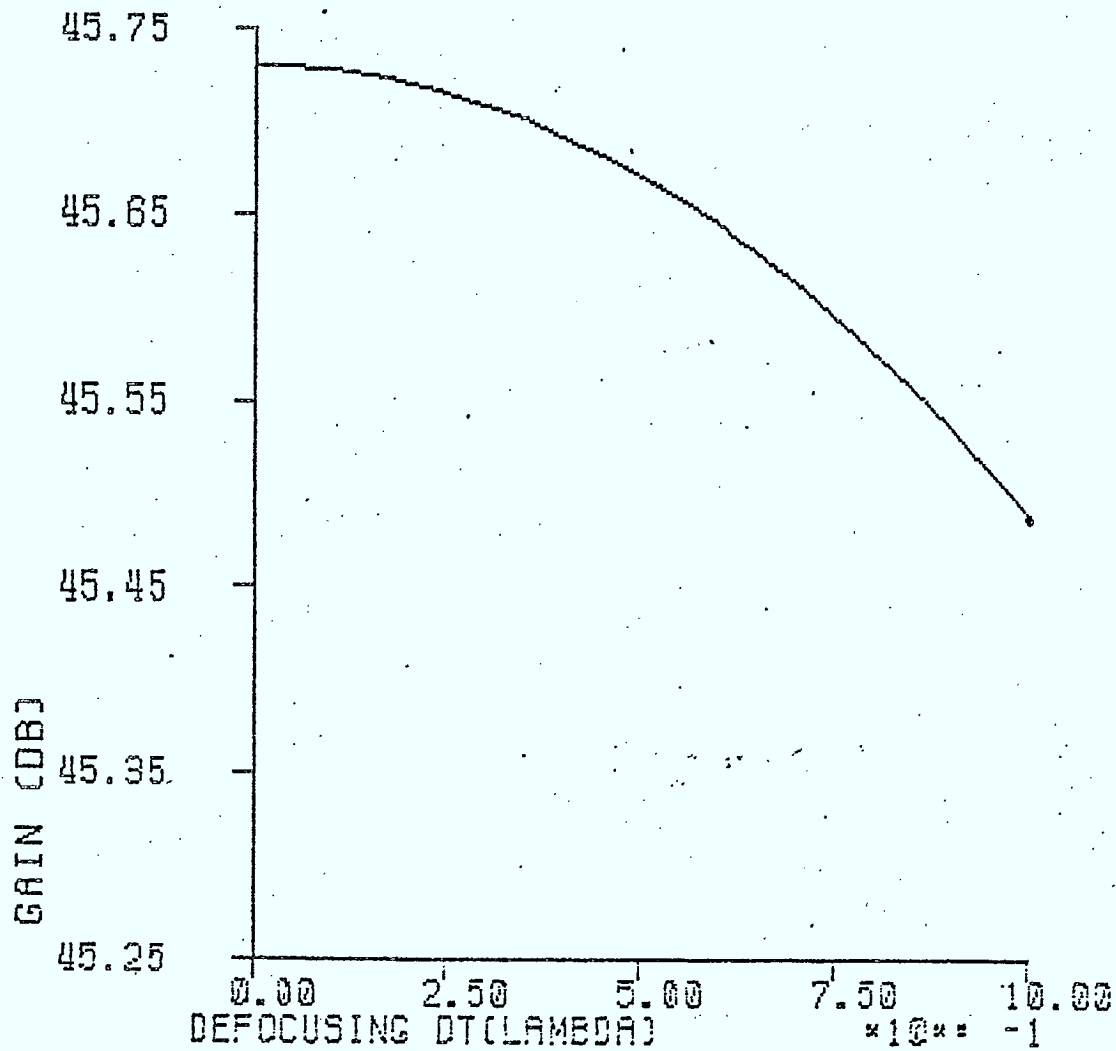


Figure 3.6.14 (b) Antenna gain loss for Figure 3.6.14 (a)

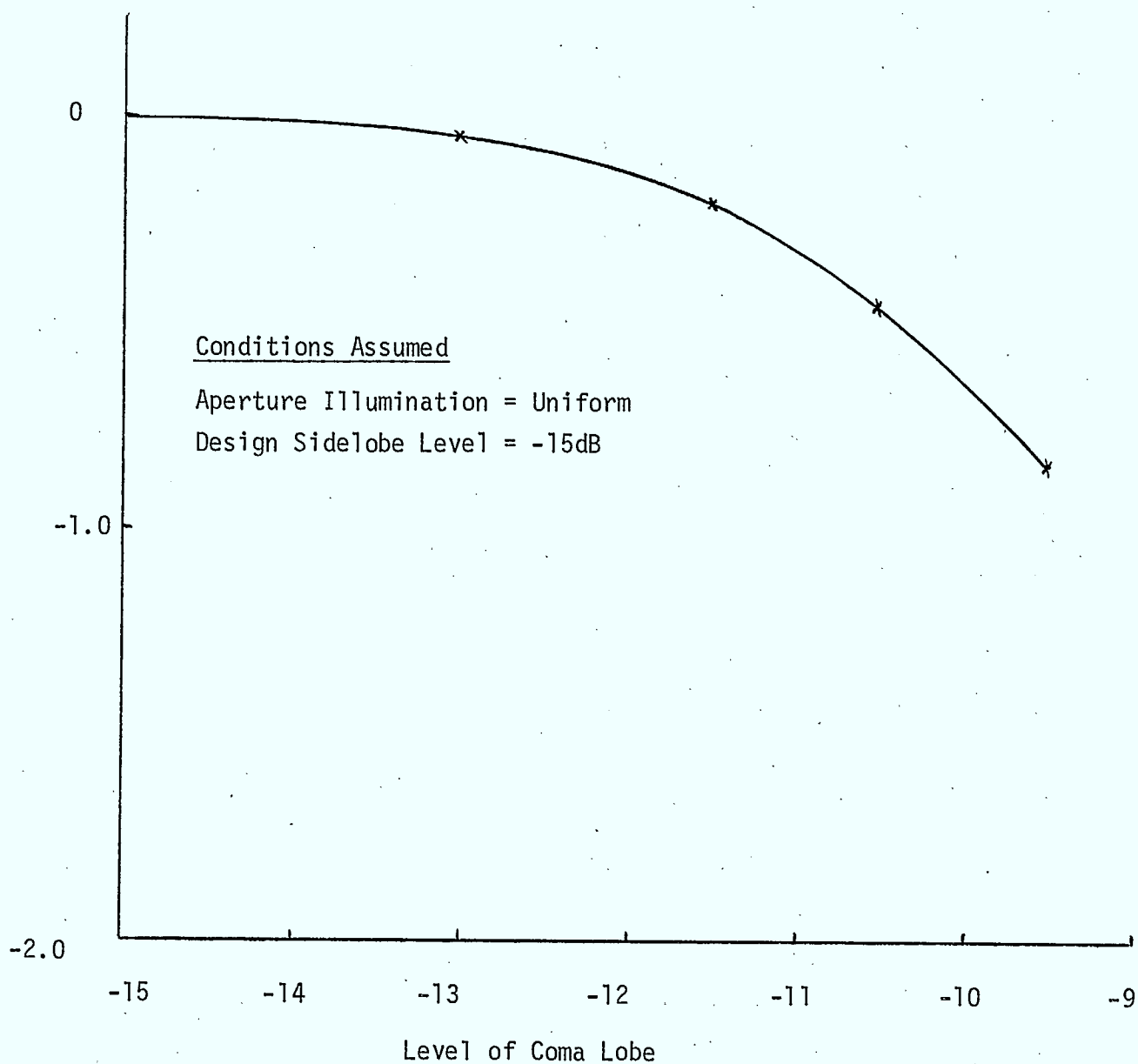


Figure 3.6.15 8m antenna-gain loss vs coma lobe level.

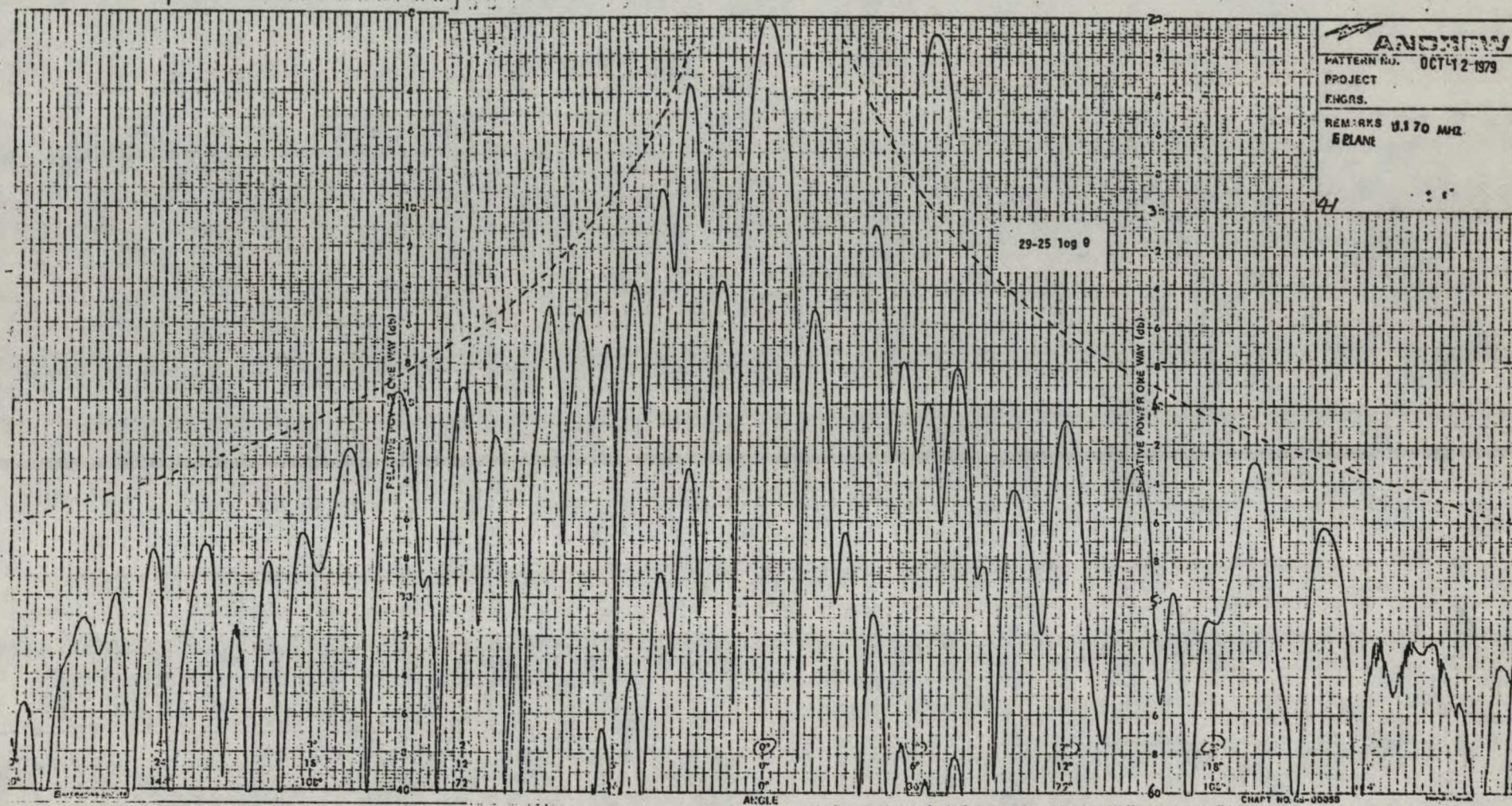


Figure 3.6.16(a) 8M Antenna E Plane pattern,

Frequency = 11700 MHz

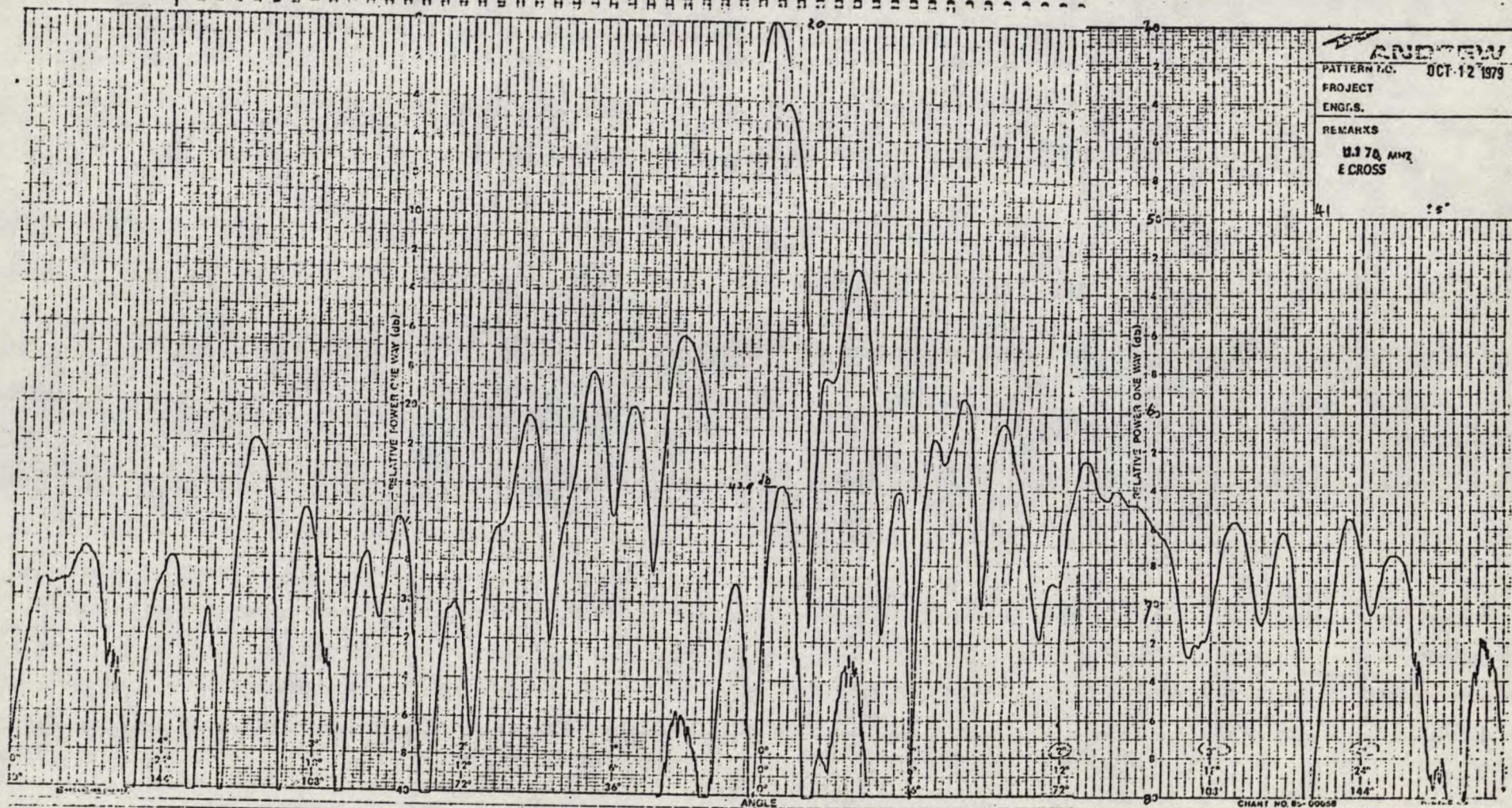


Figure 3.6.16(b) 8m antenna E plane cross polarization pattern frequency = 11700 MHz

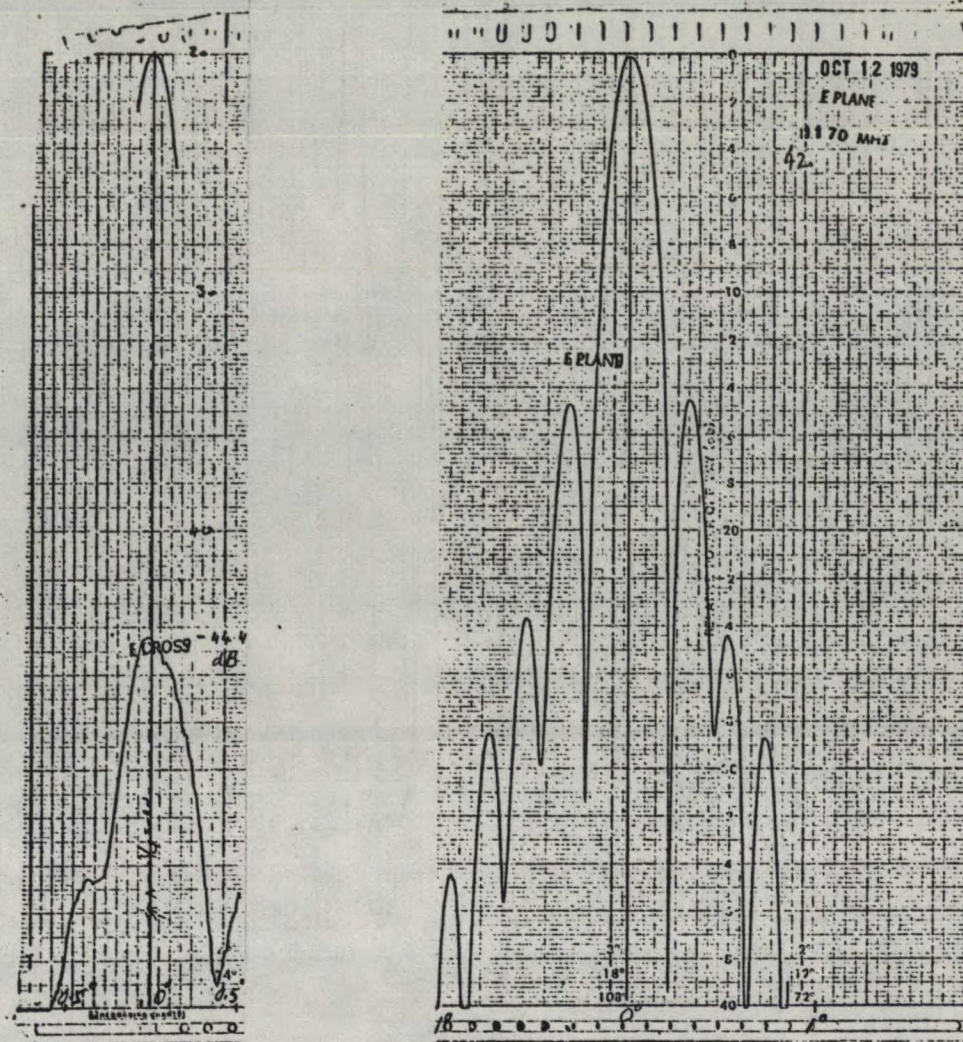
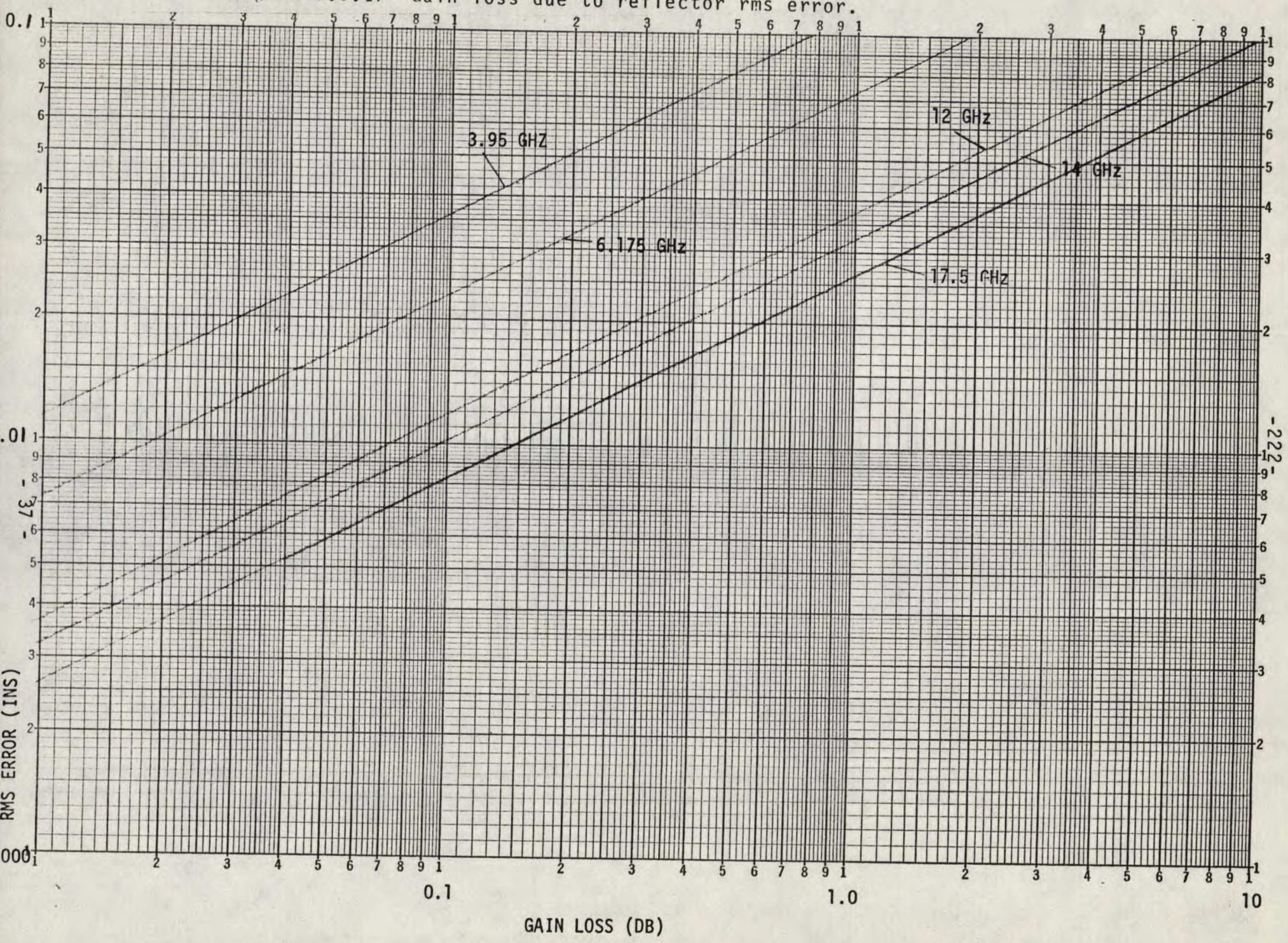


Figure 3.6.16(c) E plane cross and parallel polarization pattern
frequency = 11700 MHz

Figure 3.6.17 Gain loss due to reflector rms error.





ANDREW

PE

Approved

PATTERN ENVELOPE

ANTENNA TYPE NUMBER

Gain: GHz
 dBi at GHz
 15 dB BEAMWIDTH: DEGREES

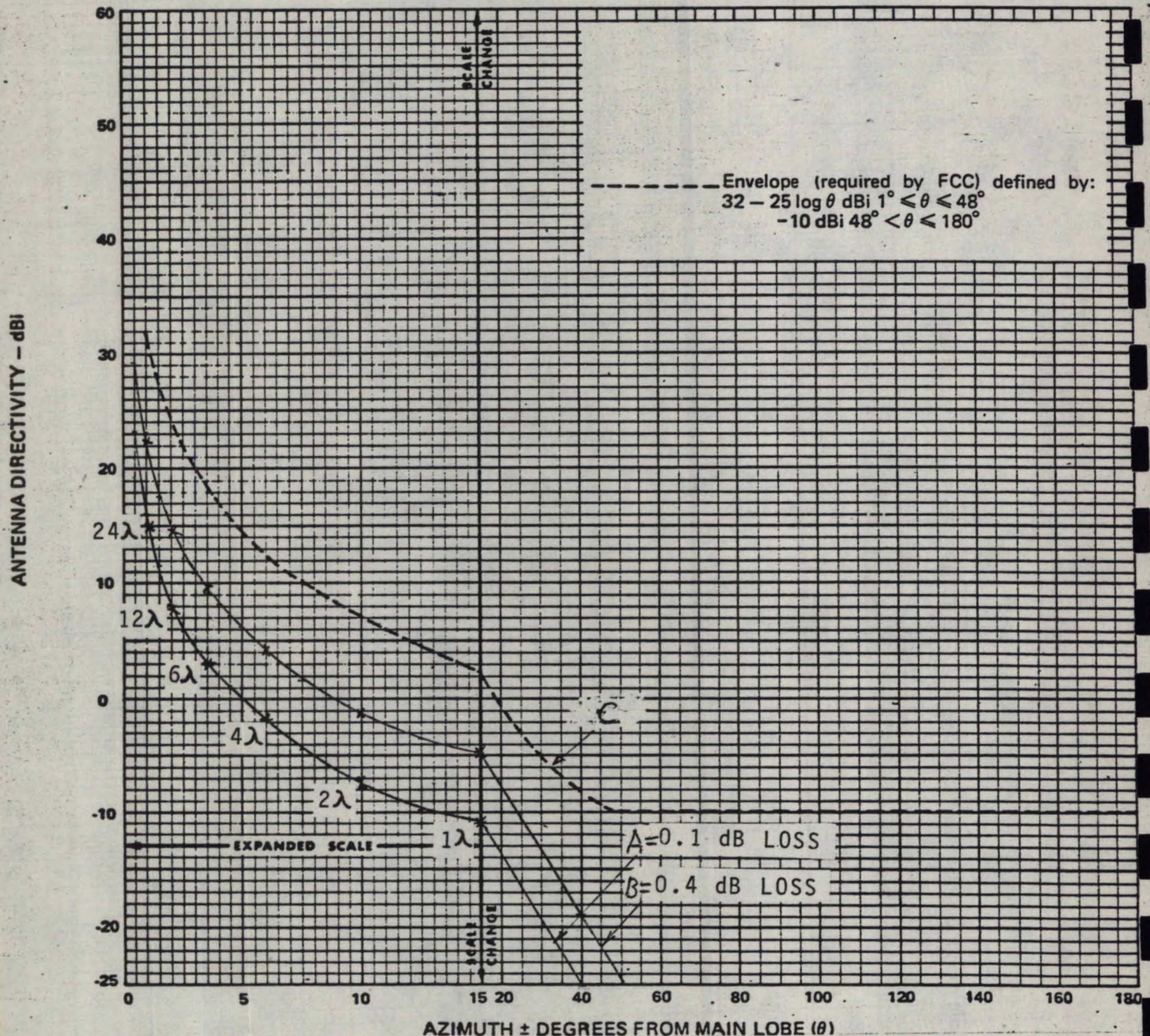


Figure 3.6.18 Envelope of Worst-Case effect of RMS error on antenna pattern

Typical measured results

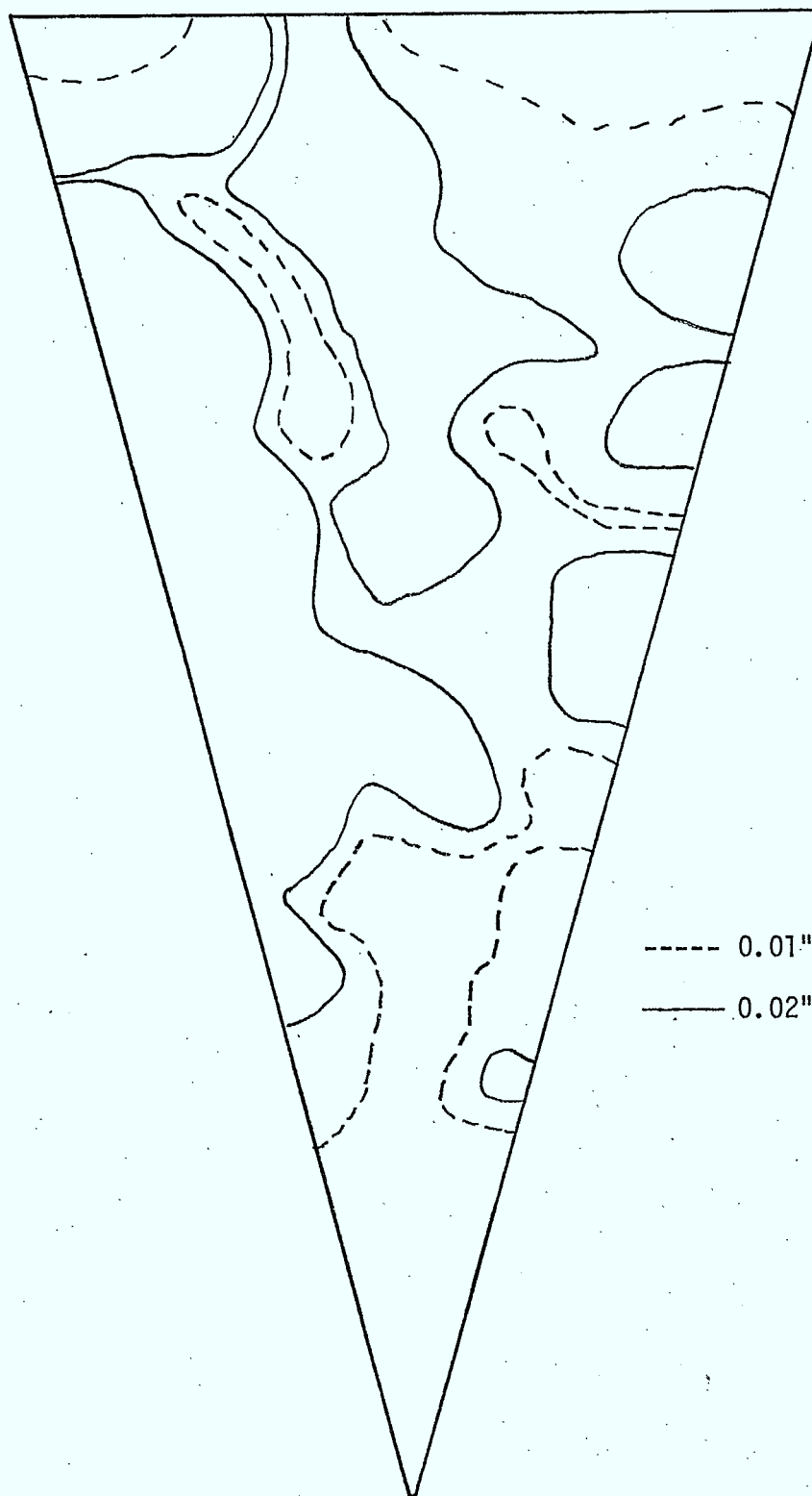


Figure 3.6.19 Andrew 10M antenna - error contour for skin panel

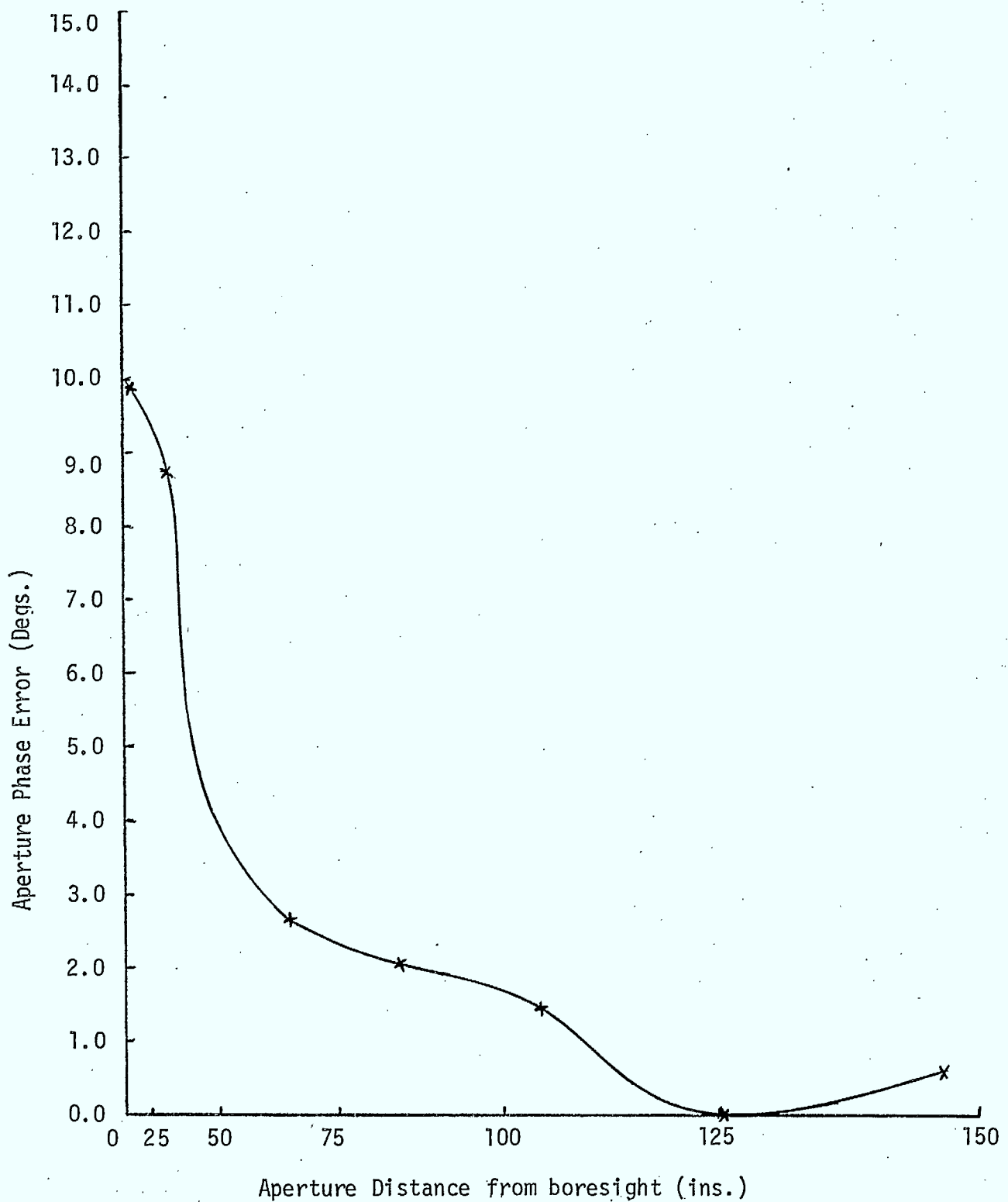


Figure 3.8.1 8M Antenna - Aperture Phase Error caused by a 20°C temperature change Case (a)

(Frequency = 12 GHz)

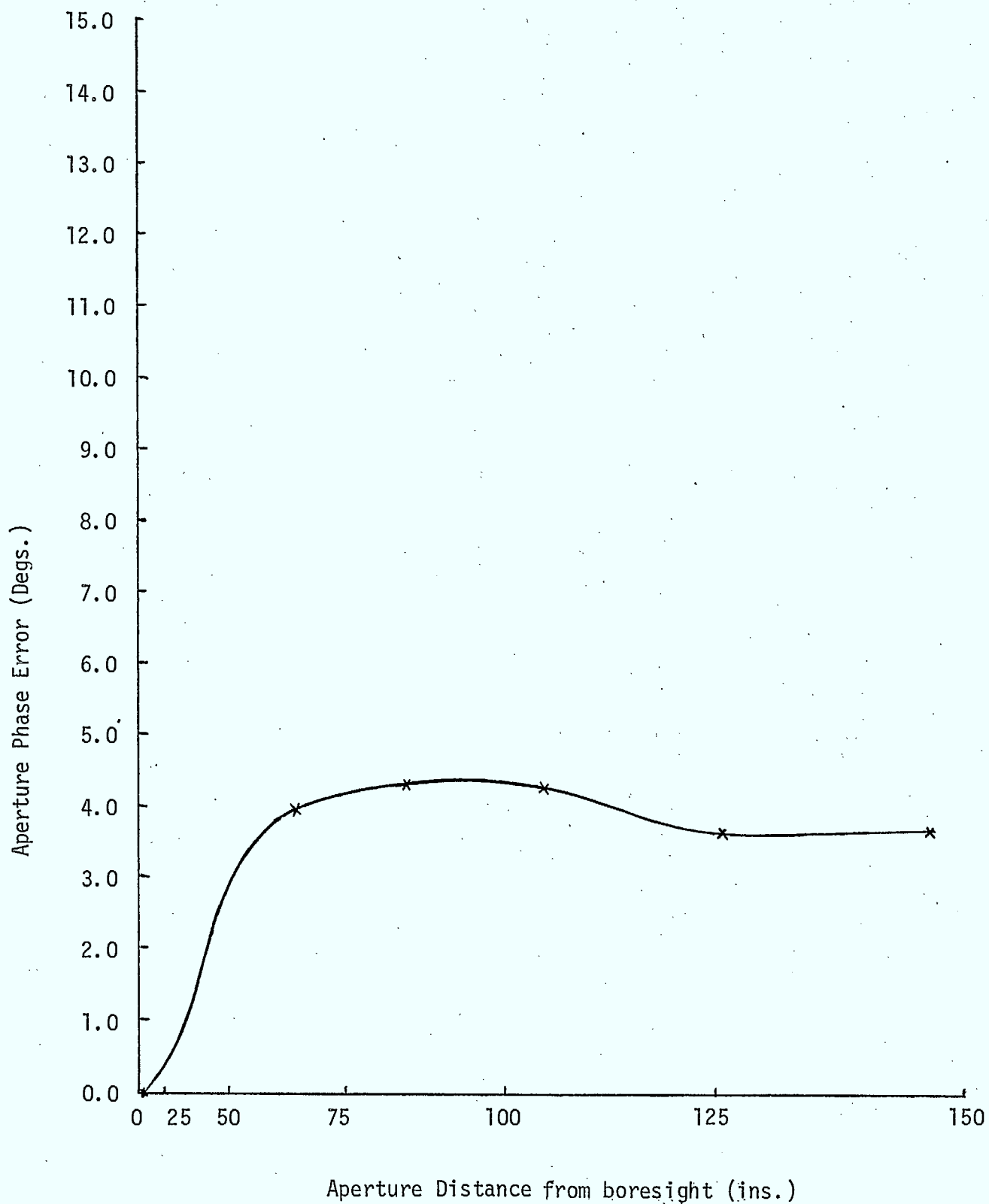


Figure 3.8.2 8M Antenna - Aperture error caused by a 10°C differential between skin and structure
(Frequency = 12 GHz) Case (b)

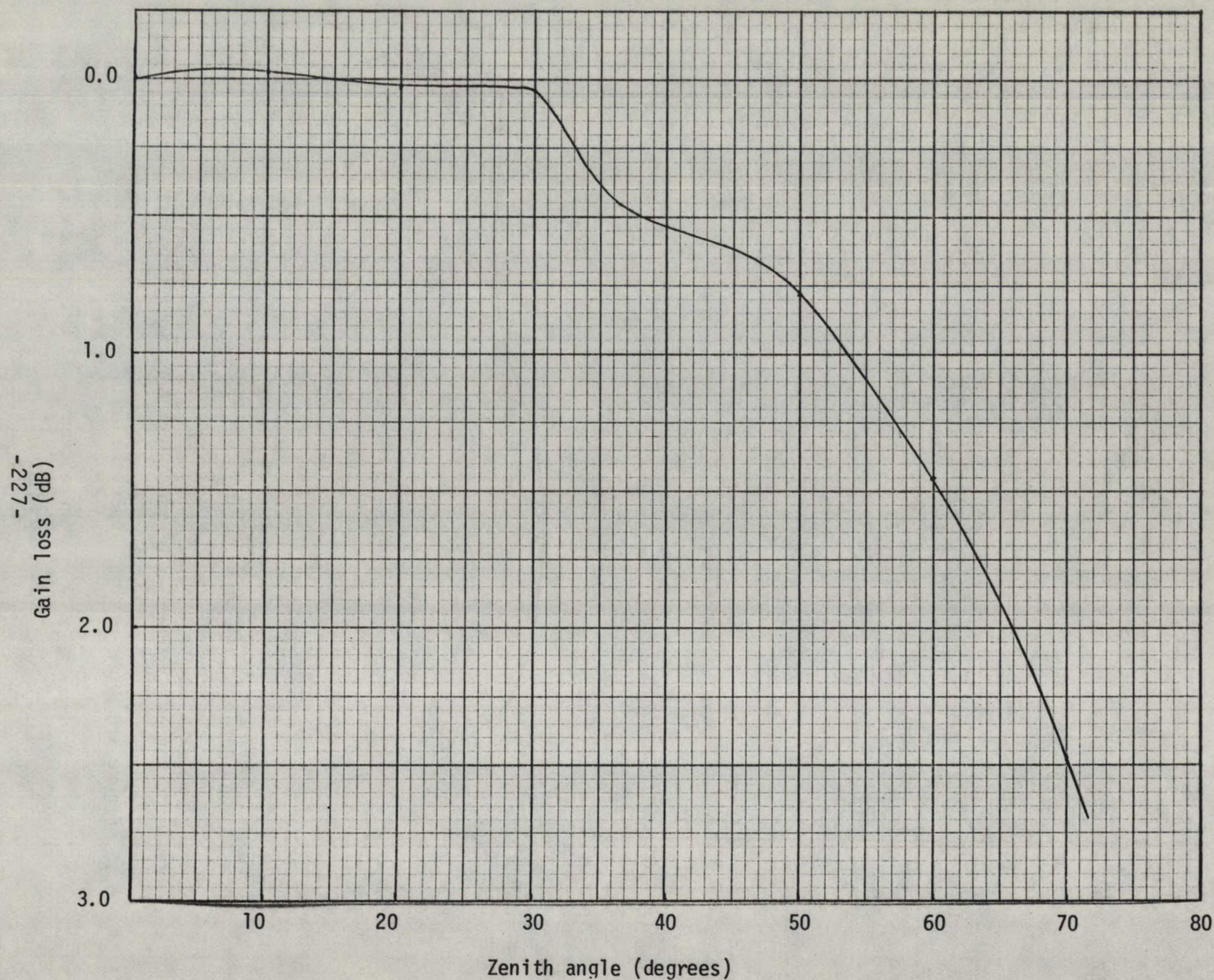


Figure 2.8.2 Measured gain loss for 140' Green Bank radio-telescope antenna 10.7 GHz
 (Plotted from data given in Hoerner and Wong (5))

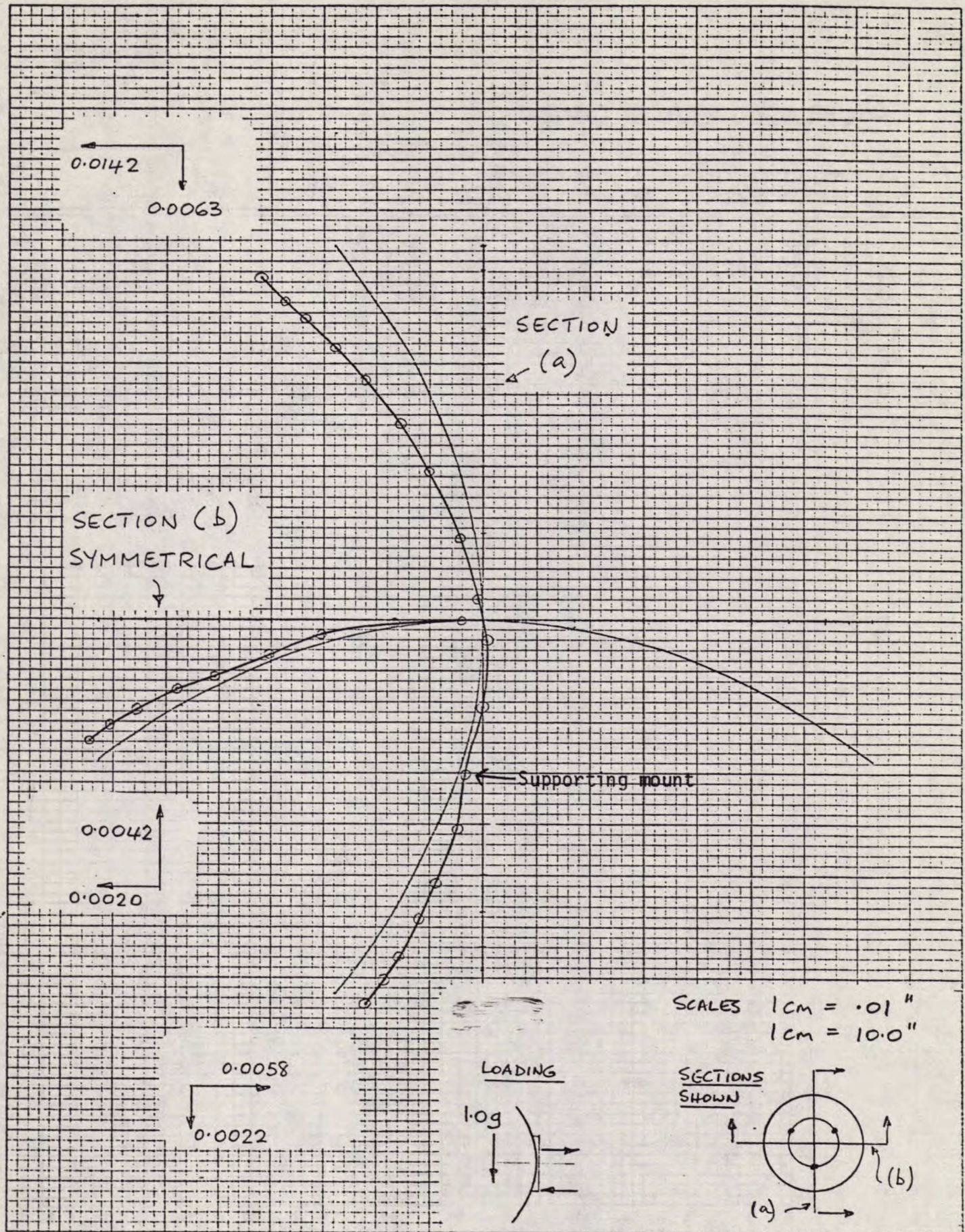


Figure 3.8.4 Gravitational sag 12 ft. reflector.

46 1612

5 X 3 TO THE CENTIMETER 18 X 24 CM.
KEUFFEL & ESSER CO. MADE IN U.S.A.



ANDREW

PE

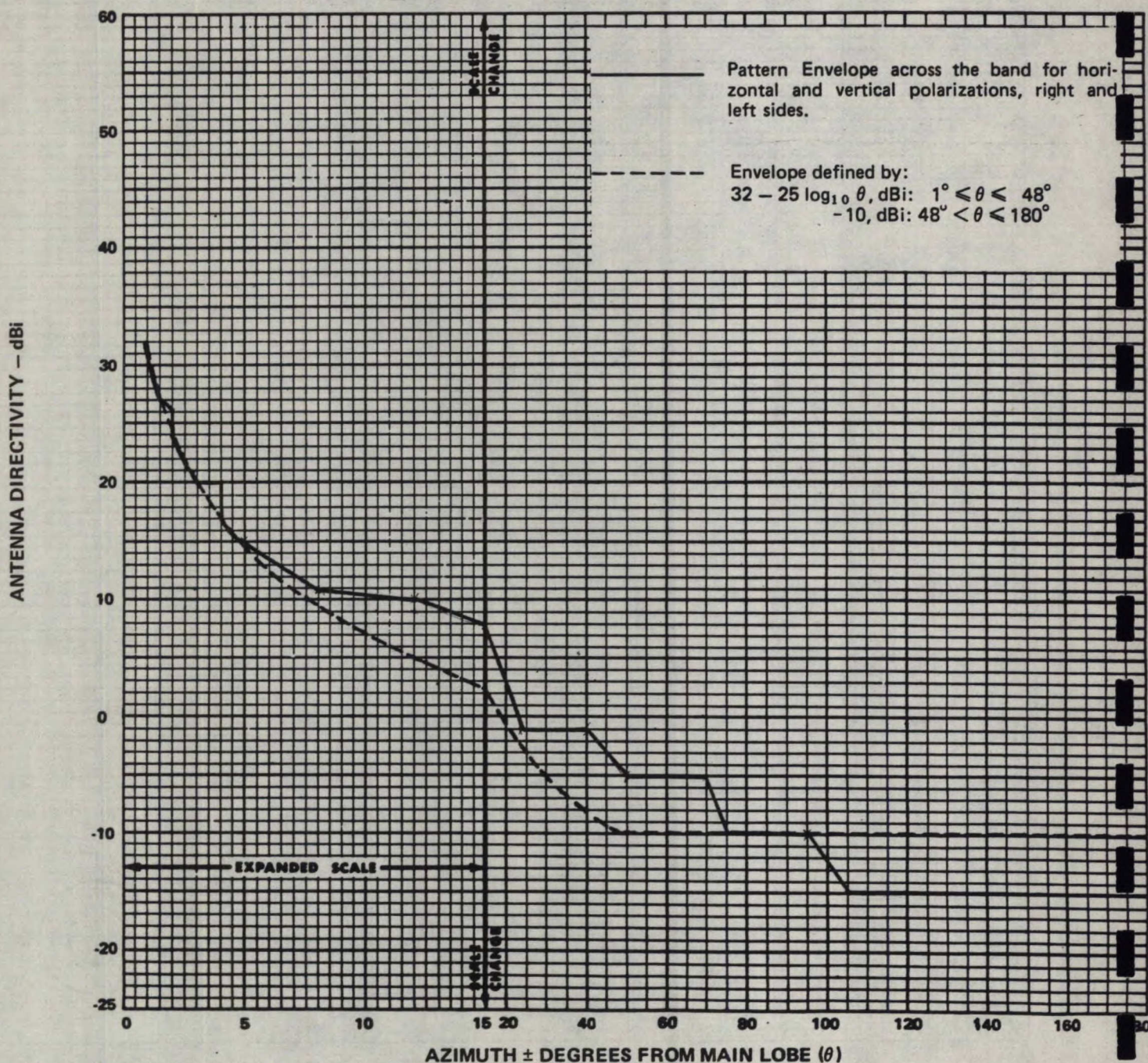
Approved

PATTERN ENVELOPE

ANTENNA TYPE NUMBER ESA 10-46
10M EARTH STATION ANTENNA

3.7-4.2 GHz

Gain: 51.0 ± 0.2 dBi at 3.95 GHz



Andrew Corporation 10500 W. 153rd St.
Orland Park, IL U.S.A. 60462

Andrew Antenna Company Ltd.
Whitby, Ontario, Canada
FORM 4016D (11/79)

Andrew A
Lochgelly,
Andrew A
Reservoir,

FIGURE 4.1.1.

Antennes Andrew S.A.R.L.
Nogent-le-Rotrou, France
Andrew S.R.L.
Milano, Italy



ANDREW

PE

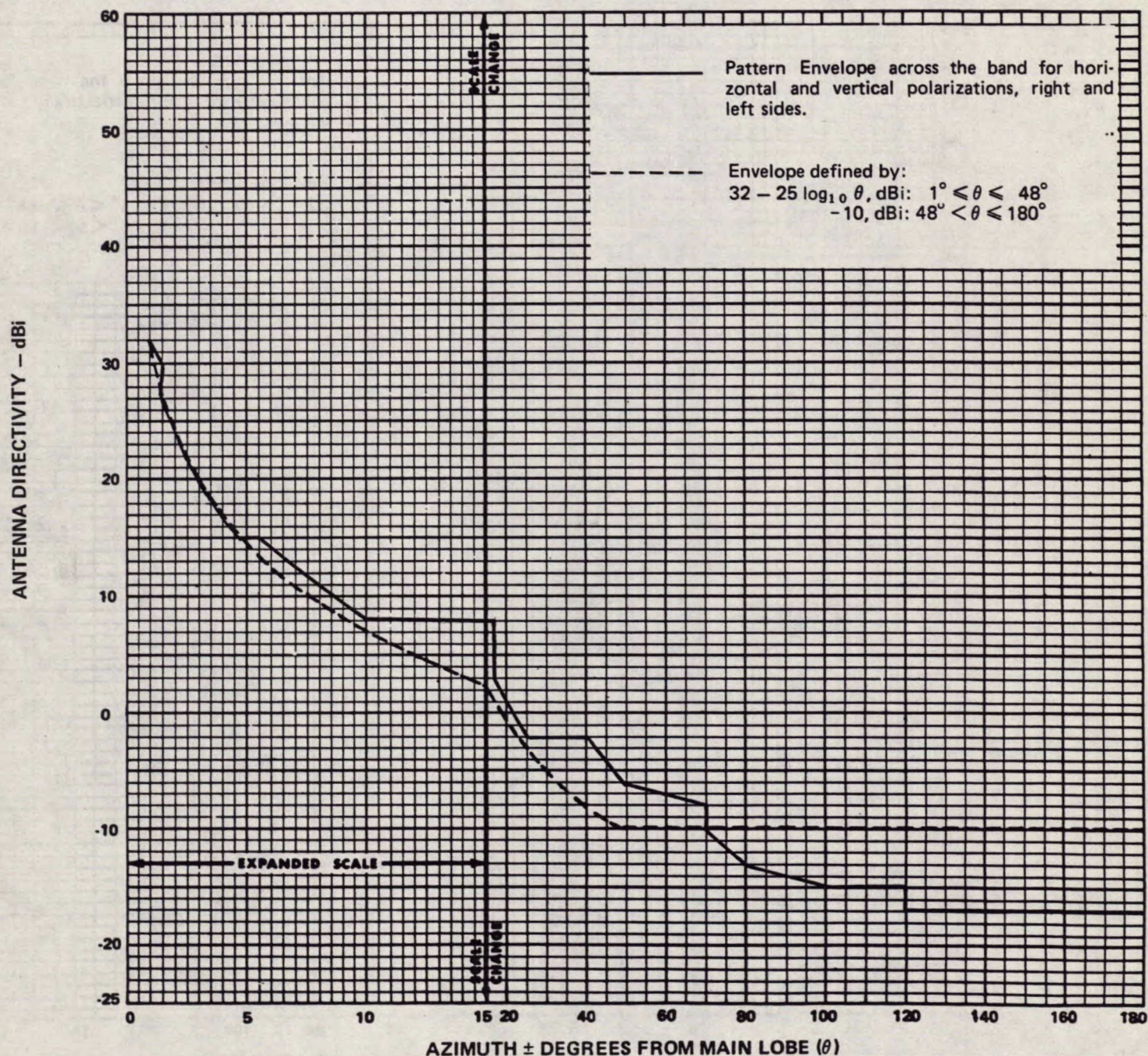
Approved

PATTERN ENVELOPE

ANTENNA TYPE NUMBER ESA 10-46
10M EARTH STATION ANTENNA

5.925-6.425 GHz

Gain: 54.5 ± 0.2 dBi at 6.175 GHz



Andrew Corporation 10500 W. 153rd St.
Orland Park, IL U.S.A. 60462

Andrew Antenna Company Ltd.
Whitby, Ontario, Canada
FORM 4016D (11/79)

Al
Lc
Ar
Re

FIGURE 4.1.2

Limitada
zil
is
ico

Antennes Andrew S.A.R.L.
Nogent-le-Rotrou, France
Andrew S.R.L.
Milano, Italy





ANDREW

PE

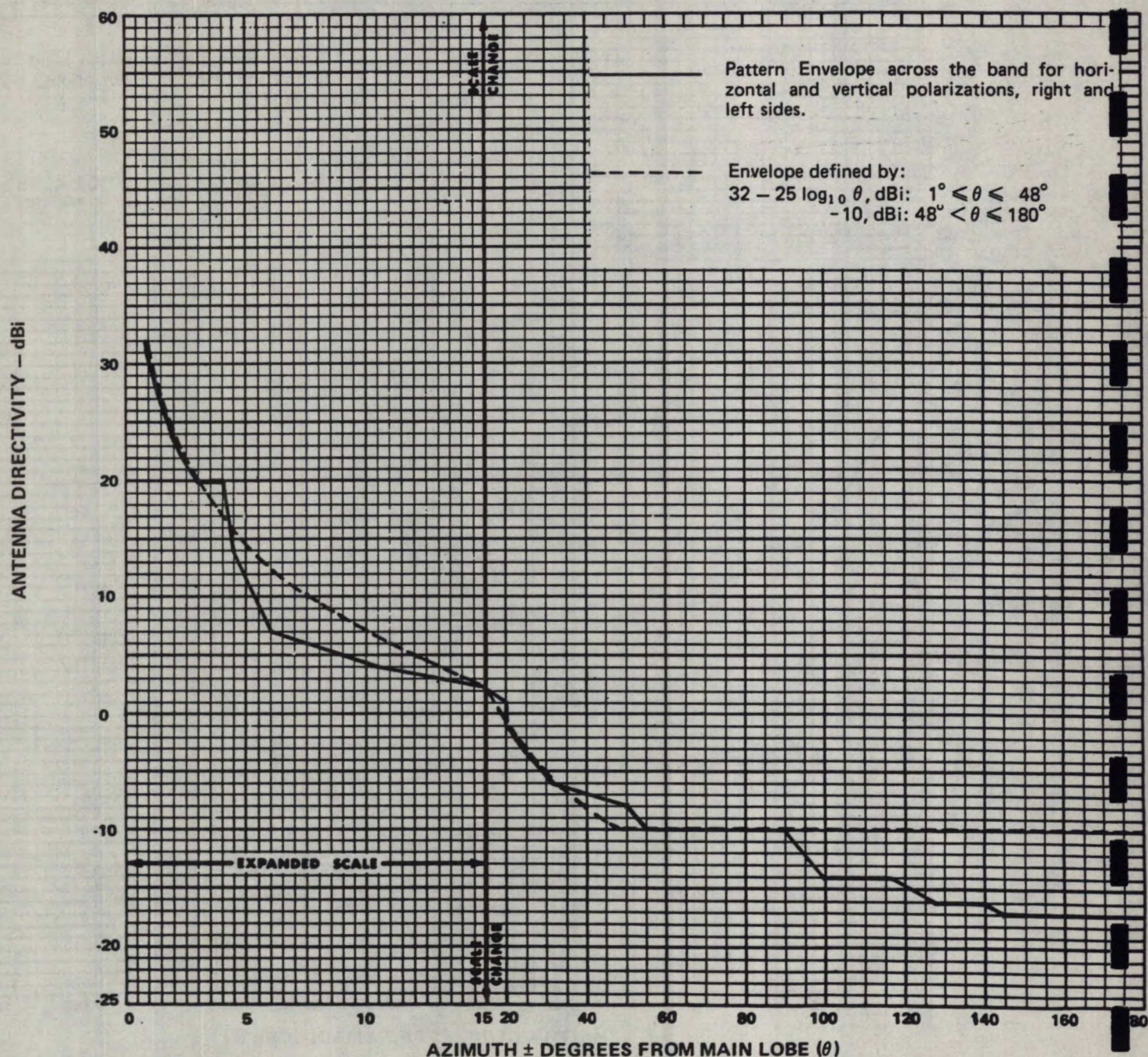
Approved

PATTERN ENVELOPE

ANTENNA TYPE NUMBER ESA10-46B
10M 4/6 GHZ EARTH STATION ANTENNA

3.7-4.2 GHz

Gain: 51.0 ± 0.2 dBi at 4.0 GHz





ANDREW

PE

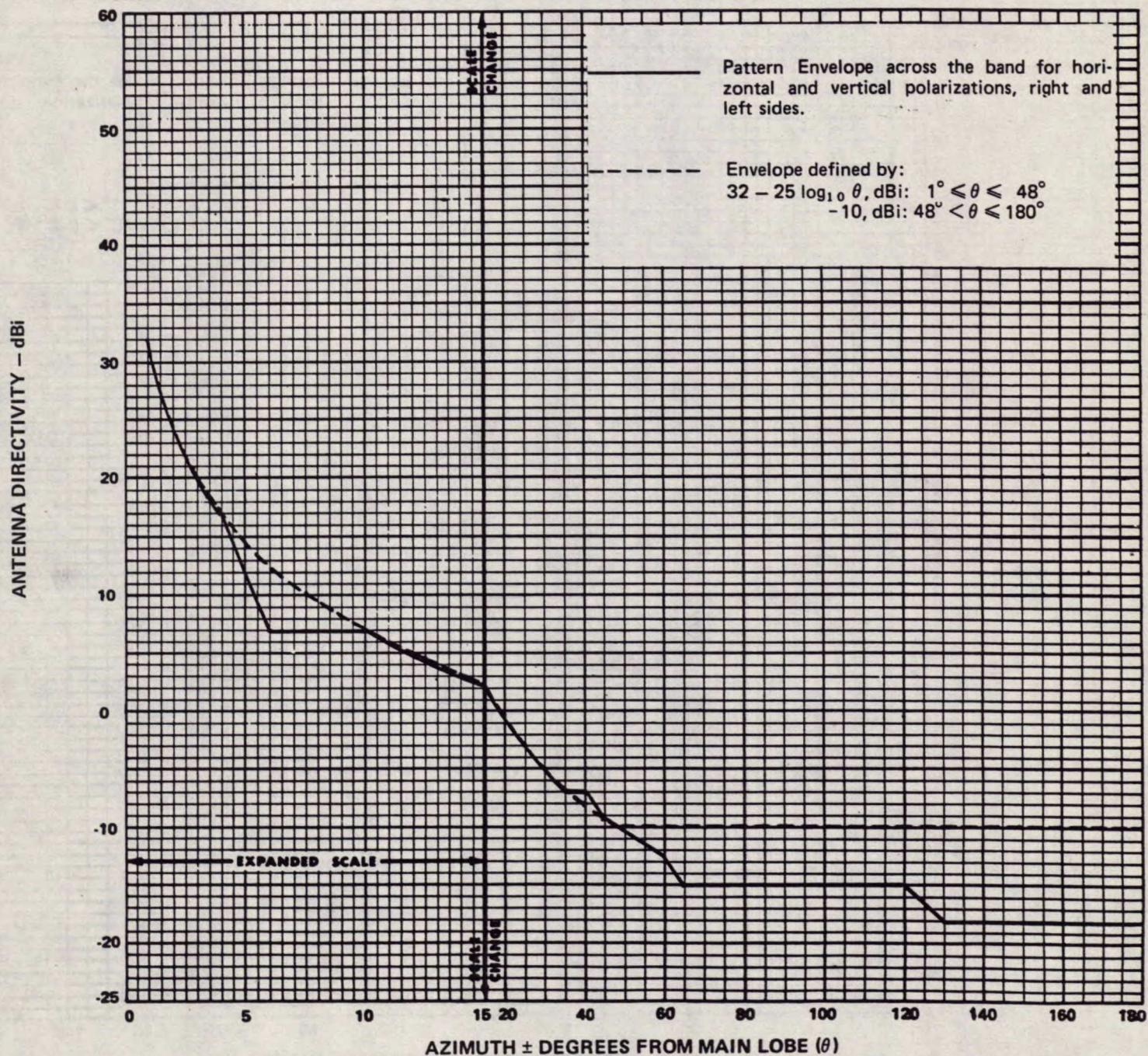
Approved

PATTERN ENVELOPE

ANTENNA TYPE NUMBER ESA10-46B
10M 4/6 GHZ EARTH STATION ANTENNA

5.925-6.425 GHz

Gain: 54.3 ± 0.2 dBi at 6.175 GHz





ANDREW

PE

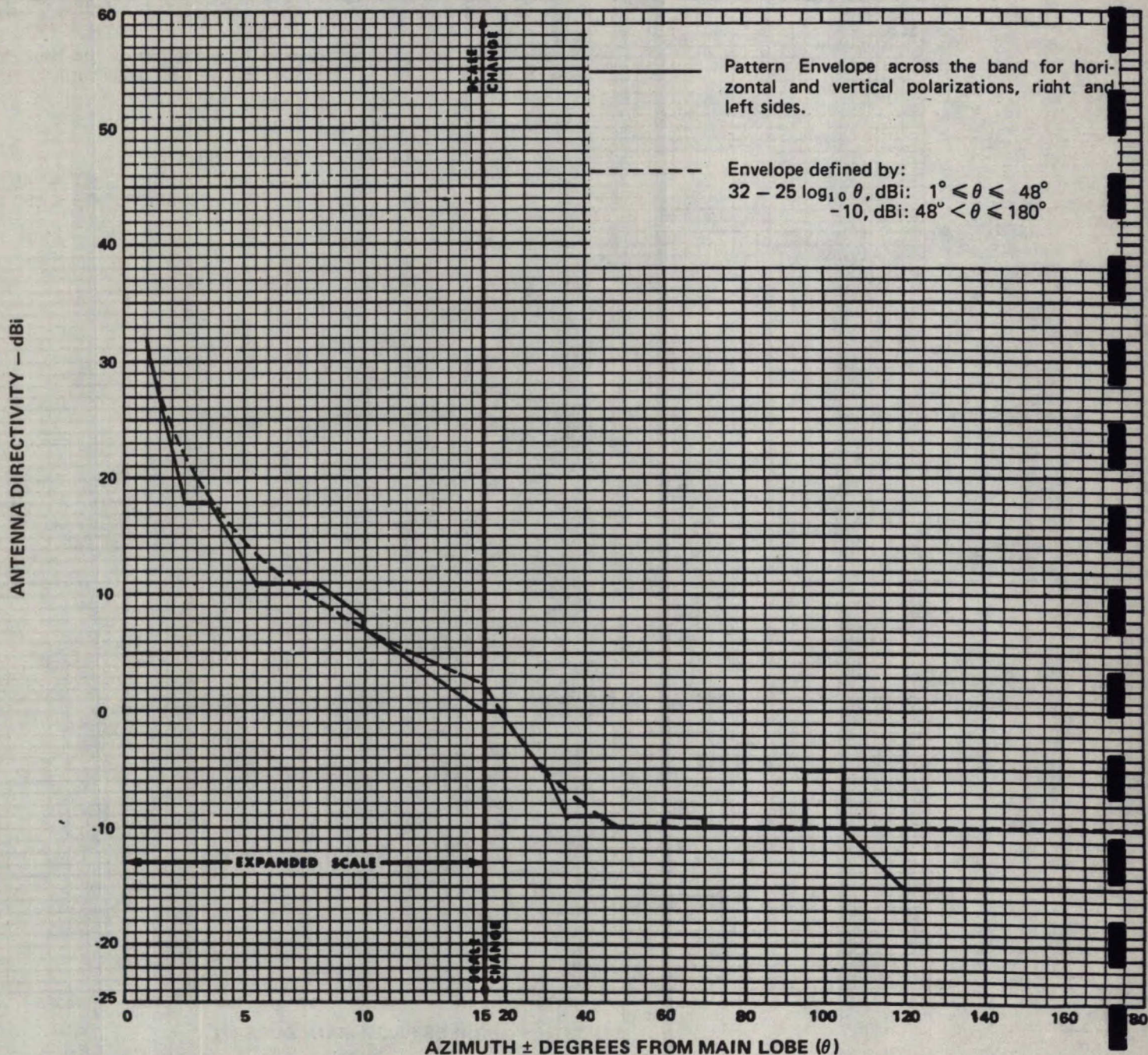
Approved

PATTERN ENVELOPE

ANTENNA TYPE NUMBER ESA12-46
12M 4/6 GHZ EARTH STATION ANTENNA

3.7-4.2 GHz

Gain: 52.6 ± 0.2 dBi at 4.0 GHz



Andrew Corporation 10500 W. 153rd St.
Orland Park, IL U.S.A. 60462

Andrew Antenna Company Ltd.
Whitby, Ontario, Canada

Andrew An
Lochgelly,

Andrew An
Reservoir, \

FIGURE 4.1.5

Antennes Andrew S.A.R.L.
Nogent-le-Rotrou, France

Andrew S.R.L.
Milano, Italy



ANDREW

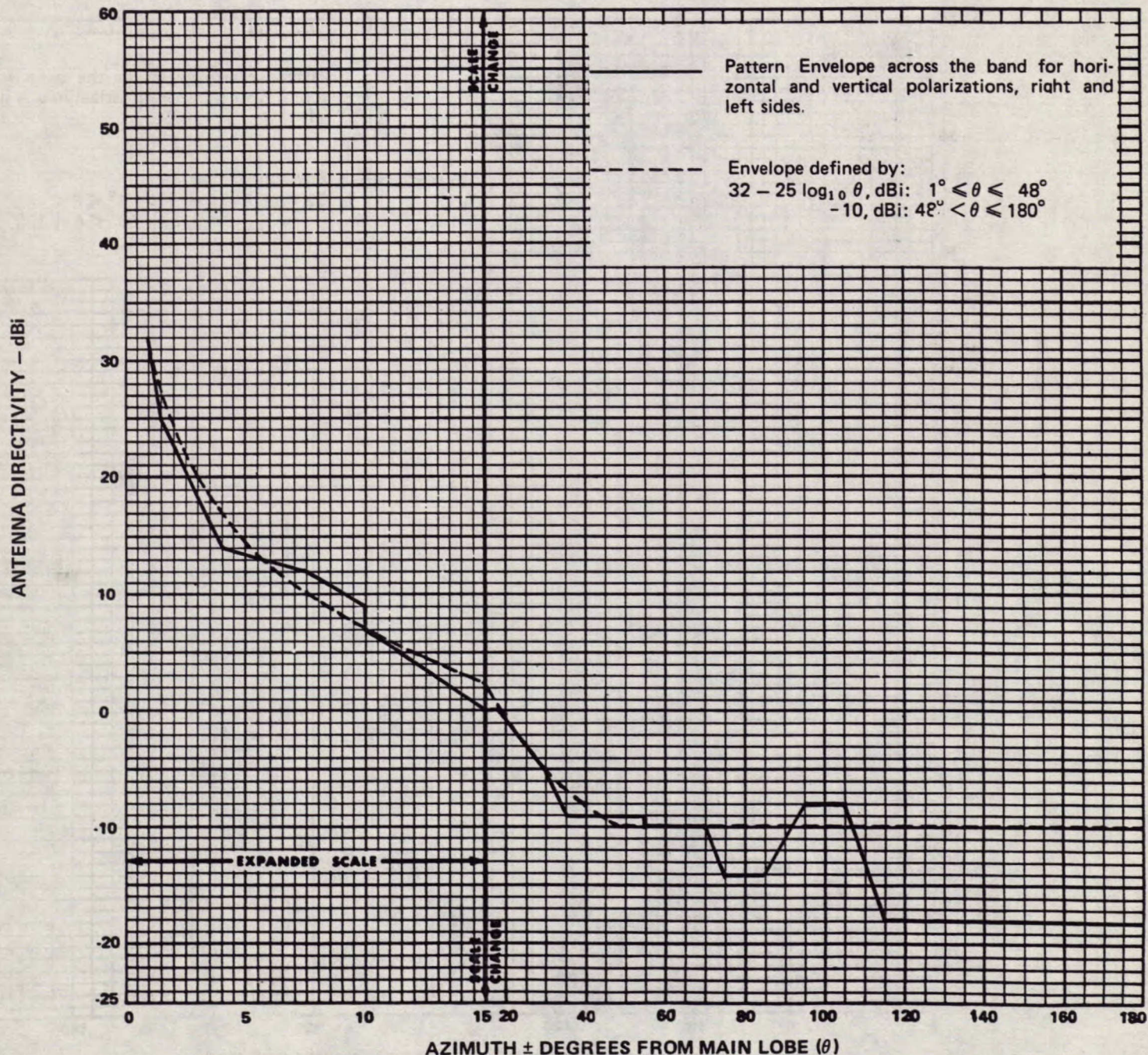
PE

Approved

PATTERN ENVELOPE

ANTENNA TYPE NUMBER ESA12-46
12M 4/6 GHz EARTH STATION ANTENNA

5.925-6.425 GHz
Gain: 56.0 \pm 0.2 dBi at 6.175 GHz



Andrew Corporation 10500 W. 153rd St.
Orland Park, IL U.S.A. 60462

Andrew Antenna Company Ltd.
Whitby, Ontario, Canada
FORM 4016D (11/79)

Andrew
Lochge
Andrew
Reservc

FIGURE 4.1.6

ida

Antennes Andrew S.A.R.L.
Nogent-le-Rotrou, France
Andrew S.R.L.
Milano, Italy





ANDREW

PE

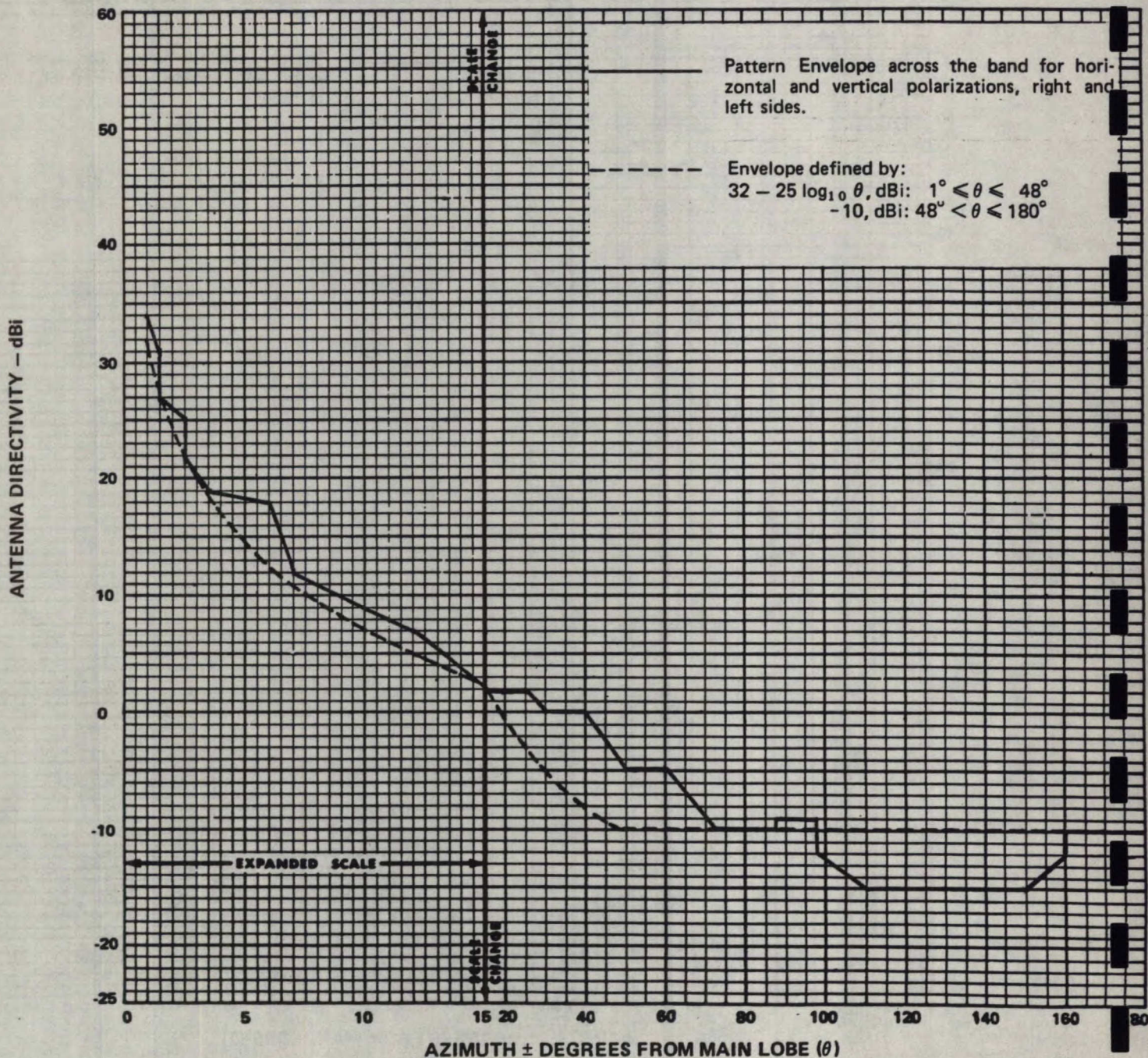
Approved

PATTERN ENVELOPE

ANTENNA TYPE NUMBER ESA 8-46
8M 4/6 GHZ EARTH STATION ANTENNA

3.7 - 4.2 GHz

Gain: 48.4 ± 0.2 dBi at 3.95 GHz



Andrew Corporation 10500 W. 153rd St.
Orland Park, IL U.S.A. 60462

Andrew Antenna Company Ltd.
Whitby, Ontario, Canada

Andrew
Lochgeil

Andrew
Reservoir, Victoria, Australia

FIGURE 4.1.7

1a

Antennes Andrew S.A.R.L.
Nogent-le-Rotrou, France

Andrew S.R.L.
Milano, Italy



ANDREW

PE

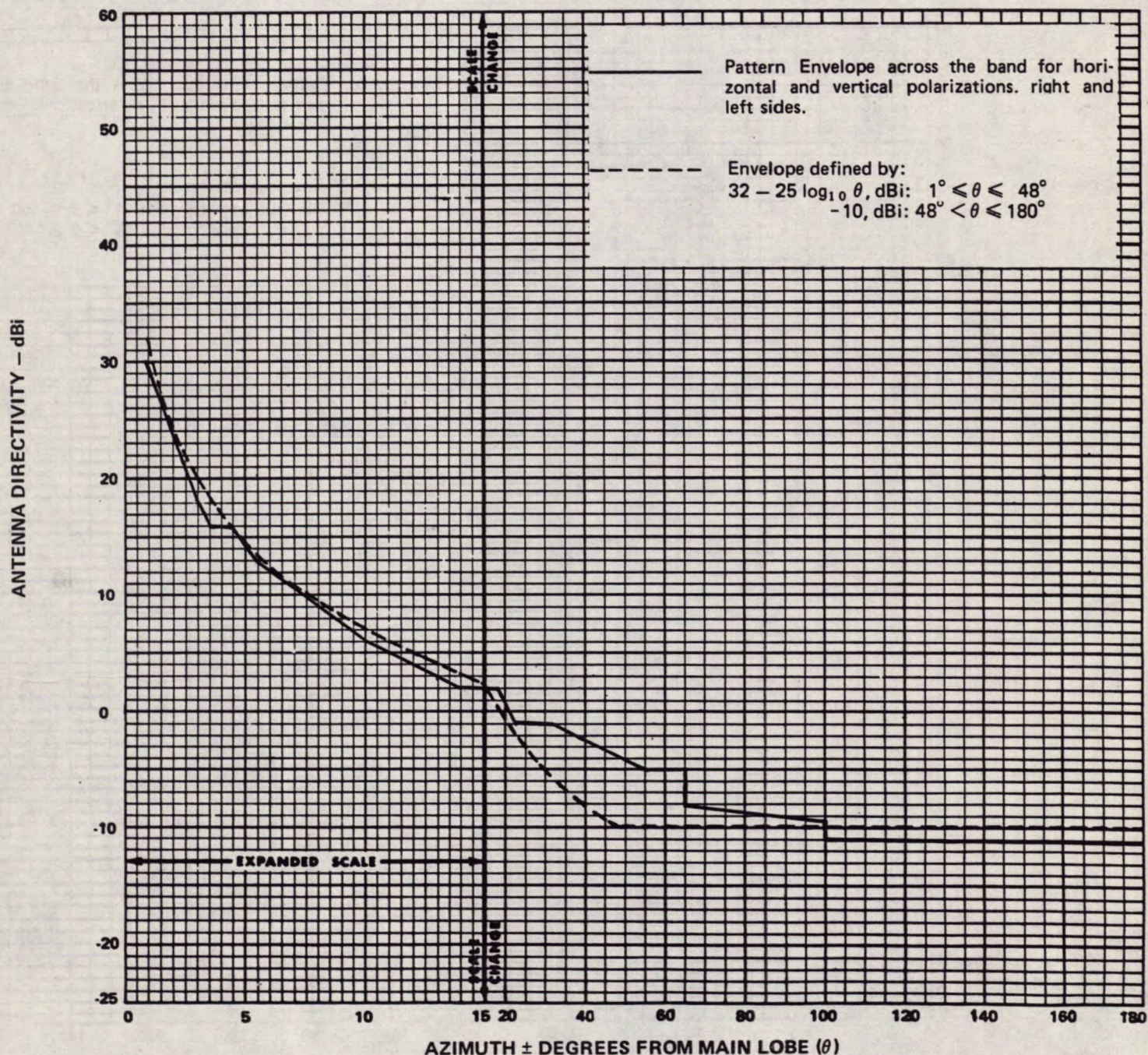
Approved

PATTERN ENVELOPE

ANTENNA TYPE NUMBER ESA 8-46
8M 4/6 GHZ EARTH STATION ANTENNA

5.925 - 6.425 GHz

Gain: 52.3 ± 0.2 dBi at 6.175 GHz



Andrew Corporation 10500 W. 153rd St.
Orland Park, IL U.S.A. 60462

Andrew /
Lochgelly

Andrew Antenna Company Ltd.
Whitby, Ontario, Canada
FORM 4016D (11/79)

Andrew A
Reservoir,

FIGURE 4.1.8

Antennes Andrew S.A.R.L.
Nogent-le-Rotrou, France

Andrew S.R.L.
Milano, Italy





ANDREW

PE

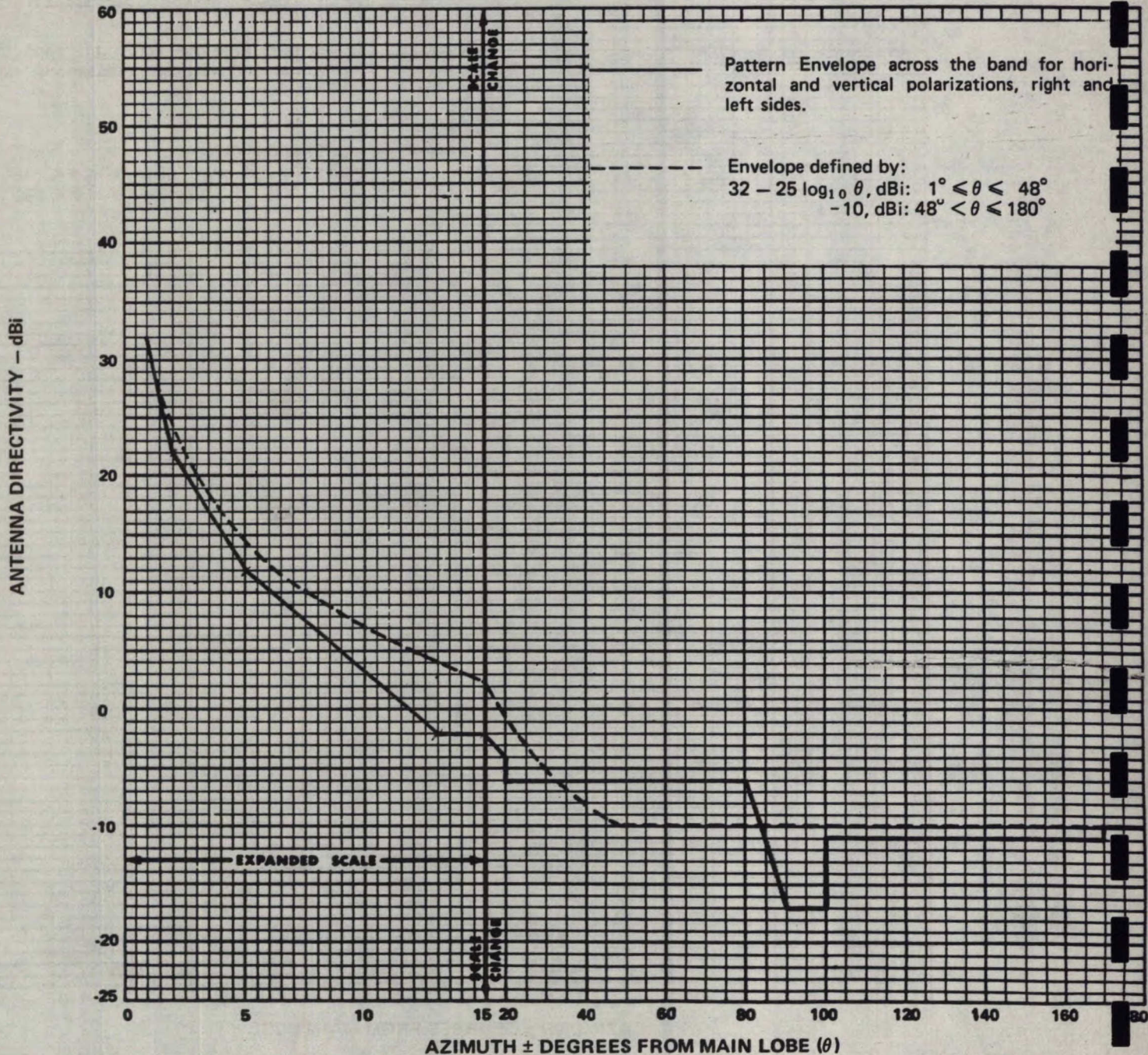
Approved

PATTERN ENVELOPE

ANTENNA TYPE NUMBER ESA8-124
8M 12/14 GHZ EARTH STATION ANTENNA

14.0-14.5 GHz

Gain: 60.4 ± 0.2 dBi at 14.25 GHz





ANDREW

PE

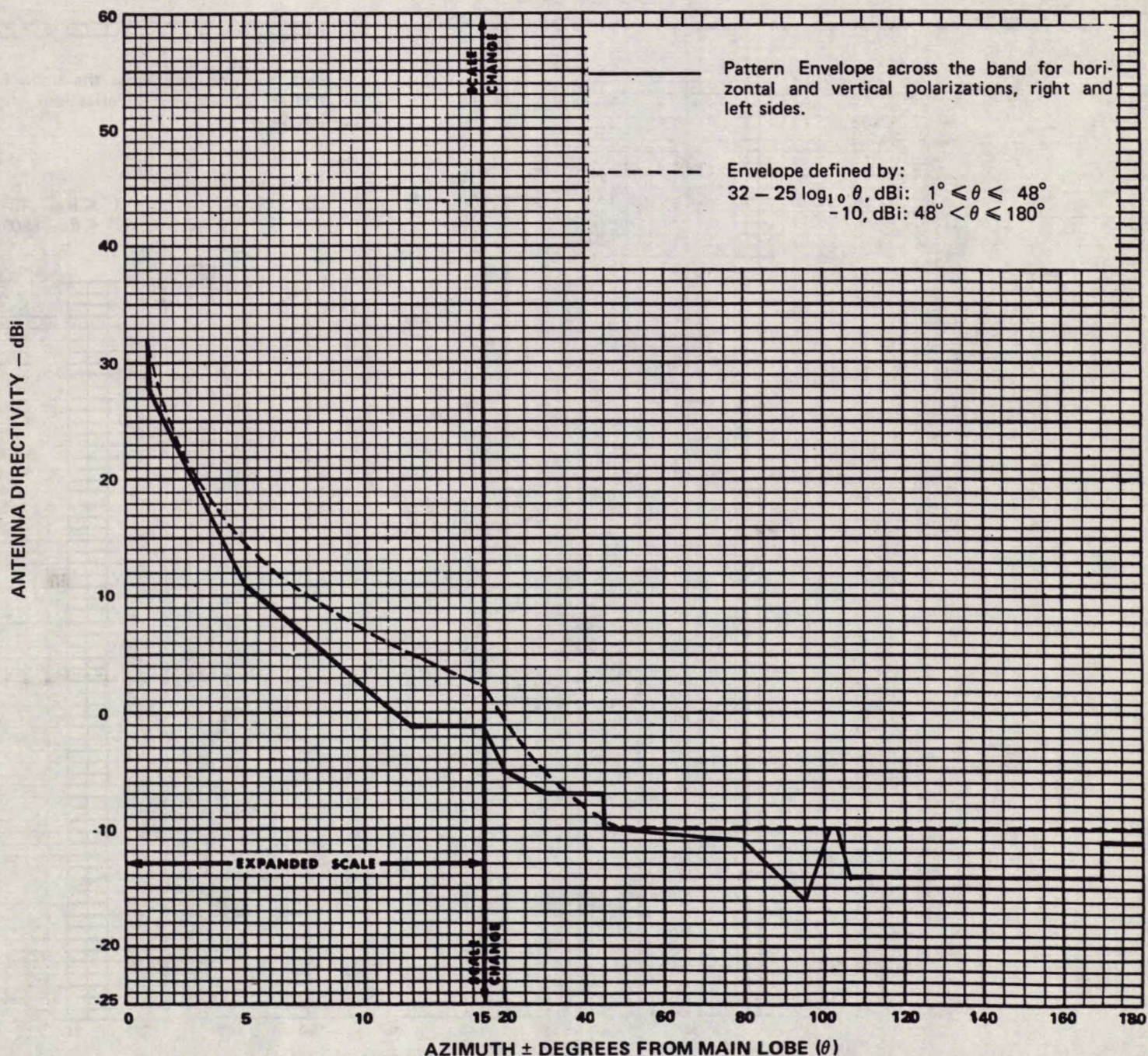
Approved

PATTERN ENVELOPE

ANTENNA TYPE NUMBER ESA8-124
8M 12/14 GHZ EARTH STATION ANTENNA

11.7-12.2 GHz

Gain: 59.0 ± 0.2 dBi at 11.95 GHz



Andrew Corporation 10500 W. 153rd St.
Orland Park, IL U.S.A. 60462

Andrew Antenna Company Ltd.
Whitby, Ontario, Canada
FORM 4016D (11/79)

Andrew Ant
Lochgelly, F
Andrew Ant
Reservoir, V

FIGURE 4.1.9

Antennes Andrew S.A.R.L.
Nogent-le-Rotrou, France
Andrew S.R.L.
Milano, Italy





ANDREW

PE

Approved

PATTERN ENVELOPE

ANTENNA TYPE NUMBER

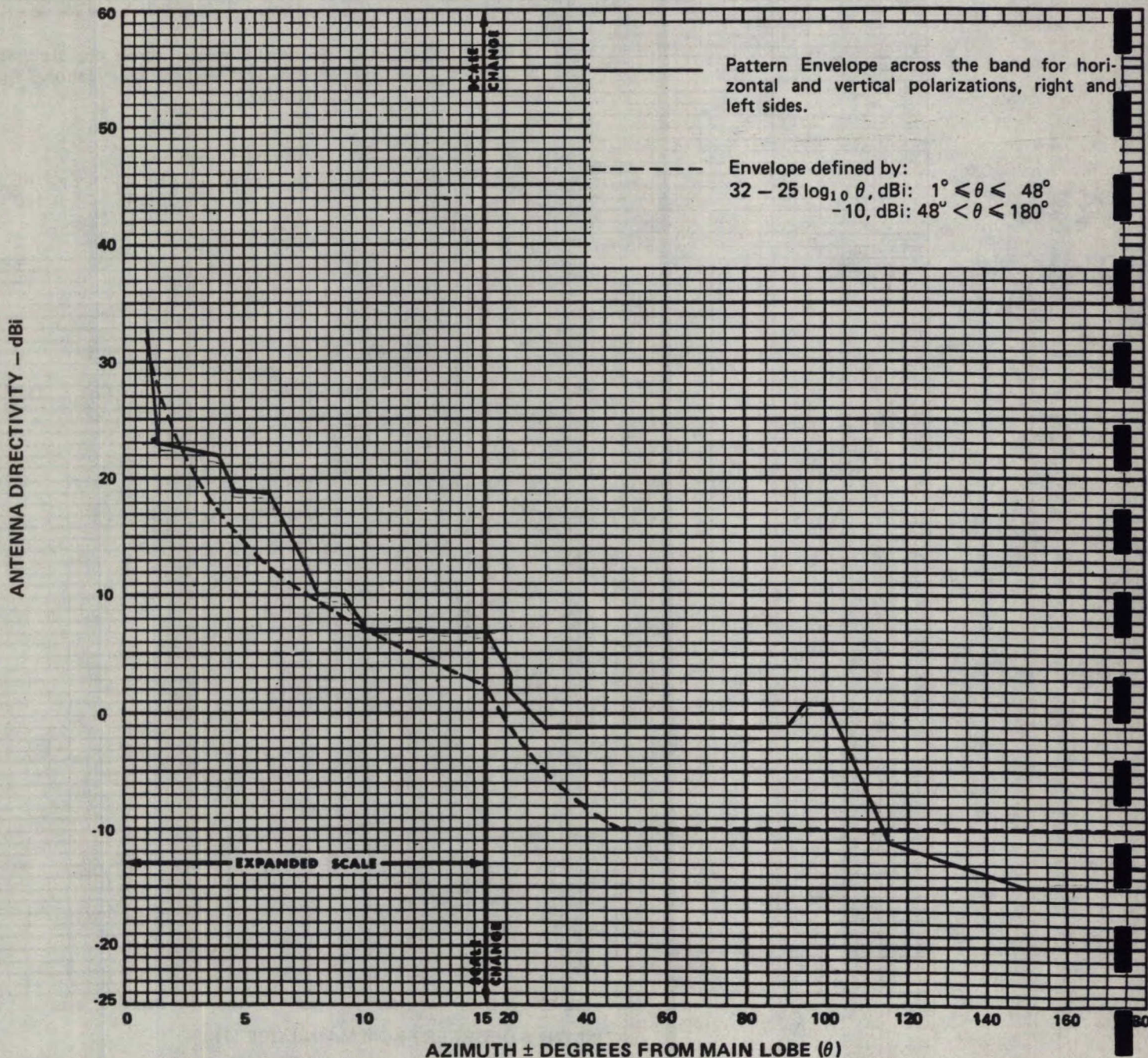
15 FT 4/6 GHZ "J" HOOK ESA

3.7-4.2

GHz

Gain: 43.3±0.2

dBi at 3.95 GHz



Andrew Corporation 10500 W. 153rd St.
Orland Park, IL U.S.A. 60462

Andrew Antenna Company Ltd.
Whitby, Ontario, Canada
FORM 4016D (11/79)

Andrew Antenne
Lochgelly, Fife
Andrew Antenne
Reservoir, Vic

FIGURE 4.1.11

Antenna
I
o

Antennes Andrew S.A.R.L.
Nogent-le-Rotrou, France
Andrew S.R.L.
Milano, Italy



ANDREW

PE

Approved

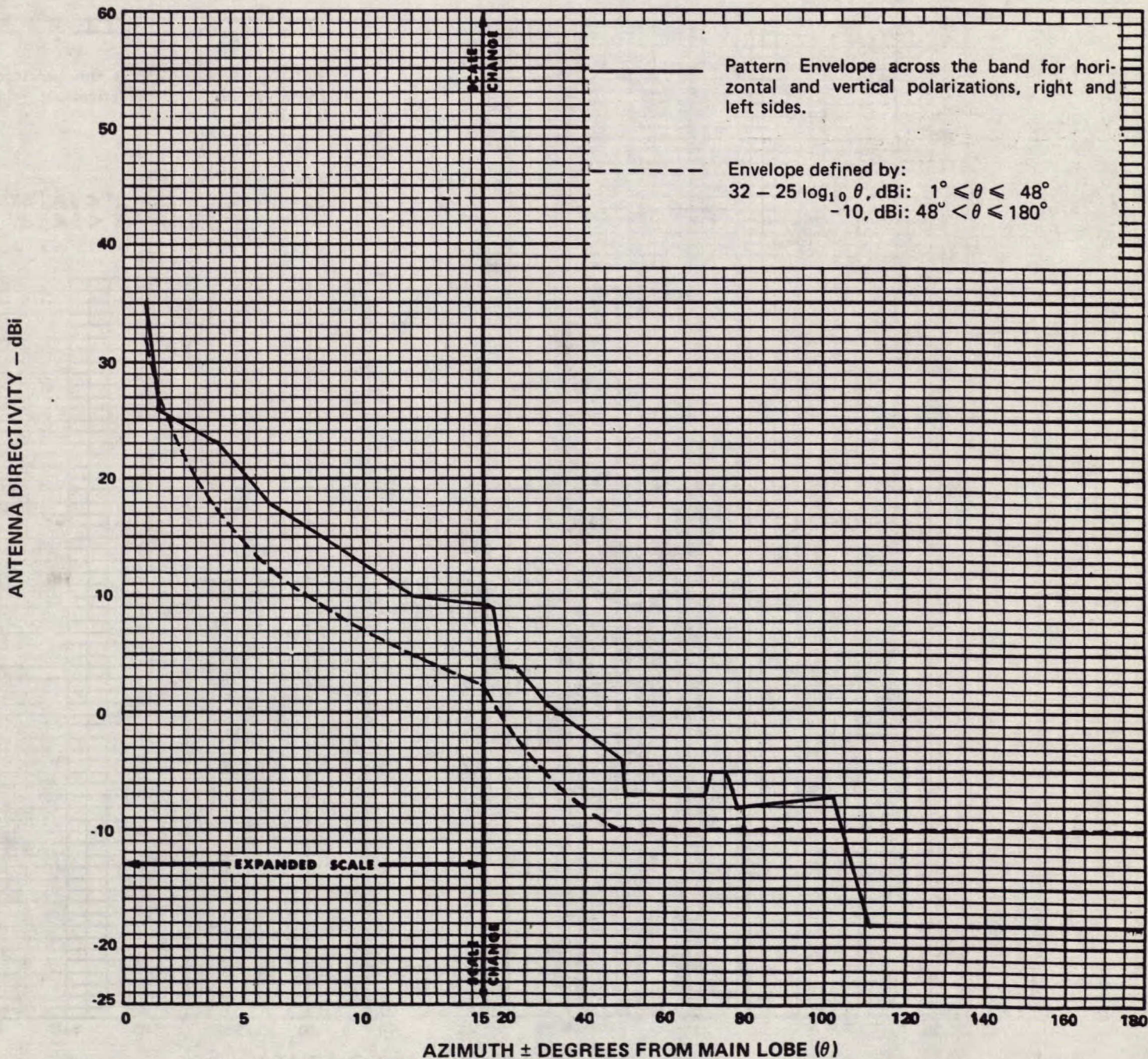
PATTERN ENVELOPE

ANTENNA TYPE NUMBER

15 FT 4/6 GHZ "J" HOOK ESA

5.925-6.425 GHz

Gain: 45.5±0.2 dBi at 6.175 GHz



Andrew Corporation 10500 W. 153rd St.
Orland Park, IL U.S.A. 60462

Andrew Antenna Company Ltd.
Whitby, Ontario, Canada
FORM 4016D (11/79)

Andrew Ante
Lochgelly, Fi
Andrew Ante
Reservoir, Vic

FIGURE 4.1.12

imitada
il
to

Antennes Andrew S.A.R.L.
Nogent-le-Rotrou, France
Andrew S.R.L.
Milano, Italy





ANDREW

PE

Approved

PATTERN ENVELOPE

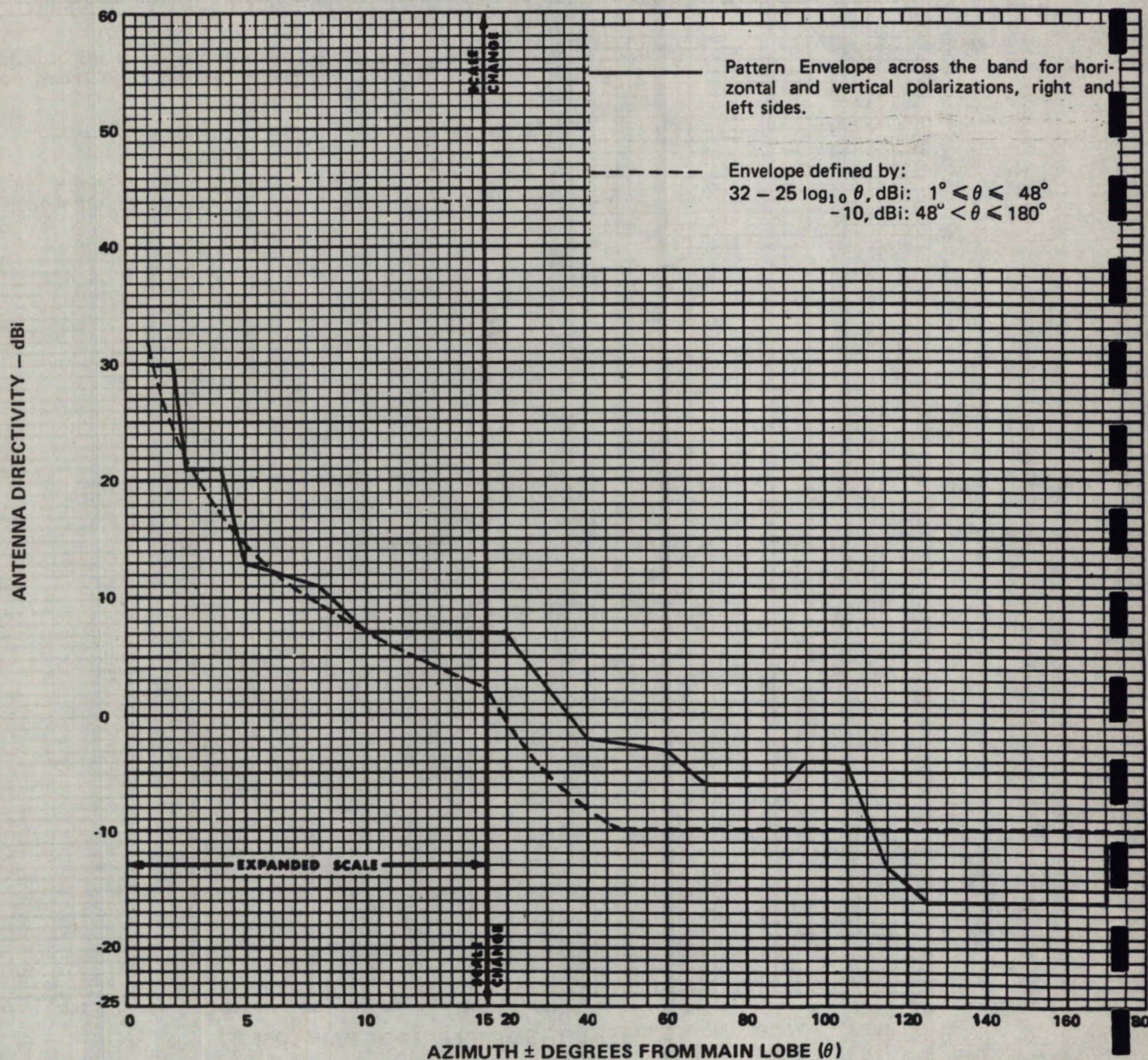
ANTENNA TYPE NUMBER

15 FT 4/6 GHZ CASSEGRAIN ESA

3.7-4.2

GHz

Gain: 43.6±0.7 dBi at 3.95 GHz



Andrew Corporation 10500 W. 153rd St.
Orland Park, IL U.S.A. 60462

Andrew Antenna Company Ltd.
Whitby, Ontario, Canada
FORM 4016D (11/79)

Andrew Anter
Lochgelly, Fifi

Andrew Anter
Reservoir, Vic

FIGURE 4.1.13

mitada

Antennes Andrew S.A.R.L.
Nogent-le-Rotrou, France

Andrew S.R.L.
Milano, Italy



ANDREW

PE

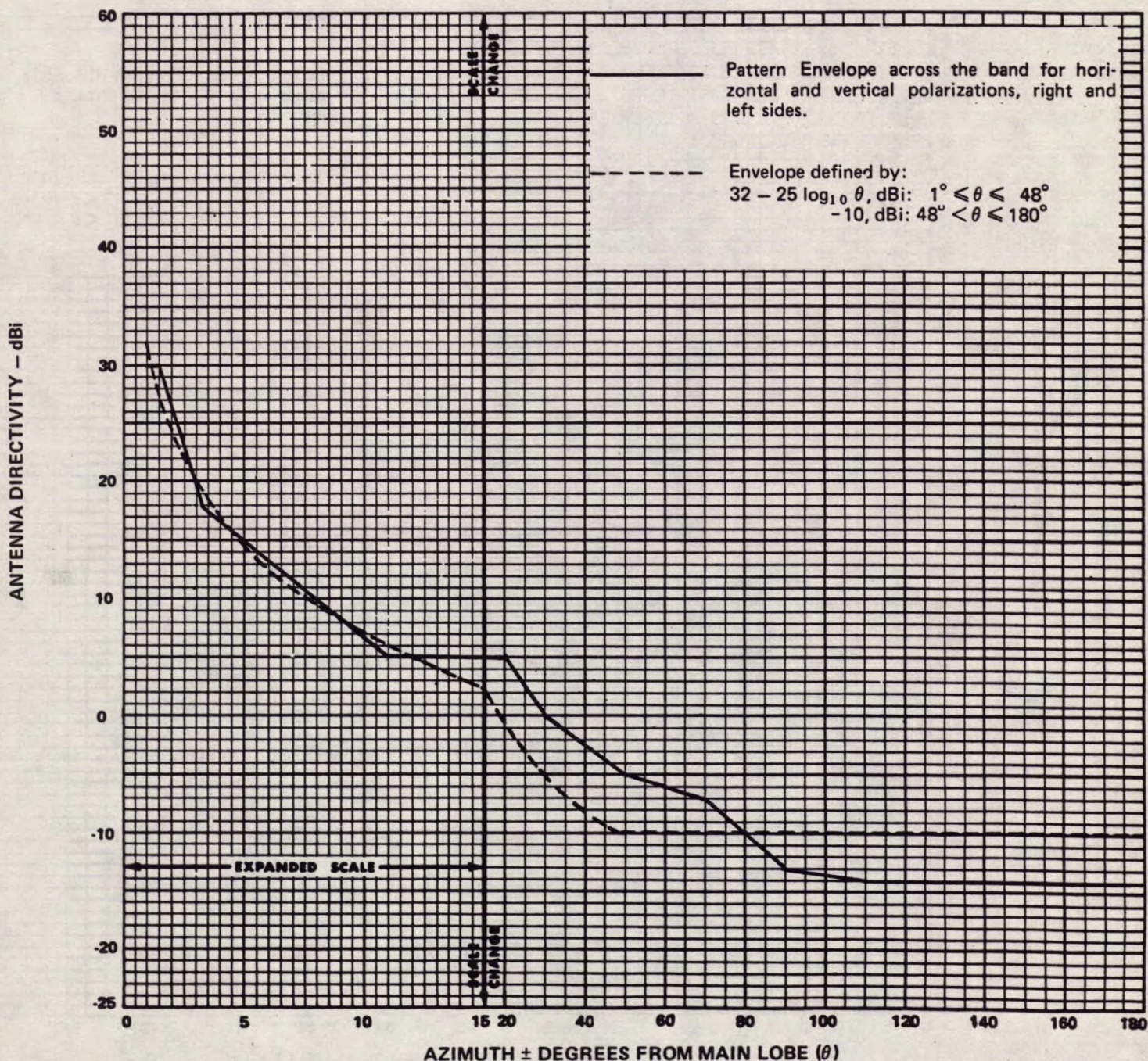
Approved

PATTERN ENVELOPE

ANTENNA TYPE NUMBER
15 FT 4/6 GHZ CASSEGRAIN ESA

5.925-6.425 GHz

Gain: 46.5 ± 0.2 dBi at 6.175 GHz



Andrew Corporation 10500 W. 153rd St.
Orland Park, IL U.S.A. 60462

Andrew Antenna Company Ltd.
Whitby, Ontario, Canada
FORM 4016D (11/79)

Andrew A
Lochelly,
Andrew A
Reservoir,

FIGURE 4.1.14

Limitada
azil
jes
xico

Antennes Andrew S.A.R.L.
Nogent-le-Rotrou, France
Andrew S.R.L.
Milano, Italy





ANDREW

PE

Approved

PATTERN ENVELOPE

ANTENNA TYPE NUMBER

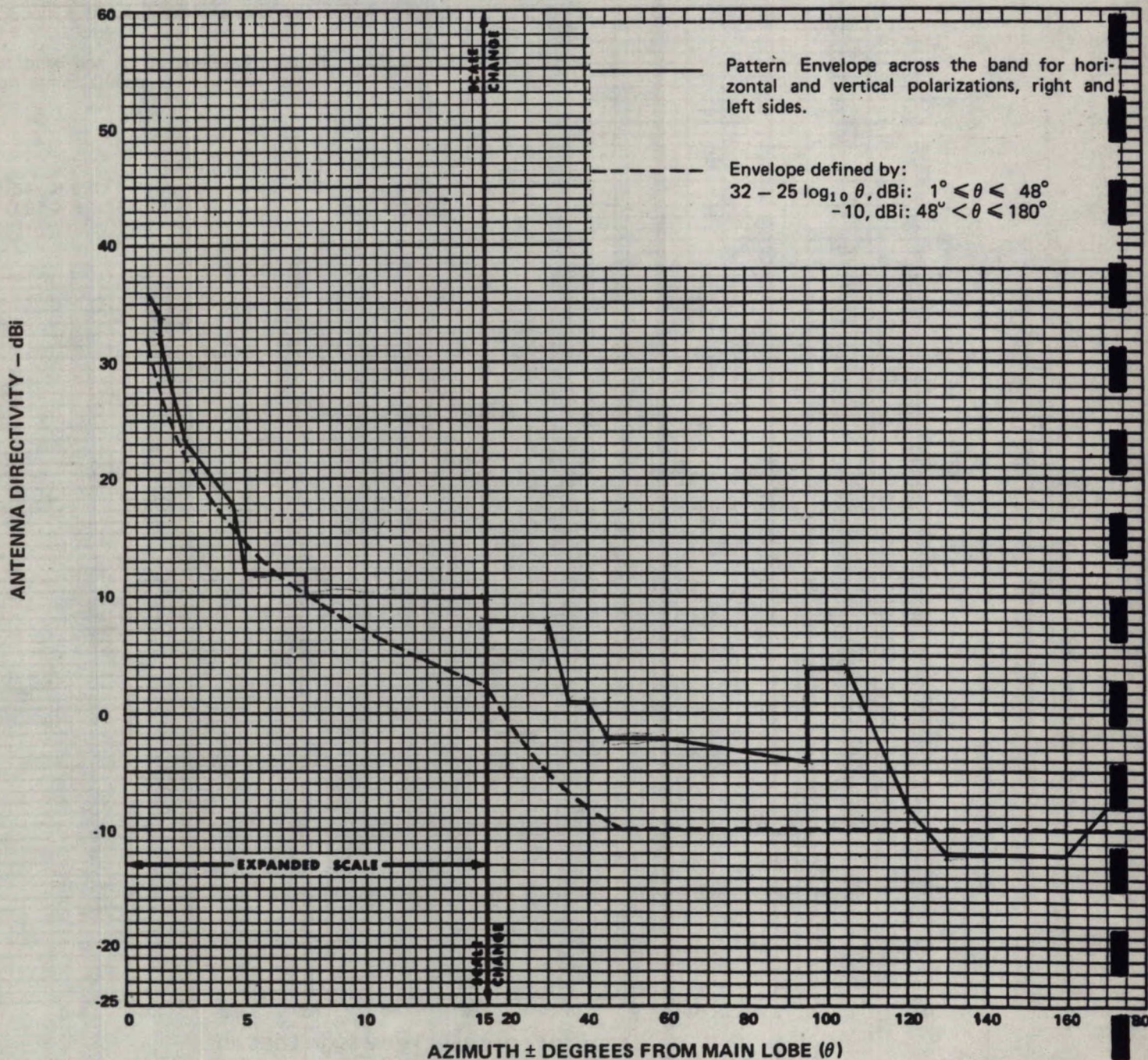
15 FT 12/14 GHZ CASSEGRAIN ESA

11.7-12.2

GHz

Gain: 53.1±0.2

dBi at 11.95 GHz



Andrew Corporation 10500 W. 153rd St.
Orland Park, IL U.S.A. 60462

Andrew Antenna Company Ltd.
Whitby, Ontario, Canada
FORM 4016D (11/79)

Andrew A
Lochgelly

Andrew A
Reservoir,

FIGURE 4.1.15

Limitada
azil
ijes
xico

Antennes Andrew S.A.R.L.
Nogent-le-Rotrou, France

Andrew S.R.L.
Milano, Italy



ANDREW

PE

Approved

PATTERN ENVELOPE

ANTENNA TYPE NUMBER

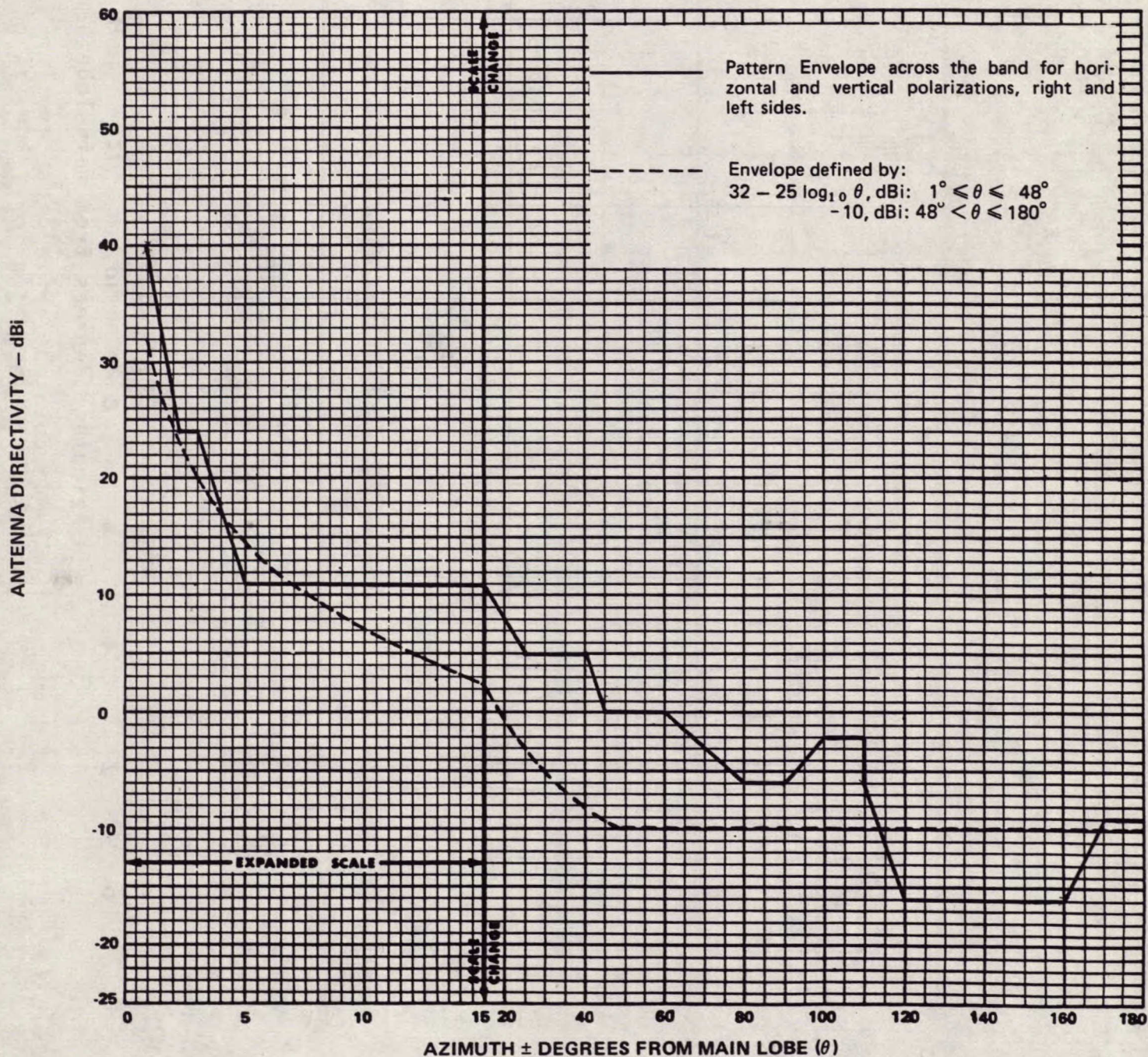
15 FT 12/14 GHZ CASSEGRAIN ESA

14.0 - 14.5

GHz

Gain: 54.2 ± 0.2

dBi at 14.25 GHz



Andrew Corporation 10500 W. 153rd St.
Orland Park, IL U.S.A. 60462

Andrew Antenna Company Ltd.
Whitby, Ontario, Canada
FORM 4016D (11/79)

Andrew Antenn
Lochgelly, Fife,

Andrew Antenn
Reservoir, Victo

FIGURE 4.1.16

Antennes Andrew S.A.R.L.
Nogent-le-Rotrou, France

Andrew S.R.L.
Milano, Italy



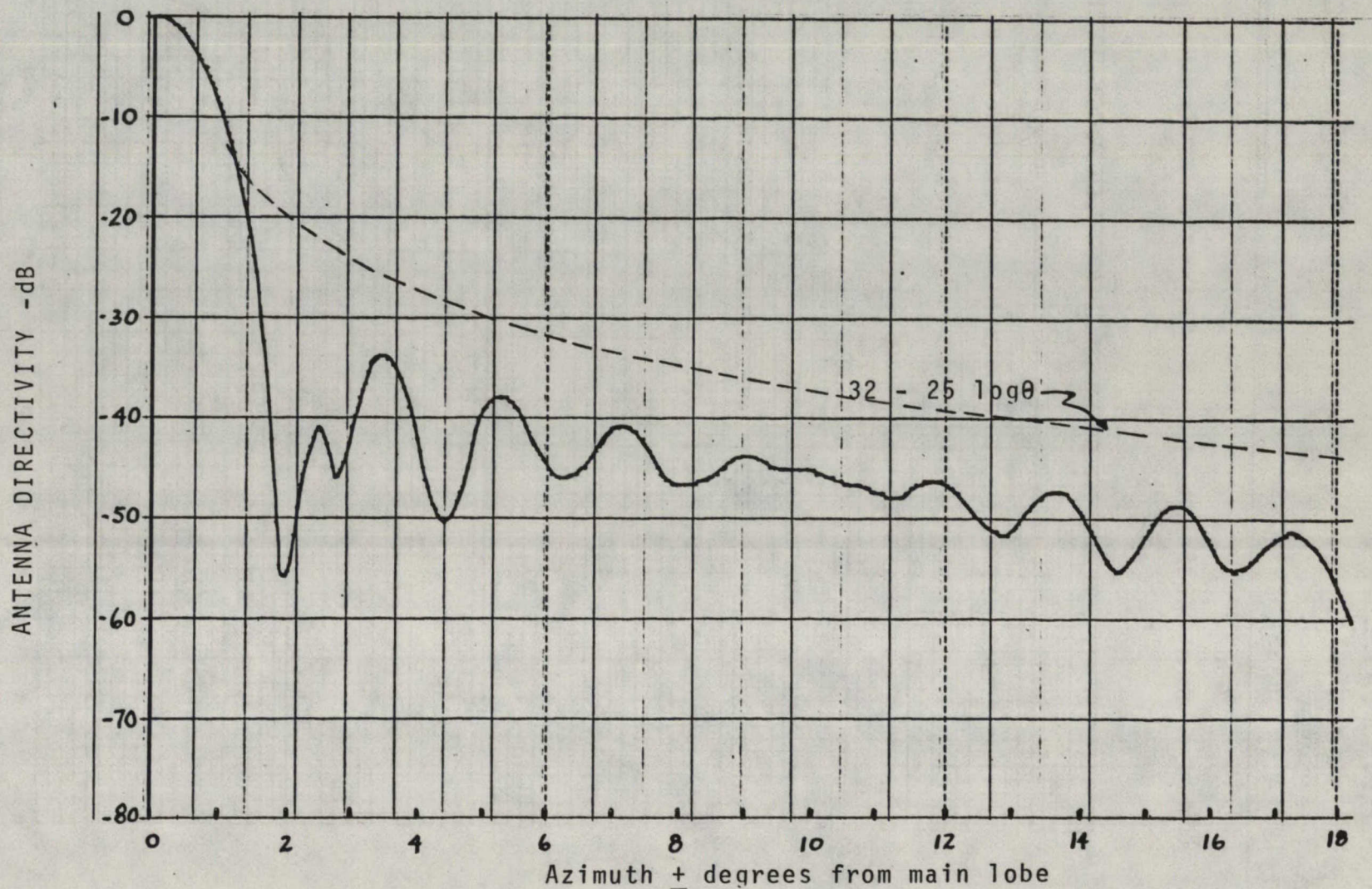


Figure 4.1.17 - Calculated farfield pattern for "J" hook feed with reference reflector illumination

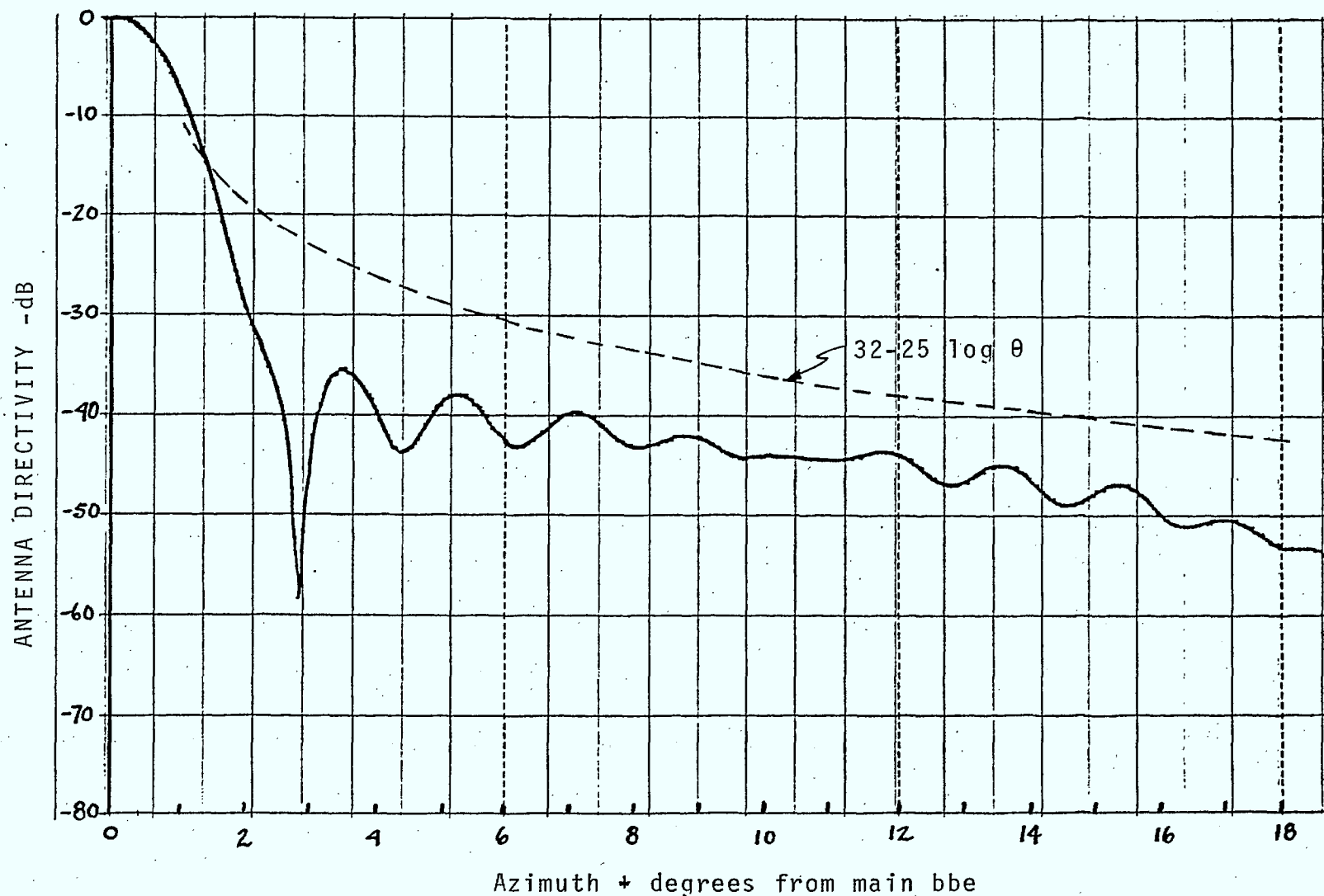


Figure 4.1.18 - Calculated far field pattern for "J" hook feed with under illuminated reflector.

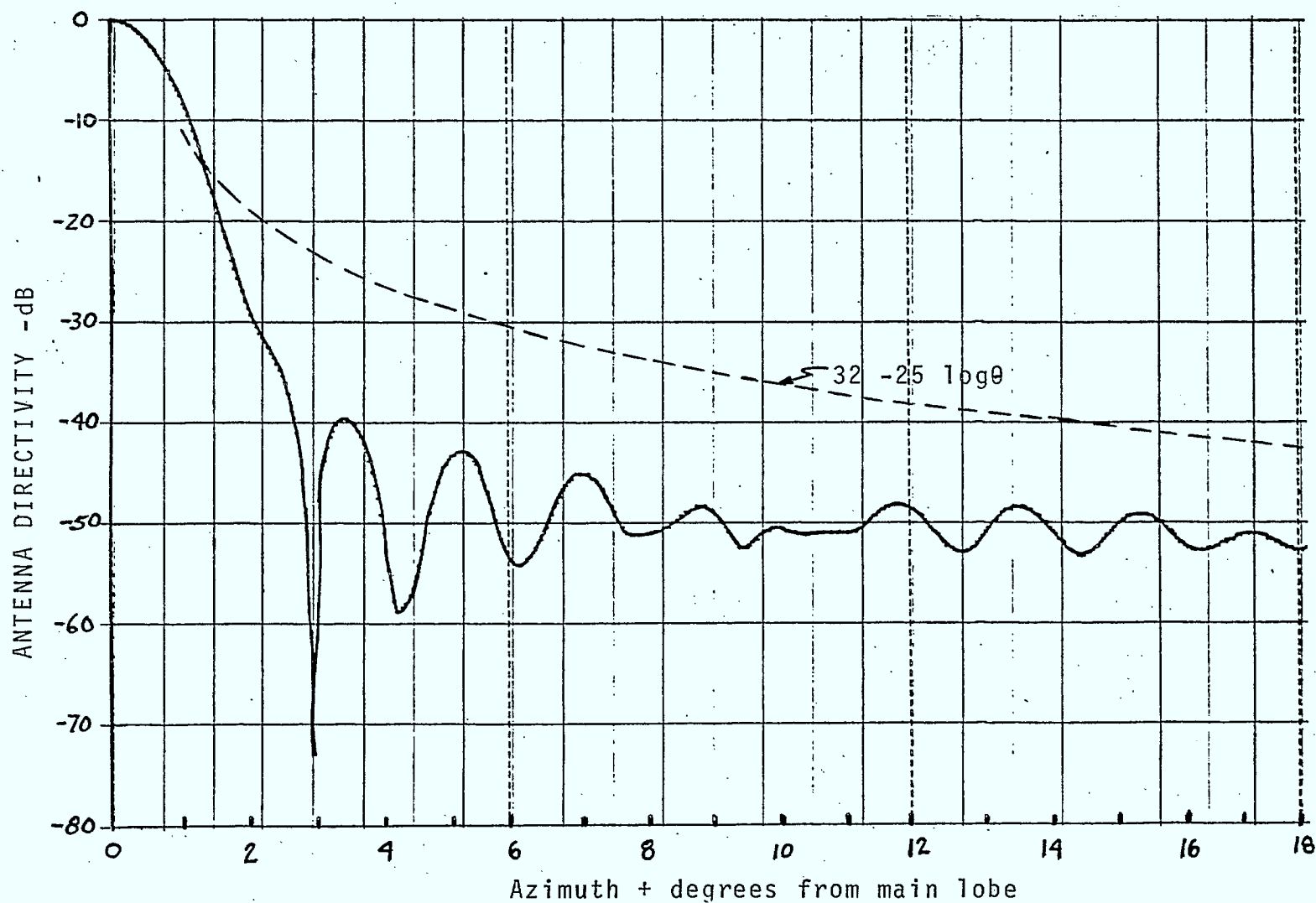


Figure 4.1.19 - Calculated far field pattern for "J" hook feed with under illuminated reflector and a 60% reduction in aperture blockage.

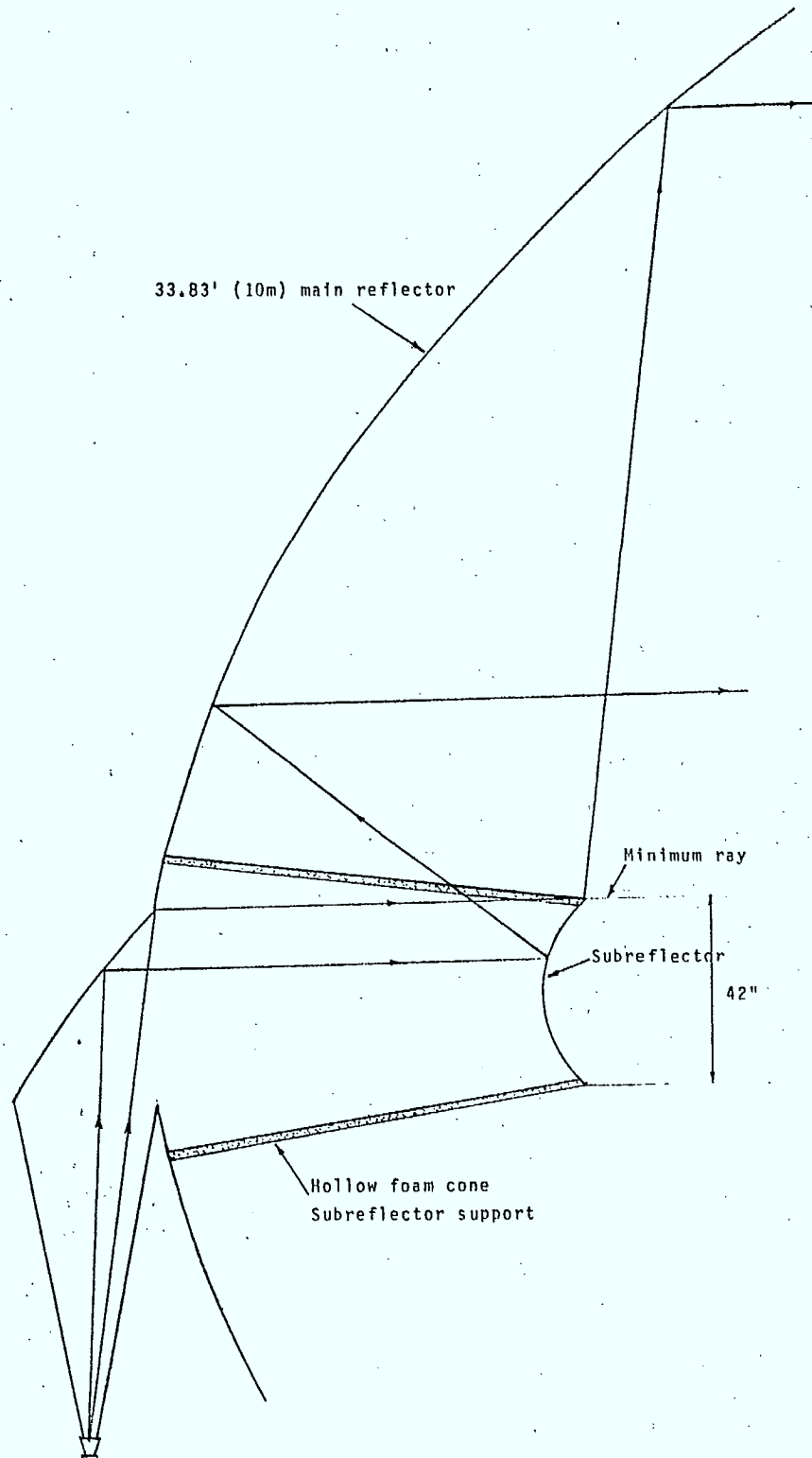


Figure 5.1.1 Shaped Cassegrain system showing reflector profiles and feed position.

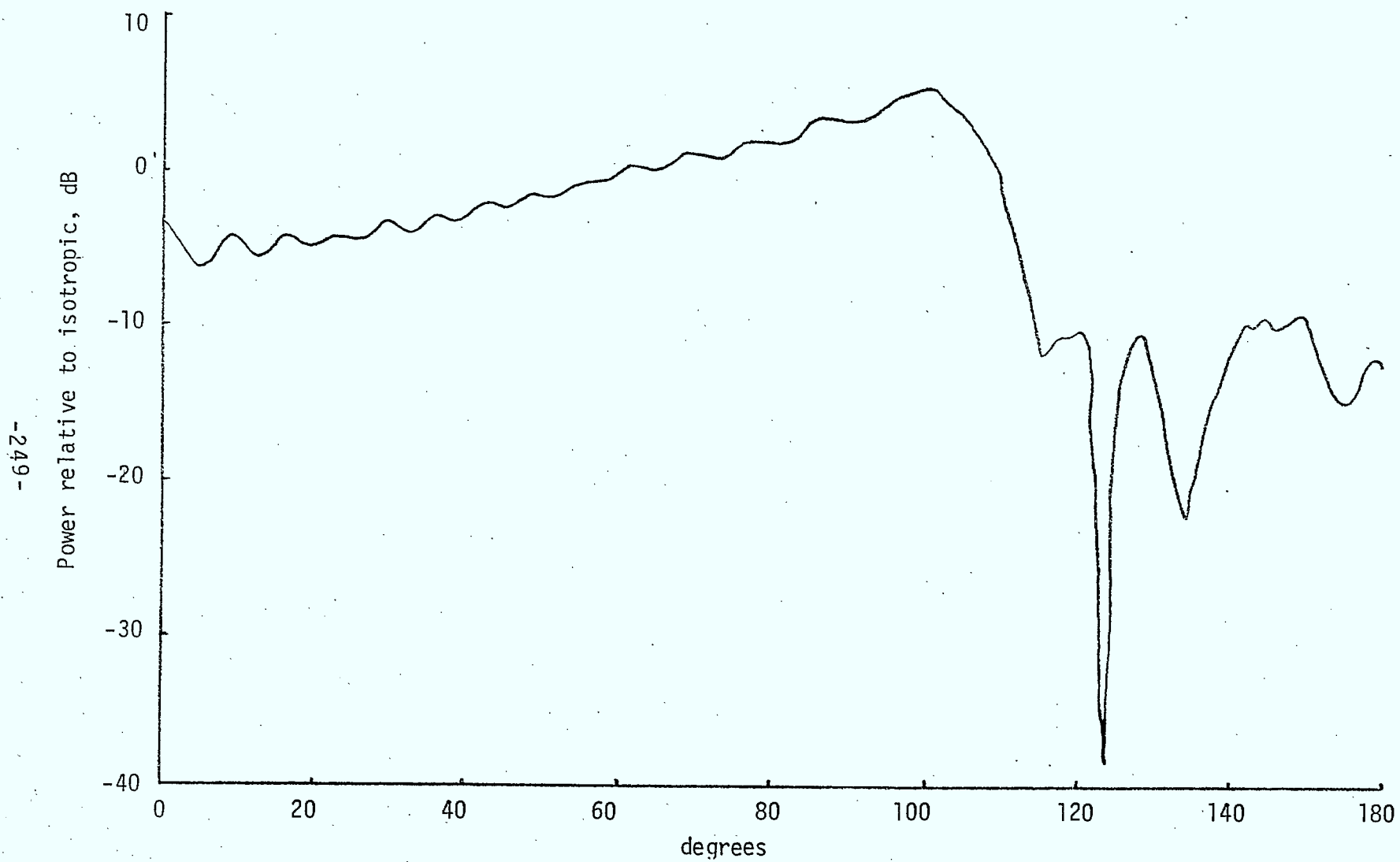


Figure 5.1.2 E Plane pattern from 14λ shaped subreflector

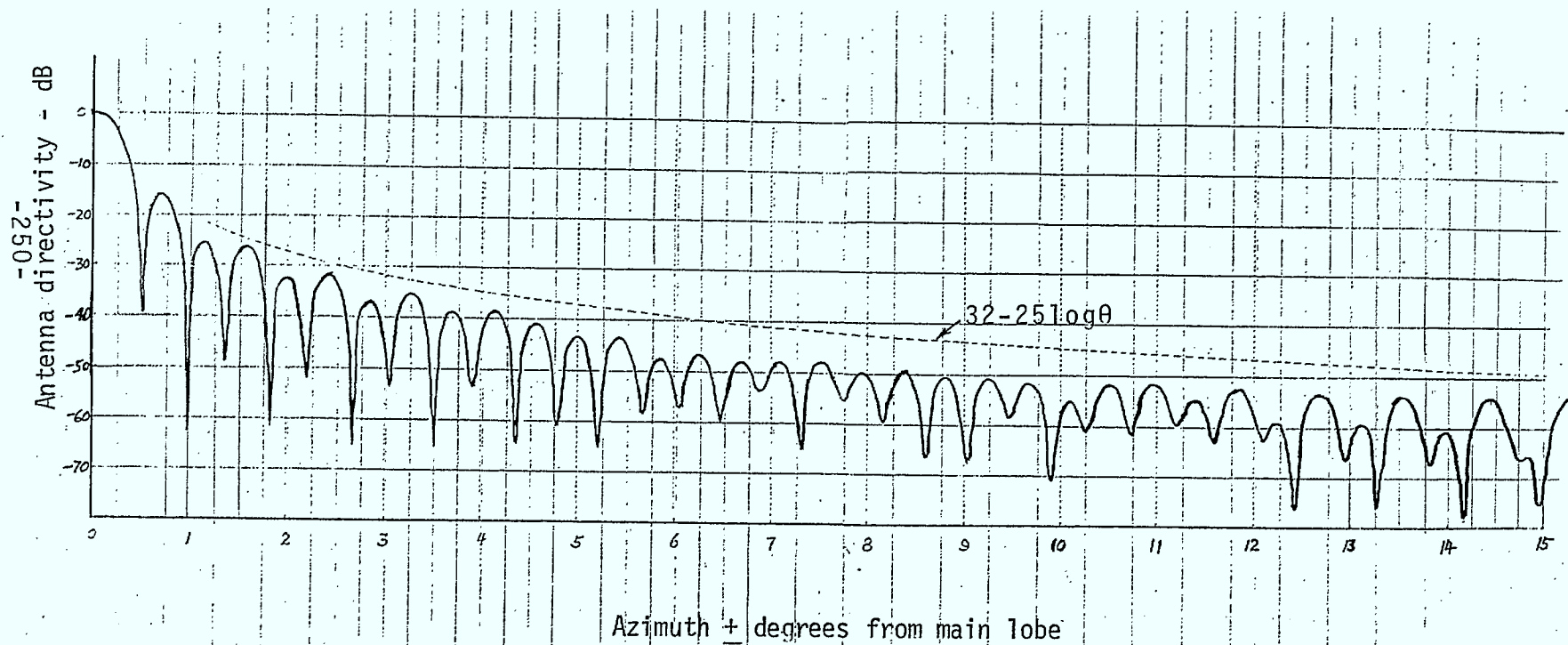


Figure 5.1.2(b) Proposed 10M antenna - calculated far field pattern for uniform illumination (0°-15°)



ANDREW

PE

Approved

PATTERN ENVELOPE

ANTENNA TYPE NUMBER

Gain: GHz
 dBi at GHz
 15 dB BEAMWIDTH: DEGREES

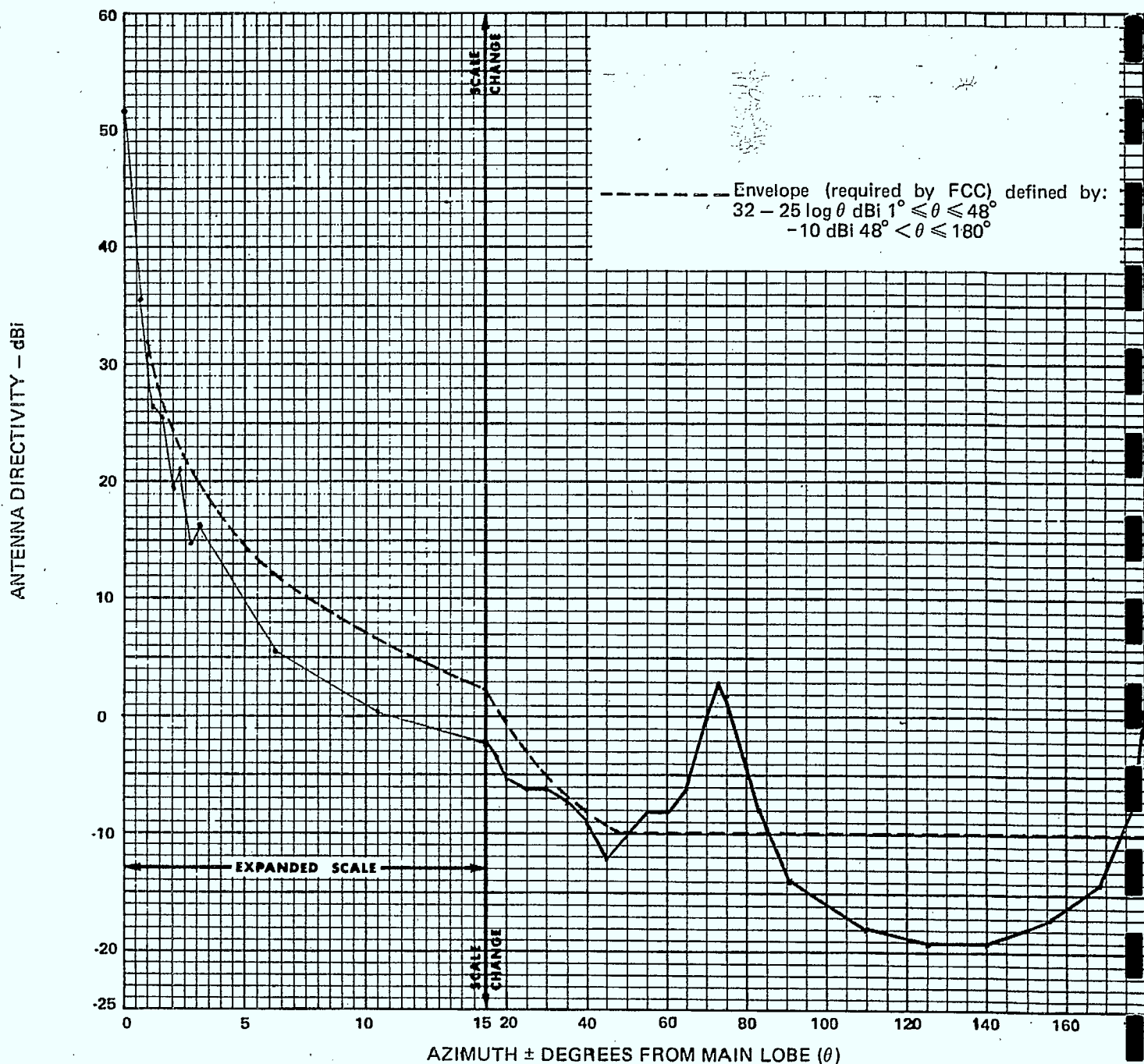


Figure 5.1.2(b)-contd.

Proposed 10M antennas - calculated far field
 RPE for uniform illumination



Figure 5.1.3(a) Proposed 10M antenna - subreflector pattern for underilluminated case

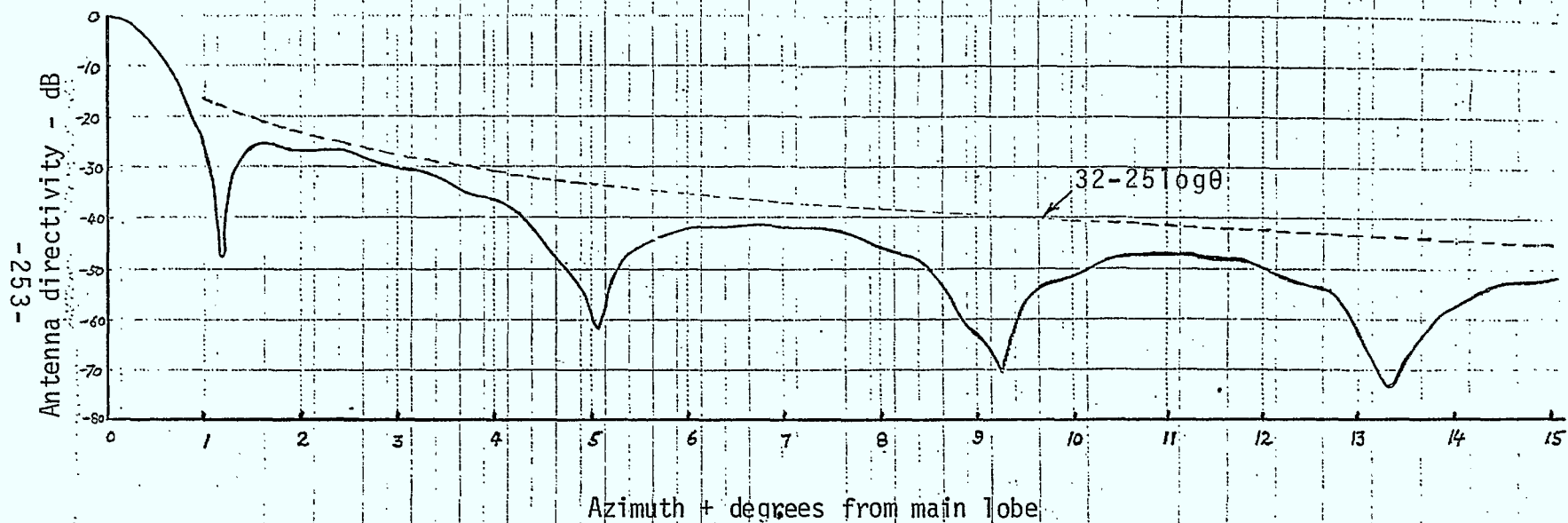


Figure 5.1.3(b) Proposed 10M antenna - calculated far field pattern for underilluminated case ($0^\circ - 15^\circ$)



ANDREW

PE

Approved

PATTERN ENVELOPE

ANTENNA TYPE NUMBER

Gain: GHz
 dBi at GHz
 15 dB BEAMWIDTH: DEGREES

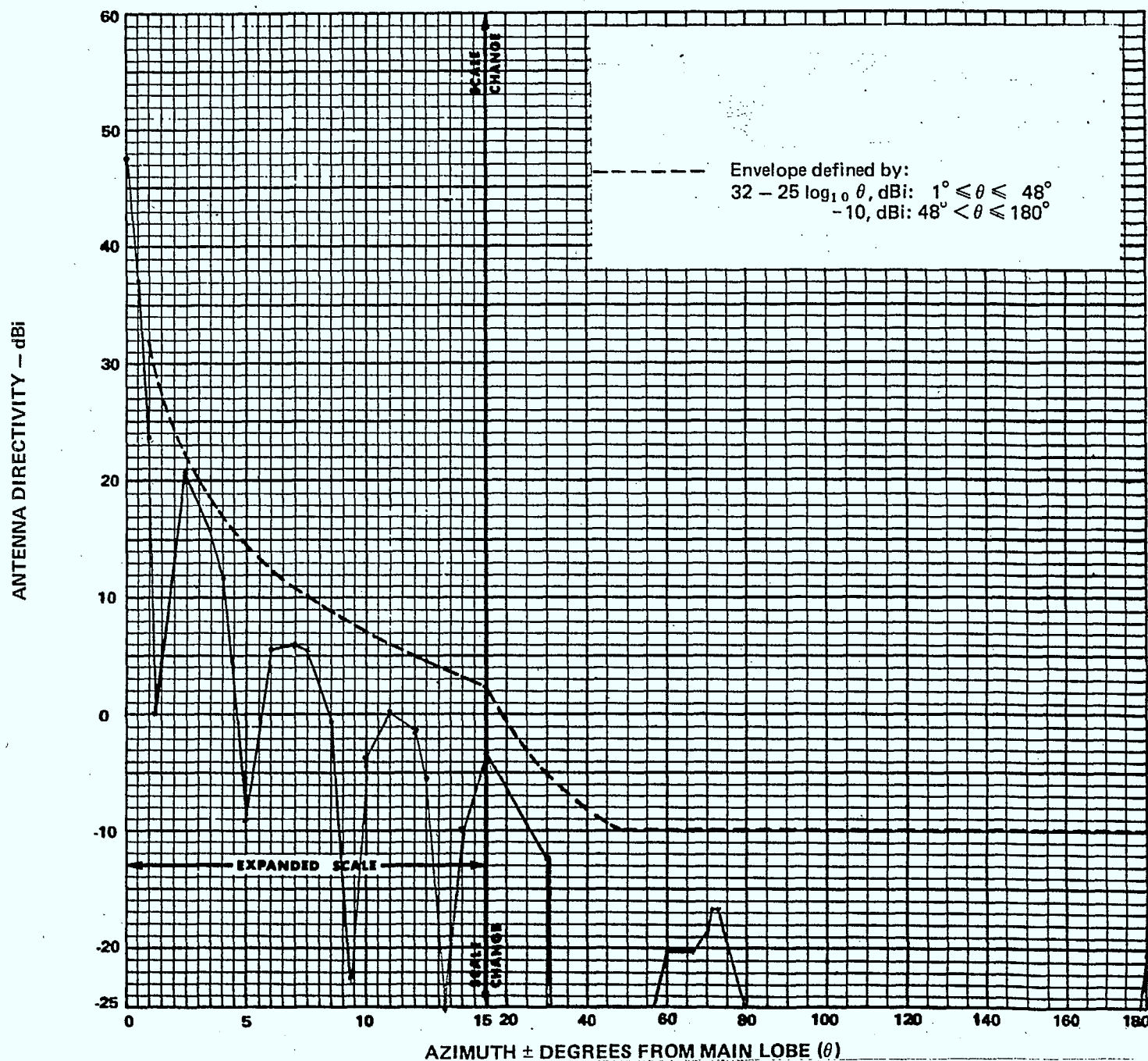


Figure 5.1.3(b)-contd.

Proposed 10M antenna - calculated far field RPE for underilluminated case.

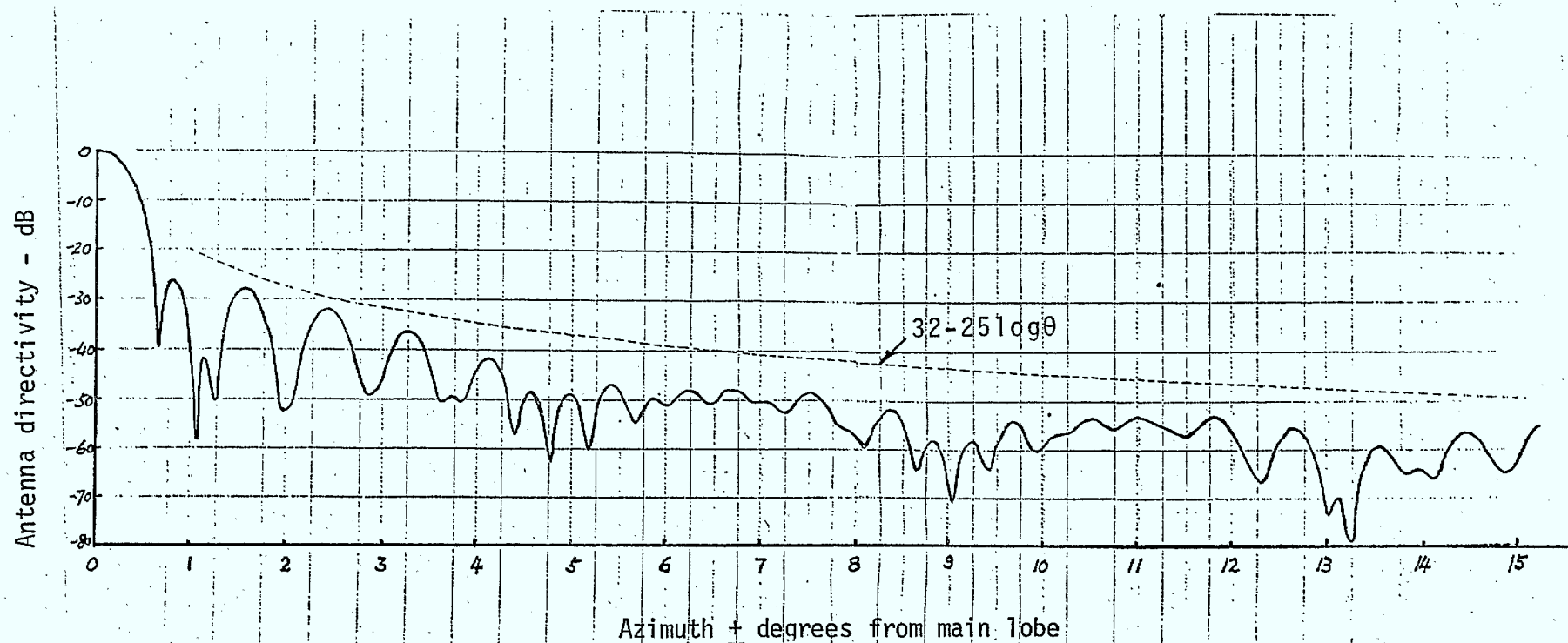


Figure 5.1.3(c) Proposed 10M antenna - calculated far field pattern for Taylor illumination ($0^\circ - 15^\circ$).



ANDREW

PE

Approved

PATTERN ENVELOPE

ANTENNA TYPE NUMBER

Gain: GHz
 dBi at GHz
 15 dB BEAMWIDTH: DEGREES

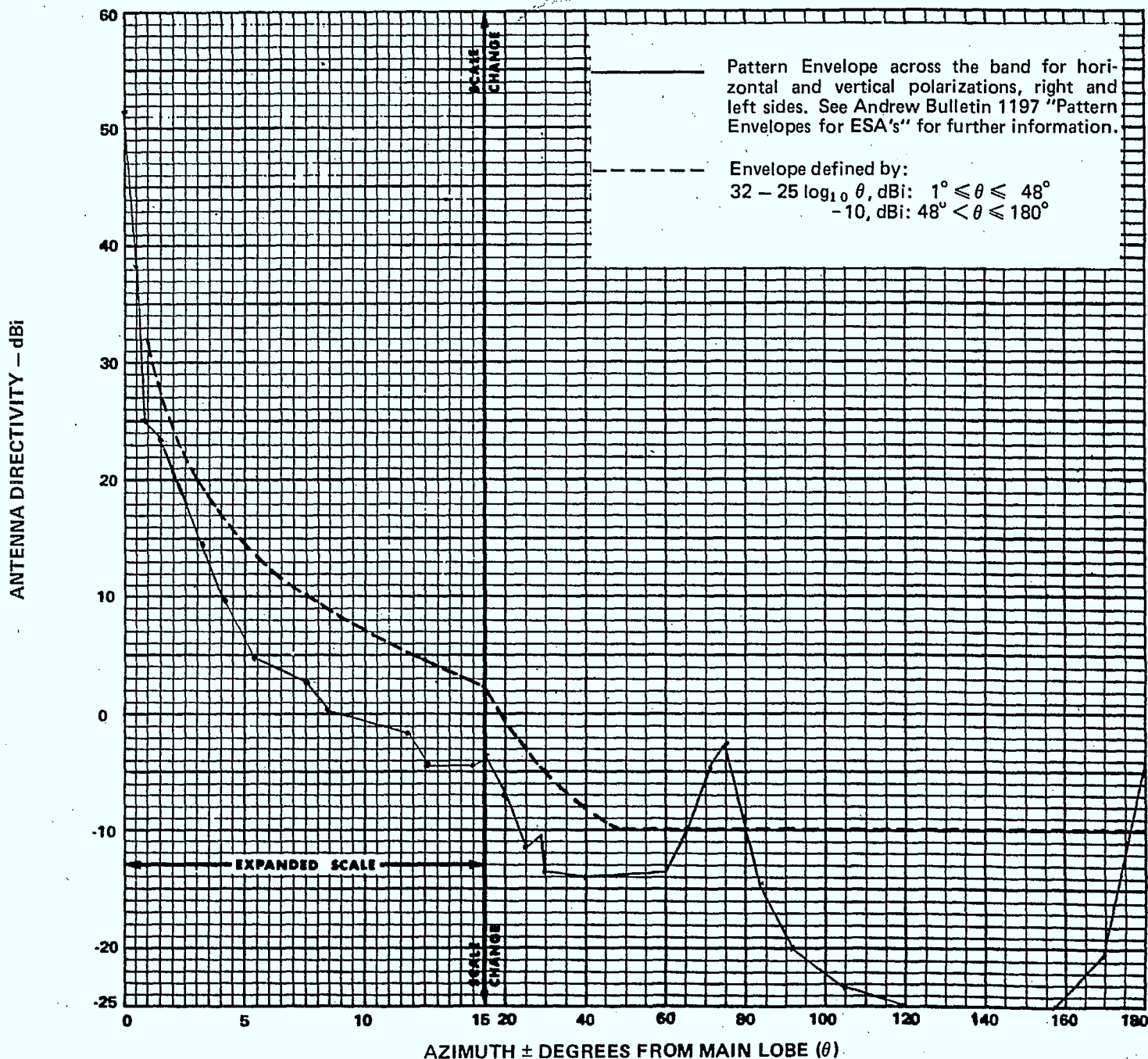


Figure 5.1.3(c)-contd. Proposed 10M antenna - calculated far field RPE for Taylor illumination.

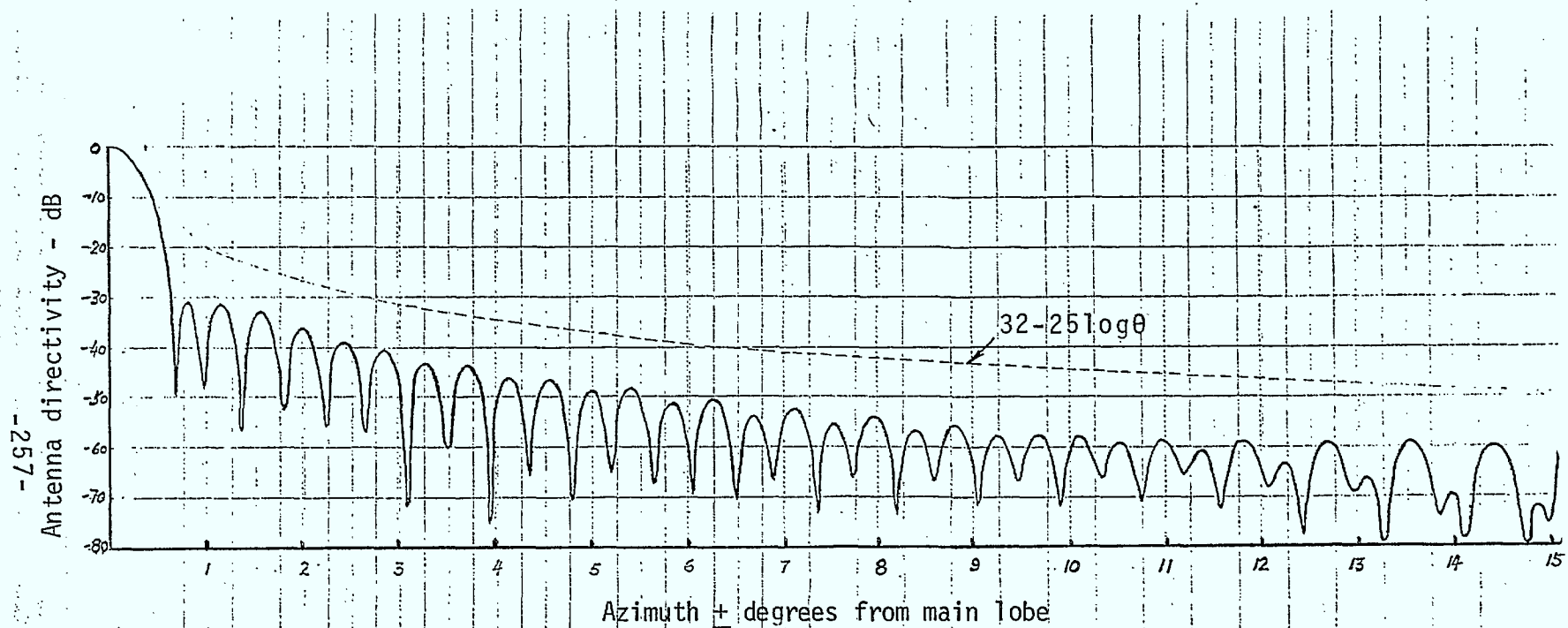


Figure 5.1.3(d) Proposed 10M antenna - calculated far field pattern for Taylor illumination without blockage ($0^\circ - 15^\circ$).



ANDREW

PE

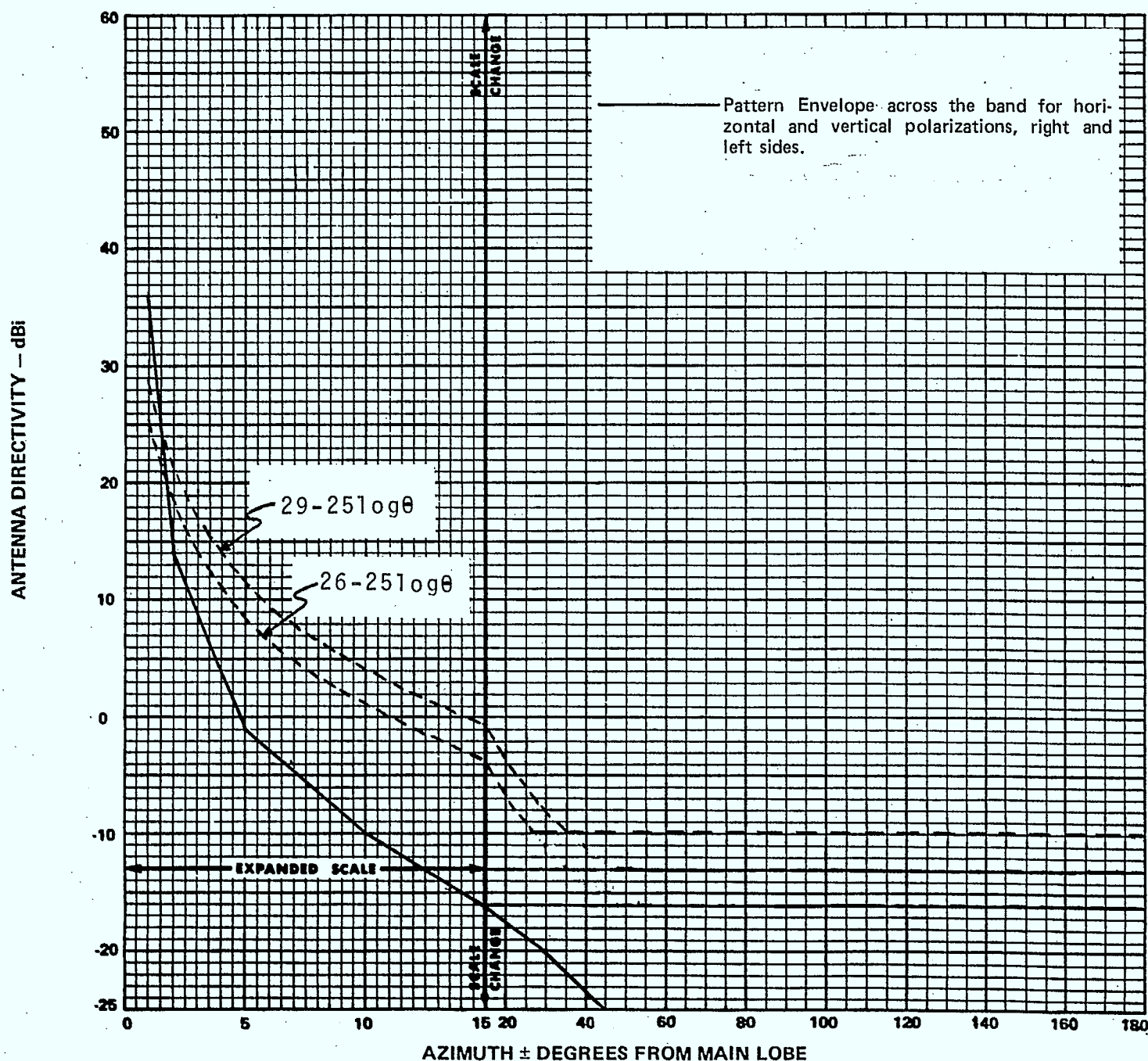
Approved

PATTERN ENVELOPE

ANTENNA TYPE NUMBER 15' OFFSET "SHELL" ANTENNA

3.7-4.2 GHz

Gain: 43.5 \pm 0.2 dBi at 4.0 GHz



Andrew Corporation 10500 W. 153rd St.
Orland Park, IL U.S.A. 60462

Andrew Antenna Company Ltd.
Whitby, Ontario, Canada

FORM 4213 (11/79)

Andrew Ant
Lochgelly, F

Andrew Ant
Reservoir, V

FIGURE 5.1.4

Antennes Andrew S.A.R.L.
Nogent-le-Rotrou, France

Andrew S.R.L.
Milano, Italy





ANDREW

PE

Approved

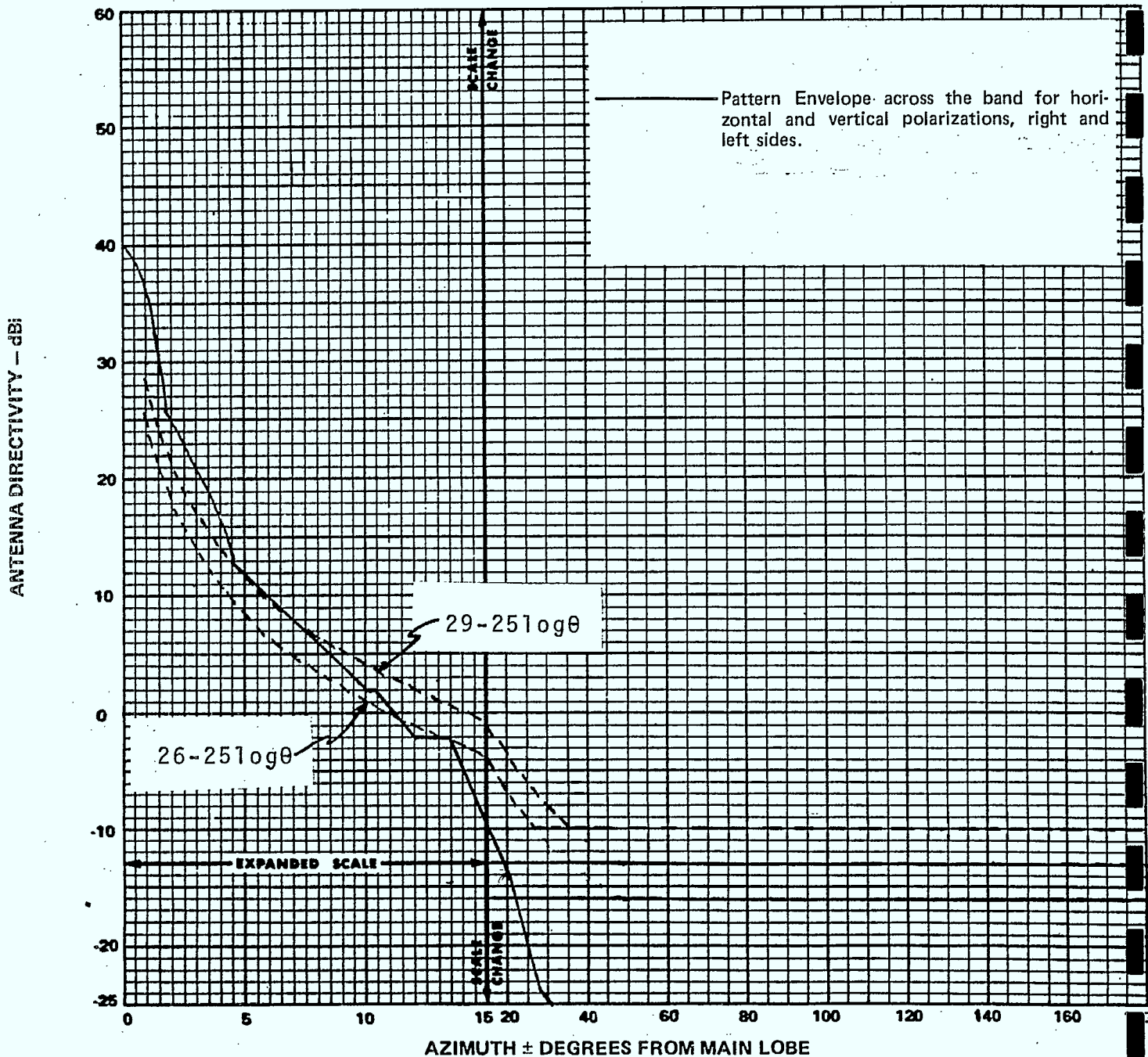
PATTERN ENVELOPE

ANTENNA TYPE NUMBER SHX10A
10FT HORN REFLECTOR ANTENNA

3.7-4.2

GHz

Gain: 39.8+0.5 dBi at 3.95 GHz



Andrew Corporation 10500 W. 153rd St.
Orland Park, IL U.S.A. 60462

Andrew Antenna Company Ltd.
Whitby, Ontario, Canada

Andrew Antenn
Lochgelly, Fife,

Andrew Antenn
Reservoir, Victo

Antennes Andrew S.A.R.L.
Nogent-le-Rotrou, France

Andrew S.R.L.
Milano, Italy



ANDREW

PE

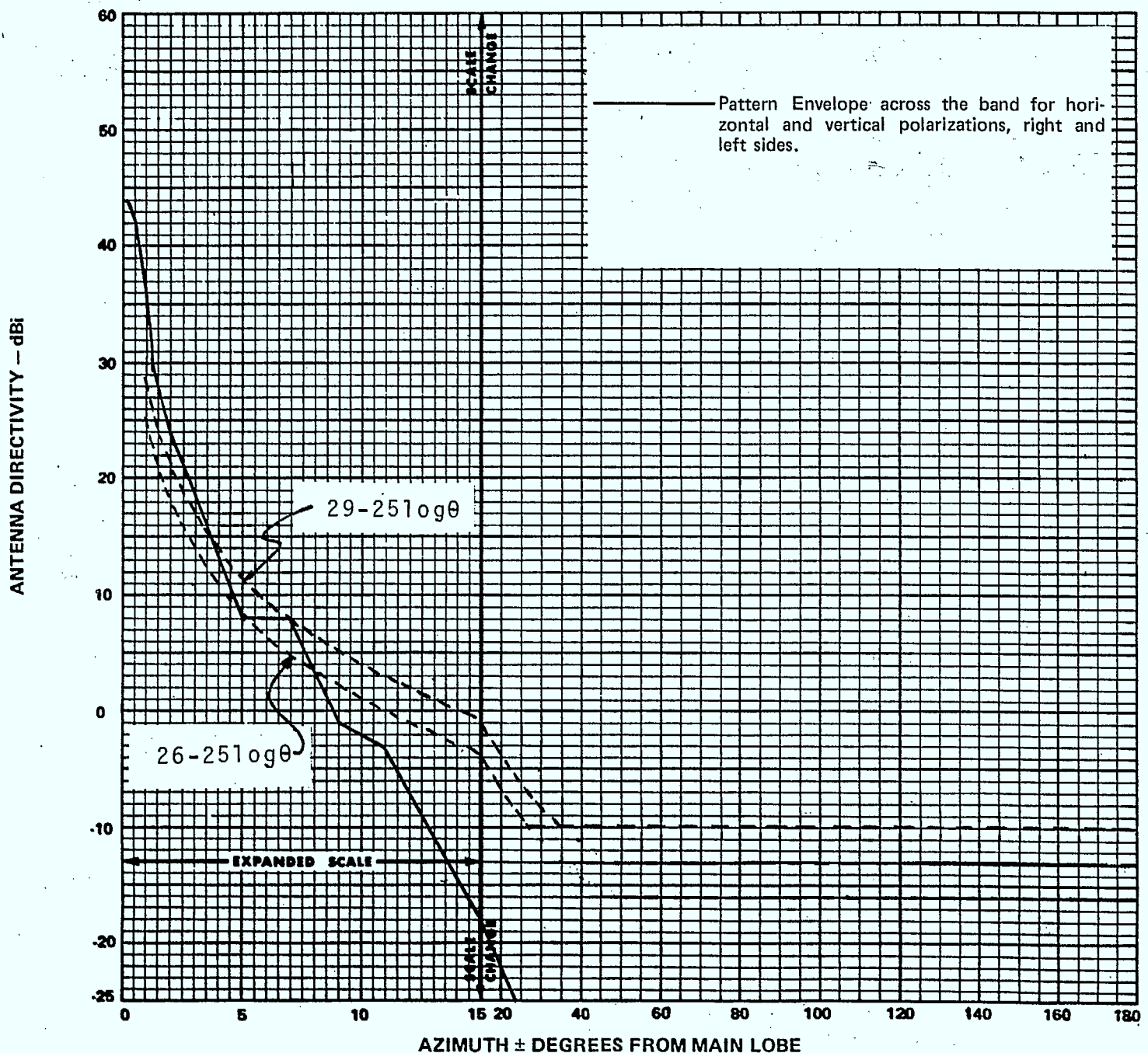
Approved _____

PATTERN ENVELOPE

ANTENNA TYPE NUMBER SHX10A
10FT HORN REFLECTOR ANTENNA

5.925-6.425 GHz

Gain: 43.5 ± 0.5 dBi at 6.175 GHz



Andrew Corporation 10500 W. 153rd St.
Orland Park, IL U.S.A. 60462

Andrew Antenna Company Ltd.
Brimley, Ontario, Canada

FORM 4213 (11/79)

Andrew An
Lochgelly, I

Andrew An
Reservoir, V

FIGURE 5.1.6

Antennes Andrew S.A.R.L.
Nogent-le-Rotrou, France

Andrew S.R.L.
Milano, Italy



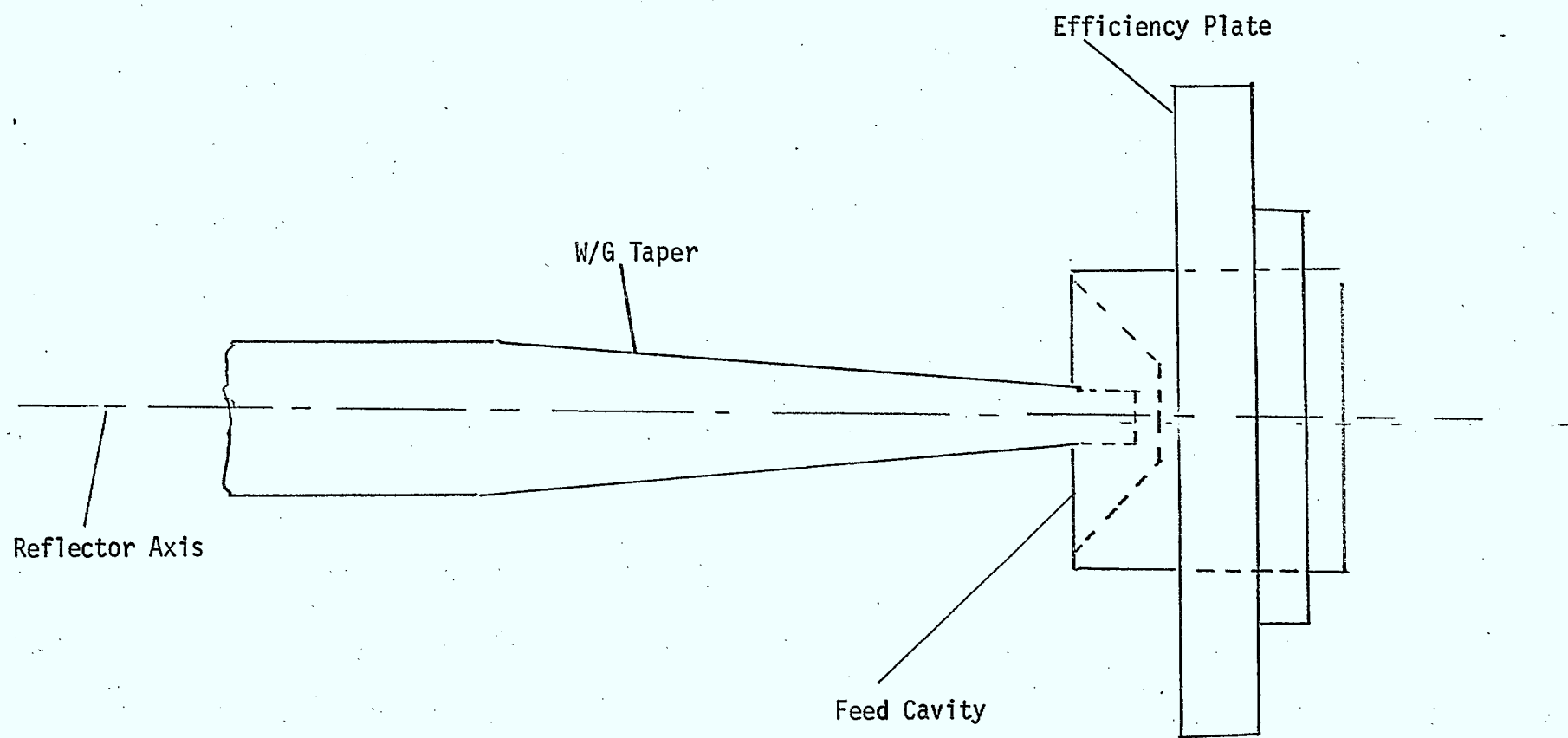


Figure 5.2.1 Cutler-type feed.

Figure 5.2.2 RPE for 15' antenna with axially supported feed



ANDREW

PE

Approved

PATTERN ENVELOPE

ANTENNA TYPE

(Curve A) defined as:

$32 - 25 \log_{10} (\theta) \text{ dBi}, 1^\circ \leq \theta \leq 48^\circ$

$-10 \text{ dBi}, 48^\circ \leq \theta \leq 180^\circ$

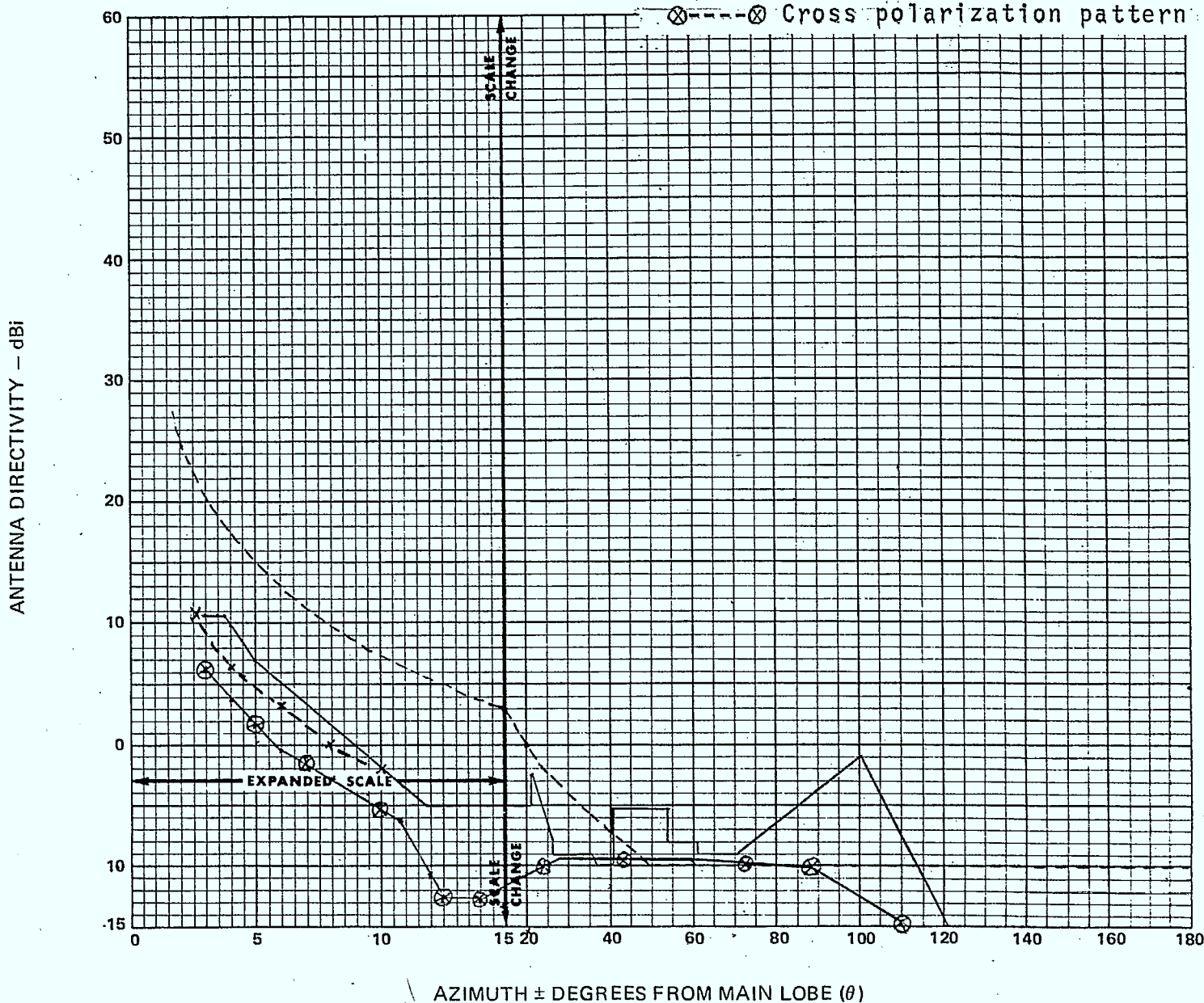
11.7 - 12.2 GHz

Gain: 52.2 dBi at 11.9 GHz

Pattern Envelope of worst case sidelobes for across the band, horizontal and vertical polarizations, right and left sides.

x-----x Calculated RPE.

⊗-----⊗ Cross polarization pattern



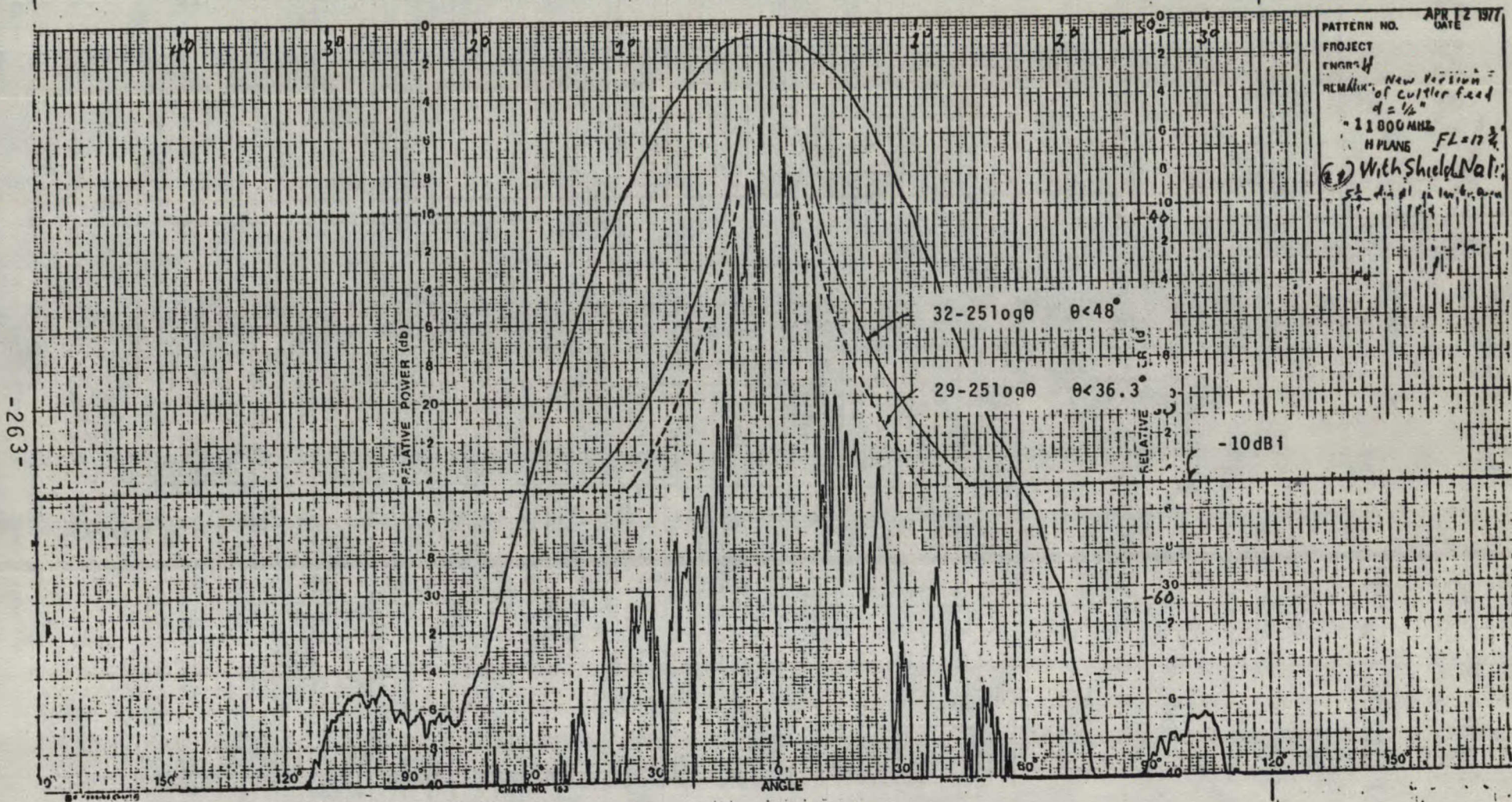


Figure 5.2.3(a) Radiation Pattern for 6' shielded antenna at 11.8 GHz - H plane

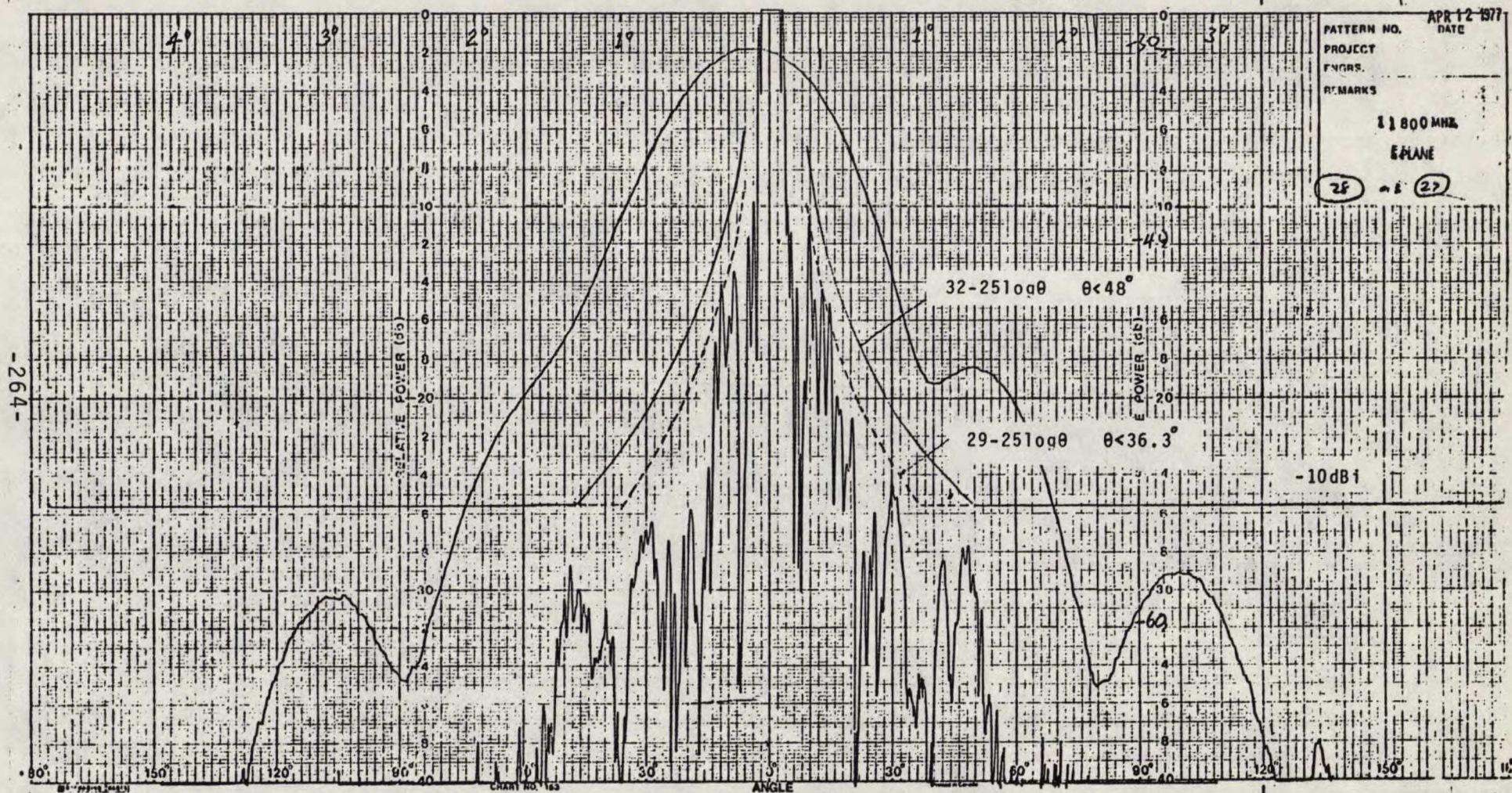


Figure 5.2.3(b) Radiation Pattern for 6' shielded antenna at 11.8 GHz - E plane

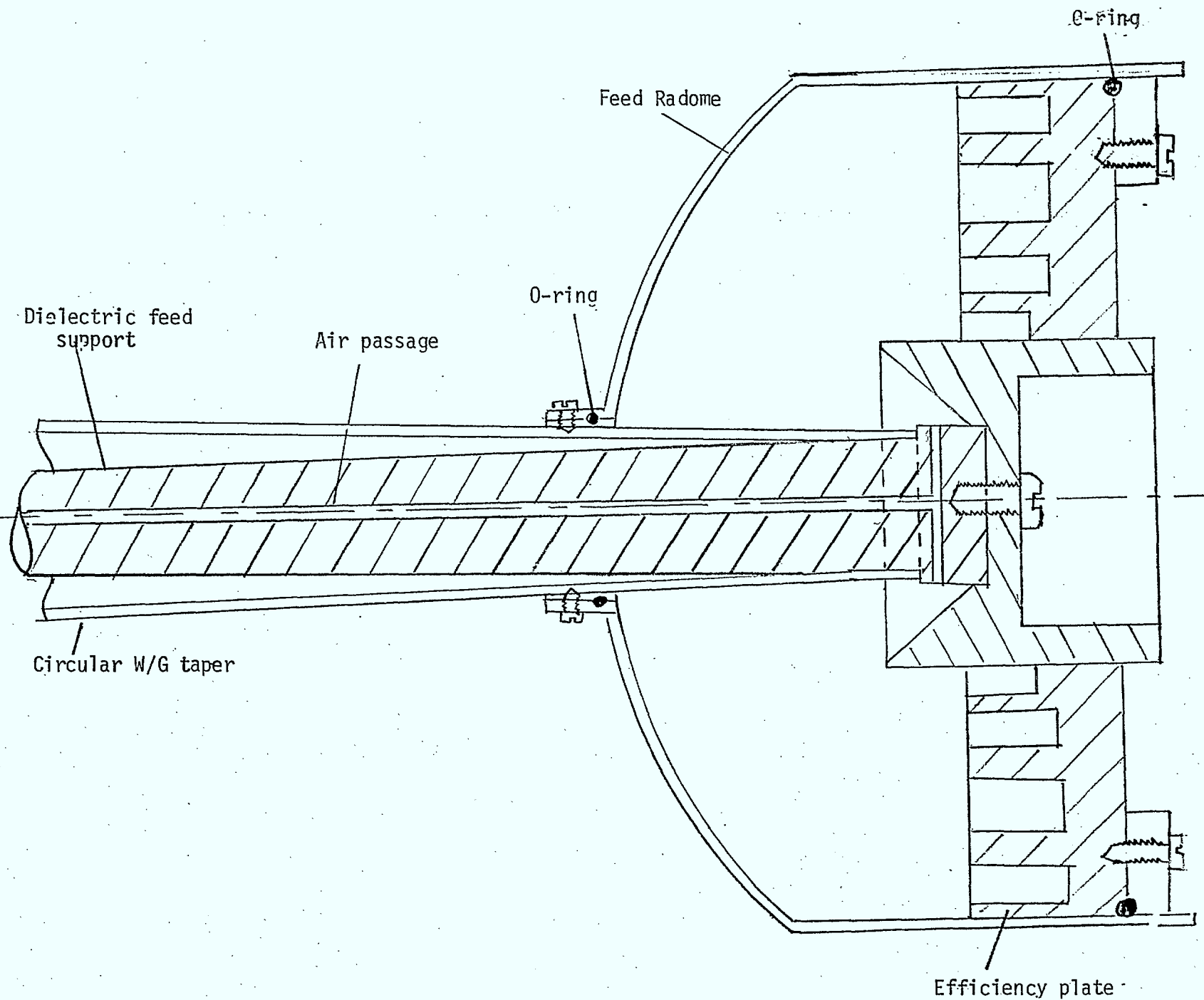


Figure 5.2.4 Receive/transmit axially supported feed

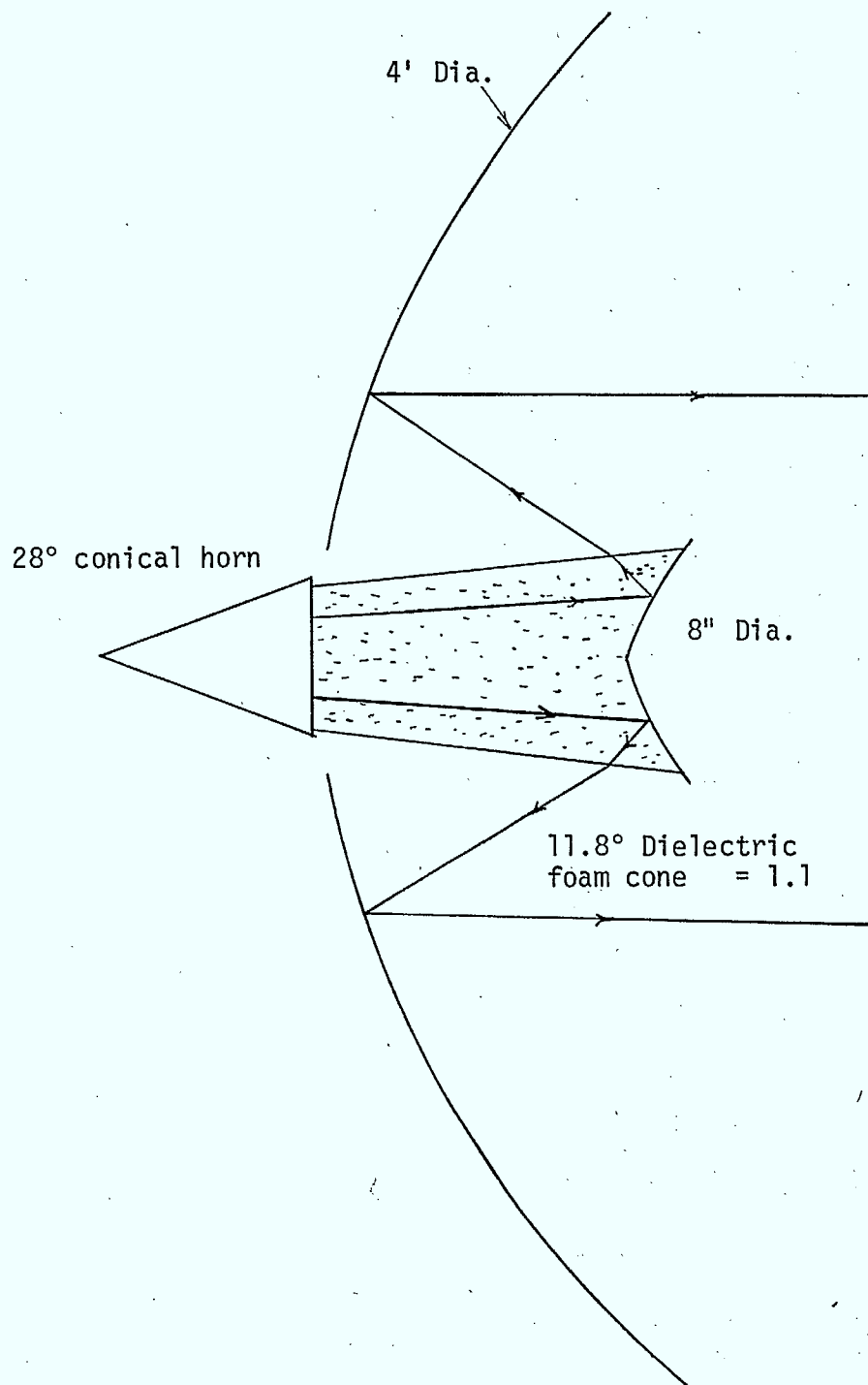


Figure 5.2.5 Reflector profiles and feed position of Cassegrain Antenna with dielectric cone feed.

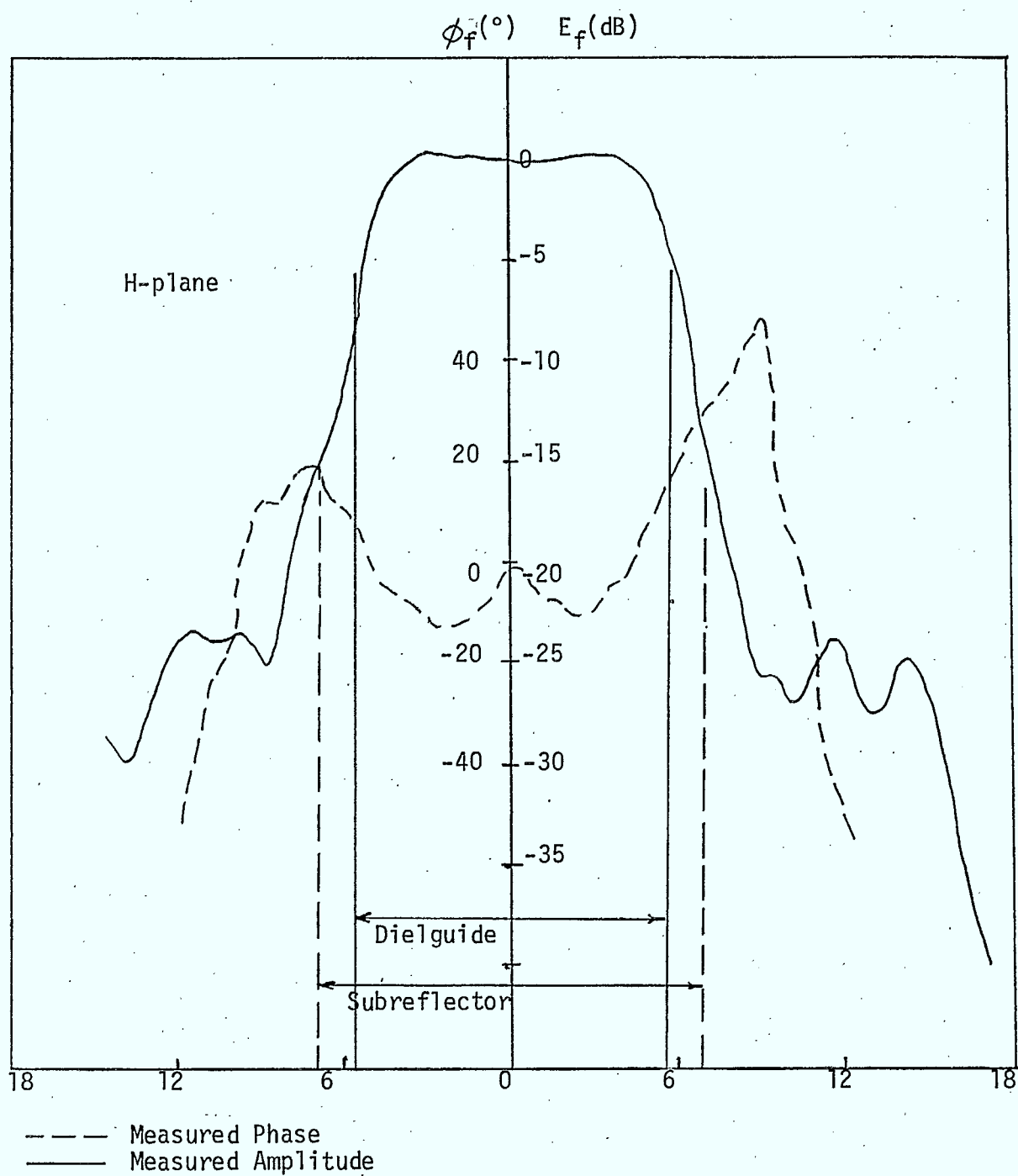


Figure 5.2.6 Aperture field pattern of a dielectric cone
excited by a conical horn
Frequency 11.2 GHz

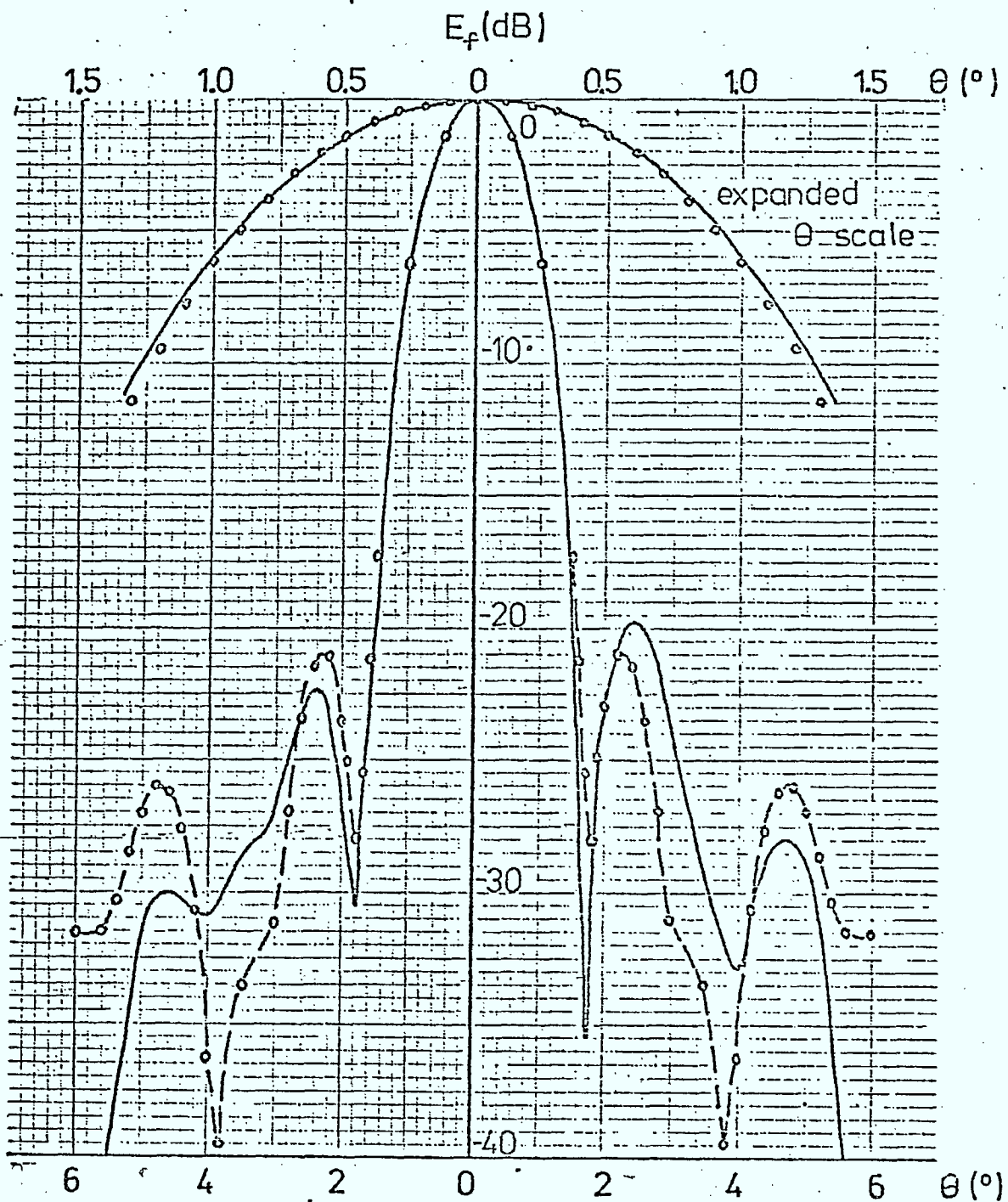


Figure S.2.7 H-plane far field radiation pattern of a 4' (1.22m) diameter cassegrain parabolic reflector. Fréq. = 11.2GHz. The centre position of the main lobe is also shown on an expanded scale.

--o--o--o-- computed, based on the measured aperture field
 ————— measured

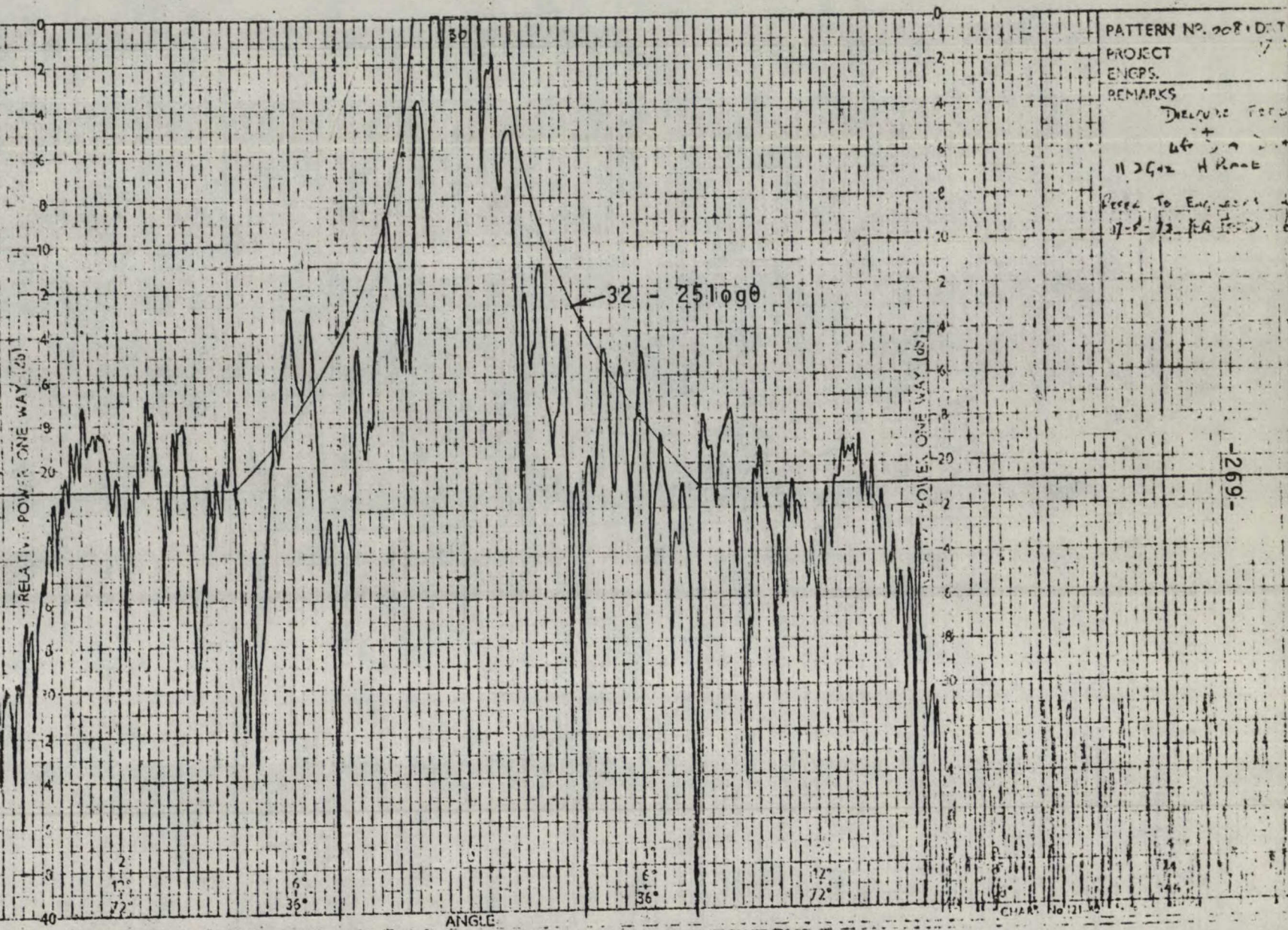


Figure 5.2.8 H-plane pattern of 4' dielguide Cassegrain Antenna, 5°-360°

-269-



ANDREW

RPE 1728

J. H. Hansen
Approved

16 November 1977

RADIATION PATTERN ENVELOPE

ANTENNA TYPE NUMBER

UGX12R-59D

FOOT ANTENNA

5.925 - 6.425

GHz

DUAL

POLARIZED

————— Envelope for a Horizontally Polarized Antenna

- - - - - Envelope for a Vertically Polarized Antenna

Gain: 45.8 ± 0.2 dBi at 6.175 GHz

For reference to a half wave dipole subtract 2.15 dB.

See Andrew Bulletin 1032, "Radiation Pattern Envelopes," for further information.

This antenna meets FCC performance Standard A.

ANTENNA DIRECTIVITY—dB DOWN FROM MAIN LOBE

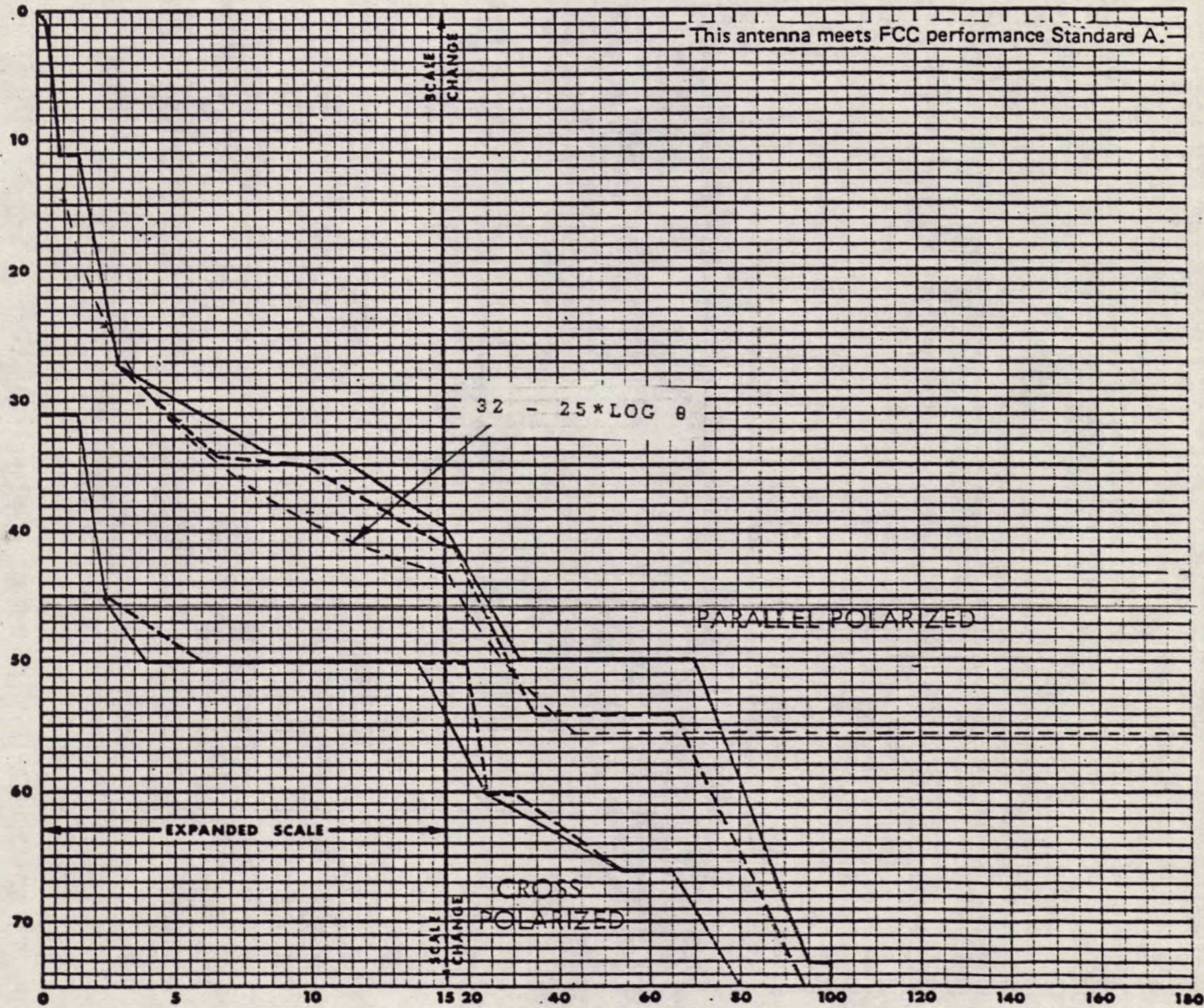


Figure 5.2.9 "Peak envelope" RPE of a Cassegrain Antenna
AZIMUTH ± DEGREES FROM MAIN LOBE

Andrew Corporation
10500 W. 153rd Street
Orland Park, IL
U.S.A. 60462

Andrew Antenna Company Ltd.
606 Beech Street
Whitby, Ontario
Canada L1N 5S2

Andrew Antenna Systems
Lochgelly, Fife
Great Britain KY5 9HG

Andrew Antennas
171 Henty Street
Reservoir, Victoria
Australia 3073

Andrew Antenas Limitada
Caixa Postal 600
18100 Sorocaba
São Paulo, Brasil



10 ft. 7" LALC 10 Jan 78
 E-658
 105 / 020: 6.175 GHz
 E-PLANE

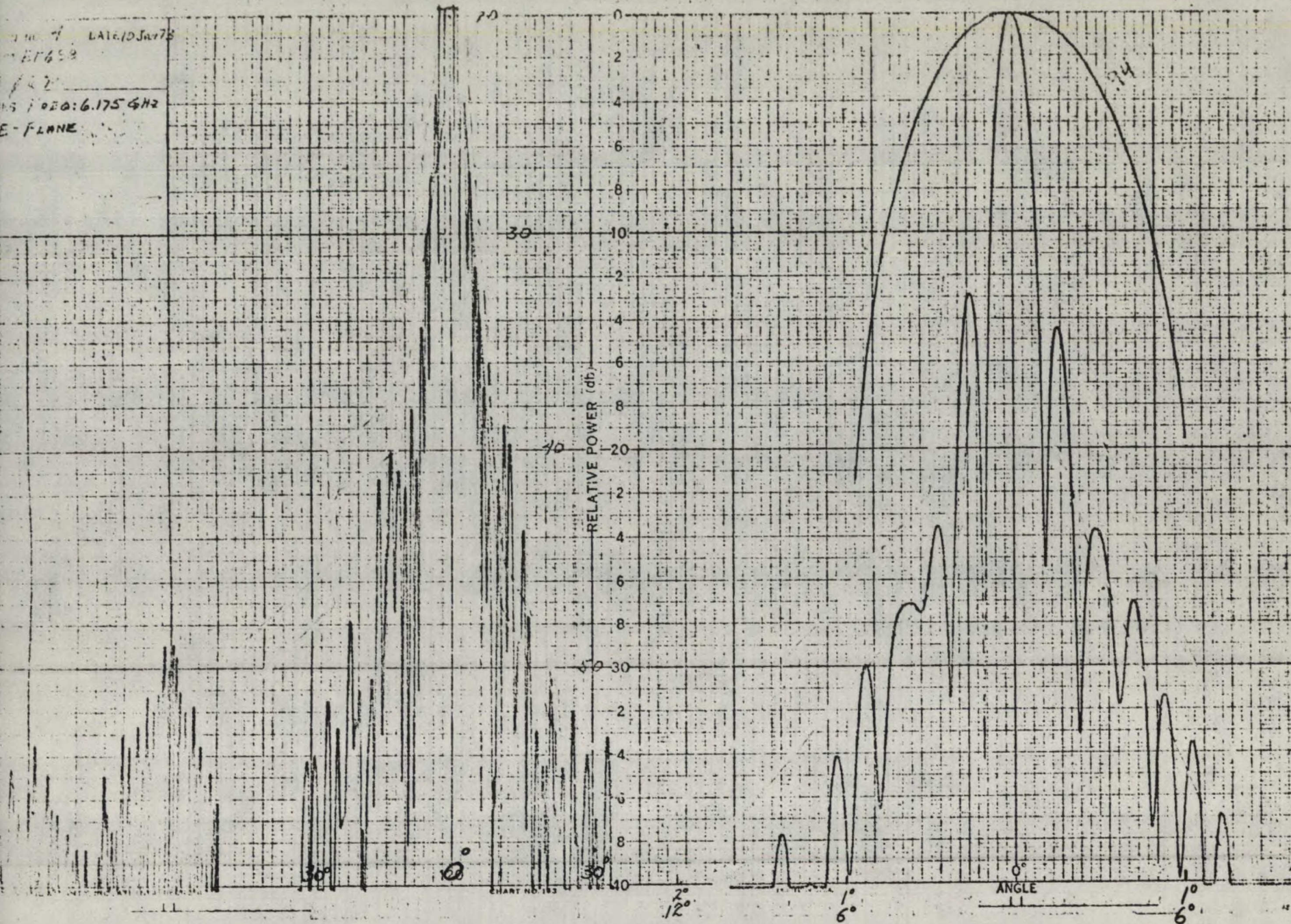


Figure 5.2.10(a). An example of the E plane radiation pattern of a 10 ft. Cassegrain ESA using cone supported subreflector

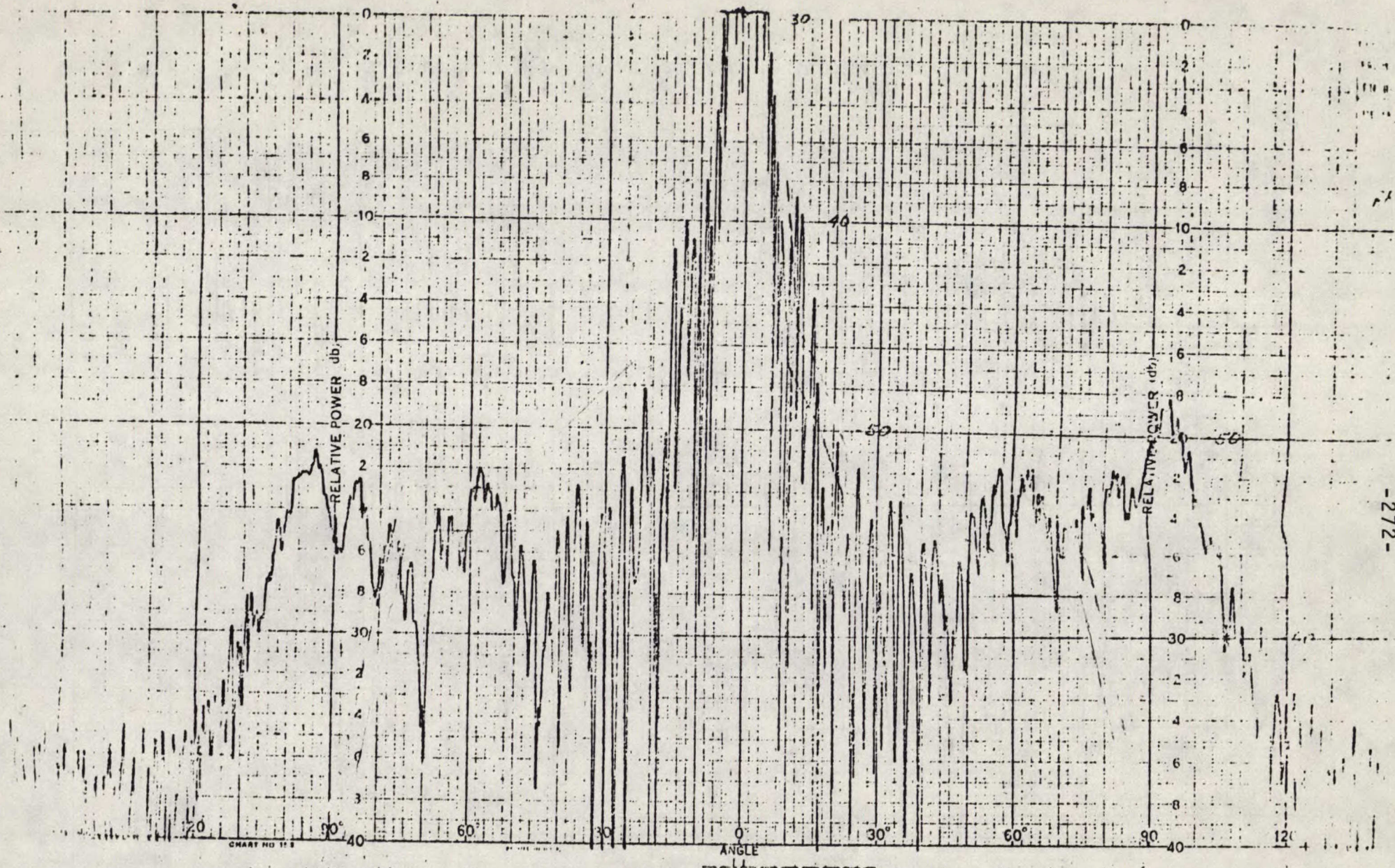


Figure 5.2.10(b) An example of the E-plane pattern of a 10 ft. Cassegrain ESA using cone supported subreflector

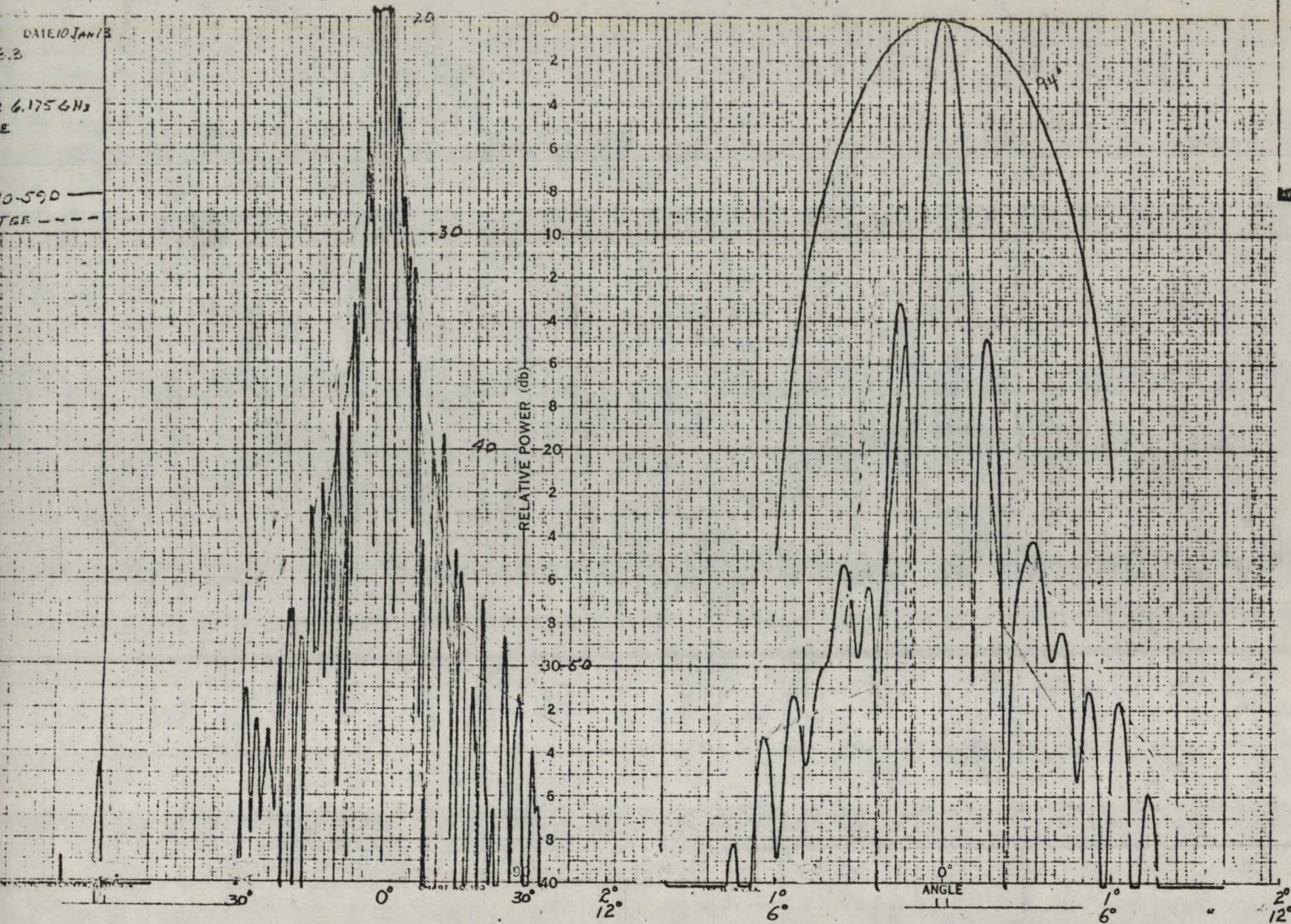


Figure 5.2.11(a) An example of the H plane radiation pattern of a 10 ft. Cassegrain ESA using cone supported subreflector

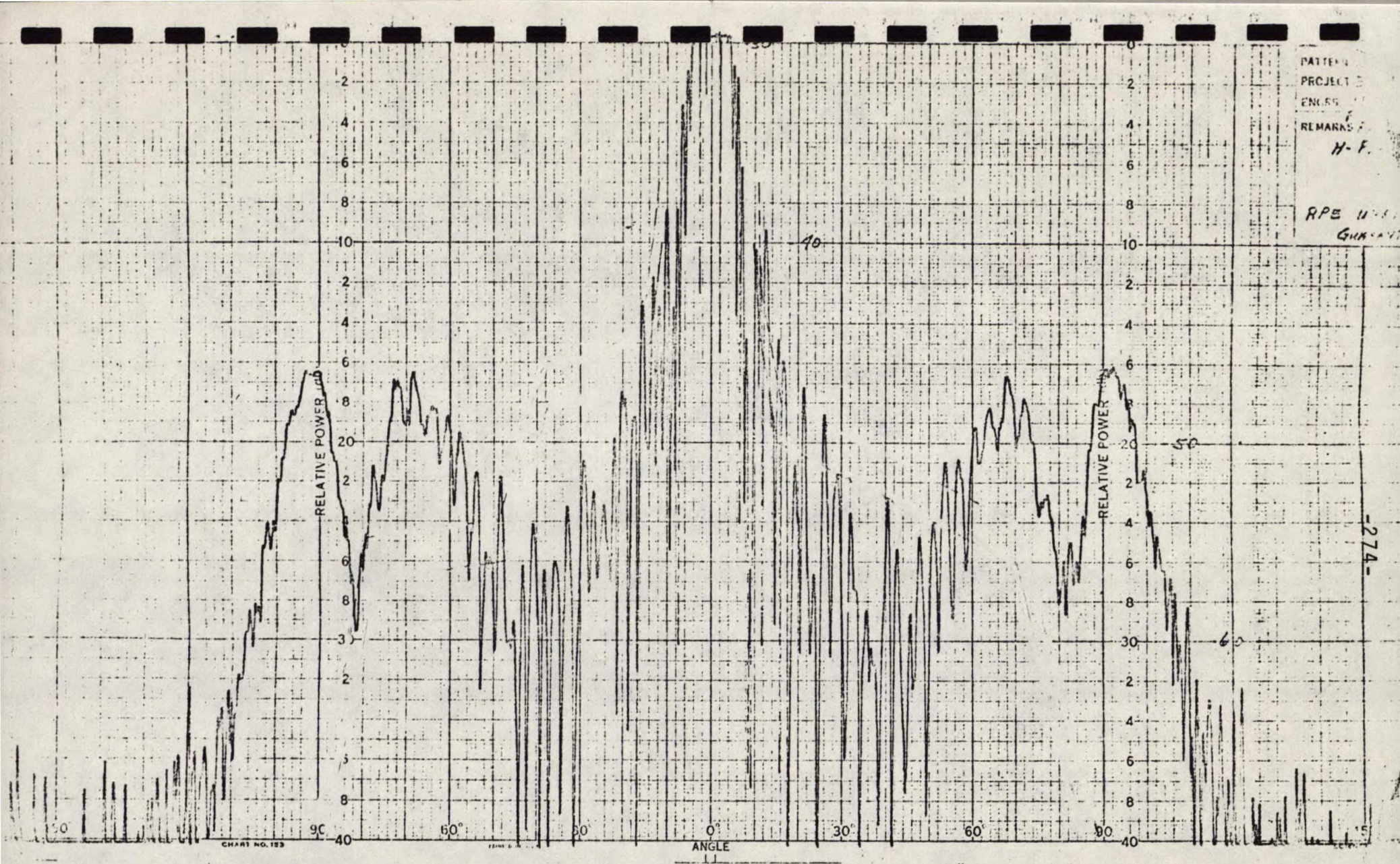


Figure 5.2.11(b) An example of the H plane pattern of a 10 ft. Cassegrain ESA using cone supported subreflector

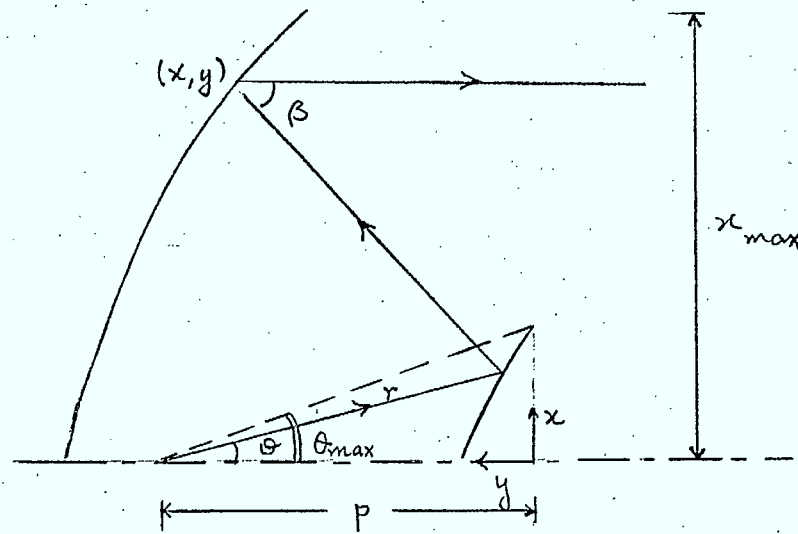


Figure A.1 Geometry for a shaped Cassegrain system.

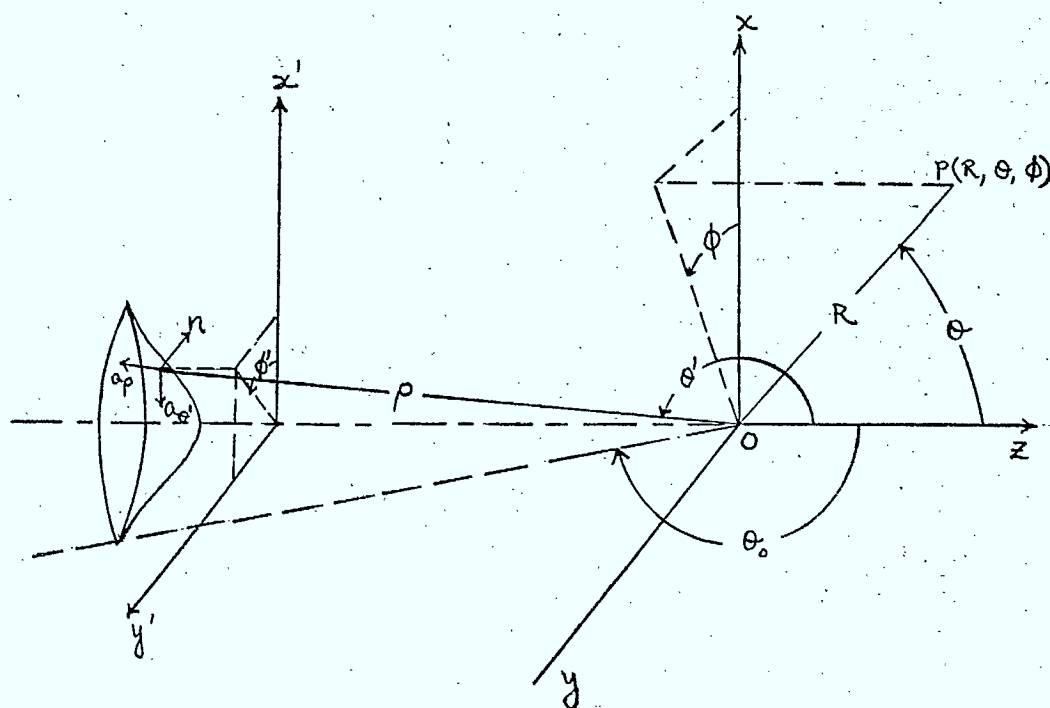


Figure C.1 Geometry for feed-reflector system.

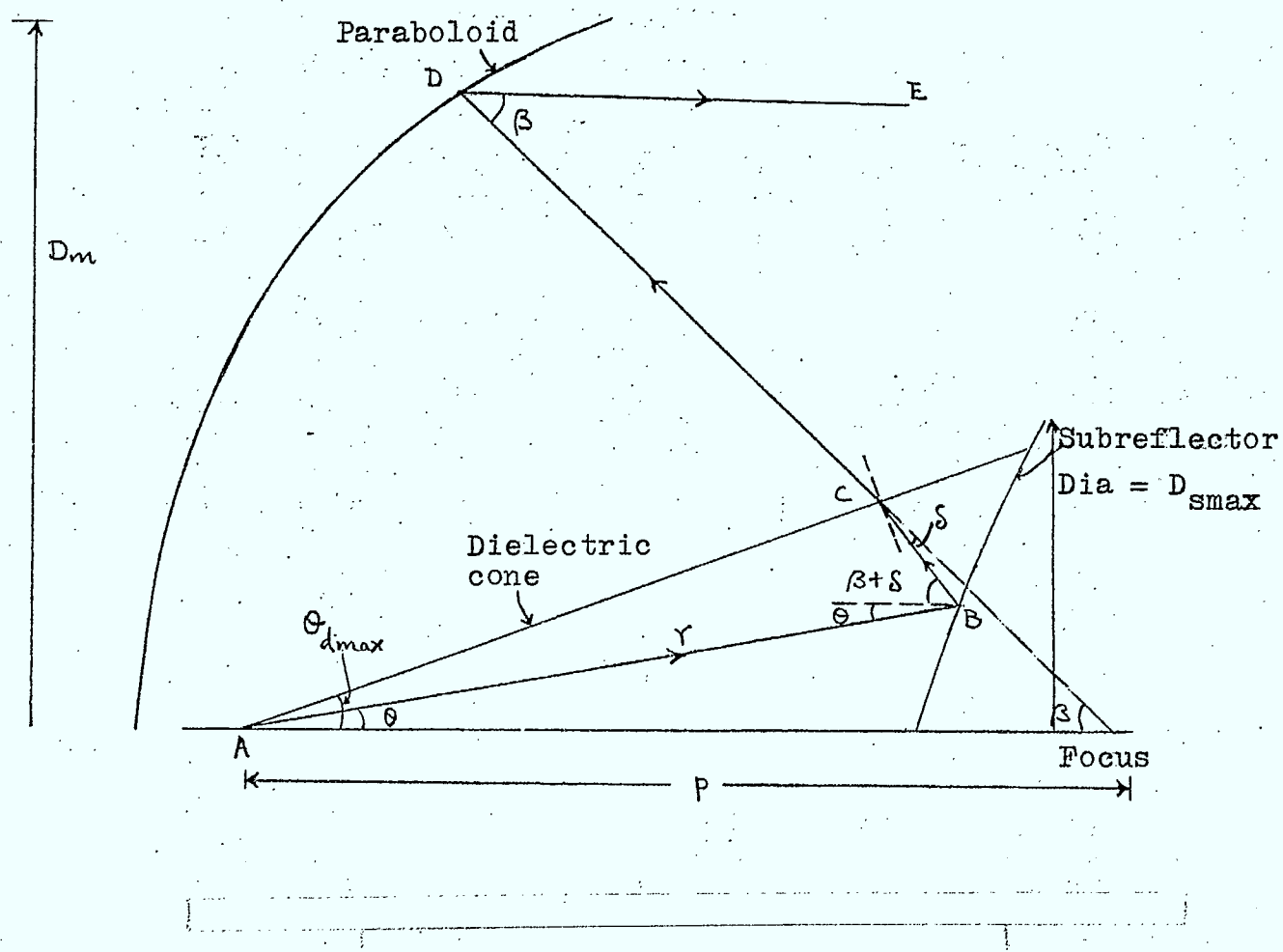


Figure E.1 Geometry of a Cassegrain system with a dielectric cone feed.



Sidelobe reduction techniques for earth station antennas

P
91
C655
L55
1982

DATE DUE
DATE DE RETOUR

OCT 22 1985

LOWE-MARTIN No. 1137

